The Influence of Solvent Reorganization on Organocatalytic Reactions

Dissertation

zur

Erlangung des Doktorgrades (Dr. rer. nat.)

der

Mathemathisch-Naturwissenschaftlichen Fakultät

der

Rheinischen Friedrich-Wilhelms-Universität Bonn

vorgelegt von

Sascha Gehrke

aus

Hannover

17. August 2020

Angefertigt mit Genehmigung der Mathematisch-Naturwissenschaftlichen Fakultät der Rheinischen Friedrich-Wilhelms-Universität Bonn

1. Gutachterin:	Prof. Dr. Barbara Kirchner
2. Gutachter:	Prof. Dr. Thomas Bredow
Tag der Promotion:	24.02.2021
Erscheinungsjahr:	2021

... meinem Vater

Statement of Authorship

I, Sascha Gehrke, hereby declare that I am the sole author of this thesis. The ideas and work of others, whether published or unpublished, have been fully acknowledged and referenced in my thesis.

Bonn, August 17th 2020

Publications

Parts of this thesis have already been published in peer-reviewed journals:

1. **S. Gehrke**, O. Hollóczki, "A Molecular Mechanical Model for N-Heterocyclic Carbenes", *Phys. Chem. Chem. Phys.*, **2016**, *18 (32)*, 22070–22080, *doi:10.1039/C6CP02624A*.

2. **S. Gehrke**, K. Schmitz, O. Hollóczki, "Is Carbene Formation Necessary for Dissolving Cellulose in Ionic Liquids?", *J. Phys. Chem. B*, **2017**, *121 (17)*, 4521–4529, *doi:10.1021/acs.jpcb.7b00631*.

3. **S. Gehrke**, M. von Domaros, R. Clark, O. Hollóczki, M. Brehm, T. Welton, A. Luzar, B. Kirchner, "Structure and Lifetimes in Ionic Liquids and their Mixtures", *Faraday Discuss.*, **2018**, *206*, 219–245, *doi:10.1039/C7FD00166E*.

4. **S. Gehrke**, B. Kirchner, "Robustness of the Hydrogen Bond and Ion Pair Dynamics in Ionic Liquids to Different Parameters from the Reactive Flux Method", *J. Chem. Eng. Data* , **2020**, *65 (3)*, 1146–1158 *doi:10.1021/acs.jced.9b00529*.

5. **S. Gehrke**, O. Hollóczki, "Hydrogen Bonding of N-Heterocyclic Carbenes in Solution: Mechanisms of Solvent Reorganization", *Chem. Eur. J.* , **2018**, *24 (45)*, 11594–11604, *doi:10.1002/chem.201802286*.

6. **S. Gehrke**, O. Hollóczki, "Are There Carbenes in N-Heterocyclic Carbene Organocatalysis?", *Angew. Chem. Int. Ed.* , **2017**, *56 (51)*, 16395–16398, *doi:10.1002/anie.201708305*;
"Treten in der N-heterozyklischen Carben-Organokatalyse wirklich Carbene auf?", *Angew. Chem.*, **2017**, *129 (51)*, 16613–16617, *doi:10.1002/ange.201708305*.

7. **S. Gehrke**, O. Hollóczki, "N-Heterocyclic Carbene Organocatalysis: With or without Carbenes?", *Chem. Eur. J.* , **2020**, *26 (44)*, 10140–10151, *doi:10.1002/chem.202002656*.

8. **S. Gehrke**, W. Reckien, I. Palazzo, T. Welton, O. Hollóczki, "On the Carbene-like Reactions of Imidazolium Acetate Ionic Liquids. Can Theory and Experiments Agree?", *Eur. J. Org. Chem.*, **2019**, *2–3*, 504–511, *doi:10.1002/ejoc.201801050*.

Further publications (not part of this thesis):

9. **S. Gehrke**, H.T. Alznauer, H.A. Karimi-Varzaneh, J.A. Becker, "Ab Initio Simulations of Bond Breaking in Sulfur Crosslinked Isoprene Oligomer Units", *J. Chem. Phys.*, **2017**, *147 (21)*, 214703, *doi:10.1063/1.5001574*.

10. C.J. Smith, **S. Gehrke**, O. Hollóczki, D.V. Wagle, M.P. Heitz, G.A. Baker, "NMR Relaxometric Probing of Ionic Liquid Dynamics and Diffusion under Mesoscopic Confinement within Bacterial Cellulose Ionogels", *J. Chem. Phys.*, **2018**, *148 (19)*, 193845, *doi:10.1063/1.5016337%40jcp.2018.ILQ2018.issue-1.*

11. J. Ingenmey, **S. Gehrke**, B. Kirchner, "How to Harvest Grotthuss Diffusion in Protic Ionic Liquid Electrolyte Systems", *ChemSusChem*, **2018**, *11 (12)*, 1900–1910, *doi:10.1002/cssc.201800436.*

12. D. Riemer, W. Schilling, A. Goetz, Y. Zhang, **S. Gehrke**, I. Tkach, O. Hollóczki, D. Shoubhik, "CO_2-Catalyzed Efficient Dehydrogenation of Amines with Detailed Mechanistic and Kinetic Studies", *ACS Catal.*, **2018**, *8 (12)*, 11679–11687, *doi:10.1021/acscatal.8b03059.*

13. **S. Gehrke**, R. Macchieraldo, B. Kirchner, "Understanding the Fluidity of Condensed Phase Systems in Terms of Voids—Novel Algorithm, Implementation and Application", *Phys. Chem. Chem. Phys.*, **2019**, *21 (9)*, 4988–4997, *doi:10.1039/C8CP07120A.*

14. R. Macchieraldo, **S. Gehrke**, N. K. Batchu, B. Kirchner, K. Binnemans, "Tuning Solvent Miscibility: A Fundamental Assessment at the Example of Induced Methanol/n-Dodecane Phase Separation", *J. Phys. Chem. B*, **2019**, *123 (20)*, 4400–4407, *doi:10.1021/acs.jpcb.9b00839.*

15. T. Stettner, **S. Gehrke**, P. Ray, B. Kirchner, A, Balducci, "Water in Protic Ionic Liquids: Properties and Use of a Novel Class of Electrolytes for Energy Storage Devices", *ChemSusChem*, **2019**, *12 (16)*, 3827–3836, *doi:10.1002/cssc.201901283.*

16. O. Hollóczki, **S. Gehrke**, "Nanoplastics can change the secondary structure of proteins", *Sci. Rep.*, **2019**, *9*, 16013, *doi:10.1038/s41598-019-52495-w.*

17. O. Hollóczki, **S. Gehrke**, "Can Nanoplastics Alter Cell Membranes?", *ChemPhysChem*, **2020**, *21*, 9–12, *doi:10.1002/cphc.201900481.*

18. M. Brehm, M. Thomas, **S. Gehrke**, B. Kirchner, "TRAVIS–A Free Analyzer for Trajectories from Molecular Simulation", *J. Chem. Phys.*, **2020**, *152*, 164105 *doi:10.1063/5.0005078.*

19. C.J. Smith, D.V. Wagle, N. Bhawawet, **S. Gehrke**, O. Hollóczki, S.V. Pingali, H.M. O'Neill, G.A. Baker, "A Combined Small-Angle Neutron Scattering, Diffusion NMR, and Molecular Dynamics Study of a Eutectogel: Illuminating the Dynamical Behavior of Glyceline Confined in Bacterial Cellulose Gels", *J. Phys. Chem. B*, **2020**, *accepted manuscript doi:10.1021/acs.jpcb.0c04916*

20. R. Elfgen, **S. Gehrke**, O. Hollóczki, *Ionic Liquids as Extractants for Nanoplastics*, ChemSusChem **2020**, *accepted manuscript doi:10.1002/cssc.202001749*

Abstract

In the last decades N-heterocyclic carbenes has shown a certain potential as organocatalysts. In addition to the formation of regio- and stereoselective C–C coupling reactions, their scope of application includes the activation of CO_2. The active site of the carbene — the electron lone pair on the hypovalent carbon atom — is on the one hand a very strong nucleophile, but on the other hand it also serves as a potential interaction acceptor site for hydrogen bonds and can therefore be blocked by solvents with appropriate functional groups. In order to develop efficient catalyst–solvent systems, a deeper understanding of this interplay is essential. This thesis makes a valuable contribution to this issue by the aid of quantumchemical calculations and classical molecular dynamics simulations.

First, a summary of the current state of research in the field of carbenes is included in chapter 1.1. Thereby, the main focus is on a discussion of the assumed reaction mechanism and the observed influences by the respective solvent on the reactivity and selectivity of the catalyst. This is followed by the short chapter 1.2, which summarizes the basic knowledge about hydrogen bonds. Based on this level of knowledge, some target questions are formulated in chapter 1.3 and the work steps required to answer them are marked out in the form of milestones.

In order to process these milestones, besides others an advanced method for analyzing the dynamic properties of hydrogen bonds is required. As such a method the *Reactive Flux approach* is introduced and the corresponding mathematics are derived in chapter 2.1.

The first milestone consists of the development of a molecular dynamics model which is suitable for simulations of catalyst–solvent systems of sufficient size over a period which is long enough to represent the reorganization of the hydrogen bond network formed by the solvent with the catalyst incorporated therein. Such a model is presented in chapter 3.1 and applied to a first test in chapter 3.2. As a second milestone, an implementation of the *Reactive Flux* approach was proposed. The successful completion of this task is described in chapter 3.3 and the robustness of the method is demonstrated in the following chapter 3.4. The processing of the third milestone requires simulations of various potential catalysts in different solvents with the aid of the model developed in milestone 1 and a subsequent analysis of the structure of the corresponding hydrogen bonds, as well as their dynamic behavior using the method from milestone 2. This central study is described in chapter 3.5. Finally, milestone 4 requires an investigation of the activation step of the catalytic cycle by means of quantum chemical calculations in order to achieve a complete picture. In this first reaction step a precursor cation is first deprotonated and the formed carbene afterwards performs a nucleophilic attack on the substrate to form the so-called *Breslow-Intermediate*. In the investigations presented in chapter 3.6, a new, energetically much more favorable transition state is presented,

which enables these two reactions in a single concerted step. Finally, in chapter 3.8 some observations that initially appear to be contradictory are discussed and brought into line with the results shown above.

Zusammenfassung

In den letzten Jahrzehnten zeigten sich das Potential von N-heterozyklischen Carbenen als Organokatalysatoren. Ihre Anwendungsgebiete umfassen neben der Vermittlung von regio- und stereoselektiven C–C Kopplungsreaktionen auch die Aktivierung von CO_2. Das aktive Zentrum der Carbene — das freie Elektronenpaar am hypovalenten Kohlenstoffatom — ist einerseits als sehr starkes Nukleophil aktiv, anderseits dient es jedoch auch als potentieller Wechselwirkungsakzeptor für Wasserstoffbrücken und kann somit von Lösemitteln mit entsprechenden funktionellen Gruppen blockiert werden. Um effeziente Katalysator-Lösemittel-Systeme zu entwickeln ist ein tiefergehendes Verständnis dieses Wechselspiels unumgänglich. Diese Doktorarbeit liefert hierzu einen wertvollen Beitrag mit Hilfe von quantenchemischen Rechnungen sowie klassischen Moleküldynamik Simulationen.

Zuerst erfolgt in Kapitel 1.1 eine Zusammenfassung des aktuellen Standes der Forschung auf dem Gebiet der Carbene. Hierbei wird der Hauptaugenmerk auf eine Diskussion des angenommenen Reaktionsmechanismus sowie der beoachteten Einflüsse durch das jeweilige Lösemittel auf die Reaktivität und die Selektivität als Katalysator gelegt. Anschließend folgt mit 1.2 ein kurzes Kapitel, welches das grundsätzliche Wissen über Wasserstoffbrücken zusamenfasst. Basierend auf diesem Wissenstand werden in Kapitel 1.3 einige grundlegende Fragen formuliert und die zu deren Beantwortung nötigen Arbeitsschritte in Form von Meilensteinen erfasst.

Zur Bearbeitung dieser Meilensteine ist unter anderem eine fortgeschrittene Methode zur Analyse der dynamischen Eigenschaften von Wasserstoffbrückenbindungen nötig. Mit dem *Reactive Flux* Verfahren wird eine solche Methode in Kapitel 2.1 vorgestellt und die mathematischen Hintergründe näher ausgeleuchtet.

Der erste Meilenstein beinhaltet die Entwicklung eines molekulardynamischen Modelles welches geeignet ist, ein Katalysator-Solvent-System ausreichender Größe über einen Zeitraum zu simulieren der lang genug ist um die Reorganisation des durch das Lösemittel gebildeten Wasserstoffbrückennetzwerkes mitsamt des darin inkorperierten Katalysators darzustellen. Ein solches Modell wird in Kapitel 3.1 vorgestellt und in Kapitel 3.2 einem ersten Test unterzogen. Als zweiten Meilenstein wurde eine Implementierung des *Reactive Flux* Verfahrens vorgeschlagen. Die erfolgreiche Bearbeitung dieser Aufgabe wird in Kapitel 3.3 beschrieben und die Stabilität der Methode im darauf folgenden Kapitel 3.4 demonstriert. Die Bearbeitung des dritten Meilensteins erfordert schließlich die Durchführung von Simulationen verschiedener potentieller Katalysatoren in verschiedenen Lösemitteln unter Zuhilfenahme des in Meilenstein 1 entwickelten Modelles und eine anschließende Analyse der Struktur der entsprechenden Wasserstoffbrücken, sowie deren dynamischen Verhaltens durch die Methode aus Meilenstein 2. Diese zentrale Studie wird in Kapitel 3.5 beschrieben. Meilenstein 4 erfordert schließlich eine Unter-

suchung des Aktivierungsschrittes des katalytischen Kreislaufs durch quantenchemische Rechnungen um ein vollständiges Bild zu bekommen. In diesem Reaktionsschritt wird ein Vorläuferkation zuerst deprotoniert und greift anschließend das Substrat nukleophil an wobei sich das sogenannte *Breslow-Intermediat* bildet. Bei den in Kapitel 3.6 präsentierten Untersuchungen konnte ein neuartiger, energetisch deutlich günstiger liegender Übergangszustand gefunden werden, welcher diese beiden Reaktionen in einem einzelnen konzertierten Schritt ermöglicht. In Kapitel 3.8 werden abschließend einige anfangs widersprüchlich erscheinende Beobachtungen diskutiert und in Einklang mit den zuvor gezeigten Ergebnissen gebracht.

Contents

1. Introduction

1.1. N-Heterocyclic Carbenes

Carbenes are a class of molecules that have a divalent carbon atom with an electron sextett. Due to this electron deficiency, carbenes are known to be mostly highly reactive species. In the special case of N-heterocyclic carbenes (NHCs) the hypovalent carbon atom is bound in a ring containing at least one nitrogen atom. The chemically more stable singlett state is stabilized by the sigma withdrawing effect of the electronegative groups at the carbene carbon atom as well as by the delocalized π-system of the carbon and the neighbored π-donating substituents.[21,22] In some particular cases further stabilization of the electronic situation is induced by the aromaticity of the heterocyclic ring.

The lone pair of electrons renders NHCs promising candidates as ligands for transition metals. Therefore, it is no surprise that a plethora of applications is reported in literature in catalysis[23–34] and in organometallic complexes.[35–38] The most prominent catalyst of this type is probably the second generation Grubbs catalyst for the metathesis reaction, which offers a highly efficient interconversion of alkenes.[29]

Another synthetic value can be found in the free carbenes themselves. It has been shown that NHCs act as catalysts that can even form C–C bonds without any metal complex in reactions based on *umpolung* — the inversion of chemical reactivity. The fundamental idea for these type of application in a broad scope of reactions was first introduced by Stetter,[39] who defined the scientific field known nowadays as NHC organocatalysis.[38,40–43]

1.1.1. A Brief History of N-Heterocyclic Carbenes

The history of NHCs started in the 19th century, when experiments showed that beriberi-like symptoms in chicken vanish if the chicken are fed by rice husk.[44] The responsible compound was later isolated and structurally characterized as the coenzyme thiamine, also known as vitamin B_1 (see the structure in Figure 1.1).[45] Its mode of action was found in the decarboxylation reaction of pyruvate to acetaldehyde.[46] Interestingly, it could be shown that it is possible with the corresponding enzyme to couple two acetaldehyde molecules together to yield acetoin.[47]

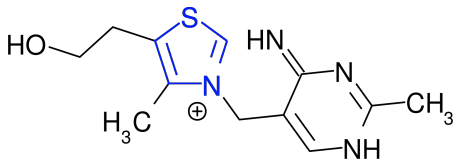

Figure 1.1.: Structure of the coenzyme thiamine in its cationic form. The thiazolium ring unit is marked as blue.

Ukai suspected the thiazolium ring to be the catalytically active component of the thiamine molecule.[48] In his ground breaking work he was able to impressively demonstrate that an analogous reaction was catalyzed by a neat thiazolium salt in ethanolic solution by coupling two benzaldehyde molecules in a benzoin condensation.[48] The role of the

thiazolium unit for the activity could later be evidenced in ^{14}C labeling experiments by Mizuhara.[49]

In this context the idea was expressed, that the active form of the thiazolium could be the corresponding carbene formed by deprotonation of the acidic ring unit.[50] Based on this idea Breslow was able to prove the suspected acidity of the proton in question by showing that the proton at position 2 of the thiazolium ring actually can be exchanged by a deuteron.[51,52] Therefore, it appeared reasonable that the active form is indeed an NHC formed by deprotonation.[52,53] On the basis of the already established mechanism for cyanide catalyzed reactions,[54] Breslow finally proposed an analogous mechanism of the benzoin reaction, which still dominates the field after 60 years and will be discussed in Section 1.1.2.[52] With growing understanding of the mechanistic details the first enantioselective reactions could be realized.[55] Finally, the work of Stetter, who used the reaction for the first time for synthetic purposes, established the term NHC organocatalysis.[39]

Even if it was already known that the scope of potential catalytically active salts is by no means restricted to thiazolium, but can also be realized with the related imidazolium derivates,[52] the efforts to find chiral organocatalysts have been mostly based on thiazolylidene structural motifs. This preference changed drastically after the seminal report of Enders and Teles in 1995[56] to NHCs containing three nitrogen atoms in their ring – the triazolylidene structure motif. Based on this type of catalyst the stereoselectivity could be significantly improved.[57] Furthermore, the activity of imidazolium salts was brought back into the focus.[58] In 2002 the preferred structural motif changed again with the introduction of an aminoindanol scaffold.[59] Over the last years a plethora of different NHC based catalysts and the corresponding *umpolung* reactions was reported and the topic was frequently reviewed in literature.[38,40–43,59–62]

1.1.2. Mechanism of the Benzoin Condensation

Over the years the benzoin condensation became the most important model reaction for investigations on the mechanism of NHC based reactions. As mentioned before, the dominating mechanism was first proposed by Breslow in 1958.[52] It is illustrated in Figure 1.2: Due to their high reactivity carbenes are not applied in their active form in synthesis. Instead, a precursor salt **1** is applied from which the active catalyst **2a** is formed *in situ* by deprotonation with a suitable base.[40–42,52,63] In his original work Breslow rendered the active species **2a** as an ylidene zwitterion. In fact, this species can be seen as in resonance with the highly nucleophilic carbene form **2b**. Afterwards, the activated catalyst reacts with an aldehyde forming an alcoholate which is protonated by a solvent molecule or the protonated base. In turn, the emerging alcohol **3** is deprotonated leading to the zwitterionic activated aldehyde **4a** which is stabilized by its neutral form **4b** — the so-called *Breslow intermediate*. The nucleophilic attack of **4a** on another aldehyde and subsequent protonation of the emerging alcoholate leads to the dialcohol **5**. After deprotonation the formed benzoin separates from the thiazole unit. This step regenerates the catalyst **2a**.

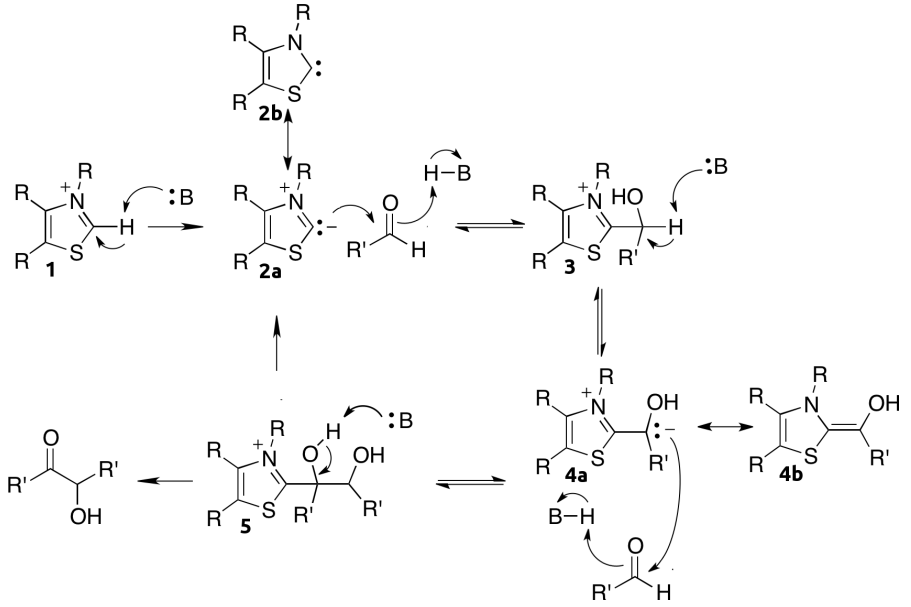

Figure 1.2.: The mechanism of a thiazolium catalyzed benzoin condensation as suggested by Breslow.[52]

With the aid of this mechanism it is in many cases possible to explain and — more importantly — predict the selectivity of the corresponding reactions.[64,65] Further, the detection of the occurrence of several intermediates[52,66,67] and resting states[66–70] of the catalytic cycle is another strong argument supporting the mechanistic picture. Especially striking in this field was the synthesis of stable Breslow intermediates[67,71,72] and analogous structures.[71,73,74] Additionally, many theoretical studies supported Breslows mechanism[64,65,75–78] or rendered the barriers for the single steps to be relatively mild.[72]

Nevertheless, there are several facts which justify reasonable doubts especially at the first part of the reaction cycle — the formation of the bond between the catalyst and the substrate. Due to the importance in terms of the selectivity of this step the understanding of this part is of a certain interest. Actually, a direct experimental evidence for the existence of a free carbene intermediate has only been reported in the very special confinement of enzymes by UV-Vis spectroscopy[79] and by mass spectroscopy in the vapor of reaction mixtures or catalytically active solutions.[80–82] However, the cations of the applied salts are characterized by very high pK_a values (imidazole p$K_a = 19 - 24$[68,70,83–89], triazole p$K_a = 14.9 - 17.4$[70], thiazole p$K_a = 17 - 19$[70,83]) but show nevertheless a relatively high catalytic activity even with a comparatively weak amine base (triethylamin p$K_a = 10.65$[90]) as an activator.[38,40–43,58]

Recently, a tandem reaction scheme of NHC catalysis and a Brønsted acid catalyzed reaction was reported.[91,92] Following the dominating reaction mechanism, this would mean that a superbasic carbene species is formed in an acidic environment in adequate amounts to be catalytically active. Obviously, this appears to be at least unlikely.

1.1.3. Discovery of Stable Carbenes

Due to the electron deficiency of the hypovalent carbon atom, carbenes are known to be a highly reactive class of substances. Nevertheless, it has been shown that the synthesis of stable carbenes is possible. The basics for this stabilization were established by Wanzlick, who studied the chemistry of NHCs in the early sixties.[93–95] Thereby, it was found that decomposition reactions — as the dimerisation of imidazolidinylidene[93,94] or nucleophilic reactions of thiazolylidenes[95] — can be suppressed by the introduction of bulky side groups on the ring unit or the π-electron donor groups which are sterically shielding the active site.

Twenty years later, the group of Bertrand reported the synthesis of a structure which is able to react as a carbene, in which the carbon atom in question is stabilized by a π-electron donor and a π-electron withdrawing substituent on the hypovalent carbon atom.[96] The molecules can also be rationalized as a triple bonded compounds, which is supported by their linear geometry. Nevertheless, their reactivity shown in capturing reactions resembles that of carbenes.[97] However, these molecules are non-cyclic and can thereby actually not be called NHCs.

Independent of this pioneer work the group of Arduengo succeeded in the preparation of another carbene, the first stable NHC, applying the idea of Wanzlick to shield the hypovalent carbon atom of an imidazolydene ring unit by sterically highly demanding adamantyl side groups.[98] Later they applied the same concept to achieve stable derivates with four methyl groups[99] or with three phenyl groups on the ring, or with diisopropylphenyl side groups.[100] Interestingly, Arduengo was able to show as well that imidazolium salts are less sensible to decomposition than the corresponding thiazole derivates.[99] Following this observation, it was shown that 1,3-dimesityl-4,5-dichloroimidazol-2-ylidene is, remarkably, even air-stable.[101]

However, for the catalytically most often applied thiazolium and triazolium derivatives bulky substituents are necessary to avoid decomposition. For instance, thiazolium salts are known to form dimers if only partly deprotonated.[102] In contrast, the catalytic activity of organocatalysts has been found to be remarkable high with very small substituents. In synthesis, larger groups are only introduced to ensure the stereoselectivity of the targeted reactions.[38,40–43] Therefore, the strategies to stabilize carbenes unfortunately mostly result in structures without further synthetic value.

1.1.4. Alternative mechanisms

Washabaugh and Jencks found, that the acidity of the thiazolium unit in aqueous solution is only marginal with a pK_a of 18.0.[83] Even considering the already known fact, that the activity of free thiamine is by four magnitudes lower than that of the corresponding enzymes[103–105], the pK_a had to be below 14 to allow a formation of carbenes in a feasible amount that explains the reactivity according to the authors.[83] As a consequence Washabaugh and Jencks speculated about an alternative mechanism with an associative pathway, but soon dismissed their idea based on the fact, that the formation of the necessary assembly would not be thinkable due to the steric hindrance in the highly confined environment of an enzyme. Therefore, they explained this inconsistency with a stabilizing effect due to the special characteristic features of the enzyme's binding pocket.

In fact, this was not the only attempt to establish an alternative mechanism for the first part of the reaction, which transforms the precursor cation into the Breslow intermediate. There have been several attempts to postulate a pathway concluding a dimer structure, build from the thiazolydene and its corresponding cation representative. Thereby, the reaction occurs either direct from the dimer[106] through a Breslow-like intermediate[107,108] or even with a stable dimer species during the entire reaction.[109] Interestingly, the thiazolium's tendency to form dimers could later been proven for the cation in solution,[102] while simultaneously the formation of dimers during the catalytic cycle were ruled out for sterical reasons.[102,110]

With the aim to falsify the dimer hypothesis, Breslow performed experiments on the reaction kinetics and was able to show that the reaction was only first order in thiazolium.[111] This means, that the transition state contains two benzaldehydes and a single thiazolydene. However, one year later López-Calahorra presented data, that was second order in thiazolium, which in turn rendered the dimer containing reaction path as more plausible.[112] The same data set was later reanalyzed by Breslow, who stated the data was originally misinterpreted and actually revealed a first order reaction.[113] Nevertheless, the dimer idea was not completely given up by its proponents.[114]

Another idea, is based on calculations with semi-empirics which renders the possibility that the mechanism goes through a biradical intermediate.[115] Later it could be shown, that the Breslow intermediate can in fact be oxidized to yield a radical.[116] These findings were recently exploited to establish a new field of redox catalysis based on N-heterocyclic carbenes,[117–119] but until today the hypothesis, that the Breslow intermediate's formation goes through a biradical could not be validated.

1.1.5. Impact of Solvents

As every molecule, catalytically active carbenes are interacting with the surrounding solvent molecules. Thereby, the high electron density of the hypovalent carbon atom's electron lone pair can act as an acceptor site for hydrogen bonds. This fact was confirmed repeatedly both theoretically[82,120–123] and experimentally.[121,124–127] The hydrogen bond interactions can be relatively strong, with an interaction energy of up to 80 kJ mol^{-1}.[82,128]

Due to the fact that the hydrogen bonding interaction site is the same as the catalytically active site the presence of potential hydrogen bond donor molecules highly influences the activity of the catalyst. This may result in a simple decrease of the reactivity.[129] However, it also has been exploited in order to control the selectivity, product ratios, and yields of certain reaction.[41,130–132]

1.1.6. Ionic Liquids as Catalytically active Solvents

As mentioned above, in synthesis the carbenes are not applied in their active form, but as precursor salt, from which the catalyst is formed by deprotonation with a suitable base.[40–42,52,63] Interestingly, some of these salts can be tailored in a way, that their melting point is below room temperature — the so-called ionic liquids (ILs).[133–136] If the anion is chosen to be basic, it is subsequently possible to design a solvent which may be catalytically active itself.

Especially for ionic liquids of the imidazolium acetate type several reactions known as catalyzed by carbenes were reported,[81] for instance with chalcogens,[137] metal ions,[138] oxides,[139,140] or CO_2.[141,142] However, the concentration of the carbene species has to be very low, because there is still no spectroscopic evidence be found to proof the carbene's presence nor a carbene could be detected in theoretical studies.[143,144] Only in *ab initio* molecular dynamics (MD) studies it was shown, that the C–H bond of the acidic proton is stretched in the presence of carbon dioxide.[144] The questions regarding the mechanism of the carbene in NHC organocatalysis arise here as well, therefore understanding that process in detail will surely reveal how carbene-like reactions in ILs can occur, facilitating the further development in the field.

1.2. Hydrogen Bonds

Hydrogen bonds (HBs) are a structure motif known for nearly a century and extensively reviewed in literature.[145–157] Their impact on the transport properties of condensed matter[158–160] as well as on the selectivity and kinetics of chemical reactions in solution[129,131,132] renders the demand of a deeper understanding of this bond type as unavoidable.

Without a doubt, the most investigated type of a hydrogen bond is found in water. Therein, the electronegative oxygen atoms of two involved water molecules are connected by one of the conjoint hydrogen atoms in a relatively weak arrangement (water dimer: 20 kJ/mol).[155] Actually, this concept can be extended to other kinds of hydrogen donor X and acceptor Y. The donor atom X does not mandatory need to be a strongly electronegative element as oxygen, nitrogen, or a halogen, but can be a less electronegative atom as S, C, Se, or Si.[147,161] In any case, the corresponding X–H bond is clearly polarized. The acceptor Y can be any atom or even a molecule part with a high electron density and subsequently a negative partial charge.[162] In most hydrogen bonds, the dipole of the donor's bond and the acceptor Y are found in a certain direction or in the case of strong hydrogen bonds even in a nearly linear assembly X–H$\cdots$Y.

In first attempts hydrogen bonds were simply described by the ionic interaction between the dipole of the X–H bond and the negative partial charge at Y, which has been shown to be sufficient in the case of traditional HBs, which are similar to those formed in water.[147] However, some special cases necessitates a more accurate description of the electrostatics by a distributed multipole analysis.[163,164] For instance, the dimer formation energy of the HF dimer is falsely predicted by a simple point charge or dipole model. In contrast, if a quadropole is included on the fluorine atom the description appears to be correct.[165,166]

Further experimental and theoretical investigations of nonstandard types of hydrogen bonds revealed that even this enhanced electrostatic model may fail in some cases, especially if very strong hydrogen bonds are examined. It has been shown, that the description is only sufficient if a charge transfer model is applied.[165,167] Others found evidence for a certain covalent character of the interaction.[147,168]

The dominant picture is, that electron density is transferred from the acceptor Y into the σ^* orbital of the X–H bond. Assuming a nearly linear arrangement X–H$\cdots$Y this orbital is located in the region between the hydrogen atom and the acceptor. The most prominent way to investigate this effect is Weinhold's natural orbital analysis.[156,167,169] As a consequence of the electronic repulsion the electron density of the X–H σ bond is pushed towards the donor atom X. This results in an increase of the X–H bond's polarization.[166]

The relocalization of electron density from the acceptor Y into the X–H anti–bond weakens the bond by a certain amount. Due to this weakening the frequency of the corresponding signal in infra red spectroscopy (IR) is significantly lowered, which allows the general detection of the existence of hydrogen bonds by IR experiments.[170–173]

Due to the fact, that the single electron of the hydrogen atom is shared between the two bonds the electron density at the hydrogen atom is reduced.[148,174] As a consequence

Table 1.1.: Criteria of the IUPAC definition of hydrogen bonds according to Steiner and Jeffrey[147,162,183]

	strong (covalent)	moderate (ionic)	weak (weak ionic/dispersive)
H$\cdots$Y distance / Å	$1.2 - 1.5$	$1.5 - 2.2$	> 2.2
X Y distance / Å	$2.2 - 2.5$	$2.5 - 3.2$	> 3.2
X–H *vs.* H$\cdots$Y	X–H $\approx$ H$\cdots$Y	X–H $<$ H$\cdots$Y	X–H $\ll$ H$\cdots$Y
X–H$\cdots$Y angle	$170 - 180°$	$> 130°$	$> 90°$
energy / kJ mol^{-1}	$63 - 167$	$17 - 63$	< 17
IR shift / cm^{-1}	25%	$10 - 25\%$	$< 10\%$
^{1}H-NMR shift / ppm	$14 - 22$	< 14	–

the magnetic shielding of the hydrogen's nucleus differs from the shielding of the non-perturbated hydrogen atom. Subsequently, especially in strong hydrogen bonds the NMR signal is significantly shifted.[175–180]

Nevertheless, a noteworthy number of exceptions has been reported in which not all the above mentioned criteria are fulfilled, but it is still supposed, that the interaction in question is a hydrogen bond. Successively, the hydrogen bond definition of the IUPAC was updated in 2011.[181,182] The new definition consists as a list of several different criteria as listed in Table 1.1.[147,162,183] The more of these criteria are fulfilled the more justified it is to call an interaction a hydrogen bond.

While the general detection of hydrogen bonds in experiments is in many cases possible and well established, the analysis of the hydrogen bond dynamics – that is the breaking, reordering, and reformation of the hydrogen bond network – is still a challenge. Due to the fact, that the average lifetime of hydrogen bonds is discussed to be in the lower picosecond regime, the time frame of NMR techniques is inapplicable for this task. More promising appear early attempts to tackle the problem with scattering methods,[184–186] or techniques based on IR spectroscopy, as ultrafast IR[160,187–191] and femtosecond 2D IR.[159,192–196] However, the interpretation of these kind of experiments is not straight forward and the real substance of their results still under discussion.

Based on the recent advances in the investigation of transport properties by the aid of molecular dynamics simulations[158,197–206] it is justified to assume, that this approach is a promising tool for the analysis of the dynamics of hydrogen bond networks. To do so it is unavoidable to find a way to classify an interaction state as a hydrogen bond. This can be achieved in two different ways:

First, if the forces during the integration are calculated with the aid of a method which calculates the effective interaction energy V_{eff} for each pair of potential bonding partners one can define the bonded state based on this energy. Therefore, a cutoff energy V_{HB} is introduced. Two partners i and j are defined as hydrogen bonded if $V_{\text{eff}}(i,j) < V_{\text{HB}}$.[207] The drawback of this approach is that the hydrogen bond definition has to be evaluated already during the simulation. A belated analysis on the basis of a position trajectory is not possible. Further, the application of this definition is not applicable for methods

which are not calculating forces in a pairwise manner but based on the explicit electronic structure or by considering many body terms.

A second approach is the application of a geometrical criterion.[208] To do so, a distance cutoff d_{cut} and an angle cutoff α_{cut} is defined, as visualized in Fig. 1.3. The interaction state of i and j is detected as a hydrogen bond if $d_{i,j} < d_{\text{cut}}$ and simultaneously $\alpha_{\text{XHY},i,j} < \alpha_{\text{cut}}$. This second approach is far more common.

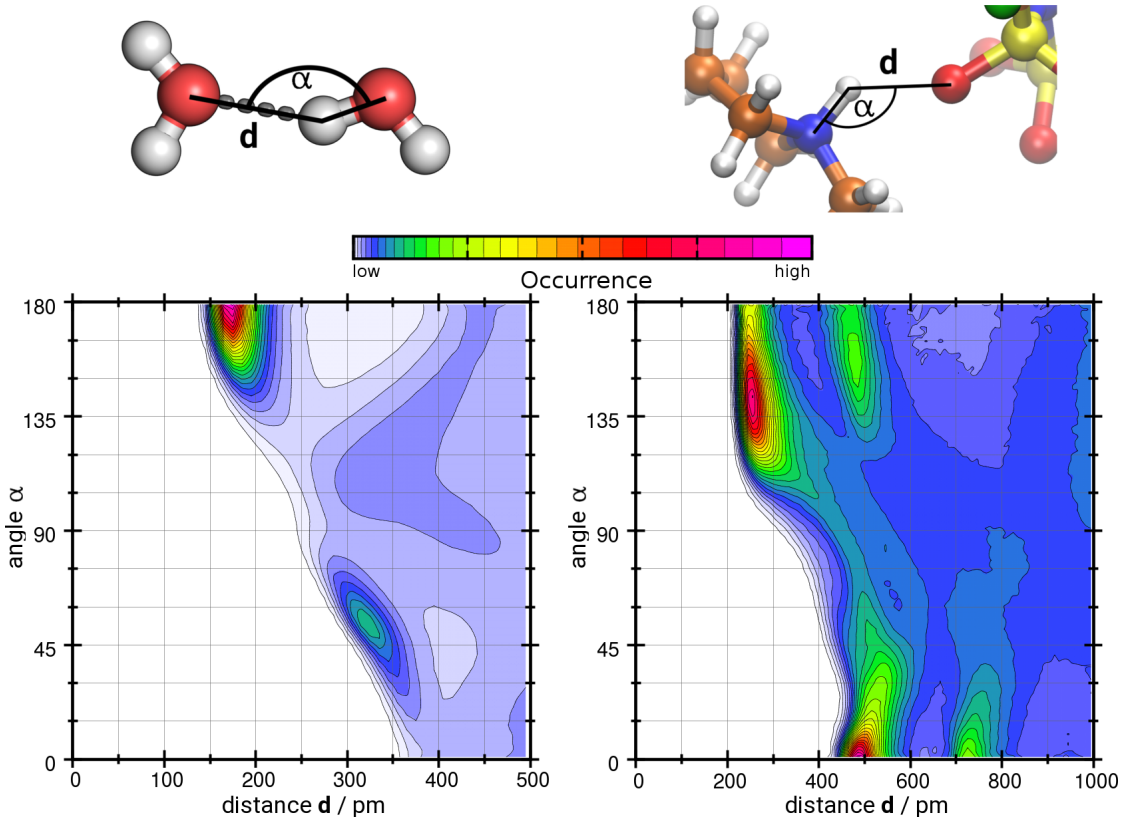

Figure 1.3.: Top: Visualization of the geometric criterion for a strong hydrogen bond (left) and a weak hydrogen bond (right). The pair is detected as a hydrogen bond if $d < d_{\text{cut}}$ and simultaneously $\alpha < \alpha_{\text{cut}}$. Bottom: The corresponding combined distribution functions (CDFs). Shown is the occurrence in arbitrary units for a certain distance d occurring simultaneously with a certain angle α. The left CDF is taken from a simulation with 512 SPC/E water molecules. The right CDF is based on a simulation of 64 ion pairs of the ionic liquid 1-butylpyridinium bis(trifluoromethylsulfonyl)imide

1.3. Scope of the Thesis

In synthesis NHC based catalysts are mostly not applied in their active form, but as a precursor cation. Even if the catalytic cycle as discussed in Section 1.1 is a multistep pathway, it starts with the activation of this precursor. Obviously, it is essential for the initial reaction that the catalyst is physically reachable for the substrate. However, due to the very strong hydrogen bond acceptor potential of the carbene's active site it is reasonable to assume that in the presence of hydrogen bond donor molecules or even in a solvent with a hydrogen bond network the carbene is sterically blocked by a hydrogen bonding partner. Moreover, due to the strong basicity of NHCs a proton transfer either from a solvent molecule or the still present protonated base to the carbene will result in the reformation of the precursor cation. Subsequently, the interplay of the catalyst with its surroundings will influence the activity and probably the selectivity of the reaction.

Based on this thoughts the following questions emerge:

1. How is the influence of different solvent system properties, as hydrogen bond donor strength and concentration on the activity of a potential catalyst? What characteristic of a solvent–catalyst–system has to be controlled to find a superior match for individual needs?

2. From this question another, more fundamental one emerge: How to quantify the "freeness" of a carbene in solution? What is the most robust way to classify the statistical and dynamical influence of a hydrogen bond network on its solutes?

3. Is it thinkable, that the initial reaction occurs without the formation of an explicit free carbene intermediate? In other words, is there a way that the cycle starts directly from the hydrogen bonded form of the carbene or the precursor cation itself?

It is the aim of this thesis to provide answers to these questions. In order to achieve this aim the following milestones are defined:

1. The investigation of the reorganization of hydrogen bond networks based on molecular dynamics simulations requires relatively large simulation times and system sizes to provide sufficient statistical data. In order to allow suited simulations a model needs to be achieved to represent the carbene species.

2. The quantification of the hydrogen bond dynamics is a non-trivial task. A method needs to be found to extract a relevant parameter from a trajectory.

3. With the aid of the model obtained in the first milestone a set of different potential organocatalysts in varying solvent systems have to be simulated. The method from the second milestone will assist in the evaluation of the catalyst–solvent interplay.

4. The activation step of the catalytic procedure needs to be investigated by the aid of quantum chemistry. All critical structures — possible intermediates as well as the barriers in between — towards the formation of a Breslow intermediate have to be located and the plausibility of their occurrence evaluated based on their enthalpies.

2. Methodology

2.1. The Reactive Flux Approach

The average lifetime is an important statistical parameter for the quantification of the dynamic processes of short living states. The lifetime of a certain assembly state A can be calculated with the help of a time dependend auto correlation function (ACF). Therefore, the population operator $h\,(t)$ is defined, which equals unity if a certain assembly fulfill the criteria for state A and zero otherwise. The average over time and ensemble of the operator $h(t)$ — denoted as $\langle h \rangle$ — can be interpreted as the probability to find an assembly in state A. Based on the fluctuations of operators $h(t)$ from equilibrium $\delta h\,(t) = h\,(t) - \langle h \rangle$ the ACF

$$c\,(t) = \frac{\langle \delta h\,(t)\,\delta h\,(0) \rangle}{\langle \delta^2 h\,(0) \rangle} \tag{2.1}$$

can be defined. If the system as well as the observed time is sufficently large the probability to find a certain assembly in state A approximates zero. Therefore, $\langle h \rangle$ is neglectable and $\delta h\,(t) \approx h\,(t)$.

Furthermore, Onsager's regression hypothesis[209,210] states, that the laws that govern the time evolution of fluctuations around an equilibrium, are the same that drive the decay of an initial non-equilibrium population $\overline{\delta h}\,(0)$ towards the equilibrium. Thereby, the overline denotes a non-equilibrium average and $\overline{\delta h}\,(t) = \overline{h}\,(t) - \langle h \rangle$. Thus, Equation 2.1 can be rewritten as

$$c\,(t) = \frac{\langle \delta h\,(t)\,\delta h\,(0) \rangle}{\langle \delta^2 h\,(0) \rangle} = \frac{\overline{\delta h}\,(t)}{\overline{\delta h}\,(0)} \approx \frac{\langle h\,(t)\,h\,(0) \rangle}{\langle h\,(0) \rangle}\,. \tag{2.2}$$

As a consequence the autocorrelation function obtained from the fluctuations around the equilibrium can be seen as the time dependend decay of an initial non-equilibration concentration of state A to state B.[211,212] If this decay is supposed to follow approximately a first order reaction A $\xrightarrow{\mathrm{k}}$ B the time dependence of the concentration reads

$$c(t) = c(0) \cdot \mathrm{e}^{-k \cdot t}. \tag{2.3}$$

Typically, $c(t)$ is normalized by the initial concentration $c(0)$ to the relative concentration

$$c'(t) = \frac{c(t)}{c(0)} = \mathrm{e}^{-k \cdot t}. \tag{2.4}$$

The integral

$$\int_0^\infty c(t)'\mathrm{d}t = \int_0^\infty \mathrm{e}^{-k \cdot t}\mathrm{d}t = \frac{1}{k} = \tau_A \tag{2.5}$$

gives the inverse of the decay rate constant k, which is by definition the average lifetime τ_A of state A.

Typically, two different types of ACFs are distinguished, depending on the basis taken for the operator $h(t)$.[213] The *intermittent* type ACF is based on one single data set for each possible assembly of atoms. The data sets are resumed independent of the occurrance of decay or reforming events of the state in question. In contrast, the *continuous*

type ACF defines one data set for each formed state A. Thereby, a new set is initiated even if a formerly broken state is reformed. As a consequence, each data set of the *intermittent* function is split into several smaller data sets in the *continuous* type of ACF. For this reason, the obtained *continuous* lifetimes are generally by one or two magnitudes shorter than their *intermittent* counterparts.

The pictured approach assumes a quasiexponential decay of $c(t)$.[213–219] However, several reports indicate a non-exponential behaviour of the decay function in the case of hydrogen bonding.[213,220–226] Furthermore, it has been shown, that for methanol the probabiltiy to form a HB is larger if the pair was bonded before than for a random pair.[227] Luzar and Chandler suggested to explain this observations with a simple diffusion picture: After the decay of the hydrogen bond the two partners are still in vacinity and subsequently the bond can easily be reformed. If the partners in contrast drift apart a reformation is obviously not possible.[228,229]

Aiming at a sophisticated model of this effects the time invariance of auto-correlation functions is exploited. As shown in Appendix A.1 the relation

$$-\left\langle \dot{f}(0)g(\tau)\right\rangle = \left\langle f(0)\dot{g}(\tau)\right\rangle \tag{2.6}$$

is guilty for the derivatives with respect to time of ACFs. As a consequence, the rate of relaxation towards equilibrium can be derived from Equation 2.2 as

$$\kappa(t) = -\dot{c}(t) \approx -\frac{\left\langle \dot{h}\,(t)\,h\,(0)\right\rangle}{\langle h\,(0)\rangle} = \frac{\left\langle \dot{h}(0)h(t)\right\rangle}{\langle h\,(0)\rangle}\,, \tag{2.7}$$

where the dot denotes the derivative with respect to time.

Due to the identity

$$\left\langle \dot{h}\,(0)\right\rangle = 0\,, \tag{2.8}$$

(which is further explained in Appendix A.2) it is possible to substract $\left\langle \dot{h}\,(0)\right\rangle$ from the relaxation rate without losing generality. Thus, Equation 2.7 becomes

$$\kappa(t) = \frac{\left\langle \dot{h}(0)h(t)\right\rangle - \left\langle \dot{h}(0)\right\rangle}{\langle h(0)\rangle} = -\frac{\left\langle \dot{h}(0)\,[1-h(t)]\right\rangle}{\langle h(0)\rangle}\,. \tag{2.9}$$

If the quantity

$$-\dot{h}\,(0) = -\left(\frac{\mathrm{d}h(t)}{\mathrm{d}t}\right)_{t=0} \tag{2.10}$$

is been interpreted as the flux departing the hydrogen bond configuration space at time zero, the function $\kappa(t)$ measures the average of that flux for those trajectories, where the bond between a tagged pair of molecules is broken at a time t. Hence, it is called reactive flux time-correlation function and thereby eponymous for the entire approach.

With the aid of the vicinity operator $H(t)$ which equals unity as long as the two molecules are found in a distance, that a formation of a hydrogen is possible and zero otherwise, it is possible to seperate the trajectories described by $\kappa(t)$ according to whether

or not the pair of interest moves apart after the decay event. Subsequently, the trajectories in which a reformation is possible are desribed by the *restrictive* reactive flux auto-correlation function

$$\kappa_{\text{in}}(t) = -\frac{\Big\langle H(t)\dot{h}(0)\left[1-h(t)\right]\Big\rangle}{\langle h(0)\rangle}\,. \tag{2.11}$$

Finally, the probability to find an initially HB to be broken but still in vicinity at time t is given by the integral

$$n(t) = \int_0^t \kappa_{\text{in}}(\tau)\mathrm{d}\tau\,. \tag{2.12}$$

According to the regression hypothesis the two probabilities $c(t)$ and $n(t)$ correspond to interconvertable local populations, which are described by the kinetic equation

$$-\dot{c}(t) = k_d c(t) - k_f n(t)\,, \tag{2.13}$$

with the rate constant of the decay reaction k_d and the rate constant of the reformation of the bond k_f. The physical meaning of the inverse decay rate $k_d^{-1} = \tau_{\text{HB}}$ is the average lifetime of a hydrogen bond.

The approach can be adopted for the analysis of the dynamics of any kind of short-living interaction by a simple adjustment of the two operators $h(t)$ and $H(t)$.

3. Results and Discussion

3.1. A Molecular Mechanical Model for N-Heterocyclic Carbenes

Sascha Gehrke[†,‡] , Oldamur Hollóczki[†,*]

Physical Chemistry Chemical Physics, 2016, Volume **18 (32)**, Pages 22070–22080

DOI: 10.1039/C6CP02624A

Received: April 19, 2016

Published: July 11, 2016

Adapted with permission from *Physical Chemistry Chemical Physics*.
For this article a Supporting Information is available free of charge at:
`http://www.rsc.org/suppdata/c6/cp/c6cp02624a/c6cp02624a1.pdf`

Contributions to the manuscript:

- Setup and maintenance of all calculations
- Fitting of parameters
- Writing the technical part of the manuscript

[†]Mulliken Center for Theoretical Chemistry, University of Bonn, Beringstr. 4+6, D-53115 Bonn, Germany

[‡]Max Planck Institute for Chemical Energy Conversion, Stiftstr. 34–36, D-45470 Muelheim an der Ruhr, Germany

[*]E-mail: holloczki@gmail.com

To evaluate the influence of solvent compositions on the reactivity of a potential catalyst, it is unavoidable to model the interaction between solvent molecules and the active species with sufficient accuracy. Furthermore, the relatively slow reorganisation of hydrogen bond networks necessitates the time observed in a suited simulation to be long enough to assure the obtained statistics of the exchange events to be sufficient for the calculation of reliable rate constants. This becomes even more severe due to the low sampling, caused by the typically low concentration of catalysts and the subsequently low number of interactions between the catalytically active species and the solvent molecules.

Therefore, the first milestone of this thesis is the development of a suited model. The targeted framework is hereby a classical force field in the style of the OPLS–AA potential. For this force field, parameters for a wide range of solvent systems are available and the representation of the relevant physics is widely accepted. In this process, the required calculations of the interaction potentials by high level wave function theory are exploited to investigate the nature of the carbene's hydrogen bonds.

Abstract

In this work we present a set of force fields for nine synthetically relevant and/or structurally interesting N-heterocyclic carbenes, including imidazol-, thiazol-, triazol-, imidazolidin-, and pyridine-ylidenes. The bonding parameters were calculated by using a set of geometry optimizations by *ab initio* methods. For fitting the non-bonding interactions, a water molecule was employed as a probe. The interaction energy between the carbene and the probe molecule was sampled along two coordinates for each carbene, representing the interaction through the lone pair, or the π system of the molecule. The corresponding reference interaction energies were obtained by CCSD(T)/CBS calculations. To describe the direction dependence of the intermolecular potential energy, an extra, massless Coulombic interaction site was included for all carbenes, which represents the lone pair of the divalent carbon atom. The resulting fitted carbene force field (CaFF) showed a robust behavior regarding the probe molecule, as changing the molecular mechanical water model, or employing, instead, an OPLS methanol molecule did not introduce significant deviations in the potential energies. The obtained CaFF models are easy to merge with standard OPLS or AMBER force fields, therefore molecular simulations of a large number of N-heterocyclic carbenes become available.

3.1.1. Introduction

The importance of N-heterocyclic carbenes (NHCs)[36,41,230–233] is represented by the extremely wide variety of processes and applications, in which they play a significant role. They are shown to be the central — albeit transient — species in the enzymatic reactions of vitamin B1 in many living organisms, being crucial for the carbohydrate metabolism.[234] These species are frequently applied in synthesis either as ligands in organometallic complexes,[35–38] or environmental friendly, metal-free organocatalysts,[40–42,235–237] enabling e.g. valuable C-C coupling reactions, in many cases even with an excellent regio- and stereoselectivity. These substances have also been used to modify the surface of metal-oxides,[139,238] while their interaction with metal surfaces has been applied to build self-assembled nanolayers on gold,[239,240] and to stabilize gold[241] and platinum[242] nanoparticles.

Beside the direct electronic, and steric effects, the interactions of the carbene molecules with their environment affect the behavior of these species to a great extent. Perhaps the most remarkable example in this respect is the aforementioned catalytic activity of thiamine in biological systems,[234] which is steered by the surrounding enzyme in a manner that it catalyzes the right reaction with optimal rates and selectivity. In synthesis, the influence of the interactions between the carbene and its environment on the reactivity can be recognized by the need for optimizing solvents for NHC-based catalysis. Such interactions can control selectivity,[41] and the stability of the carbene as well.[238]

The solute-solvent interactions and the reactivity are often both related to the same structural feature of the carbene. This common unit is often the lone pair, which — as seen from the examples above — has the capacity to form coordinative bonds with metals, or via its nucleophilicity it can initiate a reaction with organic substances as an initial step of catalysis, but also has a strong hydrogen bond acceptor character.[82,124–126] Accordingly, in the presence of hydrogen bond donor molecules, the activity of the carbene can be significantly decreased. In the light of the information above, a full control over the reactivity of NHCs can be achieved only if the interactions between the carbene and the media (especially hydrogen bonding) have been characterized and understood in details. The method of choice for such studies would be classical molecular dynamics simulations, where the large systems and long time scales can be handled, which are necessary for the proper description of the effects of interest. To do so, however, efficient and accurate molecular mechanical models have to be developed for these compounds.

In a previous work,[123] we explored, for the first time, the hydrogen bonding potential of 1,3-dialkylimidazol-2-ylidenes in solution, by fitting an OPLS/AMBER-compatible force field for describing their solute-solvent interactions, with a special emphasis on their hydrogen bonding behavior. According to the potential energies the hydrogen bonding ability of imidazol-2-ylidenes is not restricted to conformations, where the hydrogen bond donor molecule is in the plane of the ring and interacts with the lone pair of the NHC. Instead, stabilizing — albeit somewhat weaker — interactions with such substances are also accessible *via* the π system of the NHC ring. This ambident hydrogen bond accepting property is similar to the case of anisole.[243,244] To describe the strength and

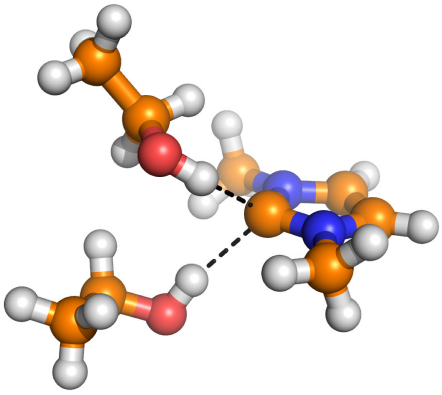

Figure 3.1.: A transient, double hydrogen bonded assembly of the carbene and ethanol, observed in the EtOH/THF 1:2 solution, as an intermediate for the associative hydrogen bond exchange mechanism.[123]

direction dependence of the hydrogen bond, we introduced an extra, massless point charge, representing the lone pair of the carbene in our model, similarly to the four and five site water models.[245–248]

We also performed molecular dynamics simulations in synthetically relevant solutions with toluene, THF and different alcohol-THF mixtures as solvents. Interestingly, in toluene and in THF the NHC solutes aggregated *via* intermolecular C–H$\cdots$C bonds formed through the ring hydrogen atoms at positions 4 and 5.[123] In the solutions, where alcohols were present, the hydrogen bonds between the hydroxyl hydrogen atom and the divalent carbon atom dominated the solute-solvent interactions, in agreement with the extreme strength[82] of the corresponding interplay. The alcohol molecules, nevertheless, showed a relatively fast exchange at the hydrogen bond acceptor site of the carbene solutes.[123] The exchange mechanism followed a predominantly associative pathway, i.e., the cleavage of the hydrogen bond was initiated by the binding of a second hydrogen bond donor alcohol molecule. This mechanism involved a transient assembly, where an NHC molecule interacts with two hydrogen bond donor molecules at a time (see Figure 3.1).[123] The formation of this intriguing structure is allowed only by the aforementioned ambident hydrogen bond acceptor character, since with the carbon atom having two different binding sites, it is able to accommodate two alcohol molecules at a time.

Since carbenes are usually applied in synthesis in their protonated form,[40–42,237] and generated in the reaction mixture *in situ* by the addition of amine bases, the mechanism, in which the proton is exchanged to the substrate of the reaction, should involve such a replacement (see Figure 3.2).[123] Therefore, the findings above will contribute greatly to our understanding of the process.

Our previous simulations showed[123] that the hydrogen bond dynamics are largely affected by the donor molecule, hence it is reasonable to assume that changing the steric and electronic environment of the carbene also has a significant effect on the rates and mechanism of the exchange. Furthermore, in many applications carbenes other than

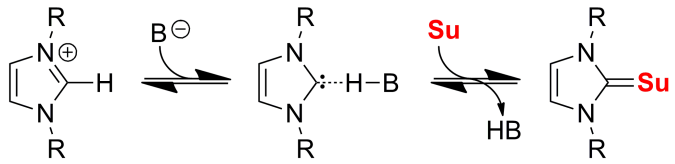

Figure 3.2.: The initial steps of carbene organocatalysis. The deprotonation of the pre-catalyst produces the hydrogen bonded structure of the carbene and the protonated base, which is then exchanged to the substrate.

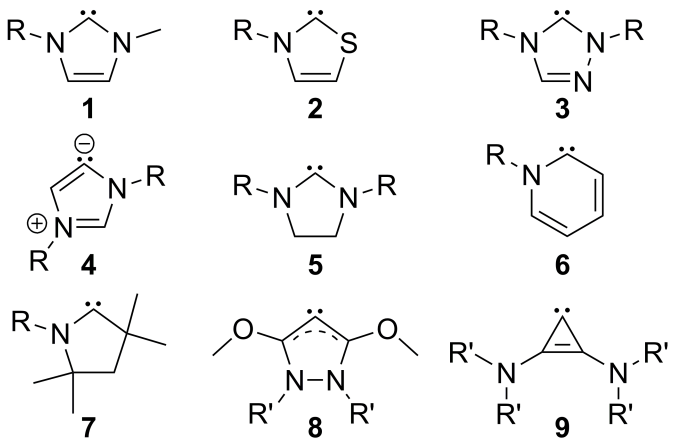

Figure 3.3.: The carbenes **1-9**, considered in this study.

1,3-dialkylimidazol-2-ylidenes are employed.[40–42,237] Therefore, although we could observe interesting interactions, and we discussed the peculiar hydrogen bond dynamics of imidazol-2-ylidenes already in our previous paper, it would be highly important to extend the molecular mechanical force field to other systems. Thus, in this study, we aim at the development of a force field for carbenes (Carbene Force Field: CaFF), which makes classical molecular dynamics simulations accessible for a large number of NHC derivatives. The molecules that we chose for parametrization are shown in Figure 3.3. These molecules are either directly relevant for synthesis (imidazol-2-ylidenes[98] **1**, thiazol-2-ylidenes[100] **2**, triazol-3-ylidenes[56] **3**, imidazol-4-ylidenes[249] **4**), or due to their remarkable, or even unique structure (imidazolidin-2-ylidenes[250] **5**, pyridine-2-ylidenes[251] **6**, pyrrolidin-5-ylidenes[252] **7**, pyrazolin-4-ylidenes[253] **8**, cyclopropen-3-ylidenes[254] **9**) they might provide an interesting comparison for the comprehensive understanding of the solute-solvent interactions of carbene derivatives to consider for future investigations.

3.1.2. Methodology

Applied Potential

In this study, the OPLS[255] potential form

$$
\begin{aligned}
V = & \sum_{ij}^{\text{bonds}} k_{l,ij}\left(l_{ij} - l_{0,ij}\right) \\
& + \sum_{ijk}^{\text{angles}} k_{\theta,ijk}\left(\theta_{ijk} - \theta_{0,ijk}\right) \\
& + \sum_{ijkl}^{\text{dihedrals}} \sum_{m=1}^{4} V_{m,ijkl}\left[1 - (-1)^m \cos\left(m\phi_{ijkl}\right)\right] \\
& + \sum_{ijkl}^{\text{impropers}} k_{\chi,ijkl}\left(\chi_{ijkl} - \chi_{0,ijkl}\right) \\
& + \sum_{i<j}^{\text{nonbonds}} f_{ij}\left\{4\epsilon_{ij}\left[\left(\frac{\sigma_{ij}}{r_{ij}}\right)^{12} - \left(\frac{\sigma_{ij}}{r_{ij}}\right)^{6}\right] + \frac{1}{4\pi\epsilon_0}\frac{q_i q_j}{r_{ij}}\right\}
\end{aligned}
$$

was used. The bonding part of the present potential contains terms for bond stretching (l_{ij}: actual distance between bonding atoms i and j; $l_{0,ij}$: reference length of the $i-j$ bond; $k_{l,ij}$: force constant for the $i-j$ bond), angle bending (θ_{ijk}: the actual $i-j-k$ bond angle; $\theta_{0,ijk}$: reference angle of the $i-j-k$ bond angle; $k_{\theta,ijk}$: force constant for the $i-j-k$ bond angle), dihedral torsion (ϕ_{ijkl}: actual dihedral angle for the $i-j-k-l$ dihedral; $V_{m,ijkl}$: Fourier constants for the $i-j-k-l$ dihedral), and improper torsion (χ_{ijkl}: angle of the $i-j-k-l$ improper torsion; $\chi_{0,ijkl}$: reference angle for the $i-j-k-l$ improper torsion; $k_{\chi,ijkl}$ force constant for the $i-j-k-l$ improper torsion). For these parameters, the molecular geometry, and the corresponding force constants have to be

determined, which can be obtained by static quantum chemical calculations, if they are not already available.

The non-bonding interactions contain the f_{ij} factor ($f_{ij} = 0$ if the atoms i and j are within the same molecule, and separated by less than three bonds, $f_{ij} = 0.5$ if the two atoms are within the same molecule and separated by exactly three bonds, and $f_{ij} = 1$ if atoms i and j are either not in the same molecule, or they are separated by more than three bonds), pairwise Coulombic interactions (q_i: the partial atomic charge of atom i; r_{ij}: distance between atoms i and j), and the van der Waals term in the form of a Lennard-Jones potential (σ_{ij}: the distance between atoms i and j where the Lennard-Jones potential between these two atoms is zero; ϵ_{ij}: depth of the energy well of the Lennard-Jones potential between atoms i and j), which require the calculation or fitting of the partial atomic charges, and the optimization of the σ_{ij} and ϵ_{ij} parameters for the Lennard-Jones part. The σ_{ij} and ϵ_{ij} parameters were calculated from the corresponding σ_{ii}, σ_{jj}, ϵ_{ii} and ϵ_{jj} parameters by the Lorentz–Berthelot mixing rules:

$$\epsilon_{ij} = \sqrt{\epsilon_{ii}\epsilon_{jj}}, \tag{3.1}$$

and

$$\sigma_{ij} = \frac{\sigma_{ii} + \sigma_{jj}}{2}. \tag{3.2}$$

Bonding Parameters

As mentioned above, the $l_{0,ij}$ and $\theta_{0,ijk}$ constants have to be determined, which was done in this study by static quantum chemical calculations. All quantum chemical calculations were performed by the ORCA 3.0.3 program package.[256] Carbenes **1**−**9** (R = Me, R' = Me) were optimized at the HF/6-31(d) level. All possible rotamers and, if applicable, ring conformations were considered, and then the most stable minima were chosen. For both the SCF cycle and the geometry optimization, tight convergence criteria of ORCA were used. After the optimization of each structures, the eigenvalues of the Hessian were calculated to confirm the nature of the obtained stationary point as a minimum.

Fitting the Non-bonding Parameters

The side chains R and R' of every carbene were systematically changed to methyl, ethyl, *n*-propyl, *iso*-propyl, *n*-butyl, *tert*-butyl, and bis(4,6-dimethyl)phenyl groups. In case of carbenes with two substitution sites, the asymmetric substitutions were created as well. In case of **9**, which contains four R' sites, the substitution was performed with all groups being the same, methyl, ethyl, *iso*-propyl, or *tert*-butyl-groups. For each kind of molecule all conceivable rotamers were created by systematic rotations within the side chain, and in case of the saturated NHCs, by changing the conformation of the ring. All the 5991 generated structures were optimized at the HF/6-31(d) level of theory. After aligning the optimized conformers of each kind of molecules onto each other *via* the hypovalent carbon atom and its neighboring ring atoms — considering also possible mirror

plane and rotational symmetry operations in the alignment procedure — two conformers were labeled identical, if all equivalent atoms of the two structures were within 0.1 Å. After removing the reoccurring conformations, the eigenvalues of the Hessian for each of the remaining altogether 2570 conformers were calculated to confirm that they are minima on the potential energy surface. The generated structures were used for the initial assignment of the partial atomic charges, using the CHELPG method[257] with the Breneman-Wiberg radii at the MP2/cc-pVTZ(-f) level of theory. For all conformations of a given molecule each partial atomic charges were averaged by weighting over the Boltzmann distribution, according to the MP2/cc-pVTZ(-f) relative energies. The obtained partial atomic charges for the ring atoms of the NHC were then averaged over all kinds of substitutions, and the values were used as a starting point in the later procedure to assign the atomic charges for the force field, as described in the next chapter.

For the systems composed of the HF/6-31(d)-optimized structure of each carbene with methyl substituents and a water probe molecule with the geometry of an SPC/E model (R_{OH} = 1.0 Å; ∢HOH = 109.47°),[258] single point energies were calculated using the DLPNO-CCSD(T)[259,260] method with tight settings[261] for the localization, as defined by Neese and Liakos. From the obtained single point energies with the def2-TZVPP as well as a def2-QZVPP basis sets the energy at the complete base set limit was obtained by extrapolation, using the scheme developed by Neese and Liakos.[262]

For the same structures the non-bonding energies were calculated by LAMMPS[263] with varying charge models and Lennard-Jones parameters. The hypovalent carbon atom was defined to be a new atom type in all cases, while the rest of the atoms were assigned to already defined and parametrized atom types of the OPLS force field (Figure 3.4).[255,264–270] The considered charge models included the insertion of an extra, massless point charge (L) at the carbene carbon atom (CC), figuratively representing its lone pair. The L point was positioned in the plane of the ring, with varying distances from the CC atom, while the charge of CC and L were also altered. The cut-off distance for the non-bonding interactions was set to 20 Å, which is longer than any interatomic distance in the investigated systems. To evaluate the quality of the model at each setting that was considered, the RMSD values, the difference of the dissociation energies $\Delta\Delta E_{\mathrm{diss}}$, and the position of the minima ΔR_{min} of the potential energy curves were calculated compared to the CCSD(T)/CBS reference.

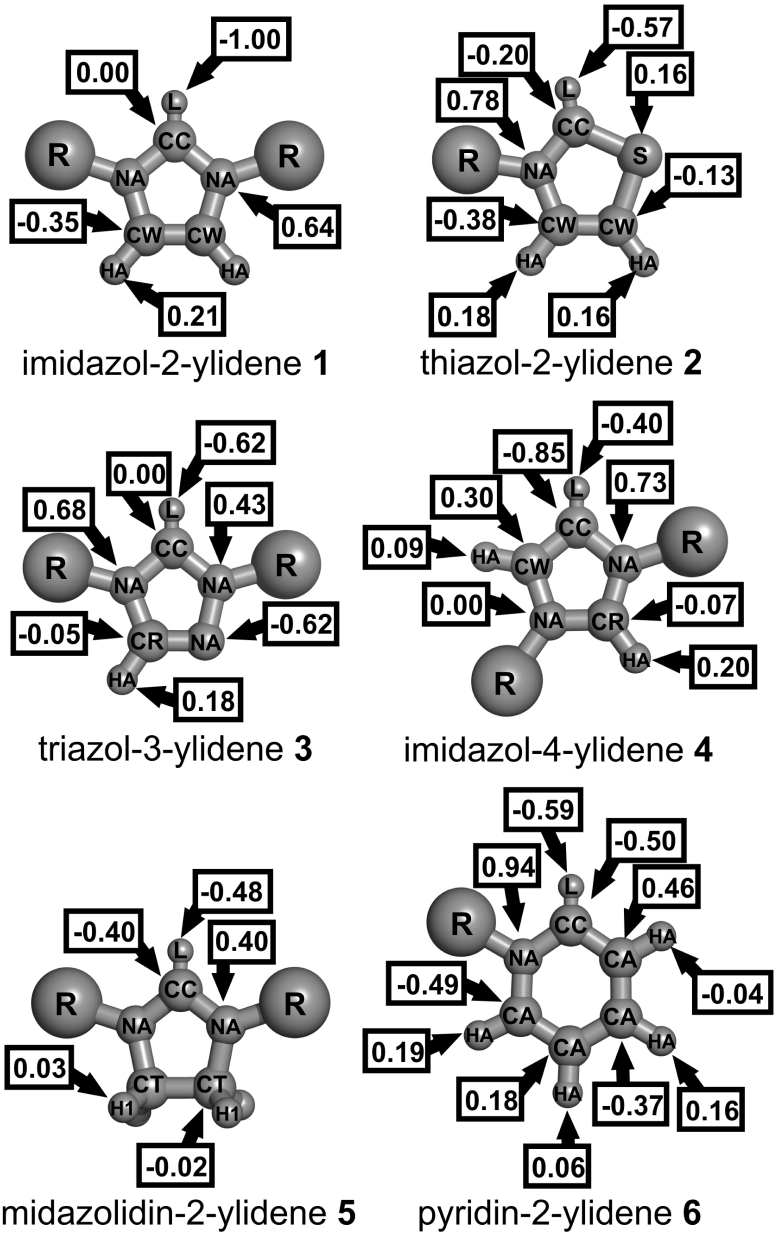

Figure 3.4.: The defined atom types and the fitted charges for carbenes **1**-**6**. The residues R can be substituted with any kind of neutral OPLS moiety.

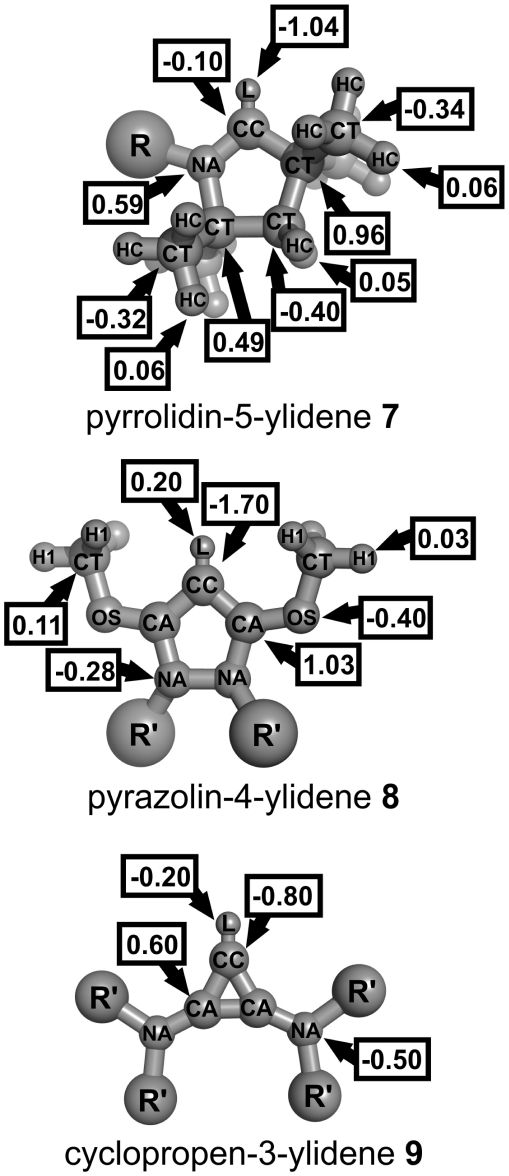

Figure 3.5.: The defined atom types and the fitted charges for carbenes **1**-**6**. The residues R can be substituted with any kind of neutral OPLS moiety. Residues R' have a total charge of $0.20e$, similarly to substituents on amines.

3.1.3. Results and Discussion

Bonding parameters

When parametrizing force field parameters, it is a general procedure to obtain the molecular geometry from low level *ab initio* geometry optimization.[255] Since compatibility of force fields is an important issue, which assures that two independently generated force fields can be used in the same simulation (or even to merge within the same molecule) to describe the physical behavior of the system, obtaining the parameters *via* an analogous approach shows clear advantages. Therefore, we chose the HF/6-31(d) level of theory for the calculation of the molecular geometries, which — beside the restrictions regarding compatibility — also allowed the facile optimization of the 5991 conformations in this study.

The geometry of carbenes **1-9** with all R and R' units substituted with methyl groups were optimized. The obtained bond lengths and angles are enlisted in the Supporting Information of the article. Here we aimed to provide parameters only for the bond lengths and angles that are directly linked to the ring, and we recommend taking those for the substituents on the carbenes from the OPLS[255] or AMBER[264] force fields.

Although the considerations regarding compatibility strongly suggest the use of the chosen method for geometry optimization, to assess how reliable the obtained geometries are, we optimized the structure of 1,3-dimethylimidazol-2-ylidene for comparison with a large set of DFT functionals (B3LYP,[271–274] BLYP,[271–273] PBE,[275,276] PBE0,[275–277] TPSS,[278] TPSSh,[278] all with and without the D3BJ dispersion correction[279,280]), and with the *ab initio* MP2 and SCS-MP2[281] methods as well, all with the def2-TZVP basis set.[282,283] The results are illustrated in Figure 3.6, and can be found in a tabular form in the Supporting Information of the article. Altogether, the errors of the chosen HF method are not severe in any cases, and the errors introduced by this approach should not have a significant effect on the results of e.g. molecular dynamics simulations. While the C-C double bond within the ring seems to be well-estimated compared to the DFT and *ab initio* methods, the rest of the bond lengths within the ring are apparently underestimated by the HF method by ca. $0.01 - 0.03\,\text{Å}$.

To avoid the CC-L vibration and the bending of the L massless point charge out of the NHC's plane, the CC and its neighboring atoms (e.g. NA-CC-NA) together with the L were defined as a single rigid body. Accordingly, fitting force constants for the bonds that include the CC atom were unnecessary. We assumed that the presence of the CC atom does not create significant differences in the moieties that are farther away from it, and also that small changes in the force constants barely influence the intermolecular structure in the liquid. Thus, for the known bond and angle types the regular OPLS[255] and AMBER[264] force constants were taken, as enlisted in the Supporting Information. For the CC-NA-CW angle, the force constant of the CR-NA-CW bending was adopted. Similarly, the dihedral force constants were taken from the known OPLS[255] and AMBER[264] parameters for the analogous heterocyclic compounds.

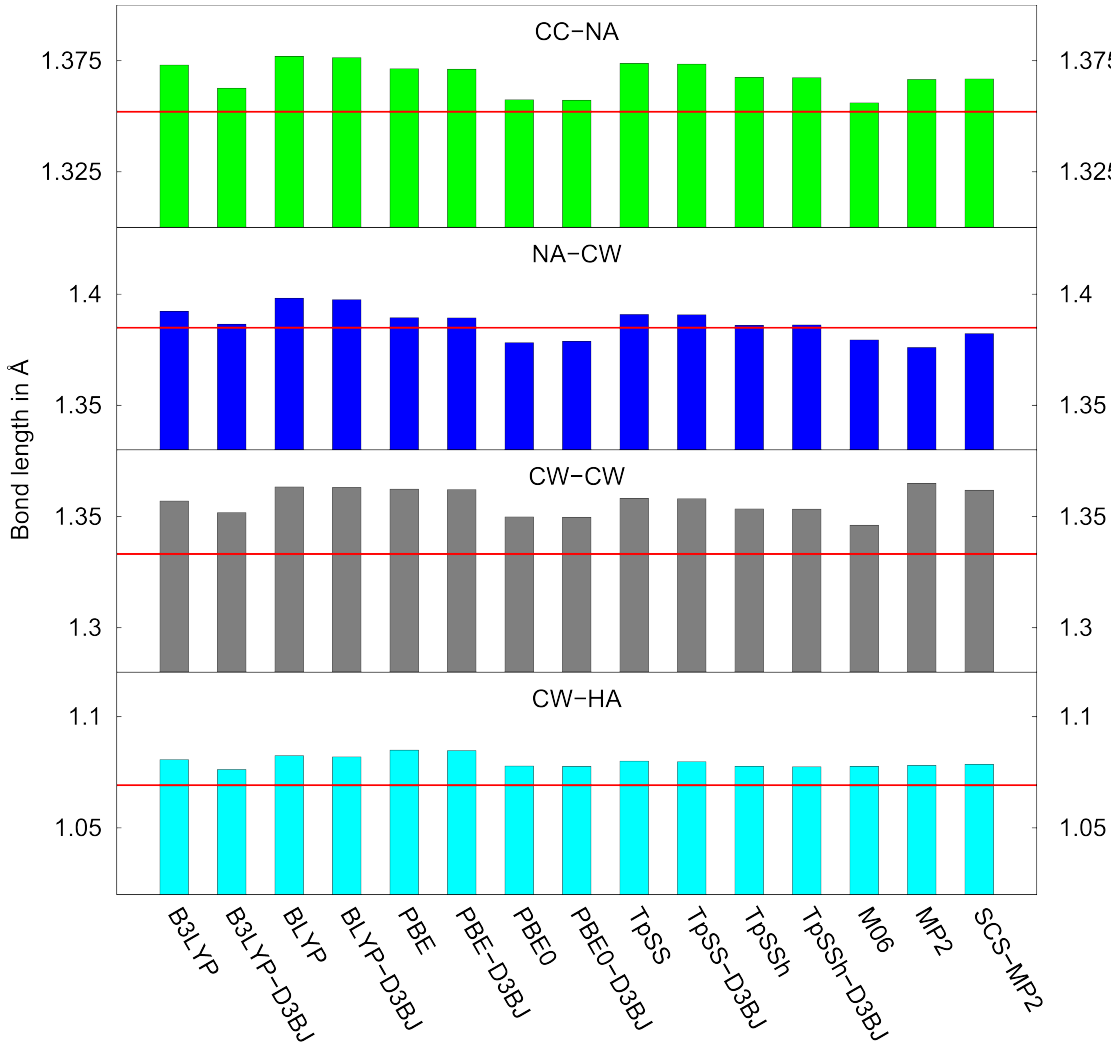

Figure 3.6.: Bond lengths of **1** (R = Me), obtained by optimizations with different methods. The basis set was chosen as def2-TZVP in all cases. The red lines represents the bond length applied in our model, obtained by HF/6-31(d) optimization.

Table 3.1.: Charges on the ring atoms of 1,3-dimethylimidazol-2-ylidene **1** (R = Me), calculated by different localization techniques.

Atom	Mulliken	Löwdin	NBO	CHELPG (COSMO)	CHELPG (BW)	CM5
CC	−0.298	−0.355	0.172	−0.964	−0.804	−0.142
NA	−0.018	0.244	−0.478	0.711	0.496	−0.075
CW	−0.093	−0.101	−0.053	−0.430	−0.320	−0.010
HA	0.131	0.001	0.202	0.233	0.184	0.045

Non-bonding Parameters

Fitting the non-bonding parameters involves the definition of the partial atomic charges q_i, and the Lennard-Jones parameters σ_{ii} and ϵ_{ii} for every atom. The determination of the charges seems straightforward, since charges can be obtained from simple quantum chemical calculations by one of the many localization schemes available in the quantum chemical program packages. An apparent choice could be the CHELPG model, which is often used to fit charges for force fields, together with other electrostatic potential-based fitting approaches. The localization models, however, may produce very different partial atomic charges for the same molecules, and therefore the robustness of these data can be a difficult issue. To observe how sensitive the partial atomic charges are to the different techniques, four charge models (Mulliken,[284] Löwdin,[285] NBO,[286] CHELPG[257]) were considered and compared for the case of 1,3-dimethylimidazol-2-ylidene. The CHELPG calculations were performed by two different set of atomic radii, one defined originally by Breneman and Wiberg,[257] and the other used by the COSMO model.[287]

The values do not only have a quantitative mismatch, but in some cases they differ even qualitatively when changing the model (Table 3.1). Considering, for example, only the hypovalent carbon atom CC, the obtained charges varied between +0.172 and $-0.964e$. While the Mulliken and Löwdin schemes produced a qualitatively similar, albeit less polarized set of partial atomic charges compared to both CHELPG models, the NBO approach resulted in a reversely polarized NA-CC bond. Thus, even if these NBO charges themselves might be physically meaningful, a molecular mechanical model based on these charges would not be able to reproduce the strong hydrogen bond accepting behavior of the NHC molecule in solution, as it would instead provide a counterintuitive electrophilic character. It is also interesting to observe how much the results from the same CHELPG approach differed, if different sets of atomic radii were taken for the electrostatic potential fitting of the charges. In this work we chose the CHELPG model with the Brenemann–Wiberg radii, due to the fact that the derived charges performed in an acceptable manner in our previous work for 1,3-dialkylimidazol-2-ylidenes.[123] However, based on the discrepancies between the different models, instead of deriving the partial atomic charges solely from the static quantum chemical calculations, we rather took a more pragmatic approach, in which the initially determined charges themselves were redistributed as an integrate part of the fitting.

Since the NHCs of interest can occur in synthesis with many different substituents — in fact, several properties, such as (stereo)selectivity in catalysis can be tuned with choosing the right substituents[41] —, it is highly important that the resulting molecular mechanical model is easy to apply with different moieties attached to the NHCs. Very often, substitution is handled in force fields by the transfer of neutral units, which avoids the lengthy, and in many cases also unnecessary fitting procedure. For example, in the OPLS force field[255] alkanes are composed of neutral CH_n (n$= 0-4$) units, so that with a single model any kind of saturated hydrocarbon can be described. In this spirit, we decided to choose the partial atomic charges at the ring in such a manner that the total charge of the ring is a well-defined value, so that the substitution by such previously established models of substituents is fairly simple.

To this end, a large number of structures were systematically generated by substituting the R and R' groups in **1-9** by methyl, ethyl, *n*-propyl, *iso*-propyl, *n*-butyl, *tert*-butyl, and bis(4,6-dimethyl)phenyl groups. By the rotation within R and R', and — if applicable — within the ring as well, all the conceivable conformations were created, as described in Section 3.1.2. According to the average total charges on the rings in the structures that were optimized (see Supporting Information), for **1-7** the ring atoms — including the attached HA (in **1-4** and **6**), H1 (in **5**) or HC (in **7**) — were assigned charges that sum up to zero, requiring models for the R groups that have a total charge of zero as well. In case of **8** and **9**, the chosen total charge for the R' groups were chosen to be $0.2e$. Since these R' substituents are connected to nitrogen atoms, this setup clearly represents the original OPLS model for aliphatic amines,[255] where the first e.g. CH_n (n$= 0-3$) unit has exactly the same, $0.2e$ total charge.

To be able to employ the same model for all derivatives of each NHC with different substituents, it is necessary that the charges at the ring atoms are nearly the same regardless the nature of the R group, and its conformation. Comparing the quantum chemically obtained partial atomic charges for all derivatives of each NHC showed that the error, which was introduced by this approximation, is notable, but not severe (see Supporting Information of the article). The R and R' substituents are all connected to a nitrogen atom, and, not surprisingly, the charge of the nitrogen atom had the largest changes by altering these groups. The hydrogen atoms at the ring, which are fairly far away from the substitution sites, showed a rather robust behavior, i.e. their charge barely changed by the substituent and its conformation. The most interesting atom is clearly the CC, which is, as a strong hydrogen bond acceptor, the site of the presumably strongest available interaction of the carbene with its environment. Although there were extreme cases, where the partial charge of this atom differed from the average value by up to $0.3e$, the charges usually scattered within a $\pm 0.1e$ interval (see Supporting Information of the article).

After having seen that the substitutable model that we tried to establish was feasible, we focused on fitting the parameters for the non-bonding potential. In many cases of force field development, the parameters are fitted to reproduce experimental thermodynamic data, such as densities, solvation free energies, or heat of vaporization. However, we are not aware of any such set of extensive information for NHCs, which is presumably due to the fact that most of these species are unstable against heat and air, making the

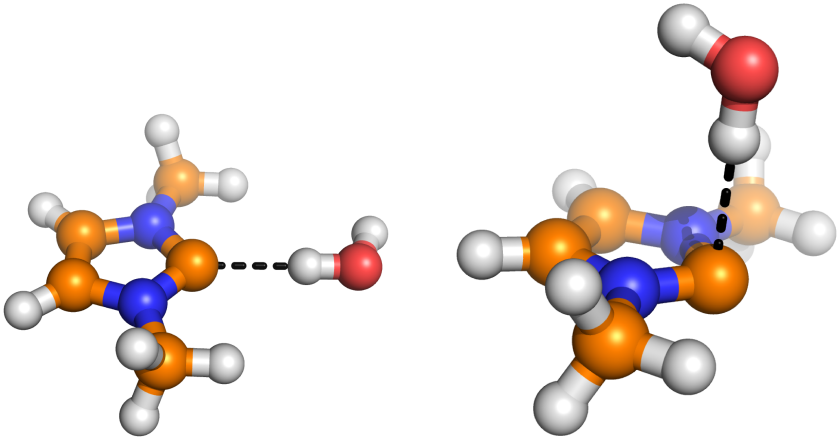

in-plane setting on-top setting

Figure 3.7.: The two coordinates for exploring the intermolecular potential of the carbenes by a water molecule as a probe. The H-C distances within the C···H–O assemblies are varied between 1.7 and 6.0 Å.

production of accurate and reliable data difficult. In a previous work,[123] we used an SPC/E water molecule[258] as a probe to map the intermolecular potential energy of an NHC as a function of position by DFT calculations. We used this information, together with the σ_{ii} and ϵ_{ii} values from literature for the already existing atom types, to fit the Lennard-Jones parameters σ_{ij} and ϵ_{ij} for the molecular mechanical model. Using the Lorentz–Berthelot mixing rules (Equations 3.1 and 3.2), the general parameters σ_{ii} and ϵ_{ii} for the carbene could be calculated, and could be used in general with other kind of interacting molecules, within the limits of these mixing rules. Such an approach had been used previously on e.g. alkanes,[270] and the UO_2^{2+} cation[288,289] as well. This procedure was found applicable in our previous study,[123] therefore we decided to perform the parametrization of the carbenes **1-9** this way.

For each carbenes two sets of geometries were generated, all consisting of the optimized structure of the carbene **1-9** (R = Me, R' = Me), and a water molecule. The water molecule had an identical geometry to that in the chosen water model. In the "in-plane" set, the water molecule was in the plane of the ring with C_S symmetry, with the O–H···C axis in the bisector of the N-C-N angle; while in the "on-top" set the water molecule was situated in a way that the C···H–O hydrogen bond was perpendicular to the plane of the ring, again in a C_S point group (Figure 3.7). While the former set could describe the interaction of the hydrogen bond donor molecule with the lone pair of the carbene, the latter set characterized the interplay between the hydrogen bond donor and the π system. The interaction energies between the two molecules were calculated according to CCSD(T)/CBS single point energies. It is important to note that the structures were not optimized. The reasons for this were that on one hand the employed water model and the NA-CC(-L)-NA moiety of the carbene are rigid, and there were not many internal coordinates to optimize. On the other hand, in molecular dynamics simulations — which

we aimed at by the fitting procedure — the system does not only explore the minima, but also the regions of the potential energy surface far away from them, hence restricting a force field to describe only the gas phase minima introduces errors.

As observed in our previous study,[123] for **1** (R = Me) the two obtained curves show clear differences in depth of the potential energy well, which was clearly due to the fact that the two potentials correspond to very different interaction sites. While this behavior is truly intriguing, and it is responsible for the facile hydrogen bond dynamics of imidazol-2-ylidenes,[123] such anisotropies make the building of a molecular mechanical model difficult, as in the applied pairwise intermolecular potentials the energy is the function of the pairwise distances, and not of the directions. To tackle this problem, in our previous study we introduced an extra, massless point charge L into the system close to the CC atom, which figuratively represents the lone pair of the carbene.[123] In that model, the CC atom possessed no charge, and it was purely a Lennard-Jones interaction site, while the L point had no Lennard-Jones, only Coulombic interactions with its environment. Due to this arrangement, the hydrogen bond donor molecules experience different combination of Lennard-Jones and Coulombic interactions when approaching the CC atom from different directions, which — if the position of L is well-chosen — introduces the required anisotropy for the system. Accordingly, similarly to the previous approach, we introduced L in all systems, where the CC→L vector is parallel to the bisector of the angle around the CC atom in the molecule (e.g. NA-CC-NA in **1**), with the L situated outside of the ring (see Figures 3.4 and 3.5).

For the atoms that fit to previously established atom types (see Figure 3.4 and 3.5), the Lennard-Jones parameters were taken from literature, from the OPLS (for the carbenes) and SPC/E (for the water) models. The σ_{ii} and ϵ_{ii} of the CC atom, the charge of the CC and the L atom (by redistributing the charges within the NHC ring), and the CC-L distance were optimized so that the obtained root mean square deviations for the potential curves were minimal compared to the *ab initio* data, while the changes in the dissociation energies and the location of the minima were also low. After the fitting the parameters for **1** (R = Me), very good agreement could be achieved between the molecular mechanical and the *ab initio* potentials.

However, since our model was built on the basis of the SPC/E water model, the quality of the force field depends on the capacity of the SPC/E model to describe carbene-water interactions. Since this issue clearly determines the applicability of the present model, the potential curves of **1** (R = Me) were recalculated by using the optimized parameters for the carbene together with other water models. The corresponding graphs and the descriptors for the quality of the molecular mechanical potential curves are shown in Figure 3.8 and Table 3.2. Clearly, the potential curves were somewhat less accurate than those fitted with the SPC/E model, but the changes were very low, and therefore the errors introduced by the choice of water model are negligible. This is especially the case, if one considers the very low improvement in quality after refitting the parameters with each individual water models (see Table 3.2). To further check the applicability of the SPC/E water model as a probe molecule for the non-bonding interactions, the analogous potentials with a methanol molecule were calculated by using the OPLS parameters for methanol,[255] and the SPC/E derived force field for **1**. Apparently, the two curves match

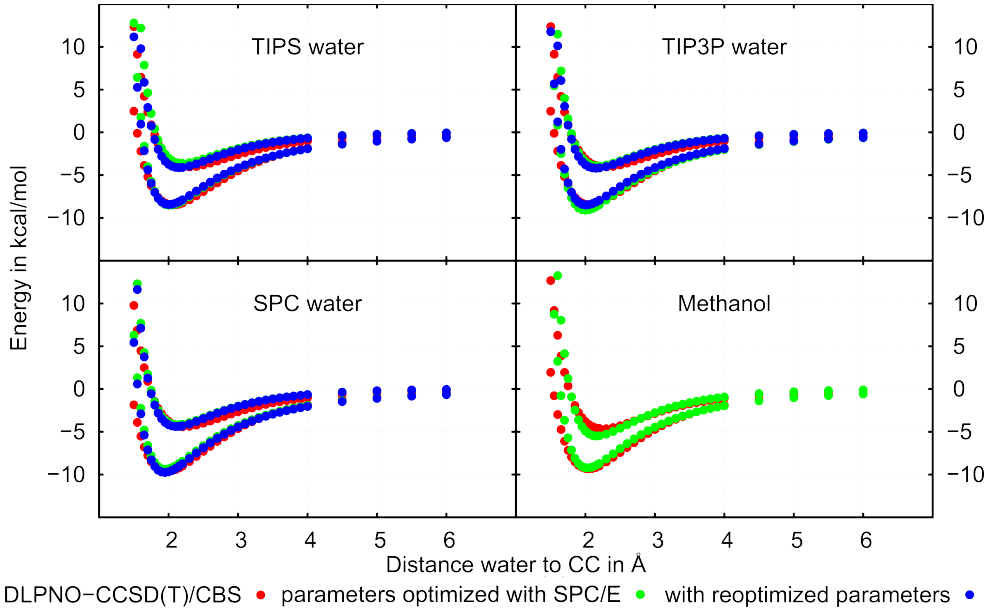

Figure 3.8.: Interaction energies between **1** (R = Me) and different water models, as a function of the C-H distance in the C···H–O assembly, obtained by the CCSD(T)/CBS reference (red), by the CaFF model with the SPC/E-fitted intermolecular potential parameters (green), and by the CaFF model with the individually fitted non-bonding parameters for each kind of probe molecule (blue).

with an excellent quality (see Figure 3.8 and Table 3.2), the observed largest error was in the dissociation energy of the on-top orientation, which was $\Delta\Delta E_{\text{diss}} = -0.9$ kcal mol^{-1}. This error is even lower than expected from e.g. most of the DFT methods, therefore for a molecular mechanical force field it is an unexpectedly good agreement.

According to the observations above, the present approach to generate the force field for carbenes is robust enough, hence we applied it also to carbenes **2**-**9**. The CCSD(T)/CBS potential curves are qualitatively similar in most cases. The in-plane curves exhibit a deep potential energy well at ca. 2.0 Å, with a dissociation energy of $8 - 12\,\text{kcal}\,\text{mol}^{-1}$, showing that all carbenes that were considered here are strong hydrogen bond acceptor molecules. The on-top curves are, in general, similar for **1**-**6** and **8**-**9**, showing a significant energy well at about $2.2 - 2.3$ Å, with a dissociation energy of $3 - 6\,\text{kcal}\,\text{mol}^{-1}$. This on-top interaction is intriguing for the non-aromatic **5**, where the interaction is not related to aromaticity as it was found for anisole,[243,244] simply to a delocalized π-system. For **7**, the on-top potential energy curve exhibits only a very shallow minimum, presumably due to the steric hindrance by the methyl groups at the carbon atom adjacent to the CC atom (compare the potentials Figure 3.9 and the descriptors in Table 3.3).

As for **1** above, the Lennard-Jones parameters of the CC atoms, the distance between the CC atom and L and the charges on the CC and L atoms were varied — together with some slight changes in the partial atomic charges of the ring atoms to maintain the

Table 3.2.: Descriptors of the fitting for the potentials of different water models and methanol with **1** (R = Me), by using the SPC/E-fitted, or refitted (in parenthesis) non-bonding potential model for the carbene.

Probe	RMSD in kcal / mol		Minimum shift $\Delta R_{\min}$ in Å		Dissociation energy $\Delta\Delta E_{\text{diss}}$ in kcal / mol	
SPC/E[258]	**0.36**					
in-plane	0.26		−0.05		−0.1	
on-top	0.44		−0.10		0.1	
TIPS[290]	**0.53**	(0.40)				
in-plane	0.33	(0.34)	−0.05	(−0.05)	< 0.1	(0.1)
on-top	0.67	(0.46)	−0.10	(−0.15)	0.4	(0.1)
TIP3P[245]	**0.43**	(0.40)				
in-plane	0.35	(0.34)	−0.05	(−0.05)	−0.6	(< 0.1)
on-top	0.50	(0.45)	−0.10	(−0.15)	0.1	(0.1)
SPC[291]	**0.45**	(0.36)				
in-plane	0.43	(0.25)	−0.05	(−0.05)	0.2	(0.1)
on-top	0.47	(0.45)	−0.05	(−0.10)	0.2	(< 0.1)
Methanol/OPLS[255]	**0.92**					
in-plane	0.57		< 0.05		0.1	
on-top	0.65		−0.15		−0.9	

total charge on the ring, if necessary —, and at the end, the settings that reproduced the CCSD(T)/CBS potential curves best were chosen as force field parameters. The presence of the L atom improved the quality of the fit in all cases, but except for **1** and **3** the CC atom also possessed some charge in the best models. The deep on-top minimum in case of **8** required the introduction of such high charge on the CC atom, that the in-plane curve become overbinding. To counterbalance this effect, we introduced a positive charge on the L atom, which in that certain case clearly cannot be interpreted as a representation of the lone pair. The final charges, CC-L distances, and Lennard-Jones parameters are summarized in Figures 3.4 and 3.5 and Tables 3.4 and 3.5. Altogether, the achieved matches between the reference and the fitted values are excellent, in terms of RMSD values, and the location and depth of the minima as well. It is important to point out here that the σ values for all CC atoms are in the range that had been defined for carbon atoms in the OPLS force field (e.g. for CA $\sigma = 3.50$, for C $\sigma = 3.75$), again indicating a certain compatibility.

Finally, we also considered to create a general model for carbenes, where the Lennard-Jones parameters, and the CC-L distance, the charges of the CC and L atoms are the same for all structures, which would be an easy starting point for parametrizing any further carbenes. However, as can be seen from the potential curves, the carbenes are so different in hydrogen bond accepting properties (up to 100 % differences in dissociation energies) that creating such a general model is rather difficult, and it is surely a safer approach to refit these parameters individually for each structures.

Table 3.3.: Descriptors for the best fitting models for carbenes **1-9**.

Carbene	RMSD in kcal / mol	Minimum shift Δ_{min} in Å	Dissociation energy Δ_{disso} in kcal / mol
Imidazol-2-ylidene **1**	**0.36**		
in-plane	0.26	−0.05	−0.1
on-top	0.44	−0.10	0.1
Thiazol-2-ylidene **2**	**0.39**		
in-plane	0.31	< 0.05	< 0.1
on-top	0.46	−0.20	< 0.1
Triazol-2-ylidene **3**	**0.42**		
in-plane	0.38	−0.05	0.1
on-top	0.46	−0.15	< 0.1
Imidazol-4-ylidene **4**	**0.51**		
in-plane	0.28	< 0.05	−0.4
on-top	0.67	−0.15	< 0.1
Imidazolin-2-ylidene **5**	**0.43**		
in-plane	0.23	−0.05	−0.3
on-top	0.56	−0.15	0.3
Pyridin-2-ylidene **6**	**0.43**		
in-plane	0.34	< 0.05	−0.1
on-top	0.50	−0.15	−0.2
Pyrrolidin-2-ylidene **7**	**7.59**		
in-plane	0.31	−0.05	−0.1
on-top	10.73	−0.10	0.5
Pyrazol-4-ylidene **8**	**0.50**		
in-plane	0.26	< 0.05	−0.1
on-top	0.66	−0.10	0.3
Cyclopropan-1-ylidene **9**	**0.37**		
in-plane	0.25	−0.05	−0.3
on-top	0.46	−0.15	0.1

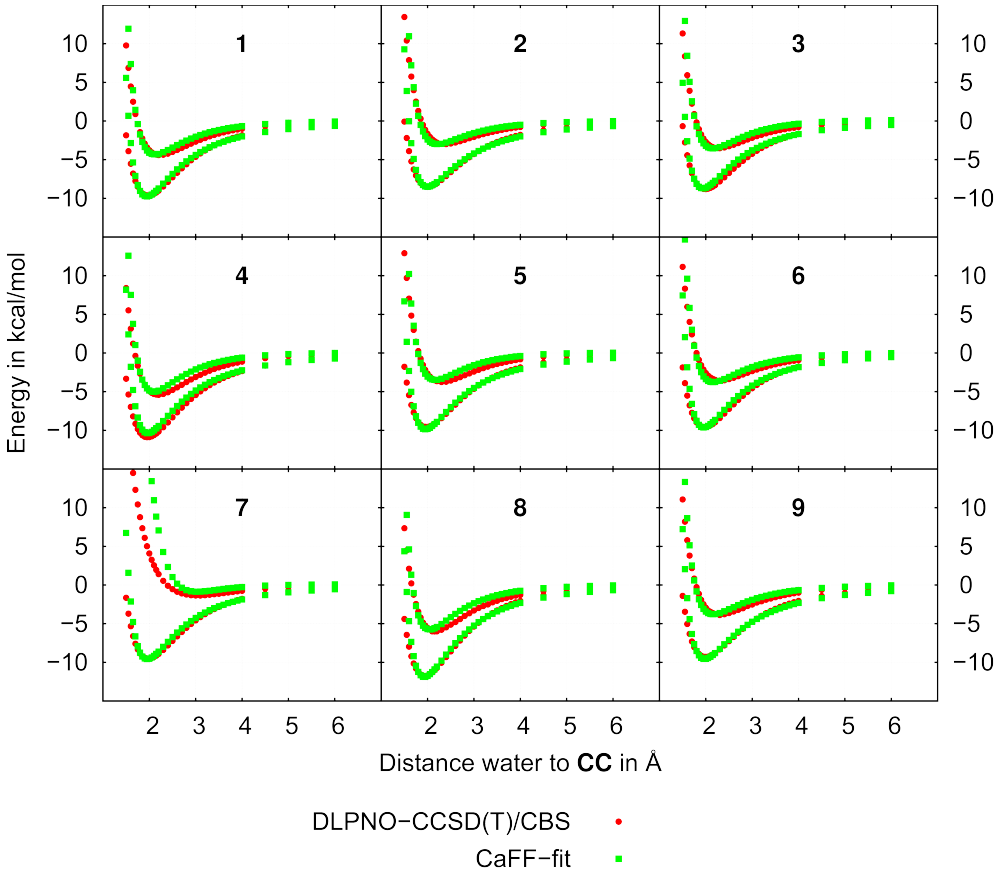

Figure 3.9.: Interaction energies between **1-9** (R = Me) and the SPC/E water model, as a function of the C-H distance in the C$\cdots$H–O assembly, obtained by the CCSD(T)/CBS reference (red), and by the CaFF model (green).

Table 3.4.: Lennard-Jones parameters used in the molecular mechanical energy calculations.

Atomtype	σ_{ii} / Å	ϵ_{ii} / kcal mol^{-1}	Source
CA	3.550	0.070	OPLS[255]
CR	3.550	0.070	OPLS[255]
CW	3.550	0.070	OPLS[255]
HC	2.500	0.030	OPLS[255]
H1	2.500	0.030	OPLS[255]
HA	2.420	0.030	OPLS[255]
HO	0.000	0.000	SPC/E[258]
NA	3.250	0.170	OPLS[255]
OH (water)	3.166	0.155	SPC/E[258]
OH (MeOH)	3.120	0.170	OPLS[255]
OS	2.900	0.140	OPLS[255]
S6	3.550	0.250	OPLS[255]
L	0.000	0.000	this work
CC (**1**)	3.55	0.38	this work
CC (**2**)	3.63	0.31	this work
CC (**3**)	3.50	0.39	this work
CC (**4**)	3.58	0.45	this work
CC (**5**)	3.51	0.49	this work
CC (**6**)	3.71	0.26	this work
CC (**7**)	3.75	0.20	this work
CC (**8**)	3.51	0.50	this work
CC (**9**)	3.58	0.35	this work

Table 3.5.: Fitted distances of the CC atom and the L atom for the different carbenes.

Carbene	Distance CC–L / Å
1	0.10
2	0.20
3	0.30
4	0.10
5	0.25
6	0.25
7	0.10
8	0.25
9	0.10

3.1.4. Conclusions and Outlook

In the present contribution we fitted force fields for N-heterocyclic carbenes (Carbene Force Field, CaFF), including many synthetically important species that are used in catalysis, and other compounds with curious electronic structure. Our aim was to produce a model, which is easy to substitute with any functional groups, in order to be able to generate parameters for a series of structures easily, without any further parametrization.

The bonding parameters of the molecules were obtained from geometry optimizations. The obtained geometries were comparable to those obtained with several of DFT and *ab initio* methods. The partial atomic charges were calculated for 1,3-dimethylimidazol-2-ylidene by the CHELPG, NBO, Mulliken and Löwdin approaches. The changes in these charges were so significant — for the most important, hypovalent carbon atom the differences were about $1e$ — that we decided to take the CHELPG charges only as a starting point, to later redistribute them during the fitting procedure to create the best possible intermolecular potential. According to the charge distributions in altogether 5991 conformations of many derivatives with a set of substituents at the possible positions, we could choose a set of atomic charges for the ring atoms for each kinds of carbenes in a way, so that the well-defined total charges at the substituents make it easy to merge the present CaFF model with the OPLS and AMBER force fields.

The non-bonding parameters were fitted by using an SPC/E water molecule as a probe of the hydrogen bonding ability, according to a CCSD(T)/CBS reference potential. For each carbenes two potential curves were produced by changing the distance of the water probe from the carbene carbon atom, one in the plane of the ring to explore the hydrogen bonding ability of the carbene *via* its lone pair, and one perpendicular to the ring plane to observe the hydrogen bond acceptor strength of the π system. Apparently, to describe both potentials well, in all cases a massless point charge L had to be introduced next to the hypovalent carbon atom CC, which introduced the necessary anisotropy to the intermolecular potential. During the fitting, the atomic charges of the NHC ring including CC and L, the Lennard-Jones parameters of the CC atoms, and the CC-L distances were optimized, to provide the best match with the reference potential curves in terms of root mean square deviations, the location of the minima, and the corresponding dissociation energies. By using the obtained parameters of 1,3-dimethylimidazol-2-ylidene with other water models (TIP3P, SCP, and TIPS), and also an OPLS model of methanol, the corresponding CCSD(T)/CBS reference curves could be well reproduced, suggesting the robustness, and accuracy of the fitting procedure.

The hereby presented molecular mechanical CaFF models for this large set of carbenes allows the investigation of these substances with their long-range environment, including solute-solvent interactions, interfacial behavior, interplay with macromolecules or nanoparticles. Since carbenes, especially NHCs are widely used in such situations, the related results will contribute greatly to our understanding in the chemistry and the corresponding applications of these compounds. Clearly, present CaFF model can be extended by including e.g. polarizability, and reactivity, or by introducing parameters for further, structurally interesting carbenes.

3.2. Is Carbene Formation Necessary for Dissolving Cellulose in Ionic Liquids?

Sascha Gehrke[†,‡] , Karola Schmitz[†] , Oldamur Hollóczki[†,*]

The Journal of Physical Chemistry B, 2017, Volume **121 (17)**, Pages 4521–4529

DOI: 10.1021/acs.jpcb.7b00631

Received: January 19, 2017

Published: April 13, 2017

For this article a Supporting Information is available free of charge at:
`https://pubs.acs.org/doi/suppl/10.1021/acs.jpcb.7b00631/suppl_file/jp7b00631_si_001.pdf`

Contributions to the manuscript:

- Setup and maintenance of all simulations
- Analysis of the trajectories
- Writing the technical part of the manuscript

[†]Mulliken Center for Theoretical Chemistry, University of Bonn, Beringstr. 4+6, D-53115 Bonn, Germany
[‡]Max Planck Institute for Chemical Energy Conversion, Stiftstr. 34–36, D-45470 Muelheim an der Ruhr, Germany
[*]E-mail: holloczki@gmail.com

In the last chapter a model for NHCs was achieved. Thereby, special importance was attached to the hydrogen bond interaction. It could be shown, that the model sufficiently reproduces the CCSD(T) potentials between carbenes and several bonding partners. However, the behavior of the model in large scale simulations still needs to be tested in terms of stability. This testing was done within the framework of a study about cellulose valorization, in which carbenes may probably play a key role.

Abstract

Many ionic liquids with basic anions have two practically important features: they can dissolve cellulose in relatively large quantities, and they show carbene-like reactions, e.g. the decomposition of the dissolved carbohydrate molecules. In this work we show that the solvation of the structural units of cellulose in 1-ethyl-3-methylimidazolium acetate barely changes by the addition of carbenes to the solution, but cellulose appears to dissolve faster in the absence of carbene molecules. Accordingly, although based on indirect experimental findings one might speculate otherwise, the solubility and carbene formation are merely two independent consequences of the basicity of the ionic liquid anion, and the presence of carbenes is not necessary for breaking up the cellulose into individual chains. Based on these results we can conclude that it is, in principle, possible to design an ionic liquid that is an ideal solvent for this biopolymer, which dissolves, but does not decompose cellulose.

3.2.1. Introduction

Utilizing cellulose from biomass has a great potential as an alternative feedstock for biopolymers, chemicals, and fuels.[292] The initial processing of the dry biomass involves dissolving its cellulose content, which allows the necessary purification of this valuable material. Among the many possible alternatives, ionic liquids[133–136] (ILs) show clear advantages,[293–299] since they dissolve this biopolymer under rather mild conditions, without the use of any toxic or environmentally harmful additive.

In cellulose, the long, linear polymer chains are held together by an extensive hydrogen bonding network, formed between the hydroxyl groups of the D-glucose monomer units.[300,301] Accordingly, it is not surprising that the hydrogen bonding ability of the IL has a pivotal role in its capacity to dissolve the cellulose. The most promising ILs for cellulose processing feature basic anions, such as acetate, phosphate and chloride, which form strong hydrogen bonds with the individual cellulose chains, disrupting the very interplay that holds them together.[293,300–303] The highest solubility could be achieved so far in 1-ethyl-3-methylimidazolium acetate ([C_2C_1im][OAc]), where up to 25 m/m% of cellulose could be dissolved.[152,293] After the dissolution and the subsequent purification processes, water is added to the solution. Since water is a stronger hydrogen bond donor than cellulose, the anion-cellulose interplay is broken, and the carbohydrate is, accordingly, precipitated from the solution,[152,294,300,303] allowing a facile and convenient separation of the solvent from the solute.

In contrast to the anion, the role of the cation has been for long disregarded. However, when the most often applied 1,3-dialkylimidazolium cation is exchanged to another, for example 1,2,3-trialkylimidazolium cation, the solubility of the cellulose decreases dramatically.[304,305] This effect was rationalized by the cations forming the second solvation shell around the cellulose chains, and since these positively charged layers repulse each other, they contribute to the separation of the chains from the cellulose bundle.[305] With respect to highly basic, 1,3-dialkylimidazolium-based ILs it should be mentioned, however, that during the last decade the accessibility of N-heterocyclic carbenes has been proven in such systems (Figure 3.10),[81,82,137,138,141] through theoretical methods and spectroscopy,[82] trapping reactions,[137,141] and via the organocatalytic activity[81] of the corresponding pure ILs. It has been shown that the carbenes derived from [C_2C_1im][OAc] may also contribute to the degradation of the cellulose product, by the repeated elimination of formaldehyde units (Figure 3.11).[306] Clearly, the degradation of the product has to be avoided, and to this end it seems straightforward to choose ILs, where the carbene formation is hindered. However, it is possible that the presence of the carbene is not only a side effect of the basicity of the strongly hydrogen bonding anions, and not only an undesirable source of degradation, but it is necessary for dissolving the cellulose. The change of the cation results in the inaccessibility of the carbene, and considering the carbene formation as a necessity, it would, therefore, at least contribute to the aforementioned drop in the solubility of the carbohydrate. Moreover, it has been shown that the formation of the carbene is diminished by the presence of water,[141,143] hence the precipitation effect by the addition of water can also be put into a different perspective.

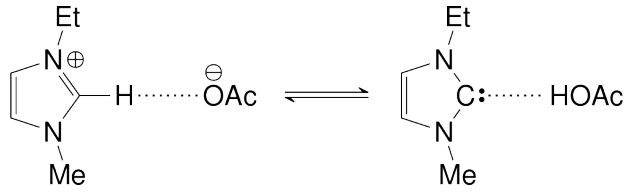

Figure 3.10.: Carbene formation from the 1-ethyl-3-methylimidazolium acetate ion pair.

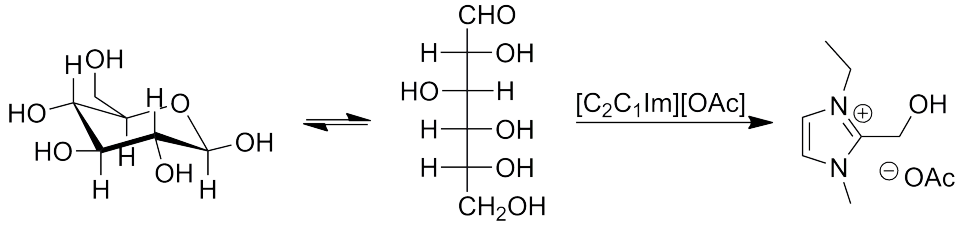

Figure 3.11.: Reaction of β-D-glucose with the $[C_2C_1im][OAc]$ solvent, a model for the degradation of cellulose induced by the ionic liquid solvent.

At that moment, when the separation of a single chain from a larger block of cellulose begins, we can postulate that there will be a particle that first fills the growing void in between these two units (Figure 3.12). Since this particle has to partly leave the bulk of the liquid, it is reasonable to assume that it is a neutral unit, thus, an ion pair, similarly to the vaporization process.[307] Such a single ion pair in a non-ionic medium usually stabilizes via reorganization,[82,308] in order to decrease its unfavorable polarity; either through decreasing the distances between the charged moieties,[308] or via a proton transfer, as was observed for $[C_2C_1im][OAc]$,[82] and for the relatively volatile protic ionic liquids.[309,310] Similar effects were surmised if neutral molecules, e.g. CO_2 were dissolved or absorbed into an ionic liquid that has the capacity for a proton transfer,[144] where the neutral molecule, by inducing a defect in the ion network,[311] enhances the formation of the carbene. Given that carbenes are very strong hydrogen bond acceptor species,[1,82,121,123,125] stronger than water or alcohols, these molecules might also interact strongly with the hydrogen bond donor carbohydrates. Thus, the presence of a carbene molecule in such a just forming void in between two departing cellulose units could indeed contribute to the dissolution process, by serving as a relatively mobile wedge. On the other hand, as mentioned above, the carbene activity of the $[C_2C_1im][OAc]$ is clearly reduced in the presence of water,[141,143] hence one might also speculate that the hydroxyl moieties of the cellulose also decrease the ability of the ionic liquid to form carbenes.

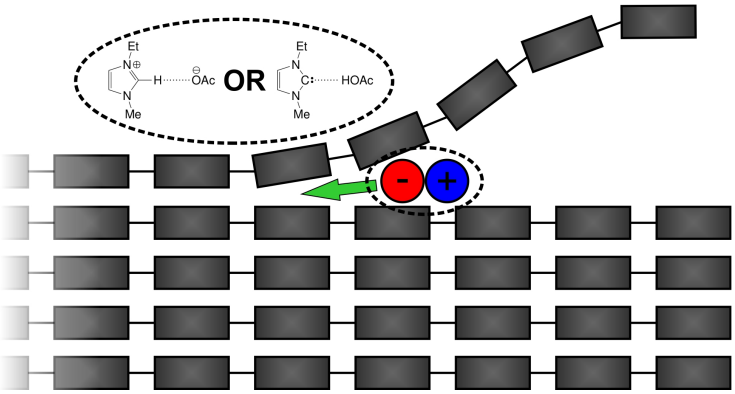

Figure 3.12.: The ion pair that participates in the detachment of a cellulose chain from the cellulose block. The polarity of this ion pair may be changed by the proton transfer, producing the strong hydrogen bond acceptor carbene molecule.

Since it has been shown that the availability of carbenes facilitates the degradation of this carbohydrate polymer, a successful application of ionic liquids for cellulose processing should employ solvents, where the cellulose chains are detached from each other also in the complete absence of carbenes. Hence there is a clear need for investigating how the accessibility of carbenes might influence the solubility in ILs, and, most of all, it has to be explored if this transient species is necessary for the dissolution process. In this article we inspect the carbene-cellulose interactions in $[C_2C_1im][OAc]$, and explore the potential effects of carbenes on the dissolution of cellulose in details through molecular dynamics simulations and static quantum chemical calculations.

3.2.2. Models and Methods

Investigated Systems

To model the solvent effects around the large macromolecules in the IL over long time scales, performing classical molecular dynamics (MD) simulations shows its clear advantages. However, the good performance of this approach comes at a price: The potentials applied in the MD simulations of ILs and biomolecules do not consider the electronic structure explicitly, and therefore the breaking and formation of bonds cannot be described by them. Accordingly, the proton transfer from the cation to the anion — thus, the carbene formation — cannot be included in such a model. Instead, we included explicit carbene molecules in the system. By tracking the interactions of these molecules with the carbohydrates a clear picture should emerge from the preferred interaction sites. Since these sites have the strongest stabilizing interactions between the solute and the carbene, this simple experiment also indicates those sites, which might prefer the formation of the carbene most, and where the formation of these species will have the largest impact. In other words, our calculations are similar to an experiment, where the effect of the carbene's inherent presence is tracked via creating carbenes from the solvent e.g. by an irreversible base.

Table 3.6.: Composition and cell data of the systems investigated by classical molecular dynamics simulations. (N_{Glu}: number of β-D-glucose molecules; N_{Glu4}: number of β-D-glucose tetramer molecules; N_{Glu8}: number of cellulose chains, composed of eight β-D-glucose units; N_{IL}: number of 1-ethyl-3-methylimidazolium acetate ion pairs; N_{NHC}: number of 1-ethyl-3-methylimidazol-2-ylidene molecules; N_{water}: number of water molecules.)

System	N_{Glu}	N_{Glu4}	N_{Glu8}	N_{IL}	N_{NHC}	N_{AcOH}	N_{water}	Cell vector /Å	ρ /g cm^{-3}
I	40	0	0	240	0	0	0	42.6395	1.030
II	40	0	0	234	12	0	0	42.7437	1.029
III	40	0	0	228	24	0	0	42.9096	1.025
IV	0	10	0	240	0	0	0	42.4869	1.029
V	0	10	0	234	12	0	0	42.5739	1.030
VI	0	10	0	228	24	0	0	42.7524	1.025
VII	0	0	10	720	0	0	0	60.5496	1.015
VIII	0	0	10	702	36	0	0	61.0125	1.011
IX	0	0	14	1	0	0	3364	49.6530	0.822
X	0	0	14	0	1	1	3364	49.8488	0.813

We considered three different kinds of solutions, containing glucose, a fraction of cellulose consisting of four β-D-glucose units, and a small bundle of Iβ-cellulose, composed of ten chains of eight β-D-glucose molecules each. All three systems were simulated in the pure [C_2C_1im][OAc] IL, and then in the presence of the carbene 1-ethyl-3-methylimidazol-2-ylidene. Finally, we also simulated a somewhat larger bundle of cellulose composed of 14 chains of Iβ-cellulose, in which a void was created by cutting out four adjacent glucose units, and replaced by an ion pair of the ionic liquid, or a carbene-acetic acid pair. These systems gave crucial information on the potential of the ionic liquid ion pairs in confined spaces of cellulose to form carbenes, and therefore helped to assess the feasibility of the mechanistic picture shown in Figure 3.12. The exact composition of the systems can be found in Table 3.6, while a snapshot of each is shown in the Supporting Information. The labeling of the atoms in the relevant molecules is presented in Figure 3.13, as used throughout the whole article.

Molecular Dynamics Simulations

All molecular dynamics simulations were carried out using the LAMMPS code.[263] The initial boxes were created to have a density of 1 g cm^{-3} by the PACKMOL program.[312] Then a 1 ns long NpT simulation was performed (T = 400 K, τ_T = 100 fs, p = 1 bar, τ_p = 1000 fs), in which the volume was averaged over the last half nanosecond. The resulting cell vectors and the corresponding densities of the simulation boxes are listed in Table 3.6. After 1 ns of further equilibration in the NVT ensemble (T = 400 K, τ_T = 100 fs), 50 ns of production run were conducted, along which the atomic coordinates were saved in every 1 ps. For the IL cations the CL&P force field was employed,[266] while

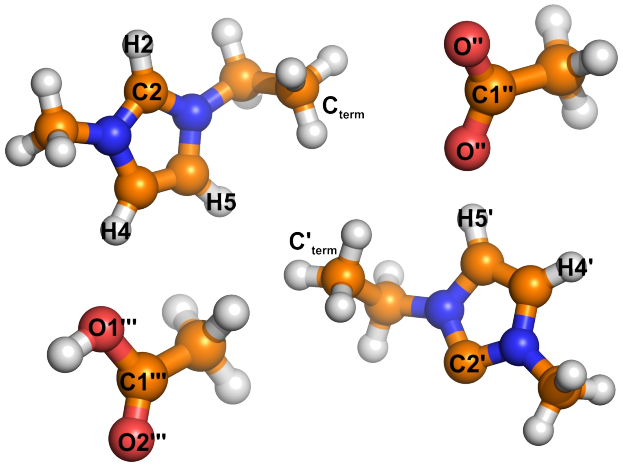

Figure 3.13.: Atom labeling as used throughout the article.

for the acetate anions and for the carbohydrates the standard OPLS parameters were taken.[255] The carbenes were modeled by the CaFF force field.[123] To account for the charge transfer between the IL ion pairs,[313–315] the partial atomic charges of the IL solvent were scaled by 0.8. The trajectories were analyzed by the Travis software.[316]

Static DFT and *ab initio* calculations

All quantum chemical calculations were performed by the ORCA 3.0.3 program package.[256] For the geometry optimizations the TPSS exchange-correlation functional[278] was used with the def2-TZVP basis set,[282,283] and the D3-BJ dispersion correction.[279,280] For both the SCF cycle and the geometry optimization the tight convergence criteria of ORCA were used. After the geometry optimization, the eigenvalues of the Hessian were calculated, in order to inspect the nature of the obtained stationary point.

Single point energies were calculated using the DLPNO-CCSD(T)[259,260] method, with tight settings for the localization as defined by Neese and Liakos.[259,260] From the obtained single point energies with the def2-TZVPP as well as the def2-QZVPP basis sets the energy at the complete base set limit was obtained by extrapolation, using the scheme developed by Neese and Liakos.[262]

3.2.3. Results and Discussion

Since cellulose is composed of D-glucose units, to characterize how this polymer interacts with the liquid, it is reasonable to understand the solvation of the monomers first. Although the solvation of glucose in this ionic liquid was characterized before by both experiments and MD simulations,[317] in order to have a direct comparison for observing the effect of the carbene on the solvation, we discuss it here as well. Focusing on the solute-solvent interactions in system **I**, it is clearly observable that — in agreement with previous results[317] — the anions dominate the solvation of glucose in $[C_2C_1im][OAc]$.

Table 3.7.: Average lifetimes of the hydrogen bonds of the RDFs in Fig. 3.14. The relative long lifetime of the bonds between the acetate and the glucose presents the extraordinary strength of this type of bond.

	Average lifetime / ps		
System	O″ ··· HO (glu)	H2,H4-5 ··· O (glu)	C2′ ··· HO (glu)
I	189.6	32.5	—
II	194.6	22.5	57.0
III	194.6	22.3	51.0
IV	278.0	63.4	—
V	299.7	38.5	78.2
VI	285.8	37.5	66.9
VII	404.8	58.4	—
VIII	436.4	49.7	89.7

All glucose -OH groups are interacting strongly with the acetate anions, as shown by the corresponding sharp and high first peak in the corresponding radial pair distribution functions (RDFs, Figure 3.14A). Dissecting the RDFs into the individual contributions from the different hydroxyl groups of the glucose molecule shows similarly strong interplay at all sites (for details, see Supporting Information).

Since the acetate anion can offer two hydrogen bond acceptor oxygen atoms, one acetate anion may interact with more than one hydroxyl groups. Comparing the number of acetate oxygen atoms in interaction with any hydroxyl moieties around the glucose molecules with the number of interacting acetate anions, one can assess how many acetate anions are interacting with the glucose through two oxygen atoms. Interestingly, we found a relatively low ratio for such bidentate interplay, only 22.67 %.

The strength of these hydrogen bonds can also be presented by their relatively long lifetime (see Table 3.7). The obtained ca. 190 ps lifetime is significantly longer, than that for the hydrogen bonds between water molecules in liquid water, which is normally in the subpicosecond range.

Beside the anion, the cation also participates in the solvation of the carbohydrate monomer molecule according to the corresponding RDFs (Figure 3.14B). Although the acetate anions are the strongest hydrogen bond acceptors in the system, the strong hydrogen bond donor glucose molecules should partly hinder their interplay with the cation in the first solvent shell. Therefore, the cations are also available for interaction with the glucose, via C-H$\cdots$O hydrogen bonds.

In system **IV** the solvation of the glucose tetramer is predominantly similar to the glucose molecule discussed above. The anion-solute interactions give rise to the highest peaks in the RDFs (Figure 3.14D), due to the strength of the anion-hydroxyl hydrogen bonds. Since a single molecule of the tetramer contains several hydroxyl groups, the possibility of each anion to form multiple hydrogen bonds with these molecules is increased compared to the system **I**. Indeed, according to the ratio of coordinating anion oxygen

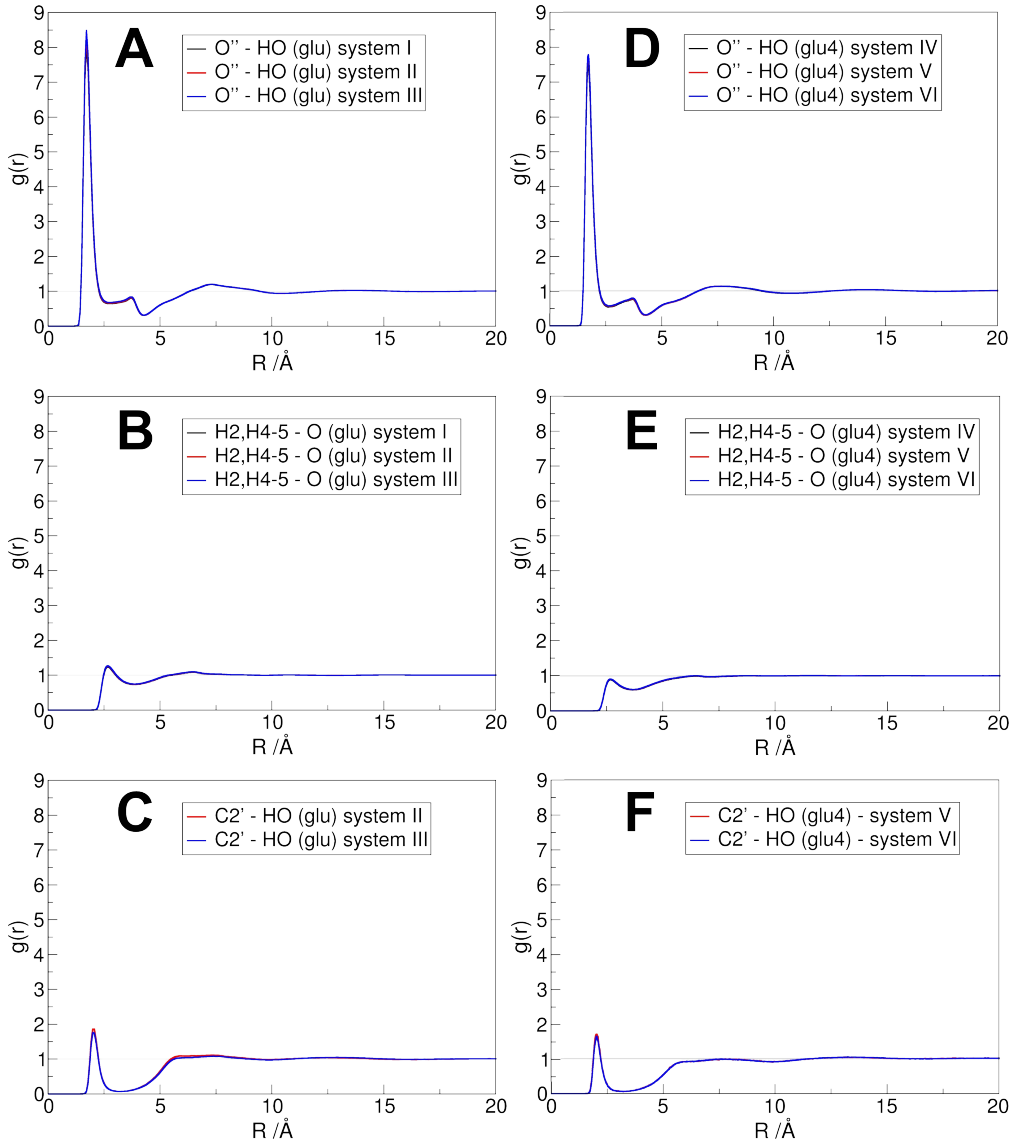

Figure 3.14.: Radial pair distribution functions in systems **I-VI**, representing the solvation of the carbohydrates.

atoms and coordinating anions, a somewhat higher, but still surprisingly low ratio of the solvating anions are in such bidentating coordination mode (24.7 %). The cation is also interacting with the solute through C-H$\cdots$O hydrogen bonds, similarly to the case of the monomer (Figure 3.14E).

In systems **II-III** and **V-VI**, the effect of the carbenes can be observed on the solvation of the carbohydrates, when compared to systems **I** and **IV**, respectively. The strongest interacting site of the carbene is the hypovalent carbon atom C2′, acting generally as a strong hydrogen bond acceptor. Thus, the carbene is in competition with the acetate for the hydrogen bond donor sites of the solute. The C2′ exhibits a notable interplay with the hydroxyl moieties of the carbohydrate molecules, but the first peaks in the corresponding RDFs (Figure 3.14C and F) are significantly lower than those for the acetate-OH interactions. The overwhelming dominance of the acetate-carbohydrate correlation over that for the carbene-carbohydrate interplay is shown perhaps best by observing how little the height of the acetate-OH RDF peaks is influenced by the presence of the carbene (Figure 3.14A). In fact, a little increase can be seen in the RDFs by introducing the carbene molecules into the system, which is due to dilution effects, that is, the similar occurrence of the acetate-carbohydrate pairs are normalized with the lower average number density of the anion when calculating the $g(r)$.

The cation-carbohydrate interactions are significantly weaker than those between the anion and the carbohydrate, and therefore one might think that they are easier to be affected by the carbene. However, due to their different nature, the cation and the carbene are interacting at different sites of the glucose or its tetramer, and therefore they are not in competition with one another. The C-H$\cdots$OH interactions are, therefore, also barely affected by the addition of the carbene to the solution, apart from a slight increase in the height of the first peak due to the aforementioned dilution effects.

It is interesting to point out that there are some notable changes in the dynamics of the systems, when carbenes are added to the solution. While the lifetime of the anion-carbohydrate interactions becomes somewhat longer, the cation-carbohydrate interplay exhibits a significantly (by ca. 30-40%) shorter lifetime.

Instead of forming hydrogen bonds with the cellulose, the carbenes should interact with the IL solvent. Strong C-H$\cdots$C hydrogen bonds between the carbene and the cation would be conceivable,[124] but the acetate anions have been shown to outperform the strong hydrogen bond acceptor strength of imidazol-2-ylidenes,[122] occupying the strongest hydrogen bond acceptor ring hydrogen atoms of the cation. Thus, the divalent carbon atom is relatively free in the solution, forming weak interactions with the ring hydrogen atoms of other carbene molecules,[123] or with the alkyl groups of the cation's side chain.[122] Accordingly, the reason for the surprisingly weak interactions between the carbene and the glucose units cannot be explained by a competing carbene-solvent interplay, but only by the significantly stronger hydrogen bond acceptor anion, which occupy the hydroxyl groups, and therefore banish the carbene from the carbohydrate.

In the carbene-free systems **I** and **IV** the carbohydrate molecules are interacting solely with the solvent, the solute-solute interplay is negligible. Thus, observing the effect of the carbene on aiding the dissolution — thus, the breaking of the carbohydrate-carbohydrate interplay — is possible only if the process for a block of cellulose is modeled. For this

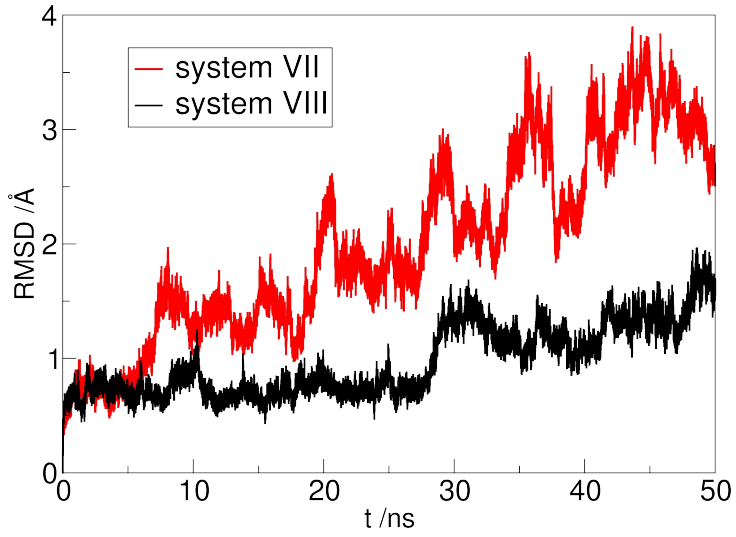

Figure 3.15.: The unwrapping of the cellulose chains of the bundle in systems **VII** and **VIII**, illustrated by the root mean square deviations of the ring-ring distances.

reason, in systems **VII** and **VIII**, a bundle of ten cellulose chains, each consisting of eight β-D-glucose units (as taken from Reference 318) was modeled in the IL $[C_2C_1im][OAc]$, and in case of the latter system in the presence of 1-ethyl-3-methylimidazol-2-ylidene molecules. The cellulose bundle suffered large structural changes in both systems, showing the detachment of several chains. To gain an impression on the rate of the process, we followed the root mean square deviations (RMSD) of the distances between the glucose rings in the bundle versus the simulation time (Figure 3.15). With this, we get an insight into how fast do the chains depart from each other, viz. how fast is the dissolution. Interestingly, as shown by the RMSD plots, the dissolution of the cellulose bundle was significantly faster in system **VII**, than in system **VIII**, showing that the presence of the carbene is not facilitating, but in fact *hindering* the process!

Analyzing the first 5 ns of the trajectory, before the dissolution takes place (cf. Figure 3.15), a similar picture emerges as in case of the glucose monomers and tetramers, with the acetate anions dominating the solute-solvent interactions, with a weaker interplay between the oxygen atoms of the cellulose and the cation. These interactions are not influenced significantly by the carbene (Figure 3.16), showing that the acetate anions outperform the carbenes in hydrogen bond accepting strength. The slightly lower peaks in the RDFs describing the acetate-cellulose interplay in system **VII** as compared to system **VIII** can be rationalized by the more intact structure of the cellulose bundle, which allows the acetate anions surround the carbohydrate chains somewhat less. Similarly, the first peaks in the RDFs are lower than for the glucose monomers and tetramers, since the cellulose chains are aggregated into a bundle, and therefore they are only partly solvated.

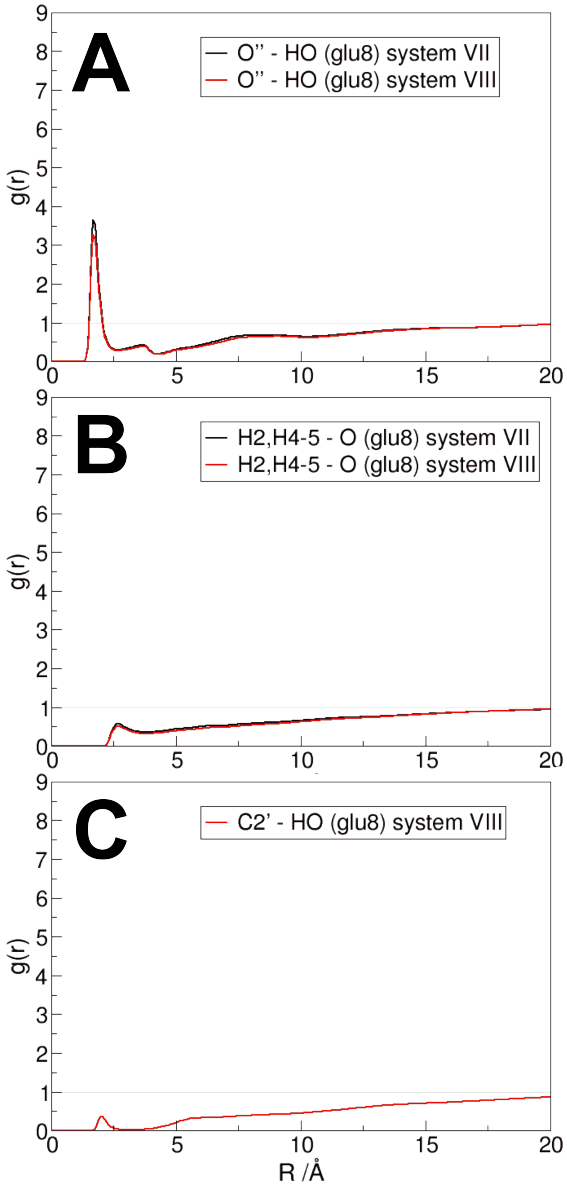

Figure 3.16.: Characteristic radial pair distribution functions for systems **VII** and **VIII**.

It is again interesting to observe that although the lifetime of the anion-cellulose interplay is increased by ca. 10 %, that of the cation-cellulose interplay is 15 % shorter when carbenes are added to the solution. Since the dissolution of the cellulose is a delicate process, where the hydrogen bonding of the chains with the anion and the repulsion between the cationic rings solvating the individual chains also plays a role, these changes might explain the differences in the dissolution process described above.

While these results give fruitful details into the interactions between the carbene and the cellulose, one might argue the simulations lack the insight into the role of the carbene formation at the confined space in between the detaching cellulose chain and the rest of the bundle, as proposed in Figure 3.12. The ion pair that first enters this particular small slit has a completely different environment than those in the bulk of the liquid. In contrast to the ionic medium, this assembly has a neutral — albeit polar — environment, and therefore it is conceivable that the ion pair would prefer certain deionization via a proton transfer. In system **VIII**, as discussed above, the carbenes have to diffuse to the spot where the cellulose block is breaking apart, and cannot be formed at the spot spontaneously. Accordingly, this spontaneous deionization by a proton transfer cannot be observed in system **VIII** directly. For this reason, we created system **IX** and **X**, where in a cellulose bundle similar to those in systems **VII** and **VIII** we created a void by removing four glucose units in the middle. In this void we inserted an IL ion pair (system **IX**), or a carbene-acetic acid complex (system **X**). To avoid dissolving the cellulose in the liquid, and the subsequent release of the ion pair to the bulk of the solvent, we chose to solvate this system not in the IL, but in water.

Again, in this model no proton transfer is possible due to the molecular mechanical potential form. However, as we will see below, by tracking the distance between the ions, or between the carbene and the acetic acid, we can gather highly relevant information regarding the carbene formation, since it shows how much does the cellulose stabilize such charge separated species in its confinement. Interestingly, the ions in system **IX** diffuse apart from each other to a distance, which is larger than that in the bulk liquid (cf. black and blue lines in Figure 3.17). This is highly unexpected, since while in the liquid there are many partners, which screen the individual interactions, in case of an ion pair a single, and therefore stronger ion-ion interplay should be present, which should precipitate in shorter anion-cation distances. In the cellulose confinement, however, there are several hydroxyl groups of the carbohydrates, which are strong hydrogen bond donor moieties, and therefore are prone to interact with the anion, and compete with the cation for it. This competition apparently disrupts the cation-anion interaction, and increase the distance between them (Figure 3.17).

In system **X**, on the other hand, the carbene and the acetic acid stay close to each other, connected by a hydrogen bond. This clear difference to system **IX** can be rationalized by comparing the hydrogen bonding abilities of the different particles in the system. The acetic acid, formed by the proton transfer (Figure 3.10), is more acidic, and therefore a significantly stronger hydrogen bond donor, than the OH groups of the cellulose. On the other hand, the carbene is a much stronger hydrogen bond acceptor, than any of the oxygen atoms in the cellulose, therefore the strongest possible hydrogen bond can be formed between these two species. Accordingly, the interactions between the carbene and

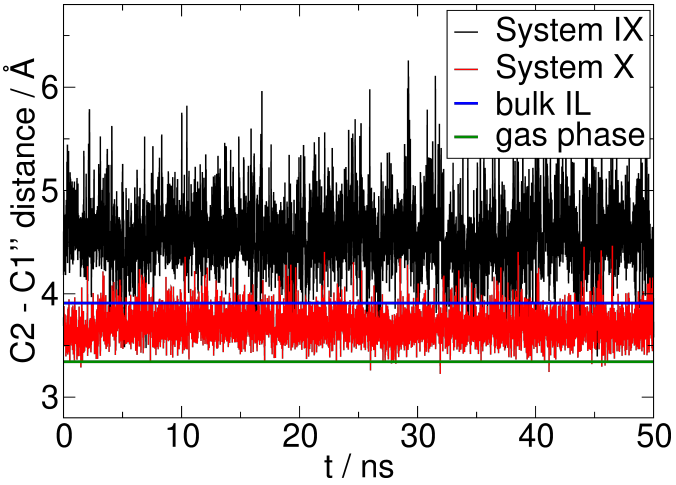

Figure 3.17.: The development of the cation-anion and carbene-acetic acid distances (through the C2-C1″ distance) over time in system **IX** (black line) and system **X** (red line). For comparison, the location of the first peak in the radial pair distribution function of the same atoms in the bulk of the liquid is indicated with a blue line. Th distance in the gas phase is shown in green. The average distance in system **IX** is at 4.57 Å and 3.70 Å in system **X**.

the cellulose, as well as the acetic acid and the cellulose are restricted to be significantly weaker, than the anion-cellulose and cation-cellulose interplay, and therefore the present medium should stabilize the ion pair more, than the carbene-acetic acid complex. In other words, the "deionization" of the IL ion pair by proton transfer is not advantageous in confined voids of cellulose, and therefore the role of carbenes in the detachment process as described in Figure 3.12 can be excluded.

To further explore the effect of the cellulose on the carbene formation, we also performed static DFT calculations, where the energy demand of the proton transfer can be directly assessed. To this end, we created clusters of a glucose molecule with an $[C_2C_1im][OAc]$ ion pair from the trajectory of the simulation of system **I**. The first 50 structures were generated by simply saving the coordinates of a glucose molecule with the closest anion and cation. The algorithm implemented in Travis[316] chooses those configurations that are possibly most different from each other, allowing the largest possible sampling of the conformational space. The 50 structures were then used to create 20 more clusters according to chemical intuition, by rotating hydroxyl groups toward the anion to maximize the glucose-IL interactions. The obtained 70 structures were then mutated into glucose-carbene-acetic acid clusters by a proton transfer, and if possible with further increase in glucose-carbene, glucose-acetic acid and/or carbene-acetic acid interactions. After optimizing these altogether 141 structures, on the geometries that were within 5 kcal mol^{-1} of that in the lowest energy structures for the carbene- and the ion pair-containing clusters, highly accurate DLPNO-CCSD(T)/CBS single point calculations were performed. The most stable isomers, and their relative energies are shown

in Figure 3.18. In the gas phase, in agreement with the experiments[82] and previous calculations[144] the carbene is more stable, than the ion pair. The presence of the glucose molecule, however, indeed destabilizes the carbene, by shifting the energy difference from -0.8 to 11.4 kcal mol^{-1} (Figure 3.18), which supports the classical MD data above.

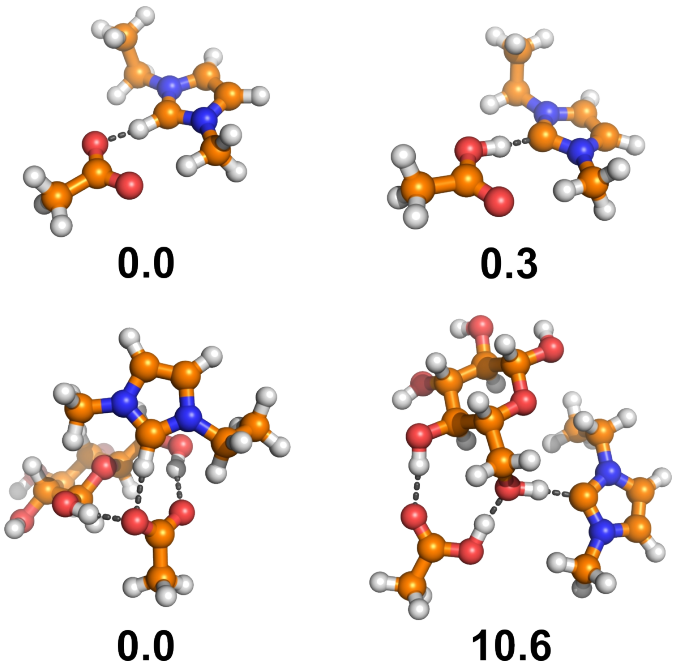

Figure 3.18.: The structure and DLPNO-CCSD(T)/CBS//TPSS-D3BJ/def2-TZVP relative Gibbs free energies of the most stable isomers of the investigated clusters, containing an ion-pair or a carbene and an acetic acid in the presence/absence of a β-D-glucose. As a comparison, the structures and relative energies of the single ion pair is also shown.

3.2.4. Conclusions and Outlook

While many ionic liquids are promising solvents for cellulose processing, the basic anions, which are necessary for the breaking of the hydrogen bonds between the cellulose chains, often allow the formation of N-heterocyclic carbenes in the same materials by a proton transfer. These carbenes damage the integrity of the biopolymer, by catalyzing its decomposition into formaldehyde-carbene adducts. However, indirect evidences point to the possibility, that these two properties are directly related, and the presence of the carbene is not merely a simple side effect of the basic medium, but in fact necessary for the dissolution process. A possible effect of the carbene formation could be a certain depolarization of the ionic liquid ion pairs at confined spaces, which would help the ionic liquid to act as a wedge that separates the cellulose chain from a cellulose bundle.

To understand the effect of the carbene's availability on the dissolution of cellulose in ionic liquids, we performed classical molecular dynamics simulations on a set of carbohydrate-ionic liquid systems, where the ionic liquid was chosen to be 1-ethyl-3-methylimidazolium acetate. The simulations were performed both in the presence and absence of carbene molecules. In agreement with previous results, the solvation of the carbohydrates is dominated by the interactions with the anions. If carbene molecules are included in the solvent, these interactions are barely changed, indicating that — albeit being present — the carbene-carbohydrate interplay is negligible in the solution. On the other hand, quantifying the rate of the dissolution of cellulose in these systems showed that cellulose bundles remain more intact if the carbene molecules are present, showing that the presence of carbenes itself is not necessary, even disadvantageous for the dissolution process.

Exploring the effects of the aforementioned deionization of ion pairs in confined spaces of cellulose, we simulated a single ion pair in a void of a cellulose bundle. We found that the ions are floating farther from one another than in the bulk of the liquid, although in a single ion pair shorter distances could be expected. The reason for this interesting finding is the presence of strong hydrogen bonds between the cellulose and the anion, which are stronger than the cation-anion interplay. In contrast, the carbene-acetic acid pair was shown to stay close to each other in a hydrogen bond, therefore these products of the proton transfer are not stabilized by the formation of cellulose-carbene or cellulose-acetic acid interactions. In agreement, by static calculations we observed that the presence of a glucose molecule destabilizes the carbene-acetic acid pair compared to the ion pair. All these data show that the carbene is less prone to form in the presence of the cellulose than in the bulk.

Thus, from the several different simulations and static calculations performed here, one can draw the conclusion that the carbene formation has a disadvantageous effect on the cellulose dissolution, even without considering the chemical degradation effect of this material. Accordingly, it seems possible to design an ionic liquid that dissolves cellulose without degrading it via the unwanted reactions of the solvent's carbene content, and it might be possible to even increase the solubility by choosing an IL without the capacity to form carbenes. These highly important findings suggest that there is further potential in ILs to improve their capacity in cellulose processing, and it is clearly worth putting more efforts into designing further ILs and processes for valorizing biomass cellulose.

3.3. Structure and Lifetimes in Ionic Liquids and their Mixtures

Sascha Gehrke[†,‡] , Michael von Domaros[†] , Ryan Clark[§] , Oldamur Hollóczki[†] , Martin Brehm[¶] , Tom Welton[§] , Alenka Luzar[‖] , Barbara Kirchner[†,*]

Faraday Discussions, 2018, Volume **206**, Pages 219–245

DOI: 10.1039/C7FD00166E

Received: May 09, 2017

Published: July 11, 2017

Adapted with permission from *Faraday Discussions*.
For this article a Supporting Information is available free of charge at:
`http://www.rsc.org/suppdata/c7/fd/c7fd00166e/c7fd00166e1.pdf`

Contributions to the manuscript:

- Setup and maintenance of all calculations
- Development of the analysis program
- Analysis of the trajectories
- Writing the technical part of the manuscript

[†]Mulliken Center for Theoretical Chemistry, University of Bonn, Beringstr. 4+6, D-53115 Bonn, Germany
[‡]Max Planck Institute for Chemical Energy Conversion, Stiftstr. 34–36, D-45470 Muelheim an der Ruhr, Germany
[§]Imperial College London, South Kensington Campus, London SW7 2AZ, UK
[¶]Theoretical Chemistry, Martin-Luther-University Halle-Wittenberg, Universitaetsplatz 10, D-06108 Halle, Germany
[‖]Department of Chemistry, Virginia Commonwealth University, Richmond, USA
[*]kirchner@thch.uni-bonn.de

As the second milestone of the thesis the introduction of a method to extract a parameter in order to quantify the availability of a carbene was proposed. Due to the fact, that the availability is among others connected to the dynamics of the carbene–solvent hydrogen bonds the average lifetime of such a hydrogen bond appears to be a promising candidate for a suitable parameter. Subsequently, a robust and reliable method for the analysis of hydrogen bond dynamics needs to be available.

One sophisticated method of this kind is the reactive flux approach described in Section 2.1. In this chapter the implementation of this analysis into the TRAVIS software package is described. Furthermore, the performance of the method is tested in a first set of case studies.

Abstract

With the aid of molecular dynamics simulations, we study the structure and dynamics of different ionic liquids systems, with focus on hydrogen bond, ion pair and ion cage formation. To do so, we report radial distribution functions, their number integrals, and various time-correlation functions, from which we extract well-defined lifetimes by means of the reactive flux formalism. We explore the influence of polarizable force fields vs. non-polarizable ones with downscaled charges (± 0.8) at the example of 1-butyl-3-methylimidazolium bromide and we use 1-butyl-3-methylimidazolium trifluoromethanesulfonate to investigate the impact of temperature and mixing with water as well as with chloride. Smaller coordination numbers, larger distances, and tremendously accelerated dynamics are observed when the polarizable force field is applied. The same trends are found with increasing temperature. Adding water decreases the ion-ion coordination numbers whereas the water-ion and water-water coordination is enhanced. A domain analysis reveals that the nonpolar parts of the ions become more dispersed when water is added and that water clusters increase in size. The dynamics accelerates in general upon addition of water. In the ionic liquid mixture, the coordination number around the cation changes between the two anions, but the number integrals of the cation around the anions remain constant and the dynamics slows down with increasing content of the chloride ionic liquid.

3.3.1. Introduction

Many properties of ionic liquids,[133] with much emphasis on their structures[152,319–322] and some references to slow dynamics (for an overview, see Reference 323), have been widely discussed from theoretical methods in literature.[152,319,321,322] For example, the mesoscopic segregation of the polar and nonpolar moieties in the liquid has been studied by theory qualitatively[324–326] and quantitatively.[321,327–330] However, their hydrogen bond (how long does a hydrogen bond (HB) exist?) and ion pair (how long does an ion pair (IP) exist?) as well as ion cage (IC) (how long is an ion surrounded by the counter-ions?) fast dynamics were not this intensively considered.[158,198–203]

Most hydrogen bonds are non-linear in ILs, especially if the ILs are apolar and based on imidazolium cations, such that the donor is a C-H group[154] which is well-known in literature to form weak hydrogen bonds.[146,331] This particular non-linearity was explained by Hunt and coworkers[157,332] as a stabilization by areas of local electron depletion, which occurs between the substituents on the imidazolium ring. The regions of reduced electron density extend over quite a large area, thus allowing anions to adjust relatively freely instead of strictly being linear.[332] Statical quantum chemical methods indicated that the hydrogen bond is not the most important interaction for ion pairs with respect to the total interaction energy.[154] In contrast, different established analysis methods gave rise to hydrogen bonding in several ion pairs, thus the presence and importance of hydrogen bonds in ILs are undoubtedly proven from theory[153,154,332–334] and experiment.[335–337] However, the question of how long a particular anion-cation co-conformer is populated in the liquid state has not been extensively studied as stated above.[153] In Reference 153 it was concluded that the term "hydrogen bond" should, for now, be treated with care to characterize the cation-anion contacts.

Besides hydrogen bonding and its duration times, already on the level of cation-anion association, i.e., ion pairing, much controversies has appeared in literature.[314,315,338] The major reason for this stems from the indirect nature of measurement of the extent of the ion pairing, which often relies on heavy assumptions, such as unity charges in the supporting equations. Previously, it was shown[313–315,339–341] that using unity charges for ILs is questionable, because a substantial charge transfer is taking place in ILs.[313–315,341] By slightly shifting from the salt-like to a molecular liquid-like system via the decreased charges, the charge transfer also fluidizes the ionic liquid.[314,315]

The dynamics of ILs in terms of lifetimes was studied previously.[158,198–200,202,203,342] In *ab initio* molecular dynamics (AIMD) simulations of $[C_2C_1Im][SCN]$ (HB donor-acceptor-hydrogen atom angle = 30°), the geometric picture indicated a superior role in terms of strength for the most acidic hydrogen bond (at H2, see Figure 3.19 for labeling) as compared to the two other hydrogen atoms at the rear, in accordance with literature.[199] However, the continuous (for definition see next section) hydrogen bond dynamics at H2 was observed to decay faster than the corresponding dynamics at the rear protons of the imidazolium ring (H4 and H5). Neglecting the directionality led to a dynamics which reflects the geometrical analysis and which is in accordance to a non-linear hydrogen bond as discussed by Hunt and coworkers.[157,334] Two movements were identified, first, a fast (<0.3 ps) hopping of the anion above and below the imidazolium ring and second,

translational motion of the anion away from the cation in-plane of the imidazolium ring (5-10 ps).[199]

In a molecular dynamics simulation (MD) study of [C_4C_1Im][PF_6] (HB angle = 30°) weak hydrogen bonds were found as indicated by their short lifetimes, which resulted from the fast rotational motion of anions.[200] As the magnitude of the activation energy related to the hydrogen bond relaxation time was observed to be close to the activation energy for anion reorientation, it was assumed that the rotation of the anion leads to rapid breaking and forming/re-forming of hydrogen bonds.[200]

Comparing the hydrogen bond and the ion pair dynamics,[202] the shortest correlation time for the continuous hydrogen bond dynamics was again observed for the most acidic hydrogen atom (H2) in [C_4C_1Im][Br] (studied at 360, 373, 402, 431, and 460 K and at an 30° angle criterion), closely followed by the continuous hydrogen bond dynamics of the rear hydrogen atoms (H4 and H5) in accordance with literature.[198–200] The correlation time for the continuous ion pair dynamics (for an ion pair consisting only of one cation and its nearest anion) was only one order of magnitude larger. If instead an ion cage dynamics based on a distance criteria to include all neighboring counter-ions was applied, the dynamics was found to be another order of magnitude larger.[202] Correlation times for the reorientation of the different cation parts were also considered and they were found to be larger than the correlation times of the continuous hydrogen bond dynamics and the correlation times of the continuous ion pair dynamics.[202] The largest correlation time for reorientation was calculated for the imidazolium ring. It was observed to be on the same time scale as the continuous cage dynamics.[202]

Using MD simulations, different charges on the cation and anion of the [C_4C_1Im][Br] IL were studied.[158] Increasing the strength of the hydrogen bond led to a reduced mobility. Interestingly, the extreme situation of the anti-hydrogen bond (negative charge at the proton) also affected the properties at the other hydrogen atoms. Large effects of the altered charges were reflected in the ion pair dynamics. This is probably due to the fact that often the next neighbor determining the IP was the one at the most acidic proton for which the charge was altered. There were also large effects in the IC dynamics if the total charge or the hydrogen bond situation was changed. The cage and ion pair dynamics correlated well to transport properties.[158]

Pensado *et al.* found while comparing for AIMD dispersion-corrected to uncorrected density functional theory[342], that a given cation of [C_2C_1Im][SCN] (398.15 K, HB angle = 50°) preserves its environment a longer time when dispersion is considered. The relaxation times of the dispersion-corrected trajectory were around twice of those from the uncorrected trajectory. The effect of including dispersion corrections led also towards slower intermittent hydrogen-bond dynamics of the system. The HBs formed survived for a shorter time when dispersion was not taken into account, suggesting that important interactions between the anions and cations are omitted.[342]

HB dynamics have been investigated for [C_2C_1Im][Cl] (450.0 K) and [C_4C_1Im][Cl] (353.15 K) by Hunt and coworkers at the HB angle of 30 and 60°.[203] The average HB number remained constant in a 100 K range, but the underlying dynamics of the HB changed dramatically.[203] The deformations of angles were found to be more relevant than bond stretching in determining the dynamics of individual HBs. A decay

occurred on two time scales related to the magnitude of the deviation from linearity. For the intermittent HB a strong temperature dependent repeated breaking and reforming over a longer timescale was observed. In $[C_2C_1Im][Cl]$ (450.0 K) hydrogen bonding with ring and alkyl chain hydrogen atoms occurred, ring reorientational dynamics was anisotropic and the corresponding dynamics were similar to the intermittent HB dynamics. In $[C_4C_1Im][Cl]$ (353.15 K) ring hydrogen atoms dominated the hydrogen bonding and intermittent HB lasted for ≈5 ns, ring reorientation occurred on a much slower timescale. The $[C_2C_1Im][Cl]$ (450.0 K) favored single HBs, but the individual ions often changed, while the $[C_4C_1Im][Cl]$ (353.15 K) favored bifurcated HBs with the same co-located ions.[203]

Very interesting model studies were carried out by Spohr and Patey.[343–345] They built up simple models in MD simulations. In the first study, the influence of ion size disparity was investigated.[343] The electrical conductivity first increased with size disparity, next it remained constant, then it decreased such that the conductivities of the 1:1 and 5:1 (cation:anion) systems were similar. This behavior was explained by competing influences of both ion diffusion leading to an enhancement and ion densities with the effect of reduction of conductivities at constant packing fraction.[343] In the second model, the influence of charge location (cation charge moved away from its center of mass) on the structure and transport properties was investigated.[344] As the charge was moved off center, the electrical conductivity initially increased, and the shear viscosity decreased. However, after a certain threshold this behavior was reversed. The formation of directional ion pairs that possess lifetimes (the correlation function decays in this case simply exponential) strongly influenced the liquid properties.[344] The further the charge was moved off, the longer the directional ion pairs existed. These lifetimes ranged from 0.03 to 90 ps. The authors concluded that the directional ion pairing explains the anomalously low conductivities and high viscosities observed for some ILs.[344] A combination of both effects (size disparity and charge location) were investigated in a third study.[345] The upturn in viscosity with larger size disparity and charge delocation was suggested to be mainly associated with directional ion pairs and the formation of such pairs was mostly determined by charge delocation. This observation was further supported by the fact that an increase in ion pair lifetimes coincided with the increase in viscosity for all models,[345] which is in turn in agreement with the correlation of ion cage and ion pair dynamics to transport properties in a realistic IL system.[158]

A pragmatic approach to harvest this correlation between ion pair dynamics and transport properties was recently suggested by Maginn and coworkers.[346] Based on previously established correlations between certain dynamics (ion pair and ion cage) in ILs and macroscopic properties[158], they suggested to correlate the inverse of the ion pair dynamics in a single universal linear relationship to self-diffusivities and ideal ionic conductivities.[346] This relationship was independent of the type of IL and temperature. Considering the variety of ILs which were studied, their observation strongly suggested that the dynamics of ILs follow a universal mechanism governed by the formation and breaking of ion pairs and ion cages.[346]

Similarly, a computational study of the molecular origin of viscosity and subsequent correlation of the quantitative structure-property relationship approach and molecular

dynamics simulations were carried out by Müller-Plathe and coworkers.[347]

HB dynamics of molecular liquids such as water (bulk and confined) has been extensively discussed in the literature.[211,213,228,229,348–356] For an excellent overview see Reference 229. In the pioneering work of Luzar and Chandler (Reference 228) it was demonstrated that the bond making and breaking are simple processes characterized by well-defined rate constants. What makes the HB dynamics apparently complicated is translational diffusion that introduces a continuum of time scales. They showed that this kinetics is understood in terms of the interplay between diffusion and HB dynamics. In their phenomenological model, translational diffusion determines whether a specific pair of water molecules are neighbors, and hydrogen bonds between such pairs form and persist at random with average lifetimes given by rate constants for bond breaking and reforming.[228]

Holm and coworkers were the first to determine reactive flux hydrogen bond lifetimes[198] for ILs (HB angle = 30°) and found them in the range of estimated values from the dielectric relaxation method. The following order of long lifetimes was observed: $[C_2C_1Im][Cl]$ (360 K) > $[C_2C_1Im][NTf_2]$ (288 K) > $[C_2C_1Im][BF_4]$ (257 K), which is due to the distribution of partial charges and the formation of networks in multi-atomic anion ILs.[198] Of course, the interactions of the anions and the imidazolium ring hydrogen atoms are stronger than those with the side chain hydrogen atoms.[198] The calculated hydrogen bond lifetimes were in the same order of magnitude as those of pure water and of some small primary alcohols.[198]

In this article, we evaluate the dynamics of one pure IL ($[C_4C_1Im][Br]$) applying a polarizable and standard (non-polarizable) force field. We investigate $[C_4C_1Im][OTf]$ (3-butyl-1-methylimidazolium trifluoromethanesulfonate) at different temperatures and mixed with water. Difficulties when simulating water and ILs have been discussed by Maginn and coworkers.[357] Furthermore we consider the dynamics in $[C_4C_1Im][Cl]/[OTf]$. We reflect on the structure and then consider continuous as well as intermittent dynamics. For the HB and the IP we also investigated reactive flux dynamics. In the final section we consider a possible correlation between intermittent as well as reactive flux IP dynamic and experimental viscosities. We end the article with some conclusions.

3.3.2. Theory of reactive flux dynamics and definitions

In the following, the methodology to describe hydrogen bond kinetics in liquid water introduced by Luzar and Chandler will be shortly summarized, for a full description the reader is referred to the original articles[228,229,349] or to Section 2.1. The method relies on the definition of a hydrogen bond population operator $h(t)$, which equals unity if a particular *tagged* pair of (water) molecules is hydrogen bonded and zero otherwise. As described below, in our selected ILs the cation is the hydrogen bond donor and the anion is the hydrogen bond acceptor for the pure ILs and for the IL mixtures. For the ILs mixed with water all three combinations cation-anion, cation-water and water-anion will be considered. Furthermore, we will also consider the population of ion pairs and ion cages as previously introduced by us.[158,202]

The time/ensemble average $\langle h \rangle$ (denoted by chevrons) of the population operator can be interpreted as the probability that a pair is hydrogen bonded. In an infinite or sufficiently large system, that probability will be zero and it is often neglected; in smaller systems, it won't, thus it shall be explicitly considered here. Using $h(t)$ or its fluctuation from equilibrium $\delta h(t) = h(t) - \langle h \rangle$, one can define a hydrogen bond time-correlation function

$$c(t) = \frac{\langle \delta h(t)\, \delta h(0) \rangle}{\langle \delta^2 h(0) \rangle} \approx \frac{\langle h(t)\, h(0) \rangle}{\langle h(0) \rangle}, \tag{3.3}$$

where the approximation holds if the system is sufficiently large, so that $\langle h \rangle \approx 0$, which implies $\delta h(t) \approx h(t)$. This function measures the fluctuations of hydrogen bond populations in time, independent of possible bond breaking events, i.e., it is an intermittent time-correlation function, as introduced by Rapaport.[213] It can also be interpreted as the conditional probability that an initially hydrogen bonded pair is still bonded at a time t later. Apart from these intermittent time-correlation functions, we will also consider the corresponding continuous functions for all dynamics (HB, IP and IC).[213] Contrary to the intermittent function the HB is broken once donor and acceptor depart from each other even for a short time only and if they reform to HB afterwards.

According to Onsager's regression hypothesis, the same laws that govern the time evolution of the hydrogen bond time-correlation function, drive the decay of an initial non-equilibrium population $\overline{\delta h}(0)$ towards the equilibrium, with $\overline{\delta h}(t) = \overline{h}(t) - \langle h \rangle$. Thus

$$c(t) = \frac{\langle \delta h(t)\, \delta h(0) \rangle}{\langle \delta^2 h(0) \rangle} = \frac{\overline{\delta h}(t)}{\overline{\delta h}(0)}, \tag{3.4}$$

where the overlines denote a non-equilibrium average. The rate of relaxation to equilibrium is given by

$$k(t) = -\dot{c}(t) = \frac{\left\langle h(t)\, \dot{h}(0) \right\rangle}{\langle \delta h^2(0) \rangle} = -\frac{\left\langle [1 - h(t)]\, \dot{h}(0) \right\rangle}{\langle \delta h^2(0) \rangle}, \tag{3.5}$$

which follows from the definition of $c(t)$, by exploiting the time invariance of time-correlation functions, and because of the identity $\left\langle \dot{h}(0) \right\rangle = 0$. The quantity $-\dot{h}(0) = -(dh/dt)_{t=0}$ is the integrated flux departing the hydrogen bond configuration space at time zero. The function $k(t)$ measures the average of that flux for those trajectories, where the bond between a tagged pair of molecules is broken at a time t later, hence its name: reactive flux hydrogen bond time-correlation function. Its zero time value is the transition state theory estimate of the rate of relaxation, k_{TST}.[211] In the reactive flux formalism k_{TST} is corrected by a time dependent transmission coefficient.[358]

In bulk water, $k(t)$ reveals several motions leading to bond breaking.[349] A quick change on the time scale of 0.1 ps which is primarily due to librations, followed by interoxygen vibrations on time scales of 0.1 to 0.2 ps. Beyond that transient period of ~ 0.3 ps, a continuum of timescales follows, resulting in a monotonic, non-exponential decay. Luzar and Chandler showed[228,229] that this behavior can be understood with a simple diffusion picture: After bond-breaking, a pair can drift apart, and similarly, diffusion of two

molecules towards each other can lead to bond-reforming. In order to investigate this, they separated the contributions to $k(t)$ according to whether a pair did or did not move apart after bond breaking i.e, by investigating the *restrictive* reactive flux time-correlation function

$$k_{\text{in}}(t) = -\frac{\left\langle H(t)\left[1-h(t)\right]\dot{h}(0)\right\rangle}{\langle \delta h^2(0)\rangle}. \tag{3.6}$$

The vicinity operator $H(t)$ is responsible for that partitioning. It is unity if the particular tagged pair has not yet drifted apart and zero otherwise. Thus, in the case of water it is usually defined as the oxygen atom–oxygen atom distance not further apart than the first minimum distance of the RDF, thus 350 pm. The conditional probability that an initially bonded pair is broken, but has not drifted apart at a time t is given by

$$n(t) = \int_0^t k_{\text{in}}(\tau)\, d\tau = \frac{\langle H(t)\left[1-\delta h(t)\right]\delta h(0)\rangle}{\langle \delta h^2(0)\rangle}. \tag{3.7}$$

The probabilities $c(t)$ and $n(t)$ correspond to *local* populations that can interconvert. A phenomenological description of their kinetics that is consistent with simulation data is

$$-\dot{c}(t) = k_f c(t) - k_b n(t), \tag{3.8}$$

where the forward and backward rate constants k_f and k_b are the rate constants of hydrogen bond breaking and forming. The physical meaning of $\tau_{\text{HB}} = 1/k_f$ is that of the average hydrogen bond lifetime.

For our three dynamics, hydrogen bond, ion pair, and ion cage we always define a population operator in analogy to Luzar's[228,229] hydrogen bond population operator $h(t)$ as described above for the hydrogen bond.

The events are populated

- as a hydrogen bond, if the donor-acceptor-hydrogen atoms are arranged in an angle of less than 60 degrees (see also Figure 3.21 as an example) and if the acceptor and the hydrogen atom are closer than the first minimum of the RDF. Furthermore, if we consider the reactive flux correlation function the center of ring of the imidazolium cation (c(R)) and the center of mass of the anion (c(A)) should be closer than the distance of the first minimum in the RDF.

- as an ion pair, if cation and anion are nearest neighbors with respect to the center of ring of the cation and the center of mass of the anion distance. Furthermore, if we consider the reactive flux correlation function the c(R) and the c(A) should be closer than the distance of the first minimum in the RDF. Please note, this definition can be generally applied to center of mass/ring. Although the name is not correct with respect to physics we keep it in order to be able to compare to literature.

- as an ion cage, if the central ion is surrounded by counter-ions in a radius smaller than the first minimum of of the RDF between the c(R) and c(A). Thus, more than one neighbor is considered for the central ion.

3.3.3. Systems investigated

In this study we consider the following IL systems:

- The $[C_4C_1Im][Br]$ liquid (standard and polarizable force field[359,360]) at 386 K.
- A temperature dependent investigation at 293 K, 323 K, 353 K, 373 K, and 393 K of $[C_4C_1Im][OTf]$.
- The ionic liquid/molecular liquid mixture $[C_4C_1Im][OTf]$ water at four different mole fractions of the IL (0.39, 0.58, 0.66 and 0.82) taken from Reference 361 at 293 K.
- The ionic liquid mixture $[C_4C_1Im][Cl]/[OTf]$ at x = 0.000, 0.192, 0.303, 0.402 mole fraction of $[C_4C_1Im][Cl]$ at 298 K.

The computational details can be found in Appendix A.4.

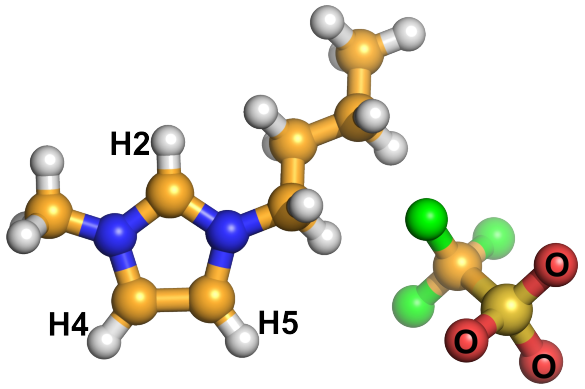

Figure 3.19.: Labeling as used in the article. Left: 1-butyl-3-methylimidazolium cation and right: trifluoromethanesulfonate (triflate) anion. (Brown: carbon; blue: nitrogen; white: hydrogen; red: oxygen; yellow: sulfur; green: fluorine)

3.3.4. Results: Structure

Polarizable force field

In Figure 3.20 we observe the typical RDF for the ring hydrogen atoms with a simple anion like $[Br]^-$. The location of the first maximum and minimum together with the coordination number obtained from the corresponding number integrals (at the distance of the minimum) can be found in Table 3.8. Obviously H2 forms stronger hydrogen bonds than the H4/5, because it is more acidic,[154,332] which is reflected in higher peaks and larger coordination number per hydrogen atom. This is in agreement with MD simulations and empirical refinement to model experimental data by Bowron *et al.*, where the authors also found a more pronounced coordination at H2.[362] Upon applying the polarizable force field larger distances are found, see also Reference 363. Furthermore,

the coordination number decreases with polarizable force field, see Table 3.8, but the relative behavior remains the same. The ions are surrounded by approximately five counterions, also here the polarizable force field decreases the number slightly.

Unfortunately, the force field is unable to resolve distance differences at the ring protons, which are, for example, observed in AIMD simulations[199] and experiments.[364] Thus, the approach by Maginn to treat the ring protons on equal footing when applying ff-MD seems reasonable.[346] In the present work, we distinguish front (H2) and rear (H4 and H5) hydrogen bonding.

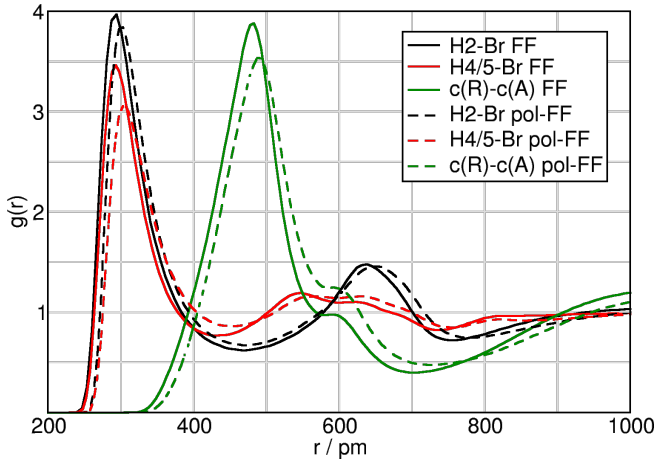

Figure 3.20.: Cation-anion radial distribution functions (RDFs). Black: H2; red: H4/5; dark green: RDFs between center of ring c(R) and center of mass anion c(A). Solid line: standard force field; dashed line: polarizable force field. Please note, for clarity we show only a range of the RDF, the full functions can be found in the SI, these decay properly to 1.

Table 3.8.: Distance of first maximum r(max), first minimum r(min) and number integral (NI) at r(min) from the reference to the observed particle in $[C_4C_1Im][Br]$ for H2 and H4/5 as well as for center of ring-$[Br]^-$ (c(R)–c(A)). $\bar{N}I$ is the number integral from the reference to the observed particle. If no number is given, NI=$\bar{N}I$. "FF": standard force field; "pol-FF": polarizable force field. $T = 386$ K.

	H2-Br	H4/5-Br	c(R)–c(A)
	r(max)/r(min)/NI/$\bar{N}I$		
FF	293/468/1.6	293/428/1.3/2.5	483/703/5.3
pol-FF	303/473/1.4	303/458/1.3/2.6	488/723/5.0

Table 3.9.: r(max), r(min), NI and $\bar{\text{N}}$I as in table 3.8, in $[C_4C_1Im][OTf]$ for H2-O, H4/5-O and c(R)–c(A) at different temperatures.

T	H2-O	H4/H5-O	c(R)–c(A)
	r(max)/r(min)/NI/$\bar{\text{N}}$I		
293	263/403/2.7/0.9	258/373/1.9/1.2	528/793/6.0
323	258/408/2.7/0.9	258/378/1.9/1.2	528/793/5.9
353	258/403/2.6/0.9	258/373/1.7/1.2	533/793/5.8
373	258/403/2.5/0.8	258/378/1.8/1.2	533/798/5.8
393	258/403/2.4/0.8	263/383/1.8/1.2	533/798/5.8

Temperature dependency

The temperature dependent RDFs are shown in the Supporting Information of the article and the corresponding distances of first maximum r(max), first minimum r(min) as well as the coordination numbers from the number integrals are listed in Table 3.9.

Obviously, there is more variation in peak height than in peak position (see SI). Since the uncertainty of the distances is ∼5 pm, we are unable to resolve these subtle changes within the present temperature range. However, a rough trend is in bond elongation with temperature and thus in a weakening of the HB, which goes along together with a decrease in coordination number *quod vide* peak heights. The exception is the very low temperature of 293 K, which is already close to the melting temperature of 290 K measured by Tokuda *et al.*,[338] and 286 K measured by Brennecke and coworkers.[365] Interestingly, the coordination number at 373 K and 393 K is much larger than that for the bromide at 386 K, which is probably due to the fact that three oxygen atoms are available for coordination instead of only one bromide ion. On average the cation is surrounded by $5.8 - 6$ $[OTf]^-$ anions, while it is surrounded by only approximately 5.3 $[Br]^-$ anions. Hardacre *et al.* obtained similar results (at 323 K by MD and neutron scattering) via integrating up to 750 pm from the ring center of mass, namely 5.3 for $[C_4C_1Im][PF_6]$ 4.9 for $[C_6C_1Im][PF_6]$ and 4.4 for $[C_8C_1Im][PF_6]$ or 6.8 for $[C_1C_1Im][PF_6]$.[366] Furthermore, Bowron obtained (at 323 K from MD and neutron diffraction) 6.9 for $[C_2C_1Im][OAc]$ by integrating up to 700 pm.[362]

In the combined distribution functions (CDFs), given in Figure 3.21, the occurrences of different HB geometries are shown for two temperatures. It is apparent that for the IL the choice of donor–acceptor-hydrogen angle of 60° is reasonable and the temperature dependency in the first (below 200 pm) but even more in the second peaks (∼ 600 pm) is visible.

Mixture of IL with water

The c(R)–c(A), c(A)–c(W) and the c(R)–c(W) RDFs are shown in Figure 3.22 color-coded for different mole fractions. It is apparent that all three functions display a pre-shoulder. Post-peaks are also observable for the c(R)–c(A) and the c(W)–c(A) function indicating a rather complex coordination pattern with multiple interaction sites.

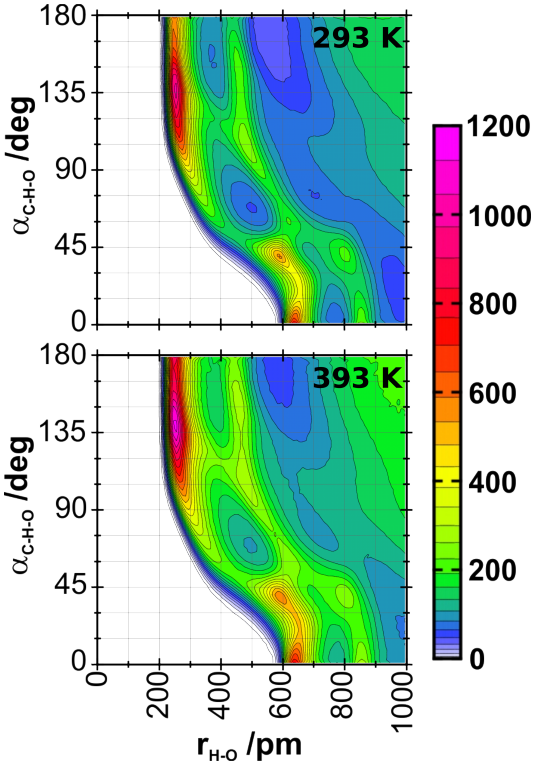

Figure 3.21.: CDFs for occurring HB geometries in $[C_4C_1Im][OTf]$, HB angle ($\alpha_{C\text{-}H\text{-}O}$) vs. the HB distance ($r_{H\text{-}O}$).

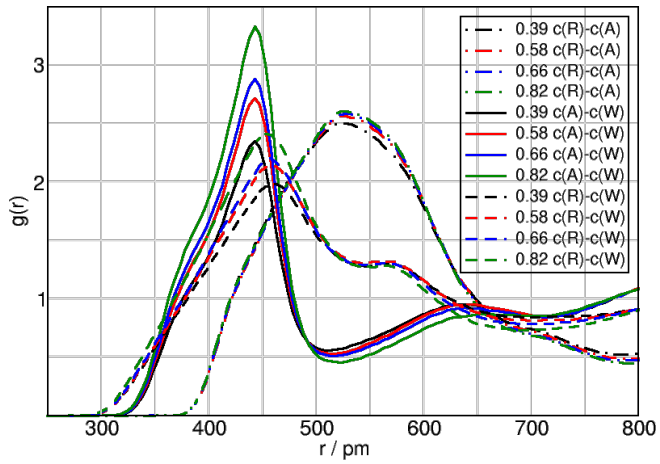

Figure 3.22.: RDFs of $[C_4C_1Im][OTf]$/water. Dashed-dotted: c(R)–c(A); Solid: c(A)–c(W); Dashed: c(R)–c(W). Black: $x_{IL} = 0.39$; Red: $x_{IL} = 0.58$; Blue: $x_{IL} = 0.66$; Green: $x_{IL} = 0.82$. Please note, for clarity we show only a range, the full functions can be found in the SI. These decay properly to 1.

Table 3.10.: R(max), r(min), NI and $\bar{\text{N}}$I as in Table 3.8, in [C_4C_1Im][OTf]-water for c(R), c(A)) and c(W) for different mole fractions. Temperature = 293 K. x_{IL} gives the mole fraction of the IL. Ring hydrogen functions are given in the SI. The last block shows the domain count[329] and the number of molecules per domain/cluster.

x_{IL}	c(R)–c(A)	c(W)–c(W)
	r(max)/r(min)/NI/$\bar{\text{N}}$I	
0.39	528/783/5.3	273/343/2.1
0.58	533/788/5.6	273/348/1.6
0.66	528/793/5.8	273/353/1.3
0.82	528/788/5.8	273/348/0.8
x_{IL}	c(R)–c(W)	c(A)–c(W)
	r(max)/r(min)/NI/$\bar{\text{N}}$I	
0.39	463/703/5.8/3.8	443/513/1.9/1.2
0.58	458/703/3.0/4.0	443/513/1.1/1.4
0.66	458/703/2.1/4.1	443/513/0.8/1.5
0.82	453/713/1.0/4.2	443/523/0.4/1.8
	Domain count	
x_{IL}	Polar	Nonpolar	Water
0.39	1.0 (197)	5.9 (33)	24.8 (12)
0.58	1.0 (288)	6.8 (42)	53.0 (4)
0.66	1.0 (330)	6.8 (49)	59.1 (3)
0.82	1.0 (410)	6.6 (62)	52.8 (2)

Upon dilution, *i.e.*, going from green to black, all functions show a decrease in their first peak heights. In the case of the cation-anion interplay this means that the cation-anion coordination decreases from 5.8 to 5.3, see Table 3.10. The number integrals for water-water (c(W)–c(W)) increase upon dilution. For the mixed IL-water interactions (c(R)–c(W) and c(A)–c(W)), we observe the same trends, see Table 3.10, all coordination numbers increase when more water is added. This trend is not observed for the water-IL interaction. The number integrals decrease slightly upon dilution. Interestingly, the cations are surrounded by much more water molecules than the anions, which can be explained by the significantly lager surface of the cations, and also through considering the hydrophobic nature of the fluorinated moiety of the anion.

Beside the local structure arising from hydrogen bonding and other polar-polar interplay between the water and the IL and between the IL ions, the mesoscopic behavior of the components within the liquid must also be analyzed to discuss and understand the full structure of the IL-water mixtures, and the underlying dynamic processes. With our newly developed domain analysis tool[329] it is possible to analyze how the defined logical units (subsets) of the liquid are arranged in the system, that is, if they are systematically connected to one another to form larger clusters or domains. In this particular case we distinguished polar (anions, and the imidazolium ring with the CH_2 and CH_3 units connected to the nitrogen atoms), nonpolar (propyl group of the cation) and water as subsets. The corresponding data is presented in Table 3.10. Interestingly, the polar moi-

eties stick together in all simulations, even in the most dilute systems. In contrast, but in agreement with previous simulations on pure ILs,[321,326] the nonpolar moieties do not form a continuous domain in the liquid, as the spatial extent of the present side chains is not sufficient for such behavior. Instead, these alkyl groups apparently form smaller islands in the liquid, which gradually increase in size over the increase of the mole fraction of the IL in the solution. Finally, and perhaps most interestingly, the water molecules remarkably change their behavior through the concentration range considered here. While in case of the lowest mole fraction of the IL the water molecules form large clusters, consisting of on average 12 molecules, at the other extreme of the concentration range they are often present as single molecules in the solution, and on average as dimers.

Ionic liquid mixture

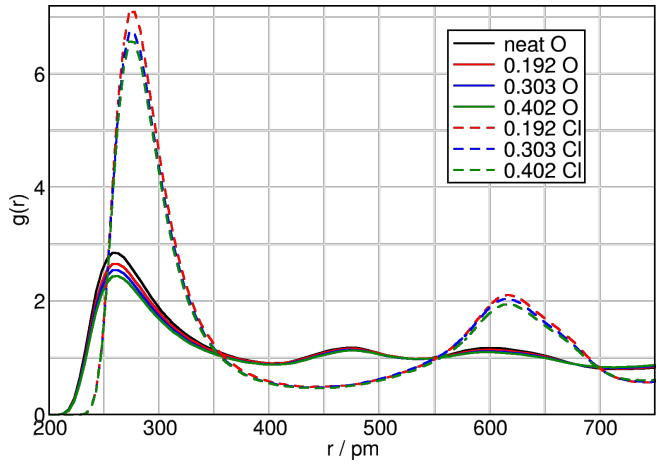

Figure 3.23.: Chloride mole fraction dependent H2-O/Cl RDFs of $[C_4C_1Im][OTf]/[Cl]$. Please note, for clarity we show only a range, the full functions can be found in the SI. These decay properly to 1.

In Figure 3.23 the chloride mole fraction dependent RDFs are given. Generally in these mole fraction regimes the oxygen atoms coordinate with shorter distances to the ring hydrogen atoms of the cations. Upon dilution of the $[C_4C_1Im][OTf]$, we observe a decrease in peak height. Inspection of the coordination numbers in Table 3.11 shows upon dilution the [OTf] anion generally decreases while the [Cl] anion coordination increases around the cation.

Table 3.11.: R(max), r(min), NI and $\bar{\text{N}}$I as in Table 3.8, in [C_4C_1Im][OTf]/[Cl] for H2-O/Cl and H4/H5-O/Cl center of mass/ring functions. x = mole fraction of [C_4C_1Im][Cl]

x	H2-O	H2-Cl	H4/5-O
		r(max)/r(min)/NI/$\bar{\text{N}}$I	
0.000	258/403/2.7/0.9	–	258/373/1.8/1.2
0.192	263/403/2.2/0.9	278/438/0.3/1.5	258/373/1.4/1.2
0.303	258/403/1.9/0.9	273/438/0.5/1.5	258/373/1.2/1.2
0.402	263/403/1.6/0.9	273/438/0.6/1.5	258/373/1.0/1.2
x	H4/5-Cl	c(R)–c(OTf)	c(R)–c(Cl)
		r(max)/r(min)/NI/$\bar{\text{N}}$I	
0.000	–	533/793/6.0/6.0	–
0.192	278/423/0.3/3.0	533/788/4.8/5.9	468/558/0.8/4.2
0.303	278/418/0.4/2.9	528/783/4.2/6.0	468/558/1.3/4.2
0.402	278/418/0.6/2.9	528/783/3.6/6.1	463/558/1.7/4.2

3.3.5. Results: Dynamics

Pure systems

Since the peak positions in the RDFs have an uncertainty of ±5 pm, the distance criteria can be defined with a certain error for the dynamic results. In order to estimate the robustness of the dynamics, we calculated the changes in the results for [C_4C_1Im][Br] with a 1 pm, 5 pm, 10 pm deviation from our standard distance criteria. For the hydrogen bond residence time we found <0.25% deviation for both the continuous and intermittent functions. For the cage dynamics the intermittent function changed by <1% for all cutoff distances, while the continuous altered by <6% for the 10 pm and only 3% for the 5 pm change in the criteria. Influences from the angular criteria (not investigated here) can be also expected.

In Table 3.12 we list the continuous and intermittent dynamics for the pure systems in order to compare to the previous simulations data.[199,202] As expected, with increasing temperature the dynamics becomes faster which fits well to the observation of increasing bond distances and reduced coordination numbers discussed in Subsection 3.3.4. The application of the polarizable force field accelerates the dynamics tremendously, even if the charge reduction should, in principle, compensate the slow dynamics in the standard force field, which it does not. Generally, the IP and HB dynamics are of the same order of magnitude. However, the IP dynamics is slower than the HB dynamics, due to the lack of directionality; the only exceptions are observed in case of the H4/5 HBs in the $[Br]^-$ system. The ion cage dynamics (considering all IPs within the first minimum radius) is one order of magnitude slower than both IP and HB in accordance with previous observations.[199,202] Interestingly, the difference between IP and IC is less pronounced in the case of the pol-FF. The continuous dynamics is in all cases faster for H2 than for H4/5. This trend is, interestingly, the opposite for the intermittent dynamics. This might indicate that the "strength" of the HB at H2 lies in its reformation, which can

make it, in that sense, longer living. This difference can clearly rise from the well-known facile switch between the "in-plane" and "on-top" positions of the anion at the H2 (shown e.g. by the spatial distribution functions[367]), which allows the frequent cleavage and formation of the corresponding HB. The anions at the H4/5 position can, on the other hand, switch between these two ring hydrogen atoms at the rear. However, to do so, the anions have to occur in the space between the H4 and H5 atoms, which is, according to the spatial distribution of the anions around the cations in such ILs,[367] not the case. This, together with the continuous and intermittent dynamics data, allows us to conclude that the change between the "on-top" and "in-plane" orientation of the anion at the H2 is more frequent than the H4-H5 change.

Table 3.12.: Continuous and intermittent dynamics of τ^{H2}: HB dynamics at H2; $\tau^{H4/5}$ at H4/5; τ^{IP} ion pair dynamics and τ^{IC} ion cage dynamics in ps. Please note, the data are obtained from the 200 ps long trajectory.

	continuous/intermittent			
system	τ^{H2}	$\tau^{H4/5}$	τ^{IP}	τ^{IC}
$[Br]^-$-FF	0.7/188	1.1/172	0.9/221	74.2/942
$[Br]^-$-pol-FF	0.6/24	0.7/ 19	0.6/27	20.6/108
$[OTf]^-$-293	0.9/1165	1.1/946	3.7/3069	169.9/14969
$[OTf]^-$-323	0.7/365	0.9/309	2.5/996	139.2/4569
$[OTf]^-$-353	0.6/180	0.8/144	2.3/490	112.0/2222
$[OTf]^-$-373	0.6/109	0.7/84	1.9/293	93.1/1295
$[OTf]^-$-393	0.5/78	0.6/60	1.7/205	84.8/896

The reactive flux hydrogen bond data is exhibited in Table 3.13. The increase in the dynamics with both polarizable force field and increasing temperature is also apparent in the reactive flux data. In all cases the lifetimes of the H2 are faster than those of H4/5. Differences in the breaking and reforming of the HB are also visible when comparing the lifetimes of the forward and the backward reaction. Comparing the reactive flux HB data with the IP results in Table 3.14, we observe also for these dynamics that IP is in general slower that the HB process. The differences reduce at higher temperatures. Again, the breaking and re-formation process are not the same, see forward and backward lifetimes. But now the differences are much more pronounced than for the HB process. However, the rate of relaxation, k_{TST} is in all cases of similar size.

For the ion pair dynamics we also show the correlation functions corresponding to the reactive flux dynamics in Figures 3.24-3.26. In Figure 3.24 the semi-log plot of the ion pair rate function $k(t)$ for $[C_4C_1Im][Br]$ exhibits the according decay. The rate function $k(t)$ and thus $c(t)$ do not decay mono-exponentially, otherwise the graph in Figure 3.24 would be a straight line. Thus, the dynamics cannot be represented by a simple decay process, and lifetimes cannot be determined simply by integration. At short times of $k(t)$ (0.35 and 0.5 ps in the inset of Figure 3.24) motions leading to ion pair breaking are visible. The restricted rate function $k_{in}(t)$ from which by integration $n(t)$ is obtained can be seen in Figure 3.25.

In Figure 3.26 we show the correlation plot relating the functions $c(t)$, $n(t)$ (see SI) and $k(t)$. At shorter times, the expected deviations occur. However, at larger values there are also deviations, which might origin from strong statistical uncertainties and which show that further simulations have to be carried out with varying simulation parameters in order to arrive at clearer behaviors of the unity plot.

Table 3.13.: Reactive flux HB lifetimes for the forward $\tau_{\mathrm{f}}^{\mathrm{HB}}$, the backward reaction $\tau_{\mathrm{b}}^{\mathrm{HB}}$, and the transition state theory estimate of the rate of relaxation, k_{TST}. All data are given in ps and are obtained from the 10 ns trajectory.

system	$\tau_{\mathrm{f}}^{\mathrm{H2}}$	$\tau_{\mathrm{b}}^{\mathrm{H2}}$	k_{TST}
$[\mathrm{Br}]^-$-FF	52	110	1.77
$[\mathrm{Br}]^-$-pol-FF	14	25	2.05
$[\mathrm{OTf}]^-$-293	304	569	1.84
$[\mathrm{OTf}]^-$-323	107	204	1.89
$[\mathrm{OTf}]^-$-353	51	97	1.81
$[\mathrm{OTf}]^-$-373	27	51	2.01
$[\mathrm{OTf}]^-$-393	21	41	1.80
system	$\tau_{\mathrm{f}}^{\mathrm{H4/5}}$	$\tau_{\mathrm{b}}^{\mathrm{H4/5}}$	k_{TST}
$[\mathrm{Br}]^-$-FF	60	125	1.14
$[\mathrm{Br}]^-$-pol-FF	23	51	1.73
$[\mathrm{OTf}]^-$-293	443	924	1.26
$[\mathrm{OTf}]^-$-323	179	408	1.34
$[\mathrm{OTf}]^-$-353	99	236	1.49
$[\mathrm{OTf}]^-$-373	60	146	1.60
$[\mathrm{OTf}]^-$-393	41	101	1.64

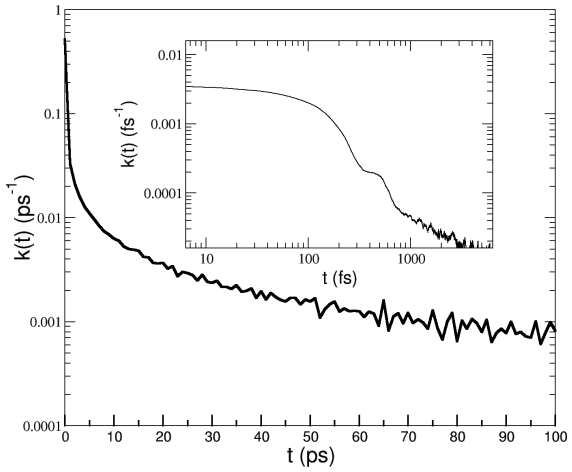

Figure 3.24.: Semi-log plot of the rate function $k(t)$ for the ion pair process in $[\mathrm{C_4C_1Im}][\mathrm{Br}]$. In the analysis the long trajectory was selected. The inset shows the analysis of the 200 ps trajectory, obviously at $0.35 - 0.5$ ps a transient period is visible.

Table 3.14.: Reactive flux IP lifetimes for the forward $\tau_{\mathrm{f}}^{\mathrm{IP}}$, the backward reaction $\tau_{\mathrm{b}}^{\mathrm{IP}}$, and the transition state theory estimate of the rate of relaxation, k_{TST}. All data are given in ps and are obtained from the 10 ns trajectory.

system	$\tau_{\mathrm{f}}^{\mathrm{IP}}$	$\tau_{\mathrm{b}}^{\mathrm{IP}}$	k_{TST}
$[\mathrm{Br}]^-$-FF	52	190	8.92
$[\mathrm{OTf}]^-$-293	611	2674	1.73
$[\mathrm{OTf}]^-$-323	240	1120	1.61
$[\mathrm{OTf}]^-$-353	126	568	1.60
$[\mathrm{OTf}]^-$-373	76	320	1.71
$[\mathrm{OTf}]^-$-393	65	228	1.65

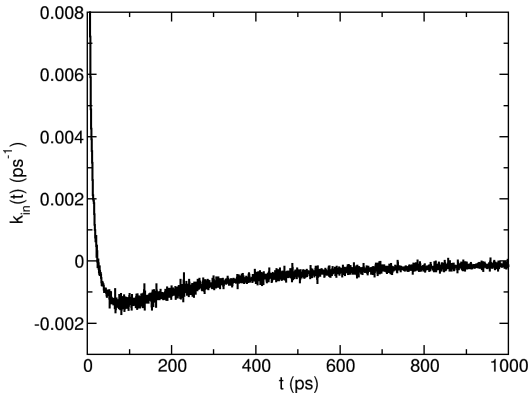

Figure 3.25.: The restricted rate function $k_{\mathrm{in}}(t)$ for the ion pair process in $[\mathrm{C_4C_1Im}][\mathrm{Br}]$. In the analysis the long trajectory was selected.

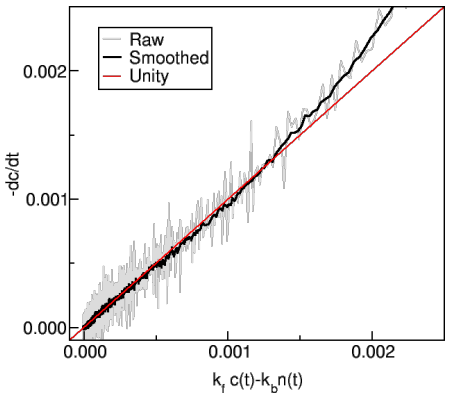

Figure 3.26.: Correlation plot for the ion pair process in $[\mathrm{C_4C_1Im}][\mathrm{Br}]$. Both axes are in ps^{-1}. In the analysis the long trajectory was selected. The fit to the line with unity slope was carried out from 160 to 8000 ps the values obtained for k_{f} and k_{b} are 0.019 ps^{-1} and 0.005 ps^{-1}, see also Table 3.12.

IL-water mixture

The intermittent c(R)–c(A) IP lifetime at $x_{\mathrm{IL}} = 0.39$ is 2048 ps, at 0.58 is 2037 ps, at 0.66 is 2552 ps, and at 0.82 is 2696 ps.

In the following we focus on the reactive flux data, since continuous as well as intermittent functions are in general problematic. The continuous HB correlation functions are ill-defined, because they strongly depend on the presumed location of the dividing surface. Thus HB lifetimes should not be extracted from continuous HB correlation function, as their values heavily depend on bond definition, as well as on the sampling frequency. While intermittent HB correlation functions are better defined in this respect, the caveat remains if these functions do not relax exponentially (which they do not in our cases, see previous Subsection 3.3.5), reflecting the fact that different dynamic processes contribute to the decay of these functions. Clearly, one should not determine intermittent HB lifetimes from the zero frequency part of the intermittent correlation function (i.e., the integral of it) or by assuming a quasi-exponential decay of these functions. Such determinations are arbitrary as the results depend on a specific interval over which these functions were studied.

It is interesting to observe that the water-water interactions exhibit slower lifetimes in the IL-rich systems, which decrease gradually toward the more moist solutions. This is somewhat surprising, since with high x_{IL} there is a higher number of available anions, which are not in interaction with other water molecules, suggesting that a cluster of water molecules would quickly break the connecting hydrogen bonds in order to interact with the stronger hydrogen bond acceptor anions instead. However, the smaller clusters of water (see Table 3.10) — often, in fact, a water dimer — in these liquids have apparently a very immobile hydrogen bond, sticking the molecules together for a longer time. With increasing water content, and therefore increasing size of water clusters, the individual water-water hydrogen bonds become significantly more mobile, which can be seen by the remarkable approximately four-fold increase in the lifetimes.

In almost all cases adding water (from $x = 0.82 \rightarrow 0.39$) leads to an acceleration of the ion pair (center of mass/ring) dynamics, see Table 3.15. An exception is given by the backward reaction of the c(R)–c(W) interplay. At low mole fraction of water, the c(W)–c(A) dynamics is faster than all the others, while at high mole fraction the water-water dynamics is the fastest. All the dynamics involving water are faster than the cation-anion function.

Considering the individual HB dynamics (Table 3.16) the lifetimes involving ions are shorter compared to those from the center of masses. It is important to point it out here that the IL anion has multiple oxygen atoms as hydrogen bond acceptors, and accordingly, while the center of mass-center of mass distance does not change notably, the individual hydrogen bonds can flip from one acceptor site to the other. Again, faster dynamics toward the more moist systems can be observed (Table 3.16). Clear trends can be observed for all forward lifetimes.

Table 3.15.: Reactive flux ion pair interplay in $[C_4C_1Im][OTf]$ water mixtures in ps. x_{IL} gives the mole fraction of the IL. 1st block: forward reaction, 2nd block: backward reaction; 3rd block: transition state theory (TST) approximation to the rate, thus a lower bound to the average IP lifetime.

		forward		
x_{IL}	$\tau_f^{c(R)-c(A)}$	$\tau_f^{c(R)-c(W)}$	$\tau_f^{c(W)-c(A)}$	$\tau_f^{c(W)-c(W)}$
0.39	399	270	287	146
0.58	454	351	328	232
0.66	487	454	387	238
0.82	500	459	407	663
		backward		
x_{IL}	$\tau_b^{c(R)-c(A)}$	$\tau_b^{c(R)-c(W)}$	$\tau_b^{c(W)-c(A)}$	$\tau_b^{c(W)-c(W)}$
0.39	1546	1201	576	156
0.58	1948	920	731	184
0.66	2064	892	933	147
0.82	2128	420	1013	467
		TST		
x_{IL}	$k_{TST}^{c(R)-c(A)}$	$k_{TST}^{c(R)-c(W)}$	$k_{TST}^{c(W)-c(A)}$	$k_{TST}^{c(W)-c(W)}$
0.39	1.56	2.57	1.14	22.20
0.58	1.56	1.70	1.69	14.12
0.66	1.64	1.28	1.86	10.61
0.82	1.62	0.68	1.95	3.37

IL-mixture

Considering the IL-mixtures in Table 3.17, slower dynamics of all interplays involving $[Cl]^-$ are found with increasing $[Cl]^-$ contents. The H-O$[OTf]^-$ dynamics becomes slower as well, except in the neat $[C_4C_1Im][Cl]/[OTf]$, where the H-O$[OTf]^-$ dynamics are slightly slower than in the mixture with the lowest $[Cl]^-$ concentration. However, the IP dynamics (which does not distinguish between $[Cl]^-$ and $[OTf]^-$) shows the same trend as the H-O$[OTf]^-$ dynamics. Furthermore, the same outlier can be identified.

3.3.6. Results: Correlating viscosity with ion pair dynamics

Correlations between lifetimes and diffusivity as well as between the latter and viscosities have been established.[158] Furthermore, linear relationship between the calculated self-diffusivities and the inverse of IP or IC lifetimes was observed by Maginn and coworkers.[346] A similar inverse linear relationship was also found for ideal ionic conductivity and these relationships were found to be independent of temperature and the nature of the IL.[346] Maginn and coworkers conclude that these observations connect macroscopic dynamic properties with local atomic-level motions and strongly suggest that the dynamics of ILs are governed by a universal ion pair or ion cage forming and breaking mechanism. Thus, in order to design an ionic liquid with enhanced dynamics, one should consider how to minimise IP lifetimes.[346]

Table 3.16.: Hydrogen bond dynamics in $[C_4C_1Im][OTf]$ water mixtures. x_{IL} gives the mole fraction of the IL.

forward			
x_{IL}	$\tau^{H2\text{-}O(A)}$	$\tau^{H2\text{-}O(W)}$	$\tau^{H4/5\text{-}O(A)}$
0.39	183	174	271
0.58	203	201	311
0.66	224	186	349
0.82	248	211	371
x_{IL}	$\tau^{H4/5\text{-}O(W)}$	$\tau^{H(W)\text{-}O(A)}$	$\tau^{H(W)\text{-}O(W)}$
0.39	149	119	175
0.58	176	127	228
0.66	193	150	264
0.82	217	181	258
backward			
x_{IL}	$\tau^{H2\text{-}O(A)}$	$\tau^{H2\text{-}O(W)}$	$\tau^{H4/5\text{-}O(A)}$
0.39	372	395	648
0.58	399	439	677
0.66	439	374	772
0.82	488	452	809
x_{IL}	$\tau^{H4/5\text{-}O(W)}$	$\tau^{H(W)\text{-}O(A)}$	$\tau^{H(W)\text{-}O(W)}$
0.39	348	198	604
0.58	403	196	771
0.66	448	231	915
0.82	546	288	896
TST			
x_{IL}	$\tau^{H2\text{-}O(A)}$	$\tau^{H2\text{-}O(W)}$	$\tau^{H4/5\text{-}O(A)}$
0.39	1.87	2.55	1.40
0.58	1.70	1.84	1.37
0.66	1.88	2.13	1.49
0.82	1.85	2.15	1.34
x_{IL}	$\tau^{H4/5\text{-}O(W)}$	$\tau^{H(W)\text{-}O(A)}$	$\tau^{H(W)\text{-}O(W)}$
0.39	1.79	2.20	0.87
0.58	1.60	1.27	3.24
0.66	1.94	2.16	1.65
0.82	1.98	2.33	6.12

Table 3.17.: Lifetimes in $[C_4C_1Im][Cl]/[OTf]$ at 298 K. Please note, we do not distinguish the anion type. x_{Cl} = mole fraction of $[C_4C_1Im][Cl]$.

			forward	
x_{Cl}	τ^{H2-O}	τ^{H2-Cl}	$\tau^{H4/5-O}$	$\tau^{H4/5-Cl}$
0.000	242	–	385	–
0.192	210	514	258	592
0.303	328	858	394	853
0.402	428	999	461	1036
			backward	
x_{Cl}	τ^{H2-O}	τ^{H2-Cl}	$\tau^{H4/5-O}$	$\tau^{H4/5-Cl}$
0.000	461	–	847	–
0.192	413	706	216	974
0.303	647	1323	334	1267
0.402	882	1406	398	1532
			TST	
x_{Cl}	τ^{H2-O}	τ^{H2-Cl}	$\tau^{H4/5-O}$	$\tau^{H4/5-Cl}$
0.000	1.86	–	1.32	–
0.192	1.96	2.17	1.45	0.99
0.303	2.05	2.40	1.35	1.14
0.402	2.37	2.24	1.57	1.06
	int		reactive flux	
x_{Cl}	τ^{IP}	τ_f^{IP}	τ_b^{IP}	k_{TST}
0.000	2289	506	2252	1.51
0.192	2148	447	1731	2.14
0.303	3716	698	2625	2.79
0.402	4912	816	2920	3.21

Another way to change macroscopic dynamics is to mix the IL with impurities such as water or investigate IL mixtures. For this reason, we correlate the viscosity with the IP dynamics of all our investigated systems.

All viscosities values are listed in the SI.[338,368–374] The temperature dependent values for $[C_4C_1Im][OTf]$ were taken from the group contribution model of Gardas *et al.*[375]

Figure 3.27 shows the correlation between the ion pair dynamics (intermittent and reactive flux) as well as the viscosities. The correlation works satisfyingly between the ion pair dynamics and the viscosity including not only temperature dependency, but also the mixture with water and with chloride. In this respect it will be interesting to further investigate the reactive flux dynamics to reveal the detailed dynamics of IL systems.

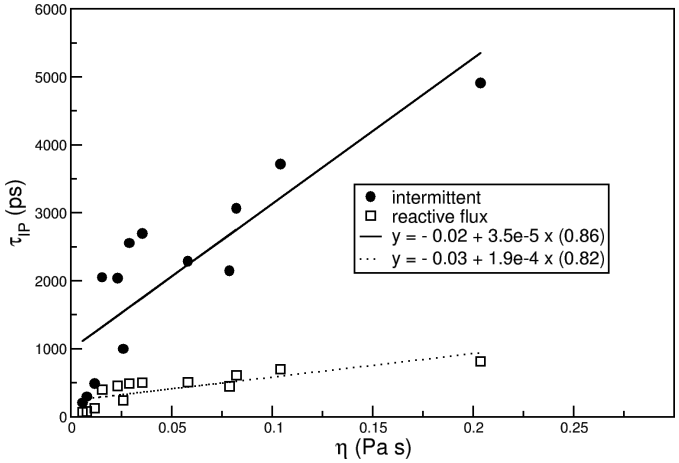

Figure 3.27.: Correlating τ^{IP} (ps) with viscosities (Pa s). Dashed and dotted line are a linear regression.

3.3.7. Conclusions

In order to obtain a broad picture of the structure and dynamics, we simulated several ionic liquids systems with the aid of flexible, atomistic, classical molecular dynamics simulations. In detail we studied the $[C_4C_1Im][Br]$ liquid with a non-polarizable and polarizable force field[359,360] at 386 K. The following systems were set up with a non-polarizable force field, namely a temperature dependent investigation at 293 K, 323 K, 353 K, 373 K, and 393 K of $[C_4C_1Im][OTf]$. This was supplemented by the ionic liquid/molecular liquid mixture of $[C_4C_1Im][OTf]$ water at four different mole fractions of the IL (0.39, 0.58, 0.66 and 0.82) taken from Reference 361 at 293 K. To complete the picture, an ionic liquid mixture $[C_4C_1Im][Cl]/[OTf]$ at x = 0.000, 0.192, 0.303, 0.402 mole fraction of $[C_4C_1Im][Cl]$ at 298 K was added.[369]

For the structure we observed the typical effects of a polarizable force field, like larger distances compared to the non-polarizable force field in accordance with previous studies.[363] Also smaller coordination numbers are observed for the polarizable variant. The temperature dependent calculation revealed that with increasing T slightly longer dis-

tances are observed. The cation is approximately surrounded by $5-6$ anions which also only slightly changes to smaller numbers within the temperature range investigated here. Considering the combined distribution functions clearly indicates that a 60 degree angle is the right choice for the hydrogen bond together with the first minimum in the according radial distribution function. In the moist IL system, adding water goes along together with a decrease in cation-anion coordination, the water-water coordination increases and so behave the IL-water number integrals. The coordination of the ions around the water decreases with added water in the IL. Our domain analysis tool reveals,[316,329] that in all mole fractions the polar parts of the ions form one connected domain. The nonpolar parts of the IL ions become more dispersed when water is added and the water clusters/molecules are distributed more when less water is present. In the mixture with the chloride the coordination number changes between the two anions, but the number integral of the cation around the anions remains constant, about six around the trifluoromethanesulfonate anion and about four around the chloride anion.

For the dynamics, we analyzed the continuous and intermittent functions in order to compare to literature, but we mainly focused on the reactive flux dynamics, because it can give information about transient relaxation, showing when most of the dynamics in a system is over. It automatically gives the transition state theory approximation to the rate, a lower bound to the average HB lifetime, that other methods extract from lengthy calculations, e.g. continuum HB correlation functions. The calculated rate function, combined with appropriate phenomenology, gives the actual HB lifetime (and even more, rate constants for both processes, breaking and reforming), which are all independent of the arbitrary HB definition in a simulation.

Obviously, temperature accelerates the dynamics of all associations (HB and ion pair and well as ion cage). The polarizable treatment of the interactions also accelerates the dynamics and this occurs to such an extend that the charge reduction does not compensate this behavior. By observing opposite trends in the continuous as well as the intermittent dynamics comparing the ring protons of the imidazolium cation, one can infer that the acidic H2 position provides more frequent breaking and reforming HB than the rear protons. In almost all cases adding water leads to an acceleration of the ion pair/center of mass/ring dynamics. Finally, mixing the IL with the chloride anion leads to a tremendous decrease of the ion pair dynamics as also reflected in the experimental viscosities.

Thus, correlating the ion pair dynamics with the viscosities provides a simple tool to estimate whether new ILs or IL mixtures will have a decreased viscosity.

3.4. Robustness of the Hydrogen Bond and Ion Pair Dynamics in Ionic Liquids to Different Parameters from the Reactive Flux Method

Sascha Gehrke[†] , Barbara Kirchner[†,*]
J. Chem. Eng. Data, 2020, Volume **65 (3)**, Pages 1146–1158

DOI: 10.1021/acs.jced.9b00529

Received: June 09, 2019

Published: October 14, 2019

For this article a Supporting Information is available free of charge at:
`https://pubs.acs.org/doi/suppl/10.1021/acs.jced.9b00529/suppl_file/je9b00529_si_001.pdf`

Contributions to the manuscript:

- Setup and maintenance of all calculations
- Development of the analysis programm
- Analysis of the trajectories
- Writing of the manuscript

[†]Mulliken Center for Theoretical Chemistry, University of Bonn, Beringstr. 4+6, D-53115 Bonn, Germany
[*]kirchner@thch.uni-bonn.de

In the last chapter a tool for the analysis of the dynamics of hydrogen bond networks was presented. Thereupon, in this chapter the robustness of this tool is evaluated. It is necessary to know how the choice of the geometric parameters of the hydrogen bond definition influences the obtained results. Further, the dependence on the details of the underlying simulation protocol needs to be clarified. Finally, the overall uncertainty of the method is estimated.

Abstract

Both, hydrogen bonding and ionic interactions have an extreme influence on properties of all kinds of material. Ionic liquids mostly possess both of them. In the present work we calculate with the aid of the reactive flux theory the dynamics of hydrogen bonds as well as of the ionic network for different 1-butyl-3-methylimidazolium based ionic liquids. In order to apply this method we carry out molecular dynamics simulations at a broad temperature and simulation parameter range. Hydrogen bond lifetimes vary with temperature in the range of 10 ps (400 K) – 60 ps (300 K) for the more fluid systems to 60 ps (400 K) – 2000 ps (300 K) for the more viscous systems. The ion pair dynamics behave differently. While the more fluid systems show ion pairs which possess a factor of 4 longer lifetimes than the hydrogen bonds, the ion pair lifetimes of the more viscous systems actually are by a factor of 0.6 smaller and thus faster than the hydrogen bond lifetimes. While the choice of the hydrogen bond angle is less sensitive, a deviation in the distance criterion of up to 5 % from the radial pair distribution functions' minimum leads to a change of less than 10 % in the calculated lifetime. The ion pair dynamics are less sensitive with respect to variation of the geometrical parameter. Interestingly, for both kinds of dynamics the impact on the activation energy is even less prone to the different cutoff values than the lifetime. In fact, the cutoff for the distance criteria remains the activation energies almost unchanged. We find that the stability of the method is sufficient if the simulation time is at least by a factor of ten longer than the according lifetime.

3.4.1. Introduction

Hydrogen bonds (HBs) are a structural motif well known for nearly a century and extensively discussed in literature.[145–147,149–151,153–157,376] Although hydrogen bonds consist of relatively weak interaction, e.g. the water dimer shows an interaction energy of about 20 kJ/mol[155], they have a "remarkable effect on the properties of fluids",[180] and their breaking and reformation is fundamental for the dynamical properties of condensed matter.[377–379] Besides the impact of the hydrogen bonds impact on transport properties,[158–160] HBs influence the reactivity of organocatalysts.[5,129,131,132] Several studies with respect to HBs were carried out by Hans Hasse and coworkers.[173,179,180,197,380–383] In References 179 and 180 HBs of methanol and ethanol in near critical and supercritical carbon dioxide at a wide range of temperature and pressures were studied from NMR experiments. Refined models for the description of HBs have been developed[197,380–382] and their predictive power were then *f.e.* tested at HB statistics.[197,382]

The general experimental detection of hydrogen bonds by the aid of IR[170–173] and NMR spectroscopy[175–180] is widely well-established today. However, the experimental analysis of dynamical processes is still challenging, yet very important. Attempts based on scattering methods,[184–186] ultrafast IR spectroscopy,[160,187–191] or femtosecond 2D IR[159,192–196] are often approaching the problem in an indirect way, rendering the interpretation of the results difficult.

Most of the HBs studies are applied to liquid water. The interactions between its molecules can be considered to contain the prototype of a hydrogen bond. The discussion becomes more complex if the hydrogen bond does not occur between two neutral molecules or a neutral molecule and an ion, but between two charged partners.[153,154] In this case it is difficult to clearly separate the attraction into a part due to the ion–ion interaction and the influence of the hydrogen bond.[147,154,384] Nevertheless, the existence and the importance of HBs in ionic systems — as ionic liquids (IL) — has been shown by several theoretical[153,154,332–334,343,344] and experimental[335–337,385] studies. Furthermore, it has been shown, that similar to the dynamics of hydrogen bonds, the dynamics of the ionic network is correlated to transport properties like viscosity, self-diffusion and conductivity of ILs.[3,158,202,343–346,386]

Particular interesting cases are provided by the subclass of imidazolium based ILs. As for many ILs, the investigation of the hydrogen bond dynamics is hindered by the interference due to the ionicity[314,315] of the system ranging from charge transfer or polarization to formation of neutral species. In the case of the imidazolium cation this means that carbene formation, with additional hydrogen bonding as acceptor, or carbene catalysis can even play a role.[6,8,81,82,144] On top of this, the HBs in imidazolium based ILs are donated by a carbon ring atom,[154] and are therefore of relatively weak type.[146,387]

Molecular dynamics (MD) simulations which often were used to tackle thermodynamic[388–390] and transport[391–395] properties also have been shown to be a promising way approaching the topic of HBs.[3,158,197–206] Recently, we analyzed ionic liquid hydrogen bond dynamics with MD simulations based on the reactive flux approach[228,229,349] and presented therein an expansion of the concept to the dynamics of ions.[3] In this work we investigate the anion and temperature variation and test boundaries of the method

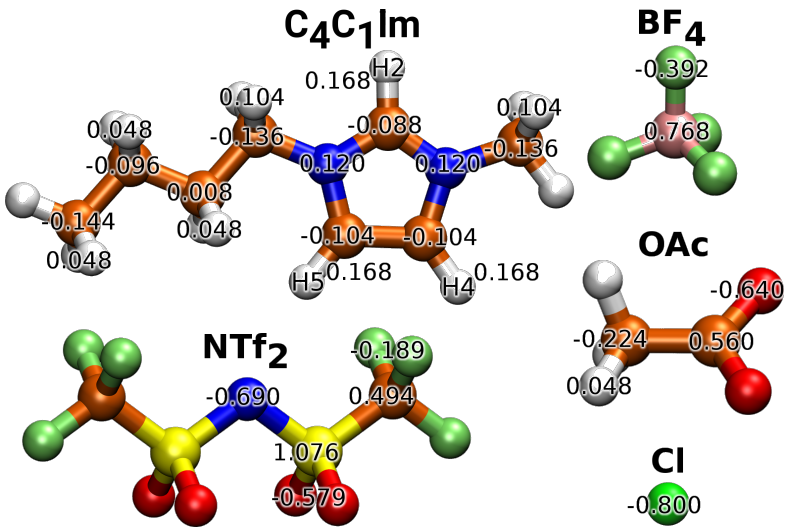

Figure 3.28.: The ions investigated in the study. The following color code is used for elements: C: orange, H: white, N: blue, S: yellow, O: red, F: lime, B: pink, Cl: green. The applied partial charges are given as numbers in the molecules. Furthermore, in the representation of the cation the hydrogen atoms of interests are marked with their names.

in terms of simulation parameters. Therefore, we performed simulations with suitable imidazolium-based ionic liquids (see Figure 3.28) chosen in a way that a broad range of different lifetimes is covered. The article is constructed as follows: First, a brief summary of the reactive flux approach is given. Second, the details of the simulations are shown. Afterwards, the influence of certain parameters of the simulation as well as of the analysis settings are presented and discussed. We end the article with a conclusion.

3.4.2. The Reactive Flux Approach

There are several attempts to define a hydrogen bond based on the electronic structure.[156,167,181,396–398] Unfortunately, the quantum mechanical calculation of the relevant properties is still very time consuming. Therefore, the most straightforward way to define a hydrogen bond in an MD simulation is the usage of a geometrical criterion,[155,197] e.g. the distance of the hydrogen atom to the acceptor site and the deviation of the angle defined by the donor – hydrogen – acceptor atoms from linearity as illustrated in Figure 3.29. Typical geometries are visualized by RDFs and combined distribution functions in the Supporting Information of the article. The time-dependent autocorrelation functions of the pair-wisely defined bonding operator $h(t)$

$$c(t) = \frac{\langle h(0)h(t)\rangle}{\langle h\rangle} \qquad h(t) = \begin{cases} 1 & \text{if criteria fulfilled} \\ 0 & \text{otherwise} \end{cases} \tag{3.9}$$

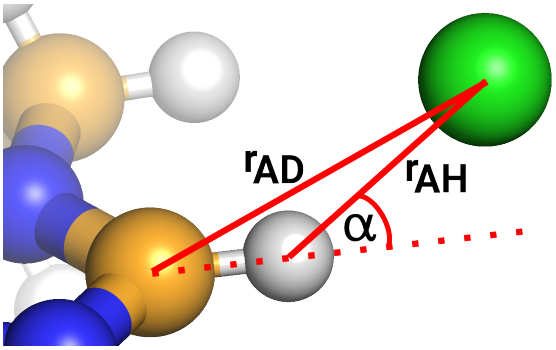

Figure 3.29.: The geometrical criterion for the hydrogen bond analysis with a chloride atom as acceptor and the H2 of the imidazolium cation (see Figure 3.28 for atom labels). The distance r_{AH} as well as the angle α have to be below a certain cutoff to define the assembly as a hydrogen bond. The distance r_{AD} sets the vicinity criterion.

describes the probability $c(t)$ to find a potential pair of acceptor and donor which was initially hydrogen bonded at time $t = 0$ still as bonded after a certain time t.

There are several approaches that estimate the lifetime directly from this probability function, i.e. the "intermittent" approach.[213,399] In contrast, the reactive flux method eliminates perturbations from diffusion, by the aid of a second state in which the pair of interest is not connected by a hydrogen bond, but still within a distance, that a hydrogen bond could be reformed. This is achieved by the vicinity operator $H(t)$, which becomes unity if the distance between acceptor and donor atom is smaller than a certain cutoff and zero otherwise. Based on the time invariance of autocorrelation functions it is possible to form a function of bond reformation

$$k_{\mathrm{in}}(t) = -\frac{\langle H(t)[1 - h(t)]\dot{h}(0)\rangle}{\langle h\rangle}\,. \tag{3.10}$$

The integral

$$n(\mathfrak{t}) = \int_0^{\mathfrak{t}} k_{\mathrm{in}}(t)\mathrm{d}t \tag{3.11}$$

gives the probability to find a certain pair of atoms initially connected by a hydrogen bond at time $t = 0$ to be not bonded anymore but still in vicinity at time $t = \mathfrak{t}$. From this it is possible to obtain the rate of decay k_d and the rate of reformation k_f by fitting the pre-factors of a linear combination of the functions $c(t)$ and $n(t)$ to the simple kinetic equation

$$-\dot{c}(t) = k_d c(t) - k_f n(t). \tag{3.12}$$

Technically, we achieve this by modifying the two parameters k_d and k_f stepwise in a way that the root mean square displacement (RMSD) according Equation 3.12 is minimized. Thereby, the first hundred data points were ignored to cancel out disturbances due to

bond vibrations, as already described in References 228, 229, and 3. The final values are excepted with a tolerance of 10^{-14}. The inverses of the rate constants give the average lifetimes of a hydrogen bond

$$\tau_{\mathrm{lt}} = \frac{1}{k_d} \tag{3.13}$$

and the "decay time"

$$\tau_{\mathrm{dt}} = \frac{1}{k_f}. \tag{3.14}$$

In the case of the hydrogen bond analysis, the second one does not have an explicit physical meaning. For a more detailed description the reader may consult the original publications by Luzar and Chandler[228,229,349] or Section 2.1.

Recently, we could show that by a redefinition of the operators $h(t)$ and $H(t)$ the approach can be extended to the dynamics of ion pairs in ionic liquids.[3] To do so, the operator $h(t)$ is transformed into the ion pair operator, which becomes unity for a pair of a certain ion and its next neighbor counterion and zero for all other pairs. The operator $H(t)$ again is defined by a distance cutoff, which is chosen in a way that it includes the first solvation shell of counterions. That is the distance between the centers of mass of the respective ions have to be below a certain cutoff, which is defined by the distance related to the first minimum in the corresponding radial pair distribution function (RDF). It needs to be mentioned here, that the existence of ion-pair-like aggregates in real ionic liquids is controversially discussed in literature (see Reference 315). Nevertheless, the formally definition of a pair-like assembly is helpful for the description of the dynamics of the ionic network. For a visualization of these operators see Figure 3.30.

The definitions of the operators are summarized in Table 3.19. The distance criteria were defined by the first minimum in the corresponding RDF. Hydrogen bonds of the imidazolium cation are mainly formed by the most acidic hydrogen atom, the H2 (see Figure 3.28), and with the other hydrogen atoms of the cation ring, the H4 and H5.[198–200] Subsequently, there are three distances to take into account:

1. The distance of the H2 at the cation ring to the hydrogen bond accepting atom of the anion, namely the oxygen atoms of the $[\mathrm{NTf_2}]^-$ ($\varnothing r_{\mathrm{AH}} = 423\,\mathrm{pm}$, see RDF in SI) and the $[\mathrm{OAc}]^-$ ($\varnothing r_{\mathrm{AH}} = 400\,\mathrm{pm}$, see RDF in SI), the fluorine atoms of the $[\mathrm{BF_4}]^-$ ($\varnothing r_{\mathrm{AH}} = 388\,\mathrm{pm}$, see RDF in SI), as well as the chloride atom itself ($\varnothing r_{\mathrm{AH}} = 443\,\mathrm{pm}$, see RDF in SI).

2. The distance between the H4 and H5 of the cation's ring and the hydrogen bond accepting atoms of the anions — the oxygen atoms of the $[\mathrm{NTf_2}]^-$ ($\varnothing r_{\mathrm{AH}} = 395\,\mathrm{pm}$, see RDF in SI) and the $[\mathrm{OAc}]^-$ ($\varnothing r_{\mathrm{AH}} = 375\,\mathrm{pm}$, see RDF in SI), the fluorine atoms of the $[\mathrm{BF_4}]^-$ ($\varnothing r_{\mathrm{AH}} = 370\,\mathrm{pm}$, see RDF in SI), as well as the chloride atom itself ($\varnothing r_{\mathrm{AH}} = 415\,\mathrm{pm}$, see RDF in SI). Due to their similarity these two atoms are treated identically in the analysis.

3. The distance between the cations and the anions. Thereby, it has to be taken into account, that the charge of the cation is mostly localized on the ring unit (total charge of the ring atoms and the directly connected groups +0.696 according to

the force field parameters), while the side chain is relatively apolar (total charge +0.104 according to the force field parameters). As a consequence, the two parts of the cation have been shown to be characterized by significantly different behavior or even separated microphases given that the side chain is long enough.[324–326,329] Subsequently, the cation is represented by the center of the ring to assure the focus on the properties of the ionic part of the molecule. The anion is simply represented by its center of mass.

The relevant RDFs are shown in the Supporting Information of the article. Furthermore, the positions of the RDFs first minima, which are crucial for the upcoming analyses, are listed in Table 3.18. Due to the fact, that in imidazolium based ionic liquids there is beside the in-plane coordination of a hydrogen bond also the possibility of an on-top coordination with angles up to 90°,[154] the angle criterion for the hydrogen bond operator $h(t)$ is difficult to define. Based on the experiences in earlier studies by us and others[3,203] a cutoff of 60° was chosen (i.e. an HB angle of 120°. Clarifying the robustness of the method concerning deviation from this values is one of the targets of this work.

Table 3.18.: Distances of the first minima r_{min} from the reference to the observed particle for H2-X and H4/5-X as well as for center of ring (cation)-center of mass (anion) (c(R)-c(A)). At this, X is the corresponding hydrogen bond acceptor atom of the anion.

	r_{min} / pm		
T	H2-X	H4/5-X	c(R)-c(A)
	[C_4C_1Im][NTf_2]		
293 K	422	398	898
323 K	425	395	898
353 K	422	392	902
393 K	422	395	902
	[C_4C_1Im][BF_4]		
293 K	388	372	754
323 K	388	368	754
353 K	388	372	754
393 K	388	368	762
	[C_4C_1Im][OAc]		
293 K	398	372	718
318 K	398	375	726
343 K	398	375	726
373 K	405	378	734
	[C_4C_1Im][Cl]		
303 K	438	415	678
333 K	445	415	678
363 K	445	415	682
393 K	445	418	686

Table 3.19.: Definitions of the operators $h(t)$ and $H(t)$ for the hydrogen bond analysis (HB) and the ion pair analysis (IP).

analysis	operator	equals unity if:
HB	$h(t)$	distance acceptor – hydrogen atom < cutoff AND
		deviation of angle donor – hydrogen – acceptor from 180° < cutoff
	$H(t)$	distance acceptor – donor atom below cutoff
IP	$h(t)$	ion A is next neighbor of ion B
	$H(t)$	distance center of mass ion A – center of mass ion B < cutoff

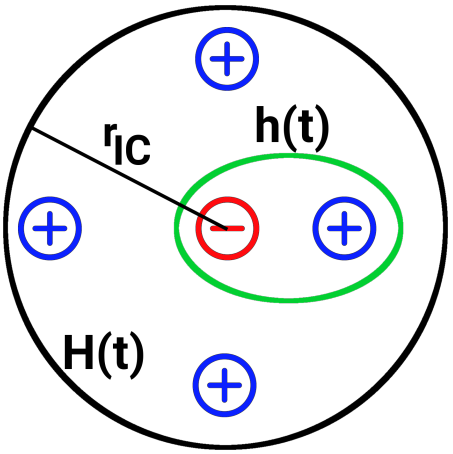

Figure 3.30.: The criteria for the operators $h(t)$ and $H(t)$ of the ion pair analysis. The green ring symbolizes the ion pair definition of the operator $h(t)$, that is the central anion and the cation within the shortest distance to it. The black ring with the radius of r_{IC} includes all neighbors in the first solvation sphere, defining the operator $H(t)$.

3.4.3. Computational Details

Molecular Dynamics Simulations

All MD simulations were performed by the LAMMPS program package.[263] The subsequent analyses of the trajectories were performed by our open source program TRAVIS.[316] The side chains of the cations were modeled by the OPLS-AA force field.[255] The ring unit of the cation, as well as all anions except the $[NTf_2]^-$ were modeled by the CL&P force field.[266,267] For the $[NTf_2]^-$ the NGOLP force field (which only exists for this anion) was applied. It gives a better representation of the minimum energy conformations and the dynamic properties of the anion compared with the CL&P.[400] Previously, it has been shown, that the ionicity in ionic liquids is better described by the CL&P if a charge transfer is taken into account than by applying unity charges.[313–315,339–341,401] Especially the modeling of dynamic properties as viscosity or diffusivity in simulations has been proven better if non-unity charges are applied.[341,401] Therefore, the charges of

all systems, except the $[NTf_2]^-$ containing system, were scaled to 0.8 and −0.8, respectively, by scaling the partial charge of each atom by a factor of 0.8. The usage of the NGOLP force field renders charge scaling in the $[NTf_2]^-$ containing system redundant.[400] Furthermore, the non-bonded interactions were computed only if the distance between the involved atoms was within the cutoff radius of 1000 pm. Coulombic interactions beyond this distance were computed via the particle-particle particle-mesh solver[402] with an accuracy of 10^{-5}.

All simulations were carried out according to the following protocol:

1. The initial configuration of each cell was generated by the PACKMOL program.[312]
2. All systems were simulated in an NVT-ensemble for 0.5 ns, to remove possible energy hotspots in the initial configurations of the molecules. Temperature was controlled by applying a Nosé–Hoover chain thermostat ($T = 400$ K, $\tau = 100$ fs)[403,404]. The timestep was chosen to be 1 fs.
3. Afterwards, the systems were simulated in an NpT-ensemble for 1 ns. Constant pressure and temperature were provided via a Nosé–Hoover-chain thermostat (target temperature, $\tau = 100$ fs) and a Nosé–Hoover barostat ($p = 1$ bar, $\tau = 1000$ fs), respectively.[403–405] The box volume was averaged over the last 0.5 ns. The resulting densities are listed together with experimental data in the Supporting Information of the article.[406–409] Due to the charge scaling the calculated densities are about 3–10 % lower then their experimental counterparts.
4. The systems were slowly forced to the average volume obtained in step 3 over 0.25 ns. Finally, the ensemble was switched back to NVT for final equilibration. Temperature control was again achieved applying a Nosé–Hoover-chain thermostat (target temperature, $\tau = 100$ fs).
5. After an equilibration period for 5 ns, the production runs were performed in an NVE-ensemble for 50 ns, saving the coordinates of the systems in every 500 fs. Additionally, the last 5 ns snapshots were saved every 50 fs as a separated trajectory. The inspection of the stability of the simulations in terms of energy and temperature during the production run reveals acceptable drifts. Data concerning the stability can be found in the Supporting Information of the article.

3.4.4. Results and Discussion

With the aim to investigate the different effects on the reactive flux analysis we divided the relevant parameters into two different groups: Simulation related and analysis related. The first group contains the time between two snapshots of the printed trajectory (named "dumpstep" to avoid confusion with the "timestep" of the applied integrator) and the total length of the trajectory. The second group contains the geometric criteria applied for the definition of a hydrogen bond or the ion cage, respectively. The investigated systems are chosen in a way, that they cover a broad range of different lifetimes at the various temperatures. Thus, they allow a deep insight into the effects of the varied parameters at different time scales.

Table 3.20.: The total length and the dumpsteps of the trajectories investigated in the present study.

name	total length	dumpstep
A	50 ns	1000 fs
B	50 ns	500 fs
C	10 ns	500 fs
D	5 ns	250 fs
E	5 ns	100 fs
F	5 ns	50 fs
G	1 ns	50 fs

Simulation related parameters

The influence of the simulation related parameters was analyzed based on the trajectories listed in Table 3.20. The 50 ns long trajectory was analyzed with a dumpstep of 500 fs and 1000 fs. Additionally, the same trajectory was split into five single trajectories with a length of 10 ns each with a dumpstep of 500 fs. These smaller trajectories were analyzed separately and based on the results the estimated unbiased standard deviation

$$s = \sqrt{\frac{1}{n-1}\sum_{i=0}^{n}(\tau_i - \overline{\tau})^2}\,, \tag{3.15}$$

of the method was calculated, with the number of data points $n = 5$ and the average lifetime $\overline{\tau}$. The 5 ns trajectory was analyzed with a dumpstep of 250 fs, 100 fs, and 50 fs. Analogously to the 50 ns trajectory, the short one is split into five very short trajectories with a length of 1 ns and a dumpstep of 50 fs and analyzed in terms of the standard deviation.

Hydrogen Bond Dynamics

For the different investigated systems we obtain lifetimes as listed in Table 3.21 and visualized in Figure 3.31. Considering the data set for the trajectories **B**, which are the most reliable data in terms of simulation parameters, we observe that the lifetimes increase in the following order $[NTf_2]^-$ (66 ps) < $[BF_4]^-$ (168 ps) < $[OAc]^-$ (391 ps) < $[Cl]^-$ (1754 ps) according to their fluidity at 298.15 K, i.e. $[NTf_2]^-$ (51.1 cP[410]; 51.58 cP[411]) < $[BF_4]^-$ (108.74 cP[411]) < $[OAc]^-$ (292.57 cP[411]) < $[Cl]^-$ (217.0 cP at 348.15 K[412]). These findings are in line with the experimentally observed correlation of local rearrangement events and viscosity.[386]

In Figure 3.31 it is revealed that a change in the dumpstep induces no significant effect on the obtained lifetimes for the chosen parameters. The results obtained for the 50 ns trajectory with dumpsteps of 500 fs and 1000 fs are nearly indistinguishable. The same statement holds with few exceptions for the results obtained with different dumpstep length from the 5 ns trajectory.

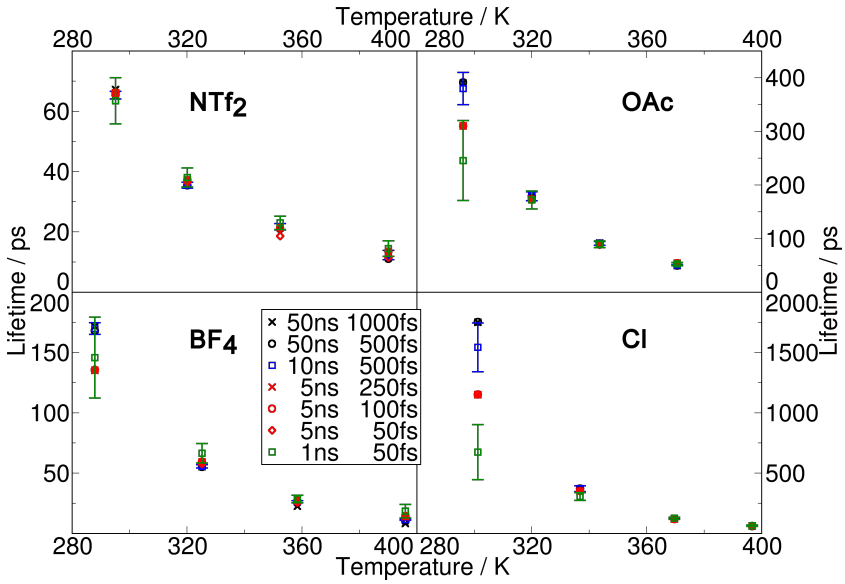

Figure 3.31.: Lifetimes $\tau_{\mathrm{lt}}^{\mathrm{HB}}$ of the H2 related hydrogen bonds plotted against temperature. The two numbers in the legend give first the total length of the trajectory and second the dumpstep. The error bars indicate the interval of the standard deviation as defined in Equation 3.15 with a confidence of 68%. The lifetimes for the hydrogen bonds at the H2-atom are listed in Table 3.21. All lifetimes can be found in the Supporting Information of the article.

A different picture is drawn if the results obtained from trajectories with different length are compared. If the trajectory is longer, the recorded number of relevant events increases. Due to this fact, the statistics become more representative and, therefore, the calculated results can be expected to be more reliable. This appears as a significantly more narrow standard deviation of the results obtained from the 10 ns trajectories compared to those of the 1 ns trajectories, as illustrated in Figure 3.31. Furthermore, the shorter the lifetime of the interaction is, the more events can be observed in the same length of the trajectory. As a consequence, the standard deviation becomes more narrow if the calculated lifetime is shorter.

According to this fact, the lifetimes tend systematically to lower values if the length of the trajectory is shortened. This holds especially if the calculated lifetime is very long as for the most extreme case, the $[\mathrm{Cl}]^-$ system at 303 K: The lifetime calculated from the 50 ns trajectory is 1.75 ns and thereby even longer than the length of the 1 ns trajectory. Therefore, it is no surprise that the lifetime calculated with the 1 ns trajectory is strongly underestimated by more than 50 % compared to the results with the 50 ns trajectory. We conclude, that as a rule of thumb, the deviation becomes negligible if the trajectory length is at least by a factor of ten longer than the calculated lifetime in question.

Table 3.21.: Lifetimes of the hydrogen bonds at the H2-atom $\tau_{\mathrm{lt}}^{\mathrm{HB}}$ and of the ion pairs $\tau_{\mathrm{lt}}^{\mathrm{IP}}$. The first column gives the temperature T of the simulation. The lifetimes are given in ps for the investigated system with a total length of 50 ns and a dumpstep of 500 fs. Lifetimes calculated from the other trajectories as well as the lifetimes for the H4/H5 containing HBs are listed in the Supporting Information of the article.

T /K	$\tau_{\mathrm{lt}}^{\mathrm{HB}}$	$\tau_{\mathrm{lt}}^{\mathrm{IP}}$
[C_4C_1Im][NTf_2]		
293	66.1	237.5
323	35.4	141.1
353	21.1	92.1
393	11.1	52.5
[C_4C_1Im][BF_4]		
293	168.0	300.3
323	55.2	116.6
353	25.2	61.5
393	10.1	31.7
[C_4C_1Im][OAc]		
293	391.3	464.9
318	179.2	209.1
343	91.2	117.2
373	49.8	68.0
[C_4C_1Im][Cl]		
303	1753.9	1098.9
333	372.4	254.9
363	121.1	88.7
393	61.4	47.5

A similar picture is drawn from the relative standard deviation of the data sets in terms of Equation 3.12 after the fitting procedure, shown in the Supporting Information of the article. Except for the highly viscous system with the $[Cl]^-$ at 303 K the deviation is lower than 1.5 % for the trajectories with 50 ns length. Generally, this demonstrates a good representation of the underlying physics of the hydrogen bond dynamics by the reactive flux approach. However, obviously if the trajectory length becomes shorter the standard deviations become significantly larger. A reason for this observation is most probably the relatively low number of breaking and reformation of the HBs. As a consequence, the obtained correlation functions are more noisy and subsequently, the uncertainty of the fitting increases.

The general findings for the hydrogen bonds including the H4 and H5 atoms (shown in the Supporting Information of the article) are similar to those of the H2 hydrogen bonds. However, for the more fluid systems with the $[NTf_2]^-$, $[BF_4]^-$, and the $[OAc]^-$ anion the H4/H5 containing HBs are characterized by longer lifetimes. Interestingly, this trend is inverted for the systems with the chloride anion.

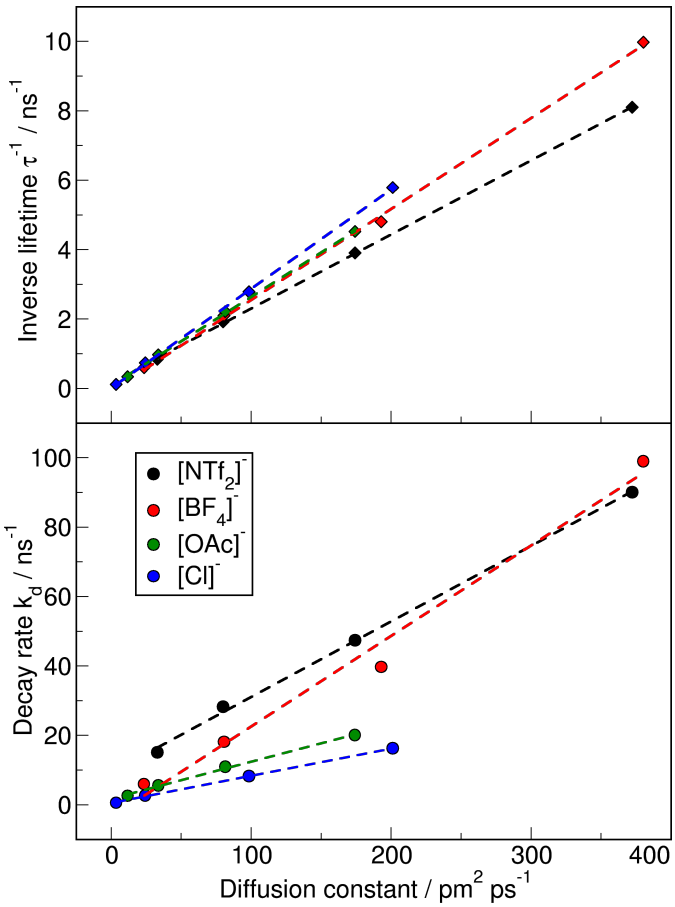

Figure 3.32.: Top panel: The hydrogen bond lifetimes obtained directly from the integral of the autocorrelation function $c(t)$ correlated with the calculated diffusion constants. Bottom panel: The same lifetimes obtained with the reactive flux method. The different systems are color coded and linked with regression lines as an eye guide.

The dominance of the reactive flux method over other approaches to calculate lifetimes is revealed, if the correlation of the inverse lifetimes (or the decay rates k_d) and the calculated diffusion constants are investigated. A direct comparison of these lifetimes is given in the Supporting Information of the article and illustrated in Figure 3.32. In the top panel this correlation is shown for the lifetimes obtained directly from the intermittent autocorrelation function of the operator $h(t)$. Obviously, the values are characterized by a clear linear trend, nearly independent of the type of anion. Longer lifetimes of the

hydrogen bonds will lower the mobility of the certain ions and thereby have a direct physical impact on the liquids transport properties. Nevertheless, this general correlation is unlikely due only to this effect. The autocorrelation function $c(t)$ does not consider if the two ions of a potential pair are close enough to form a hydrogen bond, which results in a disturbance of $c(t)$ by diffusion of the ions. However, this perturbation is just an artificial effect, which is eliminated in the reactive flux approach. Subsequently, the results shown in the bottom panel of Figure 3.32 present a different picture. Actually, the overall linearity is absent. Instead, the simulations of each anion can be grouped together. Every group is characterized by a linear trend with a different slope. In fact, these system dependent trends are attributable to physical impact of local rearrangements of the hydrogen bond network on the diffusivity of the liquid.

Ion pair dynamics

The analyzed lifetimes for the 50 ns trajectories are listed in Table 3.21. The ion pair lifetimes increase in the following order $[NTf_2]^-$ (238 ps) < $[BF_4]^-$ (300 ps) < $[OAc]^-$ (465 ps) < $[Cl]^-$ (1099 ps) similar as the hydrogen bond lifetimes. For the fluid systems the ion pair lifetimes are longer than the hydrogen bond lifetimes. However, interestingly, this is reversed for the highly viscous system $[C_4C_1Im][Cl]$.

There are several explanations for this observation possible. One obvious difference between the anions is that the chloride is a monoatomic entity, while the other anions are polyatomic. As a consequence, the motion of the small chloride is less hindered compared to the bigger anions. In fact, the ion pair definition is based on the ionic centers of the involved ions. Therefore, a translational motion of at least one ion's center has to occur to change the state of the ion pair operator. Due to its size, the chloride anion may move relatively freely between the larger imidazolium cations, changing its pairing partner more frequently, compared to the hindered, bigger anions. On the other hand, the hydrogen bond operator's state can change not only if a translational motion occurs but as well due to rotations around the center which turns the hydrogen bond acceptor side away from the involved hydrogen atom. Self-evidently, this opportunity does not exist in the case of the chloride because the acceptor side and the ionic center are one and the same. From this it follows that the hydrogen bond lifetimes of the polyatomic anion are shorter relative to the monoatomic chloride.

Another reason may lie in the physico–chemical properties of the systems. It has been shown, that some ionic liquids form stable ion pairs or ionic associates in a way that the fluid is characterized better as a molecular than an ionic liquid.[338] This possibility is strengthened by the finding from Figure 3.32 that the impact of the different kinds of interaction on the transport properties is system dependent. In this case, one could state that the ion–ion interaction of the cation and the chloride is more dominated by hydrogen bonding compared to the interaction between the cation and the polyatomic anions. Obviously, further investigations are necessary.

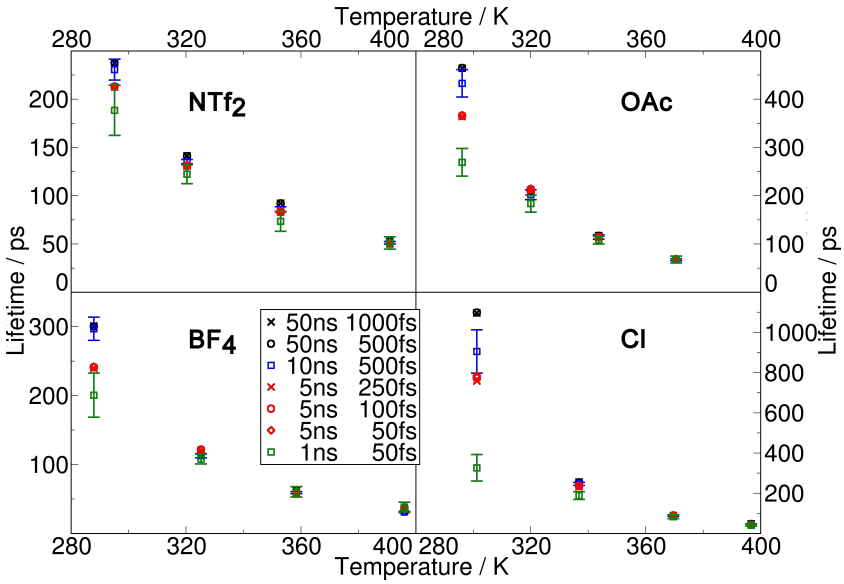

Figure 3.33.: The lifetimes $\tau_{\mathrm{lt}}^{\mathrm{IP}}$ of the ion pairs plotted against temperature. The two numbers in the legend give first the total length of the trajectory and second the dumpstep. The error bars indicate the interval of the standard deviation as defined in Equation 3.15 with a confidence of 68%.

The study of the influence on the ion pair lifetimes due to the simulation related parameters — the dumpstep and the total length of the trajectory — was carried out in the same way it was done for the hydrogen bond dynamics. Results are illustrated in Figure 3.33. Analogous to the hydrogen bond dynamics, the ion pair lifetime $\tau_{\mathrm{lt}}^{\mathrm{IP}}$ is observed to be nearly independent of the applied dumpstep. However, results based on a too short trajectory deviate significantly from those with longer trajectories. The fact, that the lifetimes $\tau_{\mathrm{lt}}^{\mathrm{IP}}$ for the ion pairs are in general longer than the lifetimes $\tau_{\mathrm{lt}}^{\mathrm{HB}}$ for the hydrogen bonds makes this effect even more critical. We conclude that it is sufficient if the trajectory has an overall length which is by a factor of ten longer than the calculated lifetimes. Please note, that increasing the temperature can help to solve the problem in that the lifetimes become generally shorter with higher temperature.

The relative standard deviation of the data sets after the fitting procedure, shown in the Supporting Information of the article reveals a similar result. For the 50 ns trajectories the deviation is lower than 2 % for all systems except these with the $[\mathrm{OAc}]^-$ at 293 K and with the chloride at 303 K.

Arrhenius behavior

In the reactive flux approach, the decay and reformation of a hydrogen bond is separated from other processes and thus it may be seen as a first order reaction described by the rate constant $k_{\mathrm{d}} = \tau_{\mathrm{lt}}^{-1}$.[229] The reactive flux approach works very well for water and similar systems in agreement with experiment.[229] It will be interesting to see whether this is also valid for our ionic liquid systems studied in the present paper. Therefore, it

should approximately follow Arrhenius' law

$$k_\mathrm{d} = A \cdot e^{\frac{E_A}{R \cdot T}} \qquad \text{or} \qquad \ln\left(k_\mathrm{d}\right) = \frac{E_A}{R} \cdot \frac{1}{T} + \ln(A) \tag{3.16}$$

with the pre-exponential factor A, the energy of activation E_A, the gas constant R, and the temperature T. Moreover, this concept should be valid for ion pairs as well. The plots in Figure 3.34 show a linear behavior for all systems and all kind of interactions. This allows the extraction of the energy of activation from the gradient as summarized in Table 3.22 together with the corresponding pre-exponential factor.

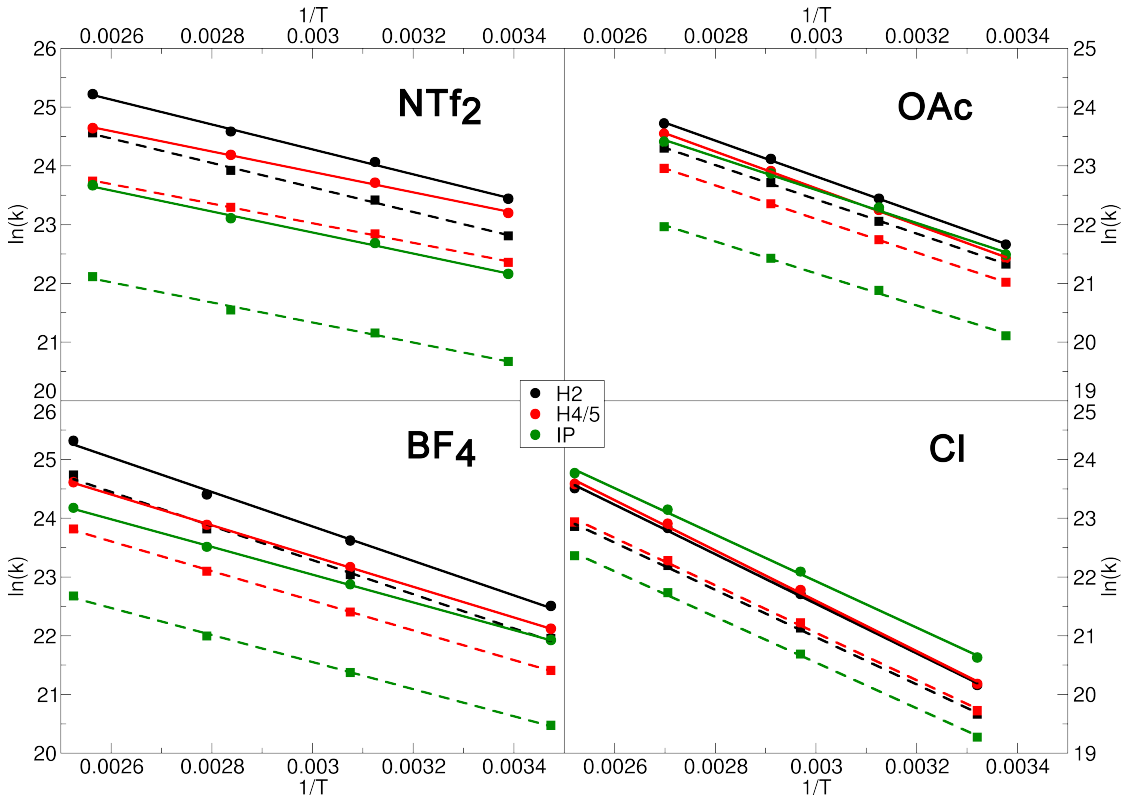

Figure 3.34.: Arrhenius plots of the different systems. The logarithm of the decay and reformation rate constant is plotted against the reciprocal temperature. The activation energy can be extracted from the gradient and the $\ln(k)$-axis intercept allows the calculation of the pre-exponential factor (both listed in Table 3.22).

The barriers E_A for the decay of the hydrogen bond and the ion pairs are very similar to those of the reformation process, despite the large differences in the decay times τ_dt compared to the lifetimes τ_lt. The height of the barriers increases in the order $[\mathrm{NTf_2}]^- < [\mathrm{BF_4}]^- < [\mathrm{OAc}]^- < [\mathrm{Cl}]^-$ for all ring hydrogen atoms as well as the ion pair dynamics, which is exactly the trend observed for the lifetimes. In general, the barrier for the decay process is slightly higher than that of the reformation process. This difference

Table 3.22.: The pre-exponential factors A and activation energies for the decay process $E_A^{\text{dec.}}$ and for the reformation process $E_A^{\text{ref.}}$ obtained from the Arrhenius plots in Figure 3.34. The last column gives the difference of the two energies $\Delta E_A = E_A^{\text{dec.}} - E_A^{\text{ref.}}$. HB2: hydrogen bond involving the H2 atom; HB4/5: hydrogen bond with the H4 and the H5 atom; IP: ion pair.

type of interaction	$A_{\text{dec.}}$ / ps^{-1}	$A_{\text{ref.}}$ / ps^{-1}	$E_A^{\text{dec.}}$ / kJ mol^{-1}	$E_A^{\text{ref.}}$ / kJ mol^{-1}	ΔE_A / kJ mol^{-1}
	$[C_4C_1Im][NTf_2]$				
HB2	20.389	9.679	17.6	17.4	0.2
HB4/5	4.419	1.480	14.5	13.9	0.6
IP	1.840	0.309	14.9	14.2	0.7
	$[C_4C_1Im][BF_4]$				
HB2	153.850	78.805	24.4	24.1	0.3
HB4/5	35.981	12.781	21.8	21.0	0.8
IP	12.049	2.300	19.6	19.2	0.4
	$[C_4C_1Im][OAc]$				
HB2	76.247	35.374	25.3	24.3	1.0
HB4/5	77.632	20.759	25.9	23.7	2.2
IP	31.093	5.518	23.5	22.6	0.9
	$[C_4C_1Im][Cl]$				
HB2	715.498	223.403	35.1	33.4	1.7
HB4/5	916.882	252.896	35.6	33.6	2.0
IP	479.613	97.512	32.9	32.3	0.6

is quite small for the $[NTf_2]^-$ and the $[BF_4]^-$ anion, and more distinct for the $[OAc]^-$ and the $[Cl]^-$ anion. Considering the pre-exponential factor which can be related to entropy increase in case of the breaking (decay) and decrease in case of the reformation of the HB or the ion pair the values for the decay are by a factor of 2–3 larger than the values for the reformation. The height of the pre-exponential factors of the hydrogen bonds involving the H4 and H5 atom and the ion pairs increase in the same order as the activation energies. However, for the H2 atom containing hydrogen bond the factor is larger for the $[BF_4]^-$ than for the $[OAc]^-$ anion.

Analyses related parameters

Hydrogen Bond Dynamics

In the analysis of the hydrogen bond dynamics the hydrogen bond has to be defined in a robust way. Due to the fact that the simple classical force field applied in this study does not provide any information about the electronic structure, the task is handled by the application of a geometrical criterion. Therefore, it is crucial to estimate the stability of the method by gaining knowledge about the influence of this criterion on the outcome of the analyses. Thus, we performed a study for both of the geometrical parameters, namely the distance between the hydrogen bond acceptor and the hydrogen atom and

Table 3.23.: Lifetimes τ_{lt} and decaytimes τ_{dt} of the hydrogen bonds at the H2 atom with different distance criterion for the $[NTf_2]^-$ anion. The first column gives the percental deviation Δr_{AH} from the RDF minimum distance. The remaining columns consist of two blocks, one for the highest simulated temperature and one for the lowest. Each includes one column with the explicit distance r_{AH} applied for the analysis, followed by a column with the resulting lifetimes τ_{lt} and decay times τ_{dt} in ps.

	$T = 293$K			$T = 393$K			
Δr_{AH}	r_{AH} / pm	τ_{lt}	τ_{dt}	r_{AH} / pm	τ_{lt}	τ_{dt}	E_A / kJ mol^{-1}
-15 %	359	47.2	64.3	359	7.1	10.1	18.9
-10 %	380	52.4	77.2	380	8.0	12.2	18.7
-5 %	401	58.5	95.6	401	9.2	15.7	18.2
-2 %	414	62.9	111.3	414	10.3	18.8	17.9
0 %	422	66.1	124.4	422	11.1	21.5	17.6
2 %	430	69.1	137.1	430	11.9	24.1	17.4
5 %	443	73.9	159.7	443	13.1	28.7	17.1
10 %	464	81.5	196.4	464	15.1	36.5	16.7
15 %	485	89.6	226.3	485	16.9	43.0	16.5

the angle defined by the donor–hydrogen–acceptor assembly. First, the hydrogen acceptor distance criterion was modified to values according to ±15 %, ±10 %, ±5 %, and ±2 % difference from the corresponding first RDF minimum, while the angle criterion was set to 60°. It should be kept in mind, that the donor acceptor distance criterion is always coupled to this one by the length of a C–H bond ($\sim$ 105 pm). Second, the angle criterion was modified by values according to ±50 %, ±40 %, ±30 %, ±20 %, and ±10 % difference from 60°, combined with a distance criterion gathered from the corresponding RDF. The explicit criteria are given together with the life and decay times exemplary for the $[NTf_2]^-$ anion in Table 3.23 and for the other ions in the Supporting Information of the article. The investigations are based on the 50 ns trajectories with a 500 fs dumpstep for the highest as well as the lowest temperature for each system.

In Figure 3.35 the relative deviation — defined by the calculated lifetime divided by the lifetime with the RDF-defined distance — for the $[NTf_2]^-$ anion is shown. The behavior of the other anions differs in a quantitative way. Obviously, the lifetime is higher with increasing distance criterion. Thereby, the impact is larger for the H2 containing hydrogen bond than for the H4/5. Furthermore, the effect for the H2 hydrogen bond is stronger with decreasing temperature. Interestingly, this trend is reversed for the hydrogen bonds containing H4 or H5.

Moreover, Figure 3.35 reveals, that the impact on the activation energies is even smaller than the effect on the lifetimes. For the H2 hydrogen bond the barrier increases by 1.3 kJ mol^{-1} for the shortest cutoff and decreases by 1.1 kJ mol^{-1} for the largest cutoff. For the H4 and H5 containing hydrogen bond the change in activation energy is only 0.4 kJ mol^{-1}. However, in this case the barrier grows if the cutoff distance increases.

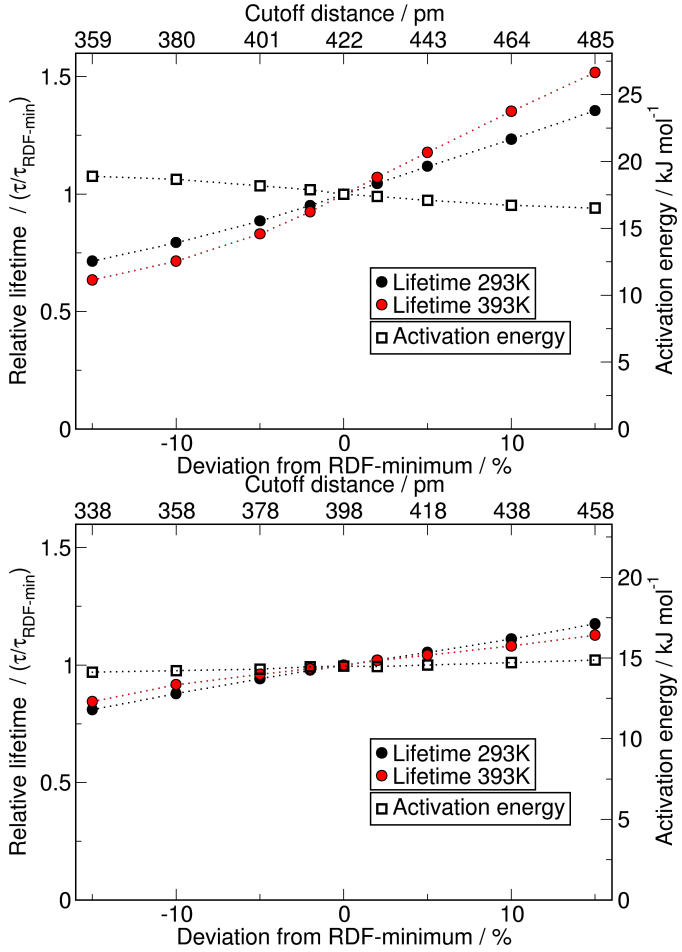

Figure 3.35.: Results of the distance criterion screening of the hydrogen bond analyses. The top panel shows the results for the H2 hydrogen bond, the bottom panel for the H4/5 hydrogen bonds. The times are given relative to the corresponding time obtained with the distance defined by the first RDF minimum. The angle criterion was in all cases defined as 60°.

In strong hydrogen bonds the donor, hydrogen, and acceptor atom are mostly found in a nearly linear assembly. However, in weak hydrogen bonds the angle between these three atoms can be deviate significantly from linearity.[146,154] Furthermore, as mentioned before, in imidazolium based ionic liquids there is next to an in-plane coordination also an on-top coordination which can assume angles up to 90°.[154] As a consequence, the angle criterion is difficult to choose — in contrast to the distance criterion. Therefore, it is important to investigate the effect of angle variations on the obtained lifetimes. The results of the investigation with the $[NTf_2]^-$ anion are illustrated in Figure 3.36. Analogously to the distance criterion, the behavior of the other anions differs only in a quantitative manner.

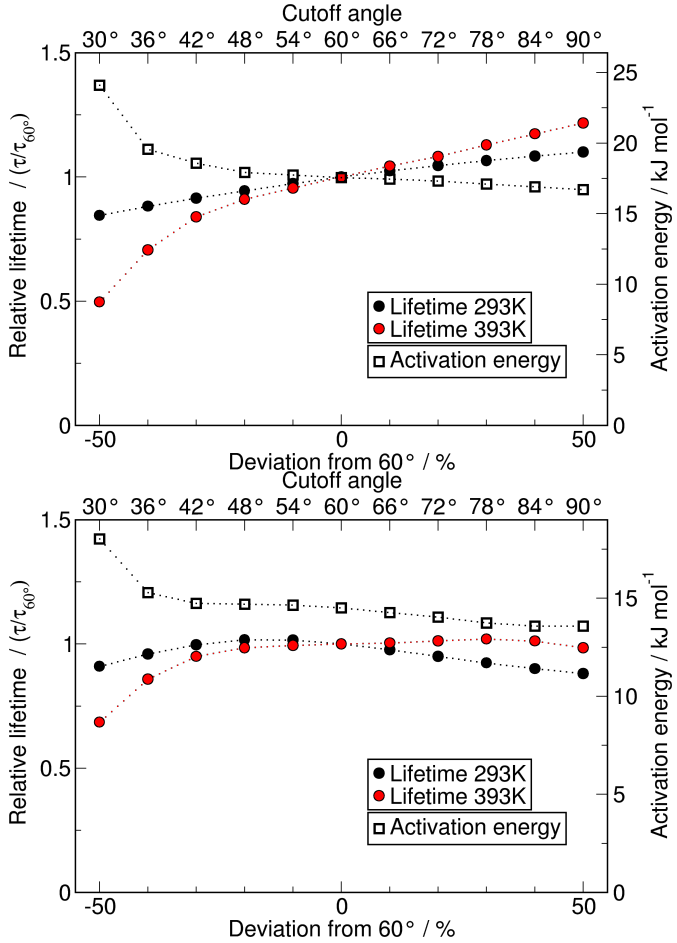

Figure 3.36.: Results of the angle criterion screening of the hydrogen bond analyses. The top panel shows the results for the H2 hydrogen bond, the bottom panel for the H4/5 hydrogen bonds. The times are given relative to the corresponding time obtained with an angle of 60°. The distance criterion was in all cases defined as first minimum of the corresponding RDF.

The impact of the angle criterion on the dynamics of the hydrogen bond at the H2 atom at low temperature is only low. The lifetime for a 30° angle is about 15% shorter than for the 60° angle, while it becomes about 10% longer with a 90° angle. Albeit the effect becomes stronger at higher temperatures, the changes are still below 10% if the angle's deviation is not more than ±20 %. However, for angle criteria smaller than −20%, that is 48°, the lifetime drops nearly exponentially to a lifetime half as long for a criterion of 30° compared to the lifetime with a 60° angle.

The impact on the activation energy is similar. Within a region from 42° to 90° the differences are only 1.0 kJ mol^{-1}. Thereby, the barrier decreases with increasing cutoff angle. If a smaller angle is chosen the increase in activation energy becomes significantly larger. In the extreme case of a 30° angle the calculated barrier peaks 24.1 kJ mol^{-1}.

For the H4/5 containing hydrogen bonds at low temperature the total deviation is below 5% for angles changed by −40% to +20%. Due to the nature of the imidazolium cation, the lifetime decreases not only for smaller angles, but as well for larger ones. At high temperature the changes in a region between −20% and +50% are below 2% and therefore clearly insignificant. For angles smaller than 48° the lifetime drops analogous to the H2 hydrogen bonds lifetime, reaching a total deviation of 32% for the 30° angle.

The behavior of the activation energy is very similar as for the H2 hydrogen bond. For a region between 36° and 90° the differences are below $1.0\,\mathrm{kJ\,mol^{-1}}$. However, for a 30° angle an increase in activation energy by $3.5\,\mathrm{kJ\,mol^{-1}}$ is observed.

Summing up, these findings show that the effect of the angle criterion on the obtained lifetimes is convincingly small as long as the criterion is not much smaller than 60°. In contrast, changes to larger angles up to at least 90° do not result in significantly different lifetimes. Therefore, results obtained with a choice of 60° are expected to be reliably robust. Nevertheless, this will probably depend on the nature of the intermolecular interaction within the substances. Thus, a careful examination of RDFs and angle distribution prior to the lifetime analysis is recommended.

Ion pair dynamics

Due to the fact, that the operator $h(t)$ is defined by a next neighbor criterion in the ion pair dynamics, there is only one related parameter, namely the cutoff distance between two ions which defines the vicinity operator $H(t)$. Analogous to the hydrogen bond dynamics, this criterion is selected through the first minimum of the corresponding RDF between the center of the cation's ring and the center of the anion's mass. We modified this distance by ±5 %, ±10 %, ±15 %, and ±20 %. The results for the $[NTf_2]^-$ anion are illustrated in Figure 3.37. For the other systems the results are only slightly, quantitatively different from these.

Obviously, the ion pair lifetimes grow with increasing distance criterion. Moreover, a higher temperature shows a more extreme behavior compared to the lower temperature. For small discrepancies below 10 % the change in ion pair lifetime is negligible small. The impact on the activation energy is more pronounced compared to the hydrogen bond dynamics but still much less changing than the lifetimes. For the shortest cutoff distance the barrier increases by $2.7\,\mathrm{kJ\,mol^{-1}}$ and decreases nearly linear with increasing distance criterion until the activation energy is $2.4\,\mathrm{kJ\,mol^{-1}}$ lower for the highest investigated cutoff.

3.4.5. Conclusions

In this article we employed the recently implemented and further developed reactive flux method to different ionic liquids systems. We investigated the dynamics of the hydrogen bonds as well as the ion pairs. The advantage of the reactive flux lies in the relative robustness of the approach towards the hydrogen bond criteria. Furthermore, it separates the dynamics of the targeted interaction from the effects due to transport properties like diffusion.

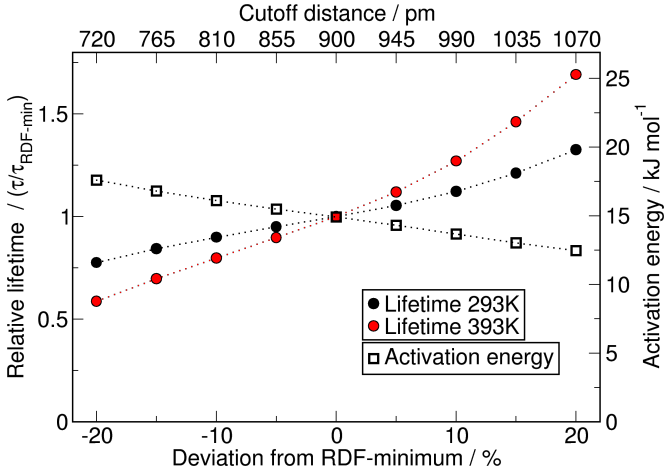

Figure 3.37.: Results of the distance criterion screening of the ion pair analyses. The life and decay times are given as multiples of the corresponding time obtained with the vicinity operator $H(t)$ defined by the distance of the first RDF minimum.

Therefore, we carried out molecular dynamics simulations based on an empirical force field for imidazolium based ionic liquids with varying anions. The aim of this work was to understand the influence of different parameters such as different anions and temperatures, but also simulations parameters and the geometrical criteria defining a pair as bonded or in contact. The simulation related group contains such factors as the total simulations lengths or the time between two snapshots of the printed trajectory. The analyses related parameters concern the geometric criteria.

We found that as a rule of thumb, the trajectory length should be at least by a factor of ten longer than the calculated lifetime. Further, we observed that a deviation in the distance criterion for hydrogen bonding of up to 5 % from the RDF's minimum results in a change of less than 10 % for the calculated lifetime. For the angle criterion we obtained a lower sensitivity: The change in lifetime is smaller than 10 % as long as the deviation of the donor-hydrogen atom-acceptor angle from linearity is chosen to be larger than 48°. Moreover, for the ion pairs, the change of the lifetime was found to be below 10 % as long as the distance deviates not more than 10 % from the RDF's minimum. Interestingly, the impact on the activation energy is less prone to the cutoff values than the lifetime.

Changing the anion leads to an increase of hydrogen bond and ion pair dynamics related to the fluidity of the ionic liquid. Thereby, the reactive flux method reveals a system dependence of this correlation which is masked in simpler analysis methods by the perturbation from diffusion. Increasing the temperature leads to a decrease in lifetime, i.e. the dynamics becomes faster. For the fluid ionic liquids the hydrogen bond dynamics is faster than the ion pair dynamics, but for the one viscous ionic liquid investigated here this trend reverses, i.e., the ion pair dynamics becomes faster than the hydrogen bond lifetime. For the investigated temperature range, the hydrogen bond as well as the ion pair dynamics do behave linearly according to Arrhenius' law.

3.5. Hydrogen Bonding of N-Heterocyclic Carbenes in Solution: Mechanisms of Solvent Reorganization

Sascha Gehrke[†,‡] , Oldamur Hollóczki[†,*]

Chemistry–A European Journal, 2018, Volume **24 (45)**, Pages 11594–11604

DOI: 10.1002/chem.201802286

Received: May 07, 2018

Published: June 08, 2018

For this article a Supporting Information is available free of charge at:
`https://chemistry-europe.onlinelibrary.wiley.com/action/downloadSupplement?doi=10.1002%2Fchem.201802286&file=chem201802286-sup-0001-misc_information.pdf`

Contributions to the manuscript:

- Setup and maintenance of all calculations
- Analysis of the trajectories, discussion of data
- Writing the manuscript

[†]Mulliken Center for Theoretical Chemistry, University of Bonn, Beringstr. 4+6, D-53115 Bonn, Germany
[‡]Max Planck Institute for Chemical Energy Conversion, Stiftstr. 34–36, D-45470 Muelheim an der Ruhr, Germany
[*]E-mail: holloczki@gmail.com

With the aim to achieve the third milestone of the thesis the achievements of the first two milestones needs to be merged. Therefore, a broad study of different NHC-based organocatalysts in varying solvent composition is simulated with the aid of the model described in Chapter 3.1. Afterwards, the statistics of the occurrence of hydrogen bonds between solvent and the carbene's active site are evaluated. An even deeper insight is gained by the application of the analysis tool presented in the last two chapters.

Abstract

Hydrogen bond dynamics of N-heterocyclic carbenes plays a central role in their proton transfer reactions, and the effects of hydrogen bonding are often invoked also in the corresponding organocatalytic applications. In the present paper the structure and lifetime of hydrogen bonds have been investigated for several carbenes in alcohol containing solutions by classical molecular dynamics simulations. The basicity of the carbene was found to be of major importance; while the least basic carbenes are often in their free form in the solvent, by increasing the basicity the simulations show increasing hydrogen bonding, often with even two alcohol molecules at a time. This peculiar bonding, where the single lone pair of the carbene is in interplay with two hydrogen bond donors, allows that despite the strong binding the alcohol molecules are readily replaced through an associative exchange mechanism. The exchange mechanism is different for carbenes with different basicities, with different substituents, and in different solvents. For example, while for the least basic carbenes it occurs through a free carbene, for the more basic compounds the double hydrogen bonded structure is involved instead. Since this process is also involved in the H/D exchange reactions, we argue that the pK values calculated from the related measurements have a varying physical meaning for the different carbenes. The lifetimes of the hydrogen bonds are apparently also clearly related to the basicity of the carbene, with gradually increasing lifetimes for the most basic compounds. Accordingly, the effects by hydrogen bond donor solvents should be more severe for basic carbenes in catalytic applications.

3.5.1. Introduction

Free N-heterocyclic carbenes attracted significant attention in the last few decades, partly because they are considered to be powerful, and environmentally benign organocatalysts.[40–42,63,235,236] The portfolio of such organocatalytic reactions contains a number of valuable C-C coupling reactions, which in many cases show an excellent regio- and stereoselectivity, including also the enzymatic reactions of thiamin (vitamin B1).[52,234] In many NHC catalyzed reactions the carbene is not used in its free form, but as a protonated precursor azolium salt, which is then deprotonated by a proper (often amine) base in the reaction mixture.[40–42,63,123] We showed recently that in many cases there is a possible way for the reaction to occur directly from the azolium species without the involvement of a free carbene intermediate.[6] However, it is not yet clear if the carbene is absent in all possible reactions, or if there are some cases, in which it is indeed generated *in situ* by deprotonation of the precursor.

Assuming the presence of the free carbene, the reaction is initiated by a nucleophilic attack of the NHC's lone pair to the substrate. This very lone pair, however, also makes the carbene a strong hydrogen bond acceptor.[1,82,124–126,413] Thus, if hydrogen bond donor molecules (e.g. solvent molecules, or the protonated base itself that originates from the carbene formation) are available in the solution, they will compete with, and potentially suppress the reaction. Therefore, the dynamics and lifetimes of the hydrogen bonds of the carbene will significantly influence its catalytic activity. There are several reports about employing solvent effects to tune carbene catalysis in terms of selectivity, yields, and reaction rates.[41] For instance, the rate of an NHC catalytic reaction in 1,3-dialkylimidazolium bis(trifluoromethanesulfonyl)imide ionic liquids has been shown to be significantly slower than in THF.[132] This effect was attributed to the presence of C-H$\cdots$C type hydrogen bonds[129] between the carbene and the imidazolium cation, although the interaction between the ionic liquid cation and the base used in the reaction may also play an important role. Inoue and co-workers showed that the ratio of the possible products of cross-benzoin condensation can clearly be affected by the solvent's composition.[130] In a similar way, the ratio of γ-butirolactones and β-lactones as products in a reaction of α,β-unsaturated aldehydes with other aldehydes in the presence of NHCs can be significantly influenced by altering the temperature and, more importantly, the solvent.[131] The highly complex reaction mechanisms, especially considering our findings[6] that the NHC is not necessarily involved in the process, suggest that the underlying origin of these solvent effects may well be other than a carbene-solvent hydrogen bond. Nonetheless, the fact that hydrogen bonding with the solvent is so often invoked as an influential factor in the reactivity of carbenes and in the related catalysis shows that understanding this feature is of high importance.

Another impressive feature of carbenes is their remarkably high basicity, which has also been in the focus for decades.[68,70,83–89,414] Among the many approaches that have been applied to determine the pK values of carbenes, those based on the kinetics of H/D exchange reactions of their conjugate acid azolium cations in deuterated solvents are prominent. The reaction follows the multistep mechanism established by Eigen,[415] which is initiated by the association of the base (e.g. a solvent molecule) and the azolium cation,

followed by a proton transfer, forming a complex of the carbene and the protonated base (Figure 3.38). Although seldomly expressed explicitly, this latter structure is a hydrogen bonded complex. To fulfill the H/D exchange, the protonated base in contact with the carbene has to be replaced by another molecule from the solvent in the solvent rearrangement step, and can then be finalized by the proton transfer to the carbene. Through the detailed analysis of the kinetics of the reaction and the corresponding kinetic isotope effects, it has been established for aqueous solutions of imidazolium, thiazolium and other analogous salts that the solvent reorganization step is rate limiting.[87,89] Thus, the hydrogen bond dynamics of the corresponding carbene is the key to understand this process comprehensively.

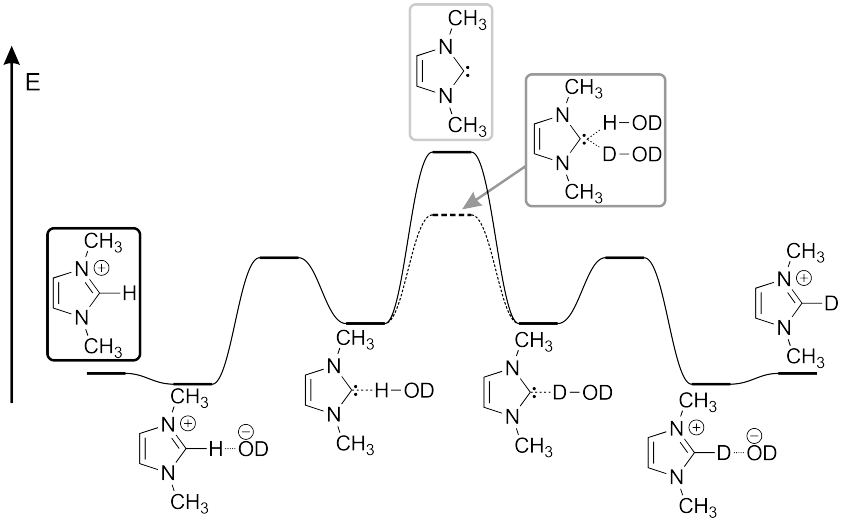

Figure 3.38.: Reaction energy profile of the H/D exchange reactions of imidazolium cations.[87] The dashed line indicates the possible additional pathway from the associative exchange[123] of the hydrogen bond donor water molecule, providing a possible "shortcut" for the solvent reorganization.

Despite the aforementioned relevance of these interactions, the knowledge in literature is still insufficient to characterize the hydrogen bonding of carbenes. The studies so far focused mostly on crystal structures[124–126] and gas phase calculations,[82,121,413] while a comprehensive study on the H-bonding structure and dynamics of carbenes in the liquid phase, to our knowledge, has not been published. In a previous work,[123] focusing solely on 1,3-dimethylimidazol-2-ylidene, we showed that the exchange rate of the alcohol molecules at the carbene is relatively fast, despite the strength of the individual interactions.[123] The mechanism of the exchange predominantly follows an associative pathway, involving a transient three-centered double hydrogen bond assembly, where two hydrogen bond donors are interacting with one NHC lone pair at the same time (Figure 3.39).

This mechanism also raises questions regarding basicity measurements for carbenes, based on the H/D exchange rate of the conjugate acids. In general, pK values correspond to equilibria, in which the acid (in this case the azolium cation) fully dissociates

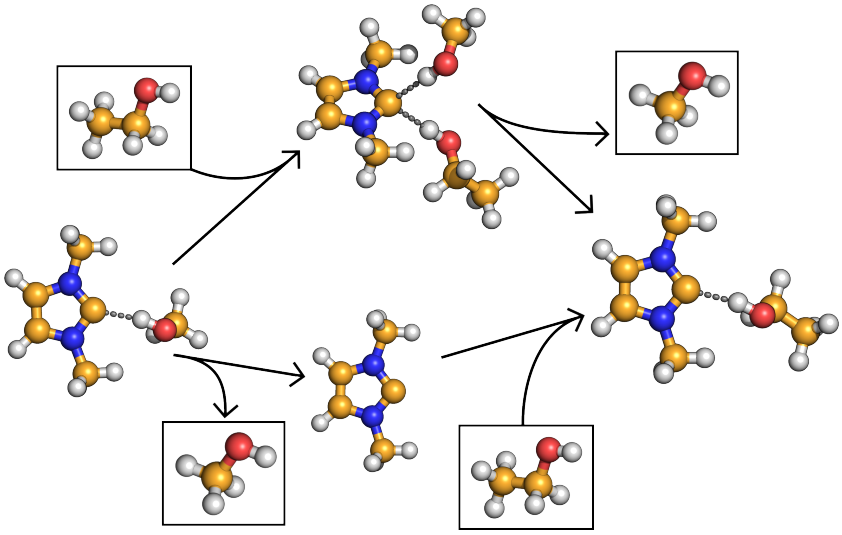

Figure 3.39.: Solvent reorganization mechanisms at N-heterocyclic carbenes illustrated by the exchange of methanol by ethanol. In the associative pathway (above) a transient three-center double hydrogen bond assembly is formed by the attachment of ethanol molecule, followed by the dissociation of the methanol molecule. In the dissociative pathway (below) a free carbene species is formed, which then forms a hydrogen bond with the ethanol.

to the deprotonated carbene (see Figure 3.40). When calculating the acidity of the corresponding molecules through H/D exchange, it is implicitly assumed that the exchange mechanism involves these free species formed through the proton transfer and the subsequent dissociation, which can then react with other proton sources in solution, fulfilling the exchange (Figure 3.38). The presence of a "shortcut", avoiding the formation of the free carbene through the associative mechanism in the process may, however, influence the rates as well (see dashed line in Figure 3.38), and hence it must be studied, too.

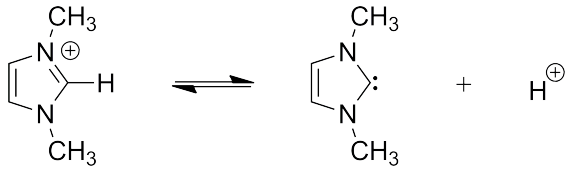

Figure 3.40.: The dissociation equilibrium of 1,3-dimethylimidazolium cation defining its pK.

These results already show how complicated the hydrogen bonding of NHCs is in a liquid. For employing the potential effect of hydrogen bonding in different NHC-based applications requires, however, a comprehensive knowledge on the influences of the heteroatoms in the NHC, the substituents, and the solvent composition as well. In the present study we discuss these effects extensively, and reveal the general aspects of the

liquid-phase hydrogen bonding of a series of NHCs. To this end, we considered altogether nine NHC rings, which have been either synthesized, or suggested to be synthetically available. For imidazol-2-ylidenes we investigated several side chains with different steric demand, and also different alcohol concentrations in the solvent mixture.

3.5.2. Computational Details

Classical Molecular Dynamics Simulations

All classical MD simulations were performed by the LAMMPS program package.[263] By using classical MD, nuclear quantum effects (NQEs) were neglected, which may have effects even on the quantitative conclusions if proton transfers are involved.[416] However, the proton transfer between the carbene and the alcohol molecules is neglected here, and since it has been shown that the dynamics of water is only slightly influenced by NQEs, while the water reorientation mechanism is not affected at all, we expect that this simplification will have no effects on the main conclusions of this study.[417] The analysis of the trajectories was performed by our open source program TRAVIS.[316,329,330,418] In order to model the carbene's side chains as well as the solvent molecules the OPLS-AA force field[255] was applied with the Lorentz–Berthelot mixing rules. Non-bonded interactions were computed within the cutoff radius of 10 Å, Coulombic interactions beyond this distance were computed *via* the particle-particle particle-mesh solver[402] with an accuracy of 10^{-5}.

The ring unit of the carbene species was modeled by the carbene force field (CaFF),[1] which is based on the OPLS force field. The CaFF has been developed specifically to describe accurately the hydrogen bonding of carbenes, using DLPNO-CCSD(T)/CBS reference interaction energies (see Chapter 3.1 or Supporting Information of the article). It has been shown to be perfectly suitable to describe the non-bonding interactions of NHCs and OPLS hydrogen bond donors and proven its value already in studies of cellulose processing.[2] It has to be mentioned here that this model is unable to describe proton transfer processes, which might also influence the hydrogen bonding of carbenes with large basicity. However, the experimental findings[87,89] that the hydrogen bond dynamics is the actual rate limiting step in the H/D exchange process suggests a certain unimportance for the proton transfer in understanding the solvent reorganization, and that the latter process can be treated separately.

To enable the calculation of the hydrogen bonds lifetimes a distance and an angle criterion has to be established first, through which it is possible to define the value for $h(t)$. For the distance criterion the position of the first minimum in the corresponding RDF was taken. In the investigated systems a nearly linear constellation within the C$\cdots$H-O unit was observed, hence the angle criterion was chosen to be $> 150^{\circ}$. This choice has shown a good performance for the similarly linear hydrogen bonds in water.[229]

All the simulations were carried out according to the following protocol:

1. The initial configuration of each cell was generated by the PACKMOL program[312] with a starting density equivalent to the experimental density of the corresponding pure solvent. The detailed compositions of the simulation cells of all simulations are shown in Table 3.24.

2. Each system was simulated in an NVT-ensemble for 0.5 ns, to remove possible energy hotspots in the initial configurations of the molecules. The temperature was controlled by applying a Nosé–Hoover chain thermostat ($T = 300\,\mathrm{K}$, $\tau = 100\,\mathrm{fs}$). The timestep for the simulations was chosen to be 1 fs.

3. Each system was simulated in an NpT-ensemble for 1 ns. Constant pressure and temperature were provided *via* a Nosé–Hoover chain thermostat ($T = 300\,\mathrm{K}$, $\tau = 100\,\mathrm{fs}$) and a Nosé–Hoover barostat ($p = 1\,\mathrm{bar}$, $\tau = 1000\,\mathrm{fs}$), respectively.[403–405] Over the last 0.5 ns the box volume was averaged. The resulting densities are summarized in Table 3.24.

4. The systems were slowly forced to the average volume obtained in step 3 over 0.25 ns. Finally, the ensemble was switched back to NVT. To assure a constant temperature again a Nosé–Hoover-chain thermostat ($T = 300\,\mathrm{K}$, $\tau = 100\,\mathrm{fs}$) was employed.

5. After an equilibration period for 1 ns, the production runs were performed for 10 ns, saving the coordinates of the systems in every 1 ps.

Static DFT and *ab initio* calculations

All quantum chemical calculations were performed by the ORCA 3.0.3 software package.[256] The geometries were optimized employing the TPSSh functional[278] enhanced by the D3 dispersion correction with Becke–Johnson damping,[279,280] using the def2-TZVPP basis set.[282,283] For both the SCF cycle and the geometry optimization convergence criteria the tight settings of ORCA were used. The obtained stationary points were identified as minima by calculating the eigenvalues of the Hessian.

Single point energies were calculated using the DLPNO-CCSD(T)[259–261] method, with tight settings for the localization as defined by Neese and Liakos. The obtained single point energies with the def2-TZVPP and with the def2-QZVPP basis sets were extrapolated to the complete basis set limit.[262]

Table 3.24.: Molecular composition of the investigated systems. Figures of the NHC ring units, as well as the side chains, are shown in Figure 3.41. Every simulation cell contains 10 molecules of the respective carbene species and 510 solvent molecules ($N_{solvent}$: number of alcohol and THF molecules in the system; ρ: densities obtained by the NpT simulations; D: diffusion coefficient of the carbenes).

			$N_{solvent}$		ρ	D
System	NHC ring	R	alcohol	THF	/ g cm^{-3}	/ 10^{-10} m^2 s^{-1}
Ia	**1**	Me	10[a]	500	0.847	16.05
Ib	**1**	Me	102[a]	408	0.827	7.19
Ic	**1**	Me	204[a]	306	0.809	14.40
Id	**1**	Me	306[a]	204	0.788	9.64
Ie	**1**	Me	408[a]	102	0.765	8.74
If	**1**	Me	510[a]	0	0.756	10.69
Ig	**1**	Me	170[a]	340	0.816	7.27
Ig-iPr	**1**	Me	170[b]	340	0.806	11.72
Ig-tBu	**1**	Me	170[c]	340	0.797	10.83
Ih	**1**	iPr	170[a]	340	0.815	8.78
Ih-iPr	**1**	iPr	170[b]	340	0.802	11.90
Ih-tBu	**1**	iPr	170[c]	340	0.798	9.19
Ii	**1**	tBu	170[a]	340	0.813	15.26
Ii-iPr	**1**	tBu	170[b]	340	0.802	7.43
Ii-tBu	**1**	tBu	170[c]	340	0.798	8.08
Ij	**1**	Me_2Ph	170[a]	340	0.822	10.61
Ij-iPr	**1**	Me_2Ph	170[b]	340	0.812	5.54
Ij-tBu	**1**	Me_2Ph	170[c]	340	0.808	3.78
Ik	**1**	iPr_2Ph	170[a]	340	0.824	3.93
Ik-iPr	**1**	iPr_2Ph	170[b]	340	0.812	3.36
Ik-tBu	**1**	iPr_2Ph	170[c]	340	0.806	3.32
II	**2**	Me	170[a]	340	0.821	15.97
III	**3**	Me	170[a]	340	0.815	8.49
IV	**4**	Me	170[a]	340	0.821	4.68
V	**5**	Me	170[a]	340	0.826	7.82
VI	**6**	Me	170[a]	340	0.824	13 29
VII	**7**	Me	170[a]	340	0.805	8.66
VIII	**8**	Me	170[a]	340	0.826	8.81
IX	**9**	Me	170[a]	340	0.846	10.34

[a]EtOH [b]iPrOH [c]tBuOH

The Reactive Flux Approach for Hydrogen Bond Lifetimes

The reactive flux approach augments the calculation of lifetimes by a correction for diffusion processes.[228,229] It is based on the autocorrelation function of the bonding operator

$$c(t) = \frac{\langle h(0)h(t)\rangle}{\langle h\rangle} \qquad h(t)\begin{cases}1 & \text{if hydrogen bonded}\\ 0 & \text{if not.}\end{cases}$$

Since autocorrelation functions are invariant with respect to time, the bond decay function

$$k(t) = -\dot{c}(t) = -\frac{\langle h(0)\dot{h}(t)\rangle}{\langle h\rangle} = \frac{\langle \dot{h}(0)h(t)\rangle}{\langle h\rangle} = -\frac{\langle \dot{h}(0)[1-h(t)]\rangle}{\langle h\rangle}$$

can be found. With the help of the neighbor operator $H(t)$ it is possible to express the diffusion corrected function of bond reformation

$$k_{in}(t) = -\frac{\langle H(t)[1-h(t)]\dot{h}(0)\rangle}{\langle h\rangle} \qquad H(t)\begin{cases}1 & \text{if neighbors}\\ 0 & \text{if not.}\end{cases}$$

The probability to find two molecules non-bonded but still next to each other is found from the integral

$$n(t) = \int_0^t k_{in}(t')dt'.$$

Finally, the kinetic equation

$$-\dot{c}(t) = k_f c(t) - k_b n(t)$$

is defined. The reciprocal pre-factors k_f and k_b have the physical meaning of the lifetime τ_f of the hydrogen bonds and the "deadtime" τ_b.

First a distance and an angle criterion has to be established, through which it is possible to define the value for $h(t)$. For the distance criterion the position of the first minimum in the corresponding RDF was taken. In the investigated systems a nearly linear constellation within the C$\cdots$H-O unit was observed, hence the angle criterion was chosen to be $> 150^{o}$. This choice has shown a good performance for the similarly linear hydrogen bonds in water.[229]

3.5.3. Results and Discussion

Influence of the NHC Ring

The hydrogen bonding and the underlying dynamics is highly dependent on the actual NHC ring,[1] due to the varying electronic effects of the heteroatoms and the different π-system of the NHC. For this reason, we modeled the whole range of carbenes that have available parameters for classical simulations,[1] covering many NHCs that have been synthesized, or have been suggested for synthesis. The complete list of structures can be seen in Figure 3.41. In the first set of simulations the R substituents were methyl groups,

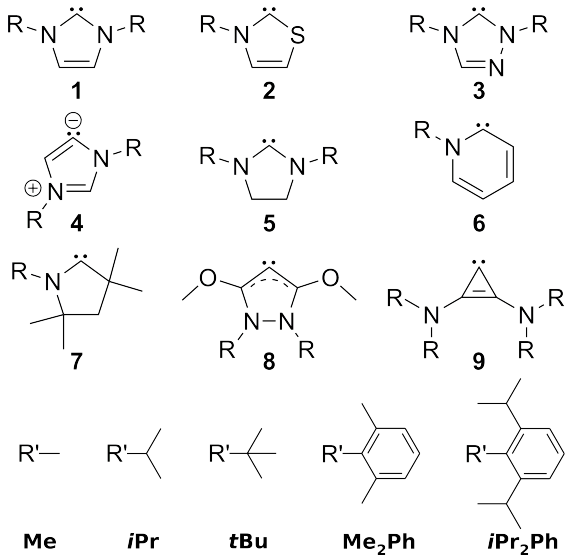

Figure 3.41.: The NHC ring units and side chains considered in this study. The R group is replaced by one of the side chains. Furthermore, the R′ group is replaced by the respective carbene ring unit. Side chains were modeled by the OPLS force field, while the ring units were modeled with CaFF.[1]

as we were interested in the electronic effects of the substituents — implicitly included in the force field — instead of steric shielding.

In the arbitrarily chosen THF-EtOH 2:1 mixture solvent all carbenes form hydrogen bonds with the alcohol according to the radial pair distribution functions (RDF) of the carbene carbon atom and the hydroxyl hydrogen atom (Figure 3.42). The first maximum — thus, the most often occurring hydrogen bond distance — was found at 1.97–2.03 Å, except for thiazol-2-ylidene **2**, where the maximum is located at 2.13 Å. The first peaks for **2** and **3** are noticeably lower, while the peaks for **4** and **8** are significantly higher than for the other systems. The number integrals (Table 3.25) of these peaks — *i.e.* the average number of alcohol molecules in hydrogen bond with a single carbene molecule — show the same trend, as they are low for **2** and **3** (0.3–0.5) and very high for **4** and **8** (1.7–1.8), as opposed to the rest of the NHCs (all are *ca.* 1). These differences show that the average number of alcohol molecules in hydrogen bond with each carbene molecules varies greatly, depending on the heteroatoms in the NHC ring. More details are shown by the distribution of the numbers of simultaneous bonding partners.

Three different bonding patterns can be observed during the simulations: the free carbene, the most commonly known structure with a single hydrogen bond donor at the single acceptor site of the carbene, and the previously observed[123] double hydrogen bonded structure. While the catalytically widely used **2** and **3** occur at least half of the time as free carbenes, **4** and **8** are not observed in their free form at all, but two-third of the time even in a double bonded assembly (Figure 3.43). The data above is well supported by the combined distribution functions (CDFs), that depict the orientation of

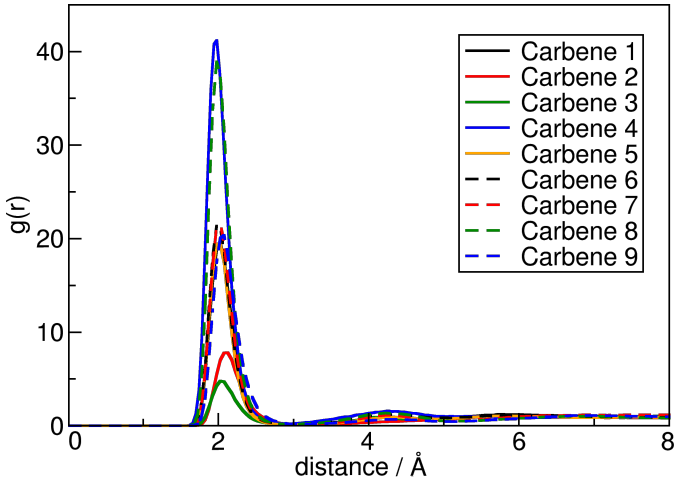

Figure 3.42.: The RDFs of the simulations with different NHC ring units. Shown is the $g(r)$ of the carbene carbon atom and the hydroxyl hydrogen atom.

Table 3.25.: Positions and number integrals of the first peak of the RDFs shown in Figure 3.42, together with the DLPNO-CCSD(T)/CBS//TPSSh-D3BJ/def2-TZVPP proton affinities.

Carbene	Maximum / Å	Minimum / Å	Number Integral	Proton affinity / kcal mol^{-1}
1	2.025	3.075	0.98	267.6
2	2.125	3.075	0.52	256.4
3	2.025	3.025	0.29	255.6
4	1.975	2.925	1.81	286.8
5	2.025	3.025	0.94	268.6
6	1.975	3.025	1.04	278.3
7	2.025	3.075	1.04	275.2
8	1.975	3.025	1.74	288.1
9	2.075	3.075	1.19	273.7

the alcohol molecules at the carbene. The three groups defined by the number integrals are characterized by a different bonding behavior. The carbenes with a high number integral, **4** and **8**, show two separate peaks slightly above and below the plane of the ring (Figure 3.44 right). The NHCs with a number integral of about 1, namely **1**, **5**, **6**, **7** and **9** show a single, but relatively broad peak centered around the ring plane, indicating a single hydrogen bond at the lone pair (Figure 3.44 middle plot). Since the mostly free **2** and **3** show almost no double hydrogen bonded structures in the solution, the occurring NHC-alcohol interactions are restricted to the single donor-single acceptor cases, where the interaction is highly directional, centered around the ring plane (Figure 3.44 left plot), with relatively low occurrences.

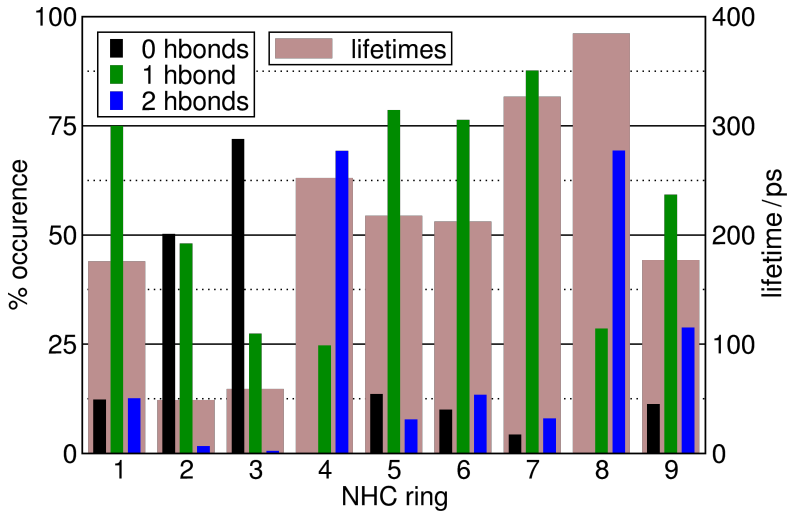

Figure 3.43.: Occurrence of the different hydrogen bond assemblies (small bars, left axis) and the lifetimes of the hydrogen bonds (broad bars, right axis) in the simulations with different NHC rings.

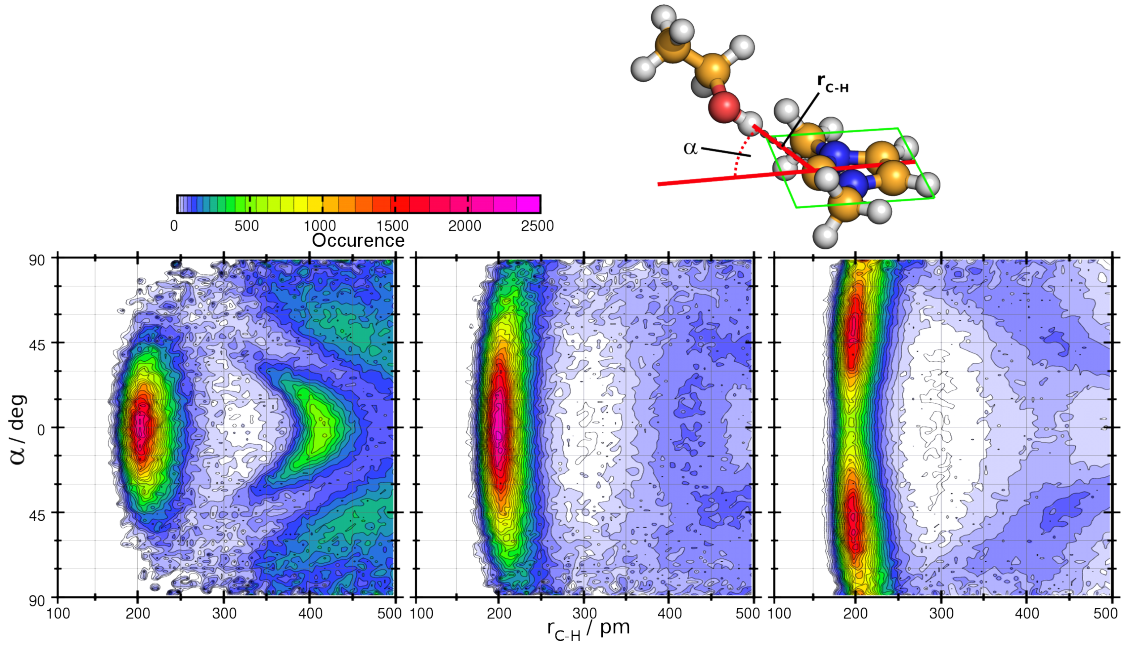

Figure 3.44.: Combined distribution functions of the carbenes hydrogen bonds. The left plot shows the predominantly free **3**, the middle plot corresponds to **1**, being mostly in a single hydrogen bond with the solvent, and the right shows the mostly double hydrogen-bonded **4**.

The hydrogen bond acceptor strength is related to the lone pair of the carbene, and so is its basicity. To verify if these two properties are connected, we determined the protonaffinity of these carbenes by static *ab initio* calculations (see Figure 3.25), and correlated them with the number integral data. Although the points show some scatter, a common trend is clearly visible (Figure 3.45), showing that the average number of hydrogen bond donor molecules at the NHC ring — that is, if the carbene is more free in solution or rather bound to one or two alcohol molecules — is strongly determined by the basicity of the carbene. Consequently, the carbenes that are easier to deprotonate are also more free in the solution from hydrogen bonds, having a distinct advantage over the other NHCs in a catalytic process, which must involve the presence of free carbenes.

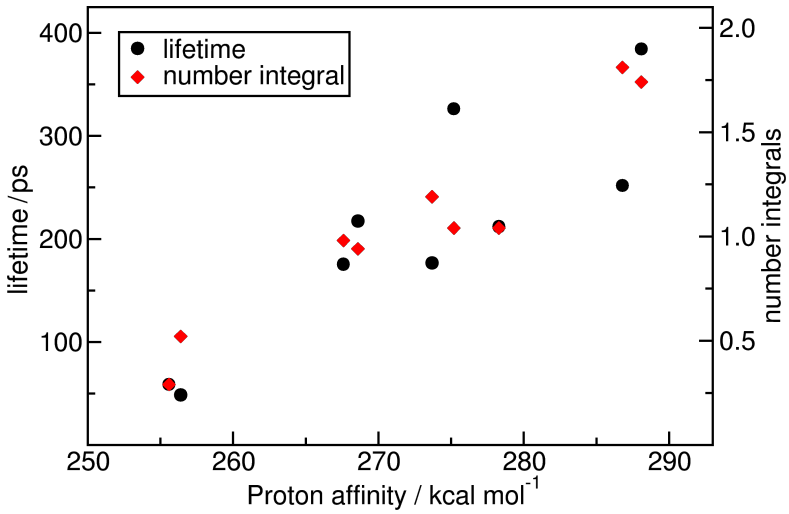

Figure 3.45.: The correlation of the proton affinity of the different carbenes with the number integral of the corresponding RDF's first peak (black) and the lifetimes of the corresponding hydrogen bonds (red).

Finally, the lifetimes[3,228,229,349] of the hydrogen bonds were calculated. The NHC ring does not only have an influence on the strength of the hydrogen bonds, but also on their dynamics. Similarly to the discussion above regarding the coordination numbers, three groups can be distinguished in terms of hydrogen bond dynamics. The average lifetime of the hydrogen bonds (Figure 3.43) of **2** and **3** are only about 50 ps, which is surprisingly short for these strong hydrogen bond acceptor solutes. The lifetimes of **7** and **8** are significantly longer, with values above 300 ps. All other lifetimes are in the range of $180 - 250$ ps. The data above shows that the NHCs mostly applied in catalysis, **2** and **3**, are only blocked for short periods by hydrogen bonding partners in this model. This feature renders these compounds mostly available for the (catalytic) reactions also in the presence of hydrogen bond donor (solvent) molecules, if they are applied in their free form, and not their conjugate bases.

The exchange mechanism also seem to vary for the different carbenes. In case of NHCs **2** and **3** with the shortest lifetimes it is clear that the mechanism is predominantly

dissociative (see Figures 3.39 and 3.46 left), initiated by the dissociation of the C$\cdots$H-O hydrogen bond, shown by the overwhelmingly high ratio of free carbene in the solution. In case of **4** and **8**, however, the free carbene is not observed at all, suggesting that the dissociative pathway is not available for these structures. In return, the high occurrence of the double hydrogen bonded structure allows the associative mechanism to facilitate the exchange, which starts with the association of a second alcohol molecule to the hypovalent carbon atom of the carbene-alcohol assembly, followed by the cleavage of the "old" carbene-alcohol bond (Figure 3.46 right). For the other carbenes the presence of all three possible coordination structures shows that both mechanisms are present, and they determine the lifetimes together (Figure 3.46 middle). However, the connection between the distribution of coordination numbers and the dynamics is apparently highly complex, since carbenes with similar coordination patterns produce very different lifetimes, see e.g. **4** and **8**.

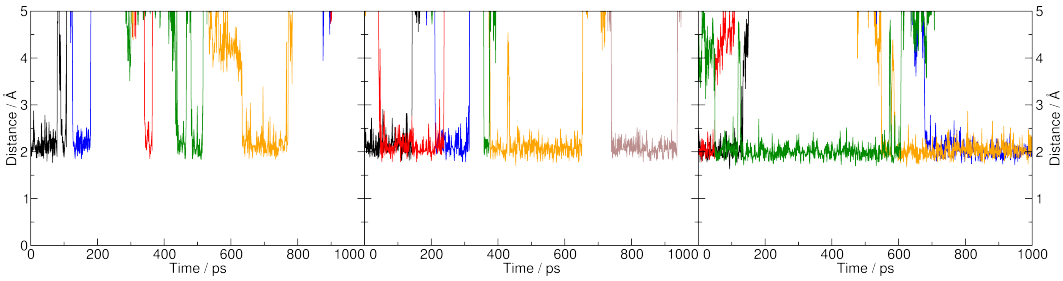

Figure 3.46.: Time development plots of the distance between the hypovalent carbon atom of the NHC and the hydroxyl hydrogen atoms of the alcohol molecules. The different curves correspond to different molecules. Hydrogen bonds are indicated by the approach of a curve to the shorter (ca. 2 Å) distances. In case of **3** (left), it is visible that the existing hydrogen bond between the carbene and the alcohol first dissociates, before a new hydrogen bond can form. In case of **4** (right), the first hydrogen bond dissociates after the formation of the second one, via the double hydrogen bonded structure, shown by the overlapping curves at ca. 2 Å. In case of **1** both mechanisms occur.

Similarly to the coordination numbers, the lifetimes show a common trend with the proton affinities, thus, more basic carbenes will have longer living hydrogen bonds. If the mechanism simply followed a dissociative path in all cases, one could argue that this correlation simply means that the cleavage of the hydrogen bond is determined by the hydrogen bond acceptor strength of the carbene, and therefore the basic, stronger hydrogen bond acceptor carbenes are less likely to release the alcohol molecule from the bond, increasing the lifetime. However, the coordination numbers show that while the least basic, therefore weaker acceptor carbenes are very often in their free state, and hence their exchange mechanism is predominantly dissociative, but with the stronger acceptor carbenes the double hydrogen bonded structures are often occurring, indicating an associative mechanism. Accordingly, the H/D exchange for carbenes with different

basicities follow a fundamentally different mechanism, hence the physical meaning of the rates, and that of the so deduced pK values should also change. While for the least basic carbenes the free carbene is indeed involved, and therefore the reaction rate truly relates to the definition of pK as shown in Figure 3.40, for the carbenes with high basicity the capacity to form double hydrogen bonded structures gives rise to the "shortcut" via the associative mechanism, which avoids the formation of the free carbene altogether (Figure 3.38). Thus, for the most basic carbenes the information on the energy requirement to remove a proton from the conjugate acid of the carbene is not included in the exchange rate *per se*.

In case of these carbenes the exchange rate, and hence the lifetimes, could follow a completely different trend against the basicity, the carbenes could exhibit, for example, a maximum in the lifetimes along the proton affinity scale. For this reason, and since the change in the mechanism could also result in large discontinuities in the trends of the lifetimes, the presence of the (albeit weak) lifetime-protonaffinity correlation is very surprising. This means, however, that the associative mechanism takes over in the exchange gradually, and therefore the trends in pK values should not be affected by it.

Influence of the Side Chains

Beside the basicity of the carbene ring, there are other effects that might influence the hydrogen bonding of the carbene ring. One of these effects can be steric hindrance, which — in the presence of groups with varying bulkiness at the nitrogen atoms — might prohibit the hydrogen bond donor to approach the carbene. To observe the extent of steric effects, we performed a series of simulations with the derivatives of the most widely investigated NHC, imidazol-2-ylidene, with an identical solvent composition to those above. The effect of the alcohol side chain was also investigated by performing the simulations with *iso*-propanol and *tert*-butanol instead of ethanol (See Table 3.24).

The RDFs of the C$\cdots$H distances in the simulations of **Ia-k** (Figure 3.47 and Table 3.26) show a significant variation in height. In case of the smallest side chains, i.e., the methyl and *iso*-propyl groups, the RDF peaks are similar in height, and the integrals of the first peaks are also close to 1. The increase of the size of the substituents, however, results in a tremendeous decrease in peak height, as well as in number integrals in the following order: 2,6-dimethylphenyl > 2,6-di-*iso*-propylphenyl > *tert*-butyl. For the latter structure even the hydrogen bonding distance, marked by the position of the first peak in the corresponding RDF, is shifted to larger values, showing again the significant weakening of the hydrogen bond by the bulkiness of the tBu group. This order is in good qualitative agreement with the increase in steric blocking at the divalent carbon atom increasing from the methyl group and the only slightly larger *iso*-propyl group through the sizable, but rather flat 2,6-dialkylphenyl groups to the spherical, and hence strongly blocking *tert*-butyl substituents.

Replacing ethanol by larger alcohols in the system, the RDFs are clearly affected, and the extent of this effect is dependent on the size of the substituents on the NHC. In case of the smaller groups on the NHC, such as the methyl and *iso*-propyl, the integral of the first peaks barely differs for the three alcohols, even if the location of the first

peak is shifted to somewhat larger values. For the 2,6-dimethylphenyl-substituted NHCs the number integral drops to ca. its half when changing the hydrogen bond donor from ethanol to *tert*-butanol, while this change for the two largest groups, the *tert*-butyl and 2,6-di-*iso*-propylphenyl, is even more significant.

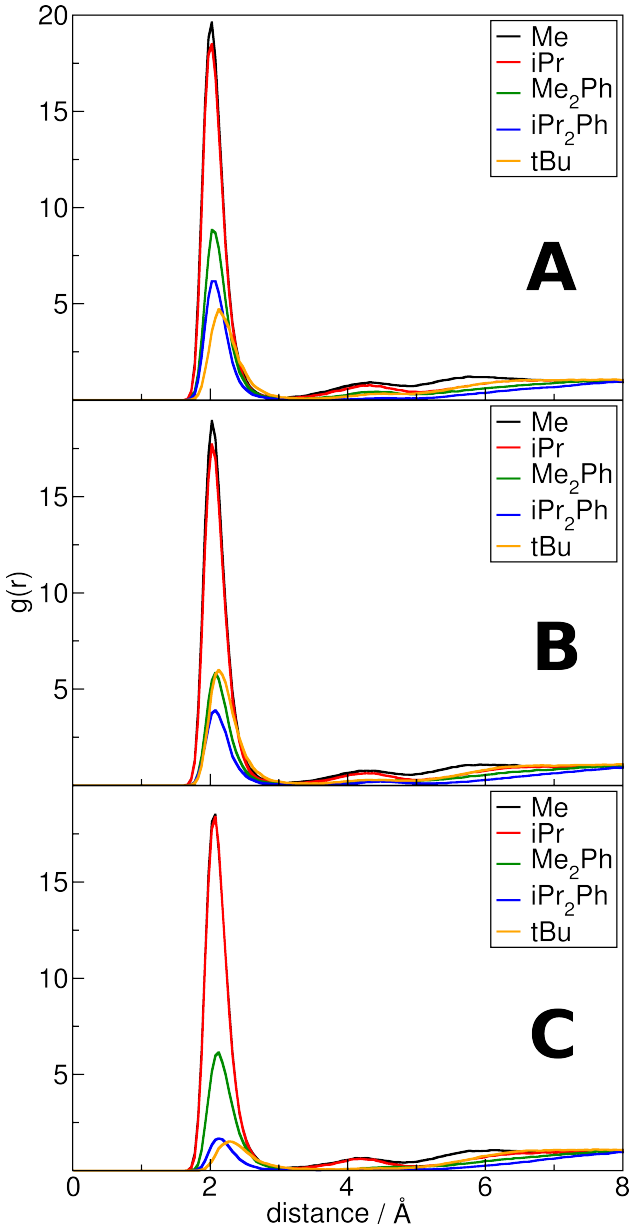

Figure 3.47.: The RDFs of the simulations with varied side chains in solvent systems with different alcohols. **A**: ethanol; **B**: *iso*-propanol; **C**: *tert*-butanol. The respective alcohol is mixed in a ratio of 1:2 with THF. Shown is the $g(r)$ of the carbene carbon atom and the hydroxyl hydrogen atom.

Table 3.26.: The number integrals of the first peak in the RDFs in Figure 3.47.

Side chain	Alcohol	Maximum / Å	Minimum / Å	Number Integral
Me	EtOH	2.025	3.075	0.98
	iPrOH	2.025	3.075	0.92
	tBuOH	2.075	3.125	0.89
iPr	EtOH	2.025	3.075	0.91
	iPrOH	2.025	3.075	0.84
	tBuOH	2.075	3.125	0.86
Me_2Ph	EtOH	2.075	3.125	0.48
	iPrOH	2.075	3.175	0.31
	tBuOH	2.125	3.425	0.35
iPr_2Ph	EtOH	2.075	3.525	0.33
	iPrOH	2.075	3.325	0.21
	tBuOH	2.125	3.575	0.10
tBu	EtOH	2.125	3.425	0.36
	iPrOH	2.125	3.425	0.42
	tBuOH	2.275	3.475	0.15

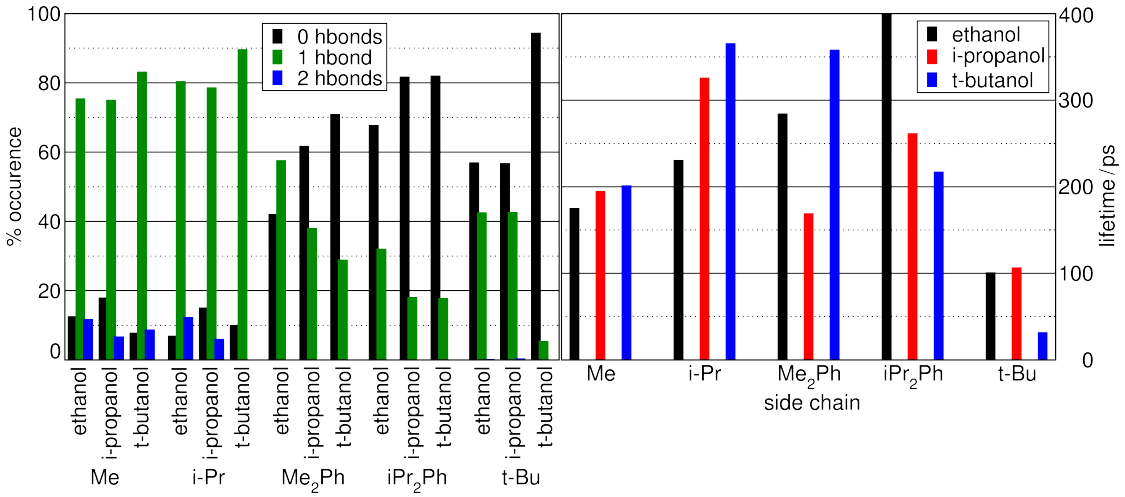

Figure 3.48.: Occurrence of the different hydrogen bond assemblies (left) and the lifetimes of the hydrogen bonds (right) in the simulations with different side chains in different solvent systems. The respective alcohol is mixed in a ratio of 1:2 with THF.

In Figure 3.48 the occurrences of the free carbenes, the single and double hydrogen assemblies are shown. Similarly to the number integrals, these occurrences are also affected by steric effects. For the methyl- and *iso*-propyl substituted NHCs the single hydrogen bonded structure is the most common with all alcohols. The ratio of the double hydro-

gen bonded structures, however, changes significantly, and 1,3-di-*iso*-propylimidazol-2-ylidene with *tert*-butanol does not form any of the double hydrogen bonded compounds. Interestingly, for R = Me or iPr, the occurrence of the free carbene is the highest with *iso*-propanol, while that of the single hydrogen bonded structures for the *tert*-butanol.

For the carbenes that have larger functional groups than *iso*-propyl at the nitrogen atoms exhibit no notable double hydrogen bonding with the present solvents. Apart from the system containing 1,3-bis(2,6-dimethylphenyl)imidazol-2-ylidene and ethanol, all simulations with the 1,3-dialkylphenyl and *tert*-butyl groups at the nitrogen atom of the NHC show the dominance of the free carbene even over the single hydrogen bond. The 1,3-di-*tert*-butylimidazol-2-ylidene in a solvent containing *tert*-butanol the ratio of the free carbene reaches over 95 %.

The average lifetimes of the hydrogen bonds (Figure 3.48, right graph) are also highly influenced by the steric demand of the carbene's and the alcohol's side chains. For the small methyl- and *iso*-propyl groups the lifetimes are increasing with an increase of the steric demand of the alcohol. The above mentioned mutual occurrence of the free carbene and the double bonded assembly shows that the exchange in these cases occurs via both the associative and the dissociative pathways. The sterically more demanding alcohol molecules are hindering the attachment of each other to the carbene carbon atom to form double hydrogen bonded structures, therefore in the exchange mechanism the associative pathway is unavailable.

By the further increase in the size of the substituents at the carbene, however, the occurrence of the free carbene is increased, making the dissociative pathway of the hydrogen bond exchange more and more favorable. This effect results in the gradual decrease of the hydrogen bond lifetimes upon approaching the bulkiest groups at the carbene, or exchanging ethanol to larger alcohols in the solvent. This trend is somewhat broken in case of the 1,3-bis(2,6-dimethylphenyl)imidazol-2-ylidene, where the hydrogen bonds show the longest lifetimes, interestingly, in *iso*-propanol, despite the otherwise clear trend in the coordination patterns. This discrepancy underlines again that the actual dynamics is a rather complex process, where the occurrences of the different coordination patterns cannot account for all the trends in the lifetimes.

Influence of the Solvent Composition

The occurrence of the different hydrogen bond patterns between the carbene solute and the alcohol in the solvents is clearly dependent on the concentration of the donor in the system. To observe the underlying effects, we performed MD simulations covering the whole concentration range for the alcohol in the EtOH/THF mixtures, while the structure and the concentration of the carbene **1** was kept constant. All the RDFs of the simulations of **1** in these solvents show a sharp peak at a distance of 2.00 Å, indicating that the local structure of the H-bond itself is barely influenced by the solvent composition. Interestingly, the number integrals are increasing nearly linear with the ethanol concentration except for very low concentrations (Table 3.27 and Figure 3.49).

Table 3.27.: The positions and number integrals of the first peak in the RDFs of the simulations with varying ethanol concentration x_{EtOH}.

ethanol concentration / x_{EtOH}	Maximum / Å	Minimum / Å	Number Integral
0.02	2.025	3.075	0.16
0.20	2.025	3.075	0.85
0.40	2.025	3.025	1.01
0.60	2.025	3.075	1.17
0.80	2.025	3.075	1.30
1.00	2.025	3.025	1.44

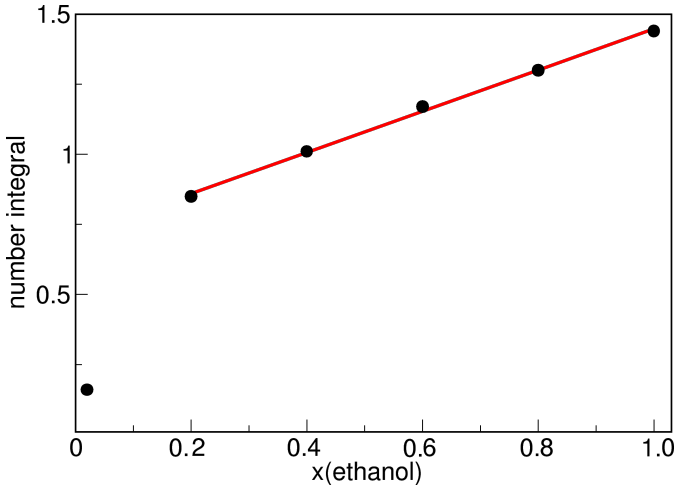

Figure 3.49.: Correlation of the number integrals of the first peak in the RDFs and the ethanol concentration.

The number of simultaneously bound alcohols (Figure 3.50) clearly shows that the number of free carbenes continuously decreases if the ethanol concentration increases, while the ratio of carbenes bound to two alcohol molecules at a time steadily grows. For low concentrations of ethanol, the number of single bonded carbenes increases until it levels out at about 80 % occurrence between $x_{\mathrm{EtOH}} = 0.2 - 0.8$ ethanol mole fraction, followed by a drop at higher ethanol content, due to the increasing amount of double hydrogen bonded structures.

We observe an exchange in the hydrogen bond donor at the carbenes in the whole concentration range. The fact that the double hydrogen bonded structures are not present at $x_{\mathrm{EtOH}} = 0.02$ of ethanol in the system shows that the exchange mechanism is dissociative in that case, while at the other extreme, in pure ethanol, the lack of free carbene molecules indicates a purely associative mechanism. Since the systems with the concentrations in between show the mutual occurrence of both free and double hydrogen bonded states, both mechanisms may occur. The lifetimes, accordingly, show an interesting dependence

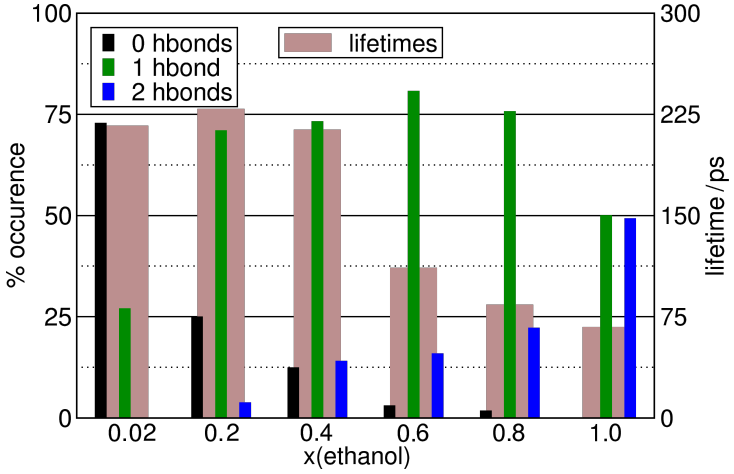

Figure 3.50.: Occurrence of different hydrogen bond assemblies (small bars, left axis) and the lifetimes of the hydrogen bonds (broad bars, right axis) in the simulations of 1,3-dimethylimidazolydene in ethanol/THF mixtures with different ratios.

on the concentration. The lifetimes are relatively unaffected by the increasing amount of ethanol in the system until ca. $x_{\mathrm{EtOH}} = 0.6$, where they suddenly drop to the half of the previous values, followed by a slower decrease toward the higher ethanol concentrations.

3.5.4. Conclusions

Hydrogen bonding of a large set of N-heterocyclic carbenes (NHCs) was explored by classical molecular dynamics simulations in different alcoholic solvents. This feature of NHCs has been invoked for explaining solvent effects in the organocatalytic applications of these compounds, since the hydrogen bond donor molecule occupies the lone pair of the carbene, hindering its reactivity. On the other hand, it has been shown repeatedly in literature that the hydrogen bond dynamics, i.e. the exchange of the donor bound to the lone pair of the carbene, is of prominent importance in the proton transfer reactions of the corresponding conjugate acid azolium salts.

The strength of hydrogen bonding and the lifetimes were found to be highly related to the basicity of these molecules. The least basic NHCs investigated here, thiazole-2-ylidene **2** and triazol-3-ylidene **3** are often free from hydrogen bond donors in the solution, and hence if these carbenes are applied in catalysis, they will be mostly available for the reactions. Approaching the more basic carbenes, e.g. imidazol-2-ylidene **1**, imidazolidin-2-ylidene **5** or the cyclic(alkyl)(amino)carbene **7**, the occurrence of the free carbene decreases by the increasing basicity, and the unusual, double hydrogen bonded structure appears. In this assembly, the single lone pair of the carbene interacts with two donor alcohol molecules simultaneously, in a geometry that resembles a tetravalent sp^3 carbon atom. Interestingly, in case of the strongest hydrogen bond acceptor NHCs, this latter structure becomes dominant, while the free carbene is not observable at all.

These trends have an effect also on the hydrogen bond dynamics of the present carbenes. While the hydrogen bond lifetimes gradually increase with the protonaffinities, the mechanism of the exchange of alcohol molecules in interplay with the carbene lone pair changes significantly. In case of the most weakly basic carbenes, where the free carbene is often available, the exchange follows a dissociative path, where the hydrogen bond dissociates, and the so formed free carbene finds an other partner in the solution. For the most basic carbenes the associative mechanism is dominant, where the formation of the new hydrogen bond precedes the dissociation of the first one.

The hydrogen bonding is strongly influenced by the substituents on the carbene rings and on the hydrogen bond donor. With increasing steric hindrance, the ratio of free carbenes rises, while that of the doubly coordinated NHCs decrease. Accordingly, while the associative mechanism of the hydrogen bond exchange becomes less favored, the dissociative pathway becomes more facile toward the bulkier substituents. This shift in mechanisms results in an initial increase in the lifetimes when the functional groups at the NHC become larger, with a subsequent drop toward the sterically most hindered carbenes. Similarly, the solvent composition affects the hydrogen bond lifetimes, and the exchange mechanism. With increasing concentration of the alcohol, the ratio of double coordinated carbenes increases, which suggest the exchange mechanism to shift toward the associative path. In accordance, the exchange becomes gradually more facile, and therefore the hydrogen bond lifetimes become lower.

Apart from the direct importance of characterizing comprehensively the hydrogen bonding of NHCs in solution for the first time, the present findings have a significant practical relevance. The basicity of carbenes is often determined by rate measurements for the H/D exchange reactions of the conjugate acid azolium cation. This method builds on the assumption that in the process the "free" carbene is formed in the solution, which provides the highest energy point in the reaction energy profile (Figure 3.38), and therefore its relative stability to the cation will determine the rate of the reaction. However, the results above show that the exchange of hydrogen bond donors may in fact avoid the formation of a free carbene, and can take a "shortcut" through the associative exchange mechanism.

At this point it is tempting to describe this phenomenon as a possible source of conceptual error in the H/D exchange-based basicity measurements, since the process may be more facile than the dissociation to a free carbene, resulting in an erroneous overestimation of the stability of the "free" carbene (cf. Figures 3.38 and 3.39), and therefore an underestimation of its basicity. However, the definition of a "free" carbene is very unclear in a protic environment, and so is the actual correct definition of the highly related pK. In an analogous manner, after deprotonating a water molecule in aqueous solution, the hydroxide anion is also not free in the sense that at every moment of a solvent rearrangement the surrounding water molecules are bound to it through hydrogen bonds. One could perhaps argue that it is due to the different number of lone pairs, and thus due to the different coordination number at a hydroxide anion as compared to the carbene, and hence this comparison is incorrect. Nonetheless, the analogy suggest a certain caution, and points out that a claim of systematic error in the corresponding measurement would be premature based solely on these findings. Nevertheless, the fact that the exchange

(i.e. the solvent reorganization) mechanism changes by the different carbene rings, substituents and solvent compositions clearly indicates that the actual physical meaning of the pK derived from H/D exchange measurements may also vary.

Fortunately, the lifetimes of the hydrogen bonds, which is clearly related to the rate constant of the exchange, show a common trend with the proton affinities, despite the variation in the exchange mechanism in case of the more basic carbenes. This shows that even if considering the existence of the associative mechanism as an error in the pK determination, the error increases gradually at higher pK values, and therefore the trends in basicity should not be affected, only the values themselves. However, the intricacies of the solute-solvent interactions show that the question should be revisited for every single carbene-solvent combination before the measurement, and the physical meaning of the measured data should be discussed carefully.

3.6. Are There Carbenes in N-Heterocyclic Carbene Organocatalysis?

Sascha Gehrke[†,‡] , Oldamur Hollóczki[†,*]

Angewandte Chemie International Edition, 2017, Volume **56 (51)**, Pages 16395–16398
German translation available in:
Angewandte Chemie, 2017, Volume **129 (51)**, Pages 16613–16617

DOI: 10.1002/anie.201708305 (german: 10.1002/ange.201708305)

Received: August 12, 2017

Published: October 26, 2017

For this article a Supporting Information is available free of charge at:
`https://onlinelibrary.wiley.com/action/downloadSupplement?doi=10.1002%2Fanie.201708305&file=anie201708305-sup-0001-misc_information.pdf`

Contributions to the manuscript:

- Setup and maintenance of all calculations
- Analyzing of results
- Writing the technical part of the manuscript
- Providing of Figures

[†]Mulliken Center for Theoretical Chemistry, University of Bonn, Beringstr. 4+6, D-53115 Bonn, Germany
[‡]Max Planck Institute for Chemical Energy Conversion, Stiftstr. 34–36, D-45470 Muelheim an der Ruhr, Germany
[*]E-mail: holloczki@gmail.com

After the first three milestones have been processed in the previous chapters, the current chapter will approach the question, if the formation of the Breslow intermediate is possible directly from the hydrogen bonded complex without the occurrence of an explicit free carbene species. To do so, an extensive DFT-study of the mechanism is performed.

Abstract

Azolium cations are widely employed in organocatalysis to catalyze highly valuable synthetic processes in the presence of a base. These reactions are called "N-heterocyclic carbene catalysis", based on the assumption that they are initiated by the formation of a free carbene through deprotonation, which can then react with the substrates and thereby affect their reactivity to obtain the desired products. However, we herein provide evidence that an electrophilic aromatic substitution mechanism is energetically more favorable, in which the azolium cation reacts directly with the substrate, avoiding the formation of the free carbene in solution.

3.6.1. Communication

Reactions catalyzed by metal-free N-heterocyclic carbenes (NHCs)[233] are of great interest in both chemistry[40–42,52,237,419,420] and biochemistry.[41,79,234] While these organocatalytic[421] processes enable synthetically valuable reactions, the analogous biochemistry of vitamin B1 (thiamine) plays a role in metabolism.[234] One of the key steps in these reactions is the formation of a bond between the NHC catalyst and the substrate as this covalent interaction is essential for the catalysis to take place. In a typical reaction, the NHC is not employed as the free carbene, but in its protonated form as an azolium salt, together with a suitable base.[40–42,52,237] According to the generally accepted reaction mechanism,[52,65] a proton is removed from the azolium ring by the base, creating a certain concentration of the free NHC in solution, which reacts with the substrate. The identified intermediates[52,66,67] and resting states[66,67,422] of the reaction and H/D exchange experiments[52] indicate that one of the ring protons can indeed be exchanged for a deuteron or an electrophile, suggesting a certain mobility for this proton. However, apart from this indirect evidence, there is no direct proof for the involvement of an NHC in the reaction as a free intermediate, and the detection of free carbenes in such reactive environments is restricted to a special case, in which the carbene is confined within an enzyme.[79]

In fact, carbenes are very basic, some with a pK value for the conjugated acid of greater than 20[68–70] (e.g., pK_a = 23.0 for 1,3-dimethylimidazol-2-ylidene in water),[87] while some of the bases that are used in such processes are significantly weaker (e.g., pK_a = 10.65 for triethylamine in water).[90] Therefore, it seems unlikely for such a proton transfer to occur frequently enough that reasonable catalytic effects could be expected. This contradiction becomes particularly intriguing if one considers some recently reported NHC catalytic processes that were conducted successfully in acidic media,[91,92] where the deprotonation of the very weakly acidic azolium cation is questionable. Moreover, persistent carbenes,[233] which are resistant to decomposition, are usually decorated with significantly bulkier substituents than those employed in carbene catalysis, suggesting the possibility of decomposition if deprotonation would occur.

Motivated by these highly contradictive interpretations and observations, we computationally explored the thus far unconsidered direct reaction between azolium cations and possible simple substrates. We selected the three NHC variants that are used most commonly in such processes (Figure 3.51), and although many modern NHC catalysts have larger substituents to introduce stereoselectivity, structures with similarly small functional groups at the nitrogen atoms have also been identified as active catalysts.[40–42,52,237,419,420] We chose trimethylamine as the base and formaldehyde, acetaldehyde, and benzaldehyde as the substrates to cover most of the possible electronic effects on the reaction.

First, we investigated the "classic", dissociative reaction mechanism, where the process is initiated by proton transfer from the azolium cation precatalyst to the amine base. The first step of this pathway is the slightly exergonic formation of a hydrogen bond between the base and the azolium cation (structure **I**; Figure 3.52). The proton transfer and subsequent dissociation into carbene **II** and the ammonium cation have a large Gibbs

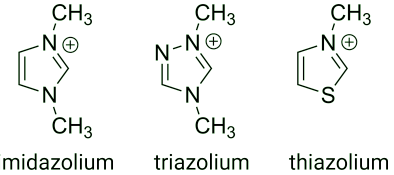

Figure 3.51.: The three catalysts investigated here.

free energy demand of $22 - 23\,\mathrm{kcal\,mol^{-1}}$ for the triazolium and thiazolium derivatives, and of even $35\,\mathrm{kcal\,mol^{-1}}$ for the imidazolium species, in clear agreement with the basicity trends of the corresponding carbenes.[68–70]

The free carbene reacts through $\mathbf{TS_{II\rightarrow III}}$ to form the catalyst–substrate bond in **III** (Figure 3.52). The highest-energy point in this mechanism is $\mathbf{TS_{II\rightarrow III}}$, rendering its relative Gibbs free energy with respect to **I** the activation Gibbs free energy of this pathway. The height of this barrier is sizable in all cases, amounting to $35-51\,\mathrm{kcal\,mol^{-1}}$ (Figure 3.53). As adduct **III** is less stable than the hydrogen-bonded assembly **I**, a final proton transfer from the protonated base is necessary to stabilize the product as structure **IV** and to provide a driving force for the reaction. The sizable barrier of this pathway suggests that the reaction should be sluggish even at elevated temperatures, in contrast to the experimental observations.

Recently, we found that a carbene center can form two hydrogen bonds at a time (e.g., in **A**; Figure 3.54).[123] In the present chapter, we successfully located transition states that are analogous to **A**, where instead of two hydrogen bonds, two reacting moieties interact with the carbene, similarly to other systems.[142,423] These transition states (e.g., **B** in Figure 3.54) allow the deprotonation of the azolium cation and the formation of the substrate–catalyst C—C bond to proceed in a simultaneous fashion, in a concerted, associative reaction mechanism.

According to this associative mechanism, **I** first forms the non-covalent complex **2** (Figure 3.52) with the substrate. Complex **2** and **I** exhibit similar Gibbs free energies. As **2** is a highly ordered complex of three molecules, entropic effects have a great impact on its accessibility. Indeed, the formation enthalpy of **2** is significantly more negative than the corresponding Gibbs free energy values (see the Supporting Information of the article). It should be noted that the calculations applied here have been shown to provide a significant (50–100 %) overestimation of the entropy compared to the values for the liquid phase.[424–426] This error results in higher Gibbs free energies for associated states, such as **2**. The observation that the Gibbs free energy of **2** is nonetheless similar to that of **I** shows that the formation of **2** is preferred in the reaction.

To arrive at **IV**, the proton must shift from the azolium cation to the base, and the aldehyde must bind to the ring. Apparently, the two steps occur in a concerted asynchronous manner,[427] that is, through a single elementary reaction step via transition state $\mathbf{TS_{2\rightarrow IV}}$. $\mathbf{TS_{2\rightarrow IV}}$ has the highest Gibbs free energy in the associative reaction mechanism in all cases; however, it is still lower in Gibbs free energy than $\mathbf{TS_{II\rightarrow III}}$ by a remarkable $19 - 29\,\mathrm{kcal\,mol^{-1}}$ (Figure 3.53). Thus the obtained barriers show a clear preference for this novel associative reaction mechanism in all cases. As the

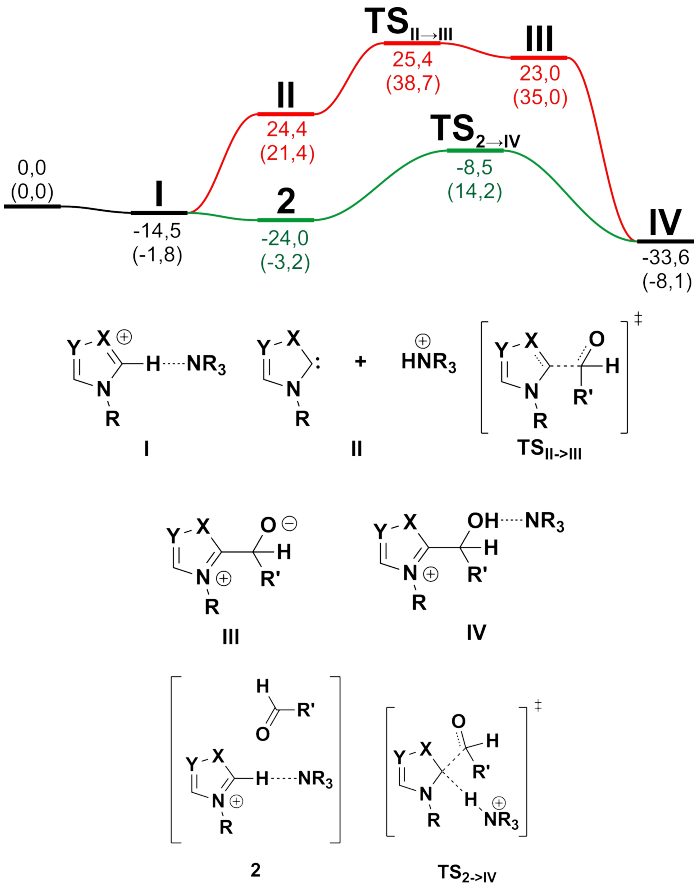

Figure 3.52.: Energy profiles of the dissociative (red) and associative (green) reaction mechanisms for the binding of the azolium catalyst to the aldehyde substrate. The relative enthalpies and Gibbs free energies (in parentheses) for the exemplary reaction between the triazolium cation and acetaldehyde are given. Lewis formulae of the structures involved are shown below (X = NMe, S; Y = CH, N; R = Me; R′ = H, Me, Ph); ball-and-stick representations are shown in the Supporting Information. For the barriers of all investigated systems, see Figure 3.53 and the Supporting Information of the article.

association of the molecules involved in the associative pathway has already occurred once **2** has been formed, entropic effects on the barriers themselves are negligible, and the activation enthalpies are similar to the activation Gibbs free energies (see the Supporting Information of the article).

It has been shown for diphenylcarbene, which is structurally very different from NHCs, that solvation can have a strong effect on its reactivity.[428] Thus we performed a series of calculations with an implicit conductor-like polarizable continuum model of toluene, THF, and DMSO, which are perhaps the most commonly used solvents in carbene catal-

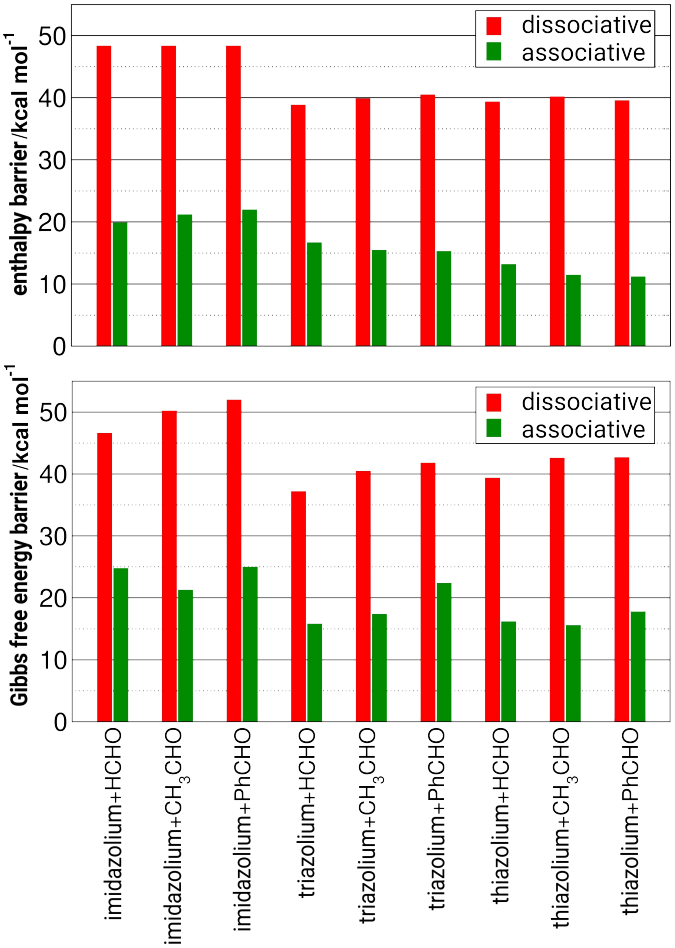

Figure 3.53.: Comparison of the CCSD(T)/CBS enthalpy (top) and Gibbs free energy (bottom) barriers of the dissociative (ΔH and ΔG of **I** and $\mathbf{TS_{II\rightarrow III}}$; red bars) and associative (ΔH and ΔG of **2** and $\mathbf{TS_{2\rightarrow IV}}$; green bars) pathways for the binding of the catalyst to the substrate (see Figure 3.52). The detailed energetics of the two mechanisms, including solvent effects and electronic energies, are included in the Supporting Information of the article.

ysis and cover a wide range of polarities. The preference for the associative mechanism was, however, not influenced at all by these solvents (see the Supporting Information of the article), suggesting that the polarity of the solvent is qualitatively unimportant for the present reaction mechanisms.

Although our associative mechanism is more favorable in all cases, the question can be raised how the dissociative pathway could be used to describe trends in the reactivity of catalysts with, for example, different basicity in previous studies for the last 50 years. Interestingly, upon correlating the dissociative and associative barriers with each

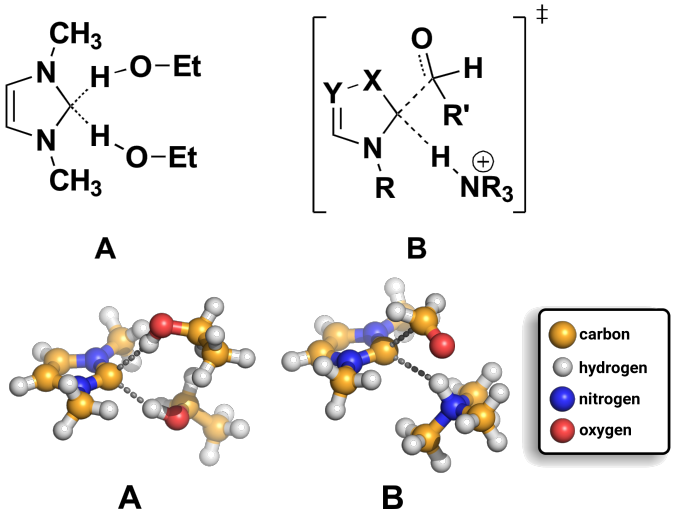

Figure 3.54.: The transient doubly hydrogen-bonded structure of an NHC (**A**) from molecular dynamics simulations,[123] and one of the optimized structures of $\mathbf{TS_{2\rightarrow IV}}$ (**B**), the key transition state of the associative mechanism (R = Me; R′ = H, Me, Ph).

other, a clear common trend is visible, showing that the higher activation energy for the dissociative mechanism will likely result in a higher barrier for the associative reaction pathway as well (Figure 3.55). This explains how using the model involving carbene formation provides information on the trends of the actual mechanism, even if the applied mechanistic picture in the free NHC model might not represent the real physical process.

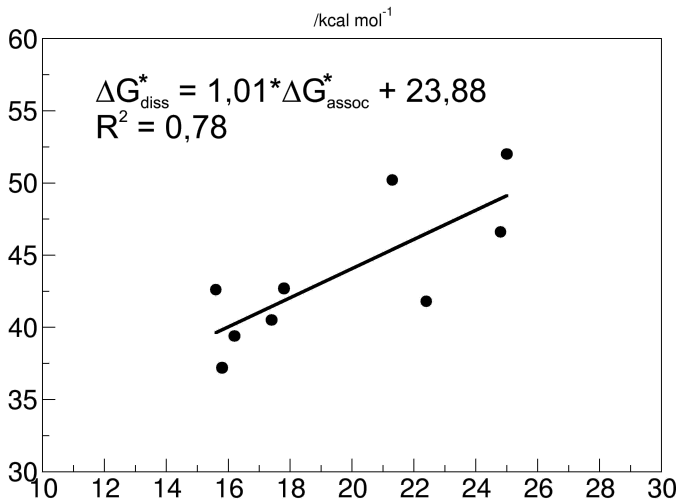

Figure 3.55.: Correlation of the barriers of the two mechanisms (see Figure 3.53) for each system.

This important finding also indicates a possible way to observe the present reaction mechanism experimentally. By varying the steric properties of the base, catalyst, and substrate, which affect $\mathbf{TS_{2\rightarrow IV}}$ and $\mathbf{TS_{II\rightarrow III}}$ differently, one should find outliers from the common trend. In agreement, the most significant outlier in this study was the reaction of the triazolium cation with bulky PhCHO, where the barrier of 23.4 kcal mol^{-1} for the associative mechanism appears to be too high compared to the general trend. In such cases, kinetic measurements, in combination with calculated activation energies, could help identifying which mechanism is operating. Surely, the complicated multistep nature of the corresponding catalytic process is another obstacle in such measurements. However, simple model reactions where the primary adduct **IV** cannot react further (for example, with benzophenone as the substrate) may enable reducing this complicated process into a single step for a detailed characterization of the process in question.

The cornerstone of this curious reaction pathway is transition state $\mathbf{TS_{2\rightarrow IV}}$, which directly connects the product **IV** and the starting cluster **2**. In light of the structure of $\mathbf{TS_{2\rightarrow IV}}$, the process itself is very similar to an electrophilic aromatic substitution (EAS), exchanging a proton at an aromatic ring for an electrophilic group. EAS reactions proceed through a structure that is very similar to $\mathbf{TS_{2\rightarrow IV}}$, where the leaving proton and the electron-deficient group are both bound to the same carbon atom at the substitution site (see structures **B** in Figure 3.54 and **C** in Figure 3.56). Furthermore, some EAS reactions[429] follow a concerted pathway, similarly to the presented associative mechanism. As azolium cations are also known to be aromatic,[132,251] it is reasonable to describe the present associative mechanism as an electrophilic aromatic substitution reaction.

Figure 3.56.: The mechanism of electrophilic aromatic substitution reactions.

Thus, instead of the generally accepted mechanism of the so-called NHC catalysis, which involves the deprotonation of an azolium salt to liberate the free NHC, an alternative reaction pathway could be identified. In this process, the proton transfer and the binding of the substrate to the catalyst occur simultaneously in a single elementary reaction step, without the involvement of an explicit carbene molecule. This process was calculated to have a low barrier, as opposed to the hindered formation of the free carbene. This finding explains various discrepancies in carbene organocatalysis, such as the absence of catalyst decomposition despite the occasionally very small substituents on the ring and the fact that reactions also take place for large pK_a differences between carbene and base or even in acidic media.

3.7. N-Heterocyclic Carbene Organocatalysis: With or without Carbenes?

Sascha Gehrke[†] , Oldamur Hollóczki[†,*]

Chemistry–A European Journal, 2020, Volume **26 (44)**, Pages 10140-10151

DOI: 10.1002/chem.202002656

Received: June 1, 2020

Published: July 1, 2020

For this article a Supporting Information is available free of charge at:
`https://chemistry-europe.onlinelibrary.wiley.com/action/downloadSupplement?doi=10.1002%2Fchem.202002656&file=chem202002656-s1-Supporting_Information_coop_template.pdf`

Contributions to the manuscript:

- Setup and maintenance of all calculations
- Analyzing of results
- Writing the technical part of the manuscript
- Providing of Figures

[†]Mulliken Center for Theoretical Chemistry, University of Bonn, Beringstr. 4+6, D-53115 Bonn, Germany
[*]E-mail: holloczki@gmail.com

The results of the last chapter demonstrated that the occurrance of a free carbene species is not necessary, but in contrast the formation of the Breslow intermediate is as well possible directly from the precursor cation. However, the reaction barriers were only obtained by calculations in the gas phase and details due to solvent effects were mostly neglected. In the following chapter the mechanism was studied with more advanced methods, not only with the aim to investigate the influence of different solvent systems, but as well to shed light on the details of the mechanism.

Abstract

In this work the mechanism of the aldehyde umpolung reactions, catalyzed by azolium cations in the presence of bases, was studied through computational methods. Next to the mechanism established by Breslow in the 1950s that takes effect through the formation of a free carbene, we have suggested that these processes can follow a concerted asynchronous path, in which the azolium cation directly reacts with the substrate, avoiding the formation of the carbene intermediate. We hereby show that substituting of the azolium cation, varying the base or the substrate, does not affect the preference for the concerted reaction mechanism. The concerted path was found to exhibit low barriers also for the reactions of thiamine with model substrates, showing that this path might have biological relevance. The dominance of the concerted mechanism can be explained through the specific structure of the key transition state, avoiding the liberation of the highly reactive, and thus unstable carbene lone pair, while activating the substrate through hydrogen bonding interactions. Polar and hydrogen bonding solvents, as well as the presence of the counterions of the azolium salts facilitate the reaction through carbenes, bringing the barriers of the two reaction mechanisms closer, in many cases making the concerted path less favorable. Thus, our data shows that by choosing the exact components in the reaction, the mechanism can be switched to occur with or without carbenes.

3.7.1. Introduction

Since the discovery of thiamine (vitamin B1),[44,45] the mechanism of the biological processes it catalyses have been in the focus of research. Next to the direct biochemical studies that revealed the role of this substance in life, numerous organic chemical model reactions have been designed to understand these reactions in further depth. The synthetic value of the knowledge that was gathered through these organic chemical studies was recognized by Stetter,[39] defining the field that we call today N-heterocyclic carbene (NHC) organocatalysis.[38,40–43] Since then, these transformations offer an ever growing portfolio of reactions, including important C-C coupling reactions, which can be often performed in a selective and asymmetric manner.

One of the most prominent examples for NHC organocatalysis is benzoin condensation, catalyzed by azolium salts in basic media. This reaction was discovered independently as an unexpected side reaction of decarboxylases in *in vitro* experiments,[47] and in organic chemical research of thiazolium salts.[48] Subsequently, the biological relevance of this process in the carbohydrate metabolism was discovered. In the underlying biochemical reactions an $H_4C_2O_2$ unit is transferred between sugar molecules, enabling the transformation of various carbohydrates into each other.[430,431] Due to the importance and simplicity of this reaction, it became a workhorse for later studies, through which the mechanism of NHC organocatalysis was investigated. Breslow observed that in deuterated solvents the position 2 proton of thiazolium salts is spontaneously exchanged to a deuteron, inferring the mobility of this proton.[51] Assuming that this mobility means that the deprotonated species, an NHC is actually present in the solution in a small quantity as an intermediate, he adjusted the mechanism of cyanide-catalyzed benzoin condensation[54] to interpret the catalytic effect of thiazolium salts.[52] Through suggesting the formation of another key intermediate (called later Breslow intermediate), he defined a mechanistic picture that is today still the main school of thought in NHC organocatalysis (Figure 3.57).

Using this mechanism as a template has allowed explaining and predicting selectivity in many related processes and understanding the role of structural features in the catalysts,[64,65] which strongly supports the aforementioned reaction path. Computational studies predict low barriers for the reaction of free carbenes with various substrates.[65] Furthermore, Breslow intermediates[67,71,72] and related compounds[71,73,74] have been synthesized and structurally characterized. Similarly, several free NHCs have been shown to be stable,[56,98,100,101,250] and extraordinary persistence has been evidenced for several of their derivatives.[98,101] In some specific cases, the formation of NHCs has also been observed by mass spectroscopy in vaporized reaction mixtures,[80] vaporized catalytically active solutions,[81,82] or confined within the active site of a thiamine-dependent enzyme.[79]

However, it is important to stress that the direct evidence that free carbenes can catalyze these reactions does not mean they play an actual role in catalysis, and similarly, the stability of NHCs prepared in an isolated environment does not prove their formation in the reaction mixture. Throughout the decades doubt has been raised regarding the first part of the catalytic cycle,[6,83,107–109,112,115,432,433] in which the bond between the azolium ring of the catalyst and the substrate is formed. In fact, already in this early

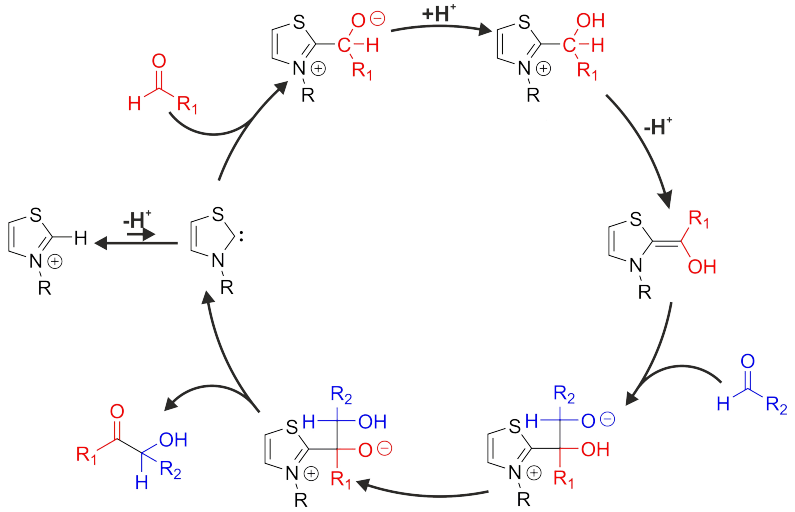

Figure 3.57.: Catalytic cycle of the benzoin condensation, as suggested by Breslow in 1958.[52]

step selectivity can become an issue, if multiple substrates are available in the reaction mixture, such as in cross-benzoin condensations, in Stetter reactions, and in the biochemical transketolase reaction. Thus, understanding this initial reaction between substrate and catalyst is of high practical relevance.[38,40–43]

Washabaugh and Jencks measured the acidity of thiamine at its active site in aqueous solution to be $pK_a = 18.0$.[83] They argued that the catalytic activity of this compound could be explained only with a $pK_a < 14$.[83] To resolve this contradiction, they tentatively suggested that an alternative, concerted pathway might bypass the formation of the energetically quite unstable free NHC, in which the deprotonation occurs simultaneously with the catalyst-substrate bond formation.[83] However, speculating that the substrate would need to approach the ring in the very direction, in which the proton should leave,[83] they dismissed this idea. Finally, they suggested that the reason for the activity of this compound within the enzyme must be due to the stabilizing effect of the protein on the carbene, which shifts the local acid-base equilibrium within the binding site.[83]

There are indeed indications that the NHC might be more stable within the active site of the enzyme,[79] including the enhanced activity of thiamine in the presence of these proteins.[103–105] However, the effect of the enzyme cannot explain how NHC organocatalytic reactions can be possible in organic syntheses in the absence of any biomolecule. Imidazolium (in water: pK_a = 19-24[68,86–89], in DMSO: pK_a = 19-24[88,434], in MeCN: $pK_a = 33.6$[87]), triazolium (in water: pK_a = 14.9-17.4[70]) and thiazolium (in water pK_a = 17-19[70,83], in DMSO: $pK_a = 14.5$[87], in MeCN: $pK_a = 25.6$[87]) salts have all been applied as catalysts,[38,40–43,58] and despite their high pK_a values, triethylamine (in water: $pK_a = 10.65$[435,436], in DMSO: $pK_a = 9.0$,[436] in THF: $pK_a = 12.5$,[436] in MeCN: $pK_a = 12.5$[436]) has been shown to be basic enough to deprotonate them in a quantity, which is sufficient to exhibit reasonable to excellent catalytic activity.[58]

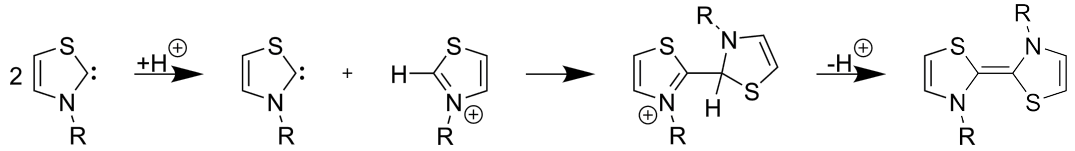

Figure 3.58.: Dimerization reaction of thiazol-2-ylidenes in the presence of acid traced, reported by Arduengo and co-workers.[100]

While the aforementioned contradictions regarding the most fundamental acid-base theory should already be enough to raise questions, the general wisdom regarding the stability of NHCs points to further interesting issues. The hitherto synthesized stable free NHCs generally possess bulky substituents on the ring to prevent decomposition reactions, e.g. dimerization, with the exception of some imidazol-2-ylidene derivatives.[99] Carbene catalysts, on the other hand, showed remarkable activity with the smallest substituents without any significant decomposition, and larger functional groups are introduced merely to increase the stereoselectivity of the reaction.[38,40–43] This is especially surprising regarding thiazolium salts. Thiazol-2-ylidenes showed a high propensity to dimerize in the presence of acid traces,[100] even with the sizable 1,3-diisopropylphenyl substituent on the nitrogen atoms. Strikingly, in the absence of acids, the same compounds did not dimerize. Arduengo and co-workeres argued that the dimerization takes place through the reaction of an NHC with a thiazolium cation (Figure 3.58). These findings can be rationalized as the protonation increases the electrophilicity of the C2 carbon atom of the ring, facilitating thereby the nucleophilic attack of the NHC at the ring, which — after deprotonation — forms the NHC dimer. Should NHCs be present in the solution in the catalytic environment, the excess of the azolium cations should result in the dimers of the catalyst in an analogous process. Such decomposition reactions of thiazolium catalysts have not been reported. In fact, the role of these dimers in the catalytic mechanism has been discussed,[107–109,112,115,433] and it was subsequently dismissed.[111,113]

For the carbene-like reactions of ionic liquids with carbon dioxide, we discovered by static quantum chemical calculations a novel reaction mechanism, which avoids NHC formation,[142] and the imidazolium cation reacts directly with the substrate. This mechanism was later observed also through *ab initio* molecular dynamics simulations.[423] Similarly, we found an alternative pathway for NHC organocatalytic reactions,[6] in which first a pre-aggregation of the components occurs. The proton transfer from the azolium cation to the base and the C-C bond formation between the catalyst and the substrate take place in a single elementary step within that aggregate, avoiding thereby the formation of free NHC intermediates, analogously to the suggestion of Washabaugh and Jencks.[83] We found that the barrier of the classical (dissociative) pathway that assumes the formation of the free NHC is by $20 - 30\,\mathrm{kcal\,mol^{-1}}$ higher than that of the concerted (associative) path.[6] This mechanism can satisfyingly explain the contradictions above regarding NHC catalyst stability and acid-base equilibria, while suggesting that the base — being present at the catalyst-substrate bond formation step — might also be a site,

through which selectivity can be enhanced.

Rico del Cerro *et al.* showed in a joint experimental-computational study that the H/D exchange of azolium salts follows a very similar associative mechanism, in which the formation of free carbenes is avoided.[437] Nolan and co-workers reported that the NHC metal complexes from imidazolium salts and metal ions can form through an analogous path,[438] in which the preparation or even the *in situ* generation of an NHC is unnecessary, allowing very simple synthetic routes to these practically highly important compounds.[438,439] Regarding the carbene-like reactions of imidazolium acetate ionic liquids with glucose,[306] we found indications that the concerted mechanism should be prevalent, as the aggregates that are required for the associative mechanism spontaneously occurred in *ab initio* molecular dynamics simulations,[440] while the barriers of this mechanism were somewhat lower than that of the reaction through carbene intermediates.[8] However, we found that in such an ionic liquid environment, and with the acetate anion as base the difference between these two mechanisms in barriers is lower,[8] which implies that there might be experimental setups, in which the dissociative mechanism is more facile. Thus, to fully uncover the mechanistic details of NHC organocatalysis, further research is necessary.

Although considering this novel reaction mechanism has already given a deeper insight into the chemistry of azolium salts,[8,142,437–440] and resulted in actual applications,[438,439] exploiting this process in its full potential — by e.g. introducing unprecedented ways to control selectivities — has not yet been achieved. To this end, hereby we aim to understand in detail the influential factors that facilitate or suppress this direct reaction mechanism, while assessing its relevance in catalytic systems. In this comprehensive work we discuss in detail the effect of possible azolium rings, substituents, solvents, bases, substrates, and counterions on this reaction.

3.7.2. Computational Methods

Static Quantum Chemical Calculations

All quantum chemical calculations were performed by the ORCA 4.0 program.[256,441] Geometry optimizations of the minima and transition states were undertaken by using the TPSSh functional[278] with the D3-BJ dispersion correction,[279,280] and the def2-TZVPP basis set.[282,283] For the SCF cycle and the geometry optimization the tight convergence criteria were applied. The nature of the obtained stationary points was verified by making sure that the Hessian had no negative eigenvalues for minima, and a single one for transition states. Steepest descent optimizations were performed in both directions defined by the imaginary normal mode for each transition state to identify the minima the given transition state connects.

On the structures obtained by the DFT calculations, DLPNO-CCSD(T) single point energies[259–261] were calculated with the def2-TZVPP and def2-QZVPP basis sets[282,283] with tight settings for the localization. The obtained single point energies were extrapolated to the complete basis set limit.[262] These electronic energies were then corrected to enthalpies and Gibbs free energies using the thermochemical data obtained from the corresponding DFT frequency calculations. Gibbs free energies of solvation were calculated

through the COSMO-RS approach,[287,442] using the BP-TZVPD-FINE method of the COSMOthermX14 software[443,444] based on BP86/def2-TZVPD calculations[282,283,445] by the Turbomole program.[446] Non-covalent interaction analysis[447–449] was performed by the Multiwfn 3.6 program package.[450]

Classical Molecular Dynamics Simulations

For performing classical molecular dynamics simulations, the LAMMPS program was used.[263] For modelling the 1,3-dimethylimidazolium cation, the chloride and triflate anions the force field parameters by Canongia Lopes and Pádua were applied.[266,267] The organic solvents were described by the OPLS-AA model,[255] while for water the SPC/E parameters were chosen.[258] In the simulations, periodic boundary conditions were applied. The starting geometry of the cubic simulation box was created by the Packmol program.[312] The initial cell vector of the simulation box was chosen according to the density of the pure solvent in question. After a geometry optimization, 1 ns simulations in the NpT ensemble have been performed, by using Nosé–Hoover chain thermostats and barostats at a temperature of 293 K and under 1 bar pressure. The timestep was chosen to be 1 fs. The volume of the periodic simulation box was averaged over the last 0.5 ns, and this value was used for the later steps of the simulations. An external harmonic potential was added to the system that kept the distance between centers of mass of the anion and the cation at a value of 3 Å. After 100 ps of equilibration, the force that was required to maintain the cation-anion distance was measured, and averaged over a production run of 250 ps. The anion–cation distance was then increased by an increment of 0.5 Å until 20 Å, repeating the equilibration and production runs at each distance. Integrating the forces versus the distance gave the free energy profile of ion pair separation.

3.7.3. Results and Discussion

In this chapter we compare the two reaction mechanisms for the initial steps of NHC catalyzed benzoin condensation, in which the catalyst-substrate bond is formed. The classical, dissociative reaction mechanism (Figure 3.59, red curve) follows the original proposal by Breslow.[52] First a free NHC intermediate **II** is formed in the reaction mixture from the azolium cation by a proton transfer to a base (e.g. an amine), which reacts with the substrate, giving primary complex **III**. Concluding the formation of the catalyst-substrate bond, **III** is protonated again by the ammonium cation, yielding **IV**. This mechanism will be referred to as dissociative mechanism. The key to this path is the availability of the free NHC intermediate, which is present in the solution in a low concentration, dissociated from the rest of the components.

In contrast, in the associative path[6] (Figure 3.59, green curve) the free NHC is not an intermediate of the reaction. Instead, the aggregation of the azolium catalyst, substrate and base occurs, producing complex **2**. The bond formation between the catalyst and the substrate is undertaken through transition state $\mathbf{TS}_{2\rightarrow\mathrm{IV}}$ by a rearrangement within aggregate **2** in a single elementary step. This step comprises the C-to-N proton transfer from the azolium cation to the base, the C-C bond formation between the catalyst

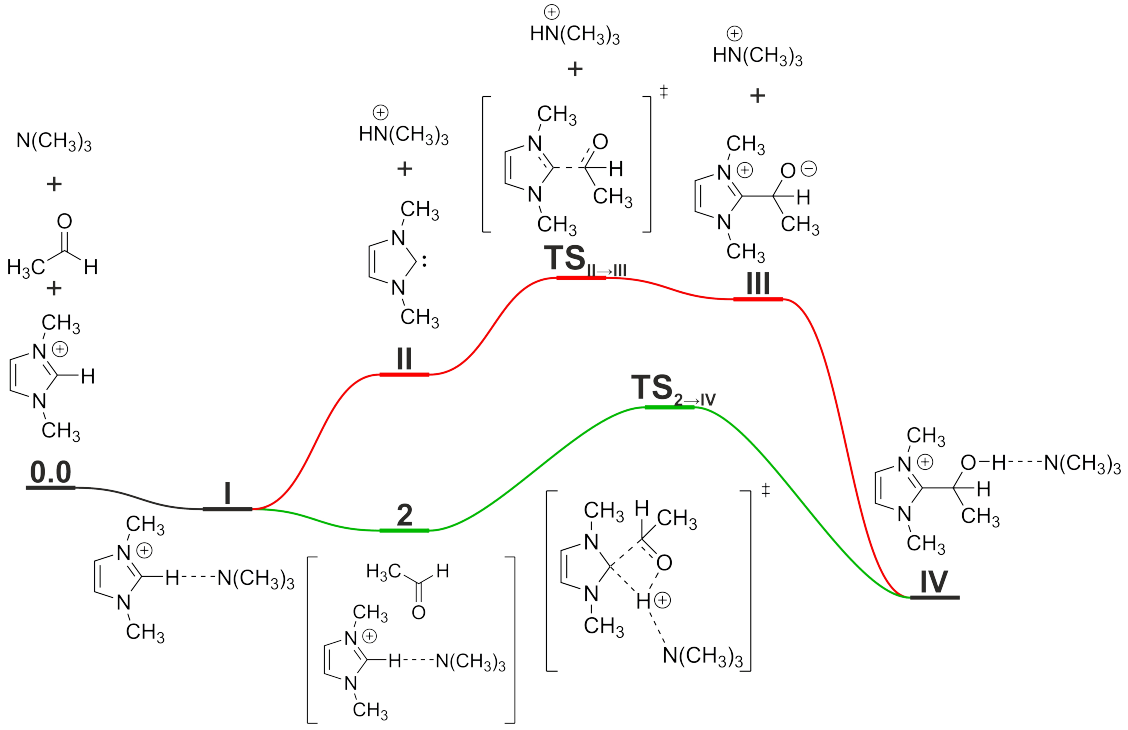

Figure 3.59.: The general Gibbs free energy profile of the dissociative (red) and associative (green) reaction mechanisms of the catalyst-substrate bond formation in the benzoin condensation, and the labeling of the different species as used throughout the article.

and the substrate, and the N-to-O proton transfer from the conjugate acid of the base (e.g. ammonium ion) to the oxygen atom of the substrate to give **IV** in a concerted asynchronous manner. An animation for the reaction mechanism is available in the Supporting Information. In this mechanism, the role of the base is to shuttle the proton from the carbon atom of the catalyst to the oxygen atom of the substrate, instead of releasing a free NHC intermediate. Formed by either of the two mechanisms, **IV** will transform to yield the Breslow intermediate, which can thereafter react with another substrate molecule in the subsequent reaction steps.

The reaction mechanisms were calculated first for the three azolium catalysts that have been applied in NHC organocatalysis (imidazolium **A**, triazolium **B**, and thiazolium **C**, see Figure 3.60) substituted with methyl groups on the relevant nitrogen atoms. The substrates were chosen to be four different aldehydes that represent a wide range of electronic effects on their reacting carbonyl group (formaldehyde, acetaldehyde, acrolein, benzaldehyde). The base was chosen to be trimethylamine.

A key question regarding the reaction is the aggregation of the reactants. The formation of a hydrogen bond between the base and the cation to give **I** was found to be

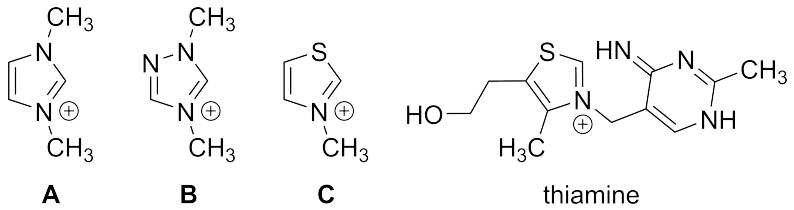

Figure 3.60.: Lewis structures of the catalysts 1,3-dimethylimidazolium (**A**) 1,4-dimethyltriazolium (**B**), and 3-methyltriazolium cation (**C**). The active tautomer of thiamine (**T**) is also shown (right), having a basic imino group in the vicinity of the mobile proton of the thiazolium ring.

Table 3.28.: DLPNO-CCSD(T)/CBS//TPSSh-D3BJ/def2-TZVPP Gibbs free relative energies and relative enthalpies for **I** and **2** with respect to the separated azolium cation, trimethylamine, and substrate in the gas phase.

catalyst	aldehyde R-CHO	ΔG(**I**) kcal mol^{-1}	ΔG(**2**) kcal mol^{-1}	ΔH(**I**) kcal mol^{-1}	ΔH(**2**) kcal mol^{-1}
A	H	−1.3	−1.0	−11.7	−19.3
A	CH_3	−1.3	−1.4	−11.7	−21.3
A	vinyl	−1.3	−1.2	−11.7	−21.3
A	Ph	−1.3	0.9	−11.7	−24.3
B	H	−2.2	−3.1	−13.2	−22.6
B	CH_3	−2.2	−3.6	−13.2	−22.9
B	vinyl	−2.2	−4.5	−13.2	−24.4
B	Ph	−2.2	−2.1	−13.2	−25.6
C	H	−2.9	−1.7	−13.1	−20.4
C	CH_3	−2.9	−0.2	−13.1	−20.4
C	vinyl	−2.9	−3.9	−13.1	−23.5
C	Ph	−2.9	−1.0	−13.1	−23.0

thermodynamically favorable in all cases, as shown by the ΔH and ΔG values in Table 3.28. The association of a substrate molecule to **I** to give **2** has an enthalpy benefit of $8-11\,\mathrm{kcal\,mol^{-1}}$, which can be explained by the polarity of complex **I** and the aldehyde (Table 3.28). This substantial ΔH value is comparable in magnitude to the $T\Delta S$ entropic contribution, and therefore the relative Gibbs free energies of **I** and **2** compared to the three dissociated components are very similar. Consequently, aggregation at least to **I** should occur in all investigated cases. The low relative Gibbs free energy of **2** suggest that this aggregate is easily accessible in the solution, and in some cases it should be even the (slightly) dominant structure in the reaction mixture.

The enthalpy and Gibbs free energy barriers ($\Delta H^{\ddagger}_{dissoc}$, $\Delta G^{\ddagger}_{dissoc}$) for the dissociative mechanism were measured in all cases as the enthalpy and Gibbs free energy difference between **I** and $\mathbf{TS}_{\mathrm{II}\rightarrow\mathrm{III}}$. For the associative mechanism, the enthalpy barriers ($\Delta H^{\ddagger}_{assoc}$)

Table 3.29.: DLPNO-CCSD(T)/CBS//TPSSh-D3BJ/def2-TZVPP activation enthalpies and activation Gibbs free energies for the reaction of 1,3-dimethylimidazolium (**A**), 1,4-dimethyltriazolium (**B**), 3-methylthiazolium (**C**) cations and trimethylamine with different aldehydes in the gas phase through the associative ($\Delta H^{\ddagger}_{assoc}$, $\Delta G^{\ddagger}_{assoc}$) and dissociative ($\Delta H^{\ddagger}_{dissoc}$, $\Delta G^{\ddagger}_{dissoc}$) reaction mechanisms.

catalyst	aldehyde R-CHO	$\Delta G^{\ddagger}_{assoc}$ kcal mol^{-1}	$\Delta G^{\ddagger}_{dissoc}$ kcal mol^{-1}	$\Delta H^{\ddagger}_{assoc}$ kcal mol^{-1}	$\Delta H^{\ddagger}_{dissoc}$ kcal mol^{-1}
A	H	26.1	46.6	22.1	46.0
A	CH_3	23.2	50.2	21.5	48.5
A	vinyl	23.5	48.6	20.4	45.8
A	Ph	26.6	52.6	24.9	47.4
B	H	18.3	37.2	15.2	37.3
B	CH_3	19.2	40.5	16.2	39.8
B	vinyl	16.8	38.7	14.7	37.1
B	Ph	20.5	41.8	16.3	39.4
C	H	17.3	39.4	11.8	38.3
C	CH_3	19.2	42.6	11.3	40.6
C	vinyl	14.1	40.8	11.5	38.1
C	Ph	19.3	42.7	13.0	39.2

were defined to be the enthalpy difference between $\mathbf{TS}_{2\rightarrow IV}$ and **2**. The reference point for calculating the Gibbs free energy barrier of the associated path ($\Delta G^{\ddagger}_{assoc}$) was defined separately for each cases, taking the more stable of **2** or **I**. The relative Gibbs free energy of $\mathbf{TS}_{2\rightarrow IV}$ compared to this reference point gave $\Delta G^{\ddagger}_{assoc}$.

The associative mechanism has significantly lower activation enthalpies in all cases than those of the dissociative path. As discussed before, the two sets of barriers exhibit a common trend, hence a higher activation enthalpy in the dissociative mechanism usually means a higher barrier for the associative path as well.[6] The difference between the enthalpy barriers is substantial, ranging between 19 and 29 kcal mol^{-1} (Table 3.29).[6] In fact, the activation enthalpies for the dissociative mechanism are so high, that these processes seem rather unlikely to occur at all at reasonable temperatures ($37-49$ kcal mol^{-1}), while the associative mechanism exhibits mild $11-25$ kcal mol^{-1} barriers. In the associative mechanism, the imidazolium catalyst showed generally higher barriers ($20-25$ kcal mol^{-1}) than those of the triazolium and thiazolium derivatives ($11-17$ kcal mol^{-1}), which is in qualitative agreement with the lower mobility of the active proton for the imidazolium derivatives.[68,70,86–89] Catalyzed by certain imidazolium derivatives, the condensation of formaldehyde in the presence of triethylamine was too slow to observe at room temperature in earlier experiments,[58] which is in good accordance with our data. The activation enthalpies were found to be only slightly different for the four substrates, but in most cases the highest values were found for benzaldehyde, while the lowest were found for

acrolein. Including entropy effects by calculating Gibbs free energies increases all barriers. The increase is generally higher for the associative mechanism ($2 - 10\,\mathrm{kcal\,mol^{-1}}$) than for the dissociative path ($0 - 5\,\mathrm{kcal\,mol^{-1}}$, Table 3.29), in agreement with the higher order in $\mathbf{TS}_{2\to\mathrm{IV}}$. Nonetheless, the entropic penalty for reaching $\mathbf{TS}_{2\to\mathrm{IV}}$ is relatively low, since the association occurred at the earlier steps of the reaction, namely at the formation of **2** (see discussion above).

Changing trimethylamine to other deprotonating agents, such as DBU and DABCO changes both reaction barriers, but the dominance of the associative mechanism is retained (see Supporting Information of the article). Substituting the ring with larger groups to arrive at frequently applied catalysts does not affect the conclusions (Figure 3.61). Some of the compounds considered here possess bulky functional groups that control enantioselectivity in the later stages of the reaction.[42] Nonetheless, the barriers of the reactions with formaldehyde and acetaldehyde indicate for all catalysts a distinct preference for the associative mechanism.

The most important catalyst is, of course, the biologically active thiamine (Figure 3.60). The calculations discussed above regarding the synthetically relevant azolium rings, bases and aldehydes, can be and have been[52] considered as model reactions for the biochemical reactions of thiamine. To test the feasibility of the associative mechanism on this biomolecule, we calculated the reactions of thiamine with pyruvic acid, and with glyceraldehyde, in which the bond between the catalyst and a substrate is formed. For these reactions it is not possible to define a dissociative mechanism, since the base and the azolium ring are covalently attached to each other within thiamine. We have, however, successfully located the transition state of the associative mechanism, bringing a novel insight into the corresponding biologically relevant reactions (Figure 3.62). The activation enthalpies were found to be reasonably low (24.4 and $15.1\,\mathrm{kcal\,mol^{-1}}$ for pyruvic acid and glyceraldehyde, respectively), which — in the presence of the enzyme — could be most likely decreased even further through stabilizing interactions within the transition state. Since the deprotonating agent and the catalyst are within the same molecule, entropy has a milder effect on this reaction, as shown by the activation Gibbs free energies (25.4 and $17.7\,\mathrm{kcal\,mol^{-1}}$, respectively).

Having seen the clear preference of the reaction to follow the associative path in the cases detailed above, the question is apparent: what effects make this mechanism so much faster than the dissociative path defined by NHC intermediate formation? One of the effects that make the associative mechanism favorable is the aforementioned high association enthalpy of the components to form **I** and **2**, which compensates for the entropy loss in the association of three molecules into a single cluster. Another reason must be that the associative path avoids the complete liberation of a highly reactive carbene lone pair, and instead this nucleophilic and basic center is simply flipped from the proton to the electrophilic carbonyl carbon atom of the aldehyde. Non-covalent interaction analysis[447–449] (see Supporting Information) reveals that the interaction between the carbonyl carbon atom and the carbene carbon atom is in general considerable, strongly supporting this hypothesis.

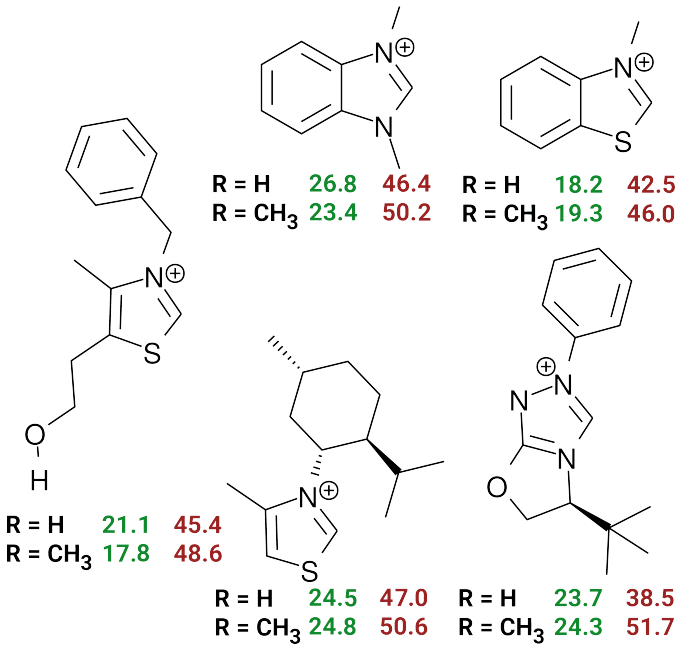

Figure 3.61.: DLPNO-CCSD(T)/CBS//TPSSh-D3BJ/def2-TZVPP Gibbs free energy barriers of the reaction between often applied catalysts, triethylamine, and formaldehyde (above) or acetaldehyde (below) through the dissociative (red) and associative (green) reaction mechanisms.

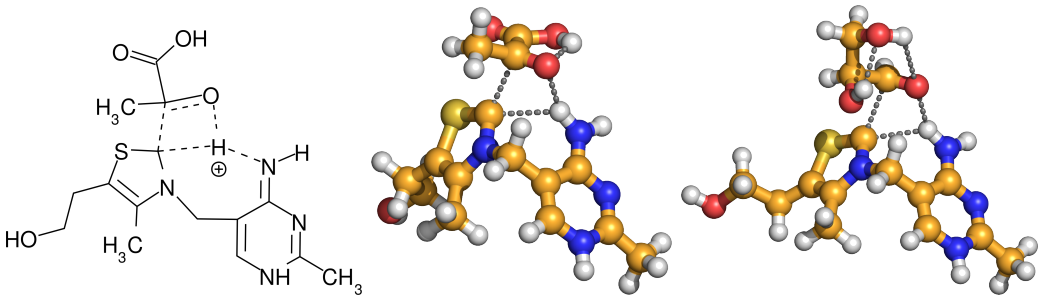

Figure 3.62.: Lewis structure of the associative transition state of thiamine with pyruvic acid as a substrate (left). Ball-and-stick representation of the same transition state with pyruvic acid (middle) and glyceraldehyde (right) as substrate.

Next to these clear advantages, there is another interaction in $\mathbf{TS}_{2\rightarrow IV}$, which deserves special attention. It has been shown that the C-to-N and N-to-O proton transfers and the C-C bond formation occur asynchronously within the single elementary step of the reaction.[6,8] The transition state is situated late along the reaction coordinate,[8] where the C-to-N proton transfer has already been completed. The mobilized proton, as departing the azolium ring and approaching the nitrogen atom of the amine base shuttle, will form a transient, but strong hydrogen bond donor species within this assembly, an ammonium cation. While the catalyst-substrate bond is being formed, the transient ammonium cation interacts strongly with the aldehyde oxygen atom through a hydrogen bond, which is observable in all transition states $\mathbf{TS}_{2\rightarrow IV}$ through various hydrogen bonding criteria (Table 3.30, and Supporting Information of the article).

Carbonyl compounds are known to be activated in their electrophilicity by hydrogen bond donor molecules, which polarize the C=O bond, and thereby decrease its strength.[451–454] Enzymatic reactions often take effect through such hydrogen bonding, which activate molecules in a manner to enhance their desired reactivity,[453,455] while the active site also offers a well-defined spatial arrangement of hydrogen bonding sites, inducing thereby selectivity through template effects. Mimicking these biochemical reactions, hydrogen bond supported catalysis has been subject to intensive scientific attention through the last few decades, using for instance urea, thiourea and guanidinium derivatives as catalysts.[451–454] Accordingly, it is reasonable to assume that the presence of the aforementioned ammonium-substrate interplay in $\mathbf{TS}_{2\rightarrow IV}$ reaches beyond a simple hydrogen bond, and it affects the reactivity of the aldehyde directly. Considering that the transition state is situated late within the concerted asynchronous elementary step that comprises the proton transfers and the C-C bond formation,[8] and it is located on the potential energy surface where the proton is already transferred to the amine, it can be expected that the barrier itself is largely determined by the C-C bond formation.[8] Therefore, the activation effect of the amine on the aldehyde may have a tremendous effect on the barrier of the reaction.

To highlight the effect of this hydrogen bond on the reaction, the changes in the structure of the four selected aldehydes induced by presence of ammonium cations are shown in Table 3.31. The activation should manifest in weaker C=O double bonds, which is a clear sign of the polarization by moving the electron density of the π bond toward the oxygen atom, rendering the molecule more electrophilic. All data indicates that the C=O bond of the substrate becomes weaker upon interacting with an ammonium cation, implying — in agreement with literature[451–454] — that this interaction has an effect on the electrophilicity of the substrate, and thus the reaction as well.

To assess how much this interaction facilitates the reaction, we compared the barriers for the reaction between a free carbene and a free aldehyde in the absence and presence of a trimethylammonium cation in hydrogen bonding with the substrate ($\Delta\Delta E^{\ddagger}$ in Table 3.30). The obtained data shows a ca. $12 - 19\,\mathrm{kcal\,mol^{-1}}$ decrease in the activation energies by the presence of the ammonium ion. This significant decrease in the barriers suggests that "umpolung" catalysis by NHCs, for instance benzoin condensation, also works partly as an inherent hydrogen bond-supported catalysis.

Table 3.30.: Hydrogen bonding between the ammonium and aldehyde moieties in the key transition state of the associative reaction mechanism $\mathbf{TS}_{2\rightarrow\mathrm{IV}}$. ($R$: O$\cdots$H distance; α: O$\cdots$H$-$N angle; BI: Mayer Bond Index; SEN: Shared Electron Number; BCP $\rho(r)$ and $\nabla^2\rho(r)$: electron density and Laplacian, respectively, at the bond critical point of the O$\cdots$H hydrogen bond; $\Delta\Delta E^{\ddagger}$: DLPNO-CCSD(T)/CBS//TPSSh-D3BJ/def2-TZVPP activation energy change in the carbene+substrate reaction if the protonated base is present).

cat.	R-CHO	R /Å	α /°	BI	SEN	BCP $\rho(r)$	BCP $\nabla^2\rho(r)$	$\Delta\Delta E^{\ddagger}$ /kcal mol^{-1}
A	H	1.87	140.0	0.056	0.078	0.030	0.110	−15.9
A	CH_3	1.67	170.1	0.171	0.127	0.050	0.131	−17.8
A	Ph	1.47	174.3	0.292	0.217	0.088	0.121	−14.3
A	vinyl	1.72	154.8	0.095	0.108	0.042	0.130	−16.4
B	H	1.72	171.4	0.156	0.107	0.046	0.120	−15.5
B	CH_3	1.56	173.8	0.233	0.172	0.069	0.127	−15.5
B	Ph	1.47	174.3	0.289	0.214	0.088	0.122	−12.0
B	vinyl	1.70	165.1	0.141	0.104	0.045	0.128	−15.2
C	H	1.71	167.8	0.154	0.105	0.046	0.120	−17.8
C	CH_3	1.55	173.5	0.244	0.136	0.072	0.126	−16.5
C	Ph	1.46	175.5	0.296	0.216	0.090	0.118	−13.1
C	vinyl	1.69	169.5	0.161	0.110	0.050	0.122	−18.6
T	glyc	2.03	140.5	0.058	0.021	0.021	0.083	–
T	pyru	1.98	150.7	0.093	0.037	0.023	0.086	–

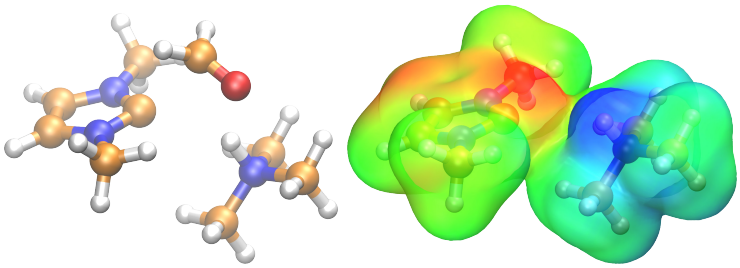

Figure 3.63.: Ball-and-stick representation of the transition state for the associative reaction mechanism for the reaction between 1,3-dimethylimidazolium cation, trimethylamine, and formaldehyde (left, C: orange; O: red; N: blue; H: white). Electrostatic potential map of the same structure, after the formaldehyde was removed (right). The negatively polarized (red) lone pair, and the positively polarized (blue) ammonium cation together define a binding site for the aldehyde, which can react with the catalyst, and can be activated by the protonated base to lower the barrier.

The nature of the interplay within the transition state can be perhaps best represented in the electrostatic potential maps of the carbene and the ammonium cation within the transition state $\mathbf{TS}_{2\rightarrow\mathrm{IV}}$ (Figure 3.63). The positively charged proton on the ammonium cation and the negatively polarized carbene lone pair are situated in such a manner that they can together encompass the substrate in the possible most favorable arrangement, through creating a sort of template. While the lone pair of the carbene interacts with the LUMO of the aldehyde at the partially positive carbonyl carbon atom, the ammonium cation can aid the nucleophilic attack through forming a hydrogen bond with the negatively polarized oxygen atom of the substrate. This cooperative effect clearly shows that through modifying the template formed by the azolium-base assembly, the feasibility of the reaction may be influenced, creating further ways to improve the selectivity of these reactions.

The effects that result in the lower barriers for the associative mechanism may also reveal the limitation of this path. Since hydrogen bonding with the aldehyde is of high importance, other species in the solution that can affect the solvation and hydrogen bonding situation of this moiety — most importantly the solvent and the counterion of the azolium cation — might flip the balance between the two mechanisms toward the dissociative path. Solvents with hydrogen bonding ability can take over the role of the ammonium cation in activating the substrate for the reaction. Furthermore, since intermediate **III** and transition state $\mathbf{TS}_{\mathrm{II}\rightarrow\mathrm{III}}$ are zwitterionic structures, the mere polarity of the solvent may alter their stabilities, and thereby the corresponding barrier. Through a proton transfer from the azolium cation to the amine, solvation energies might change significantly, since such protic ammonium ions are generally stronger hydrogen bond donors than their azolium counterparts,[154] shifting the relative free energies. Furthermore, the free NHC can be stabilized by hydrogen bonding, which also facilitates the deprotonation of the azolium cation, and hence stabilizes the dissociative path.

Table 3.31.: The activation of aldehydes in electrophilicity upon hydrogen bonding to ammonium salts (glyc: glyceraldehyde; pyru: pyruvic acid; $R_{O\cdots H}$: $O\cdots H$ distance; $R_{C=O}$: C=O distance in the aldehyde; BI: Mayer Bond Index; SEN: Shared Electron Number; obtained at the TPSSh-D3BJ/def2-TZVPP level).

aldehyde R-CHO	donor –	$R_{O\cdots H}$ /Å	$R_{C=O}$ /Å	BI (C=O)	SEN (C=O)
H	–	–	1.20	2.12	2.02
CH_3	–	–	1.21	2.13	1.97
Ph	–	–	1.21	2.08	1.92
vinyl	–	–	1.21	2.06	1.92
H	Me_3NH^+	1.76	1.21	1.96	1.98
CH_3	Me_3NH^+	1.69	1.22	1.90	1.89
Ph	Me_3NH^+	1.63	1.23	1.78	1.80
vinyl	Me_3NH^+	1.66	1.23	1.79	1.83
H	$DBUH^+$	1.87	1.21	2.00	1.98
CH_3	$DBUH^+$	1.81	1.22	1.94	1.91
Ph	$DBUH^+$	1.75	1.23	1.82	1.85
vinyl	$DBUH^+$	1.78	1.23	1.83	1.83

Thus, we investigated solvent effects on the barriers in an array of organic solvents through the COSMO-RS approach.[287,442,444] This solvent model can accurately account for the effects of the polarity of the solvent, and also hydrogen bonding interactions, making it ideal for the present purposes. In agreement with the reasoning above, the polarity of the solvent makes a big difference (Figure 3.64). Moving from the less polar solvents (toluene, hexane, THF) toward the highly polar ones (DMSO), the barrier of the associative path slightly increases, while that of the dissociative mechanism remarkably decreases. This effect is even stronger for hydrogen bond donor solvents (EtOH, MeOH, water). In aqueous solution the advantage of the associative mechanism is reduced to ca. 1 kcal mol^{-1}.

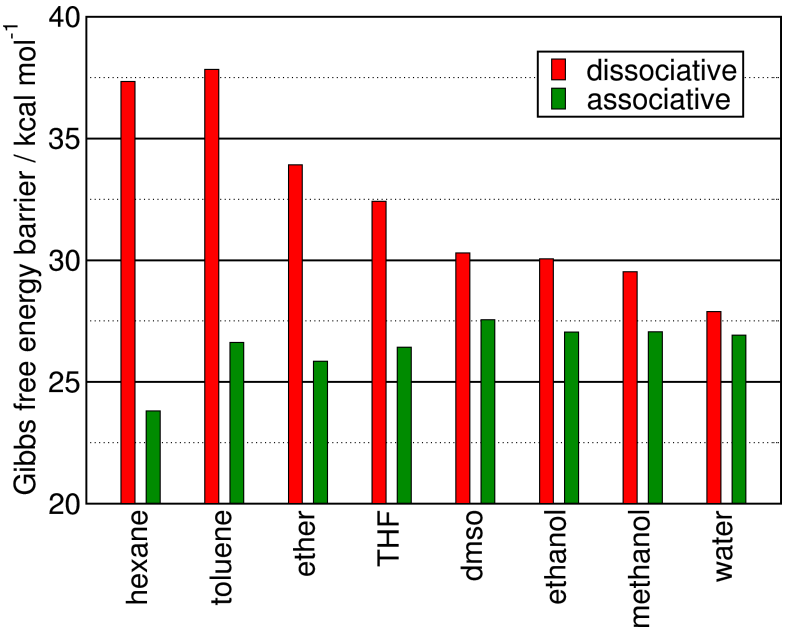

Figure 3.64.: Solvent effects on the Gibbs free energy barriers of the reaction between 1,3-dimethylimidazolium cation, trimethylamine, and acetaldehyde, using the COSMO-RS model, and the DLPNO-CCSD(T)/CBS//TPSSh-D3BJ/def2-TZVPP method. For numerical values, see Supporting Information

Thus, the polar environment and hydrogen bonding apparently decreases the barrier of the dissociative path through stabilizing $\mathbf{TS}_{\mathrm{II}\rightarrow\mathrm{III}}$. However, hydrogen bonding can also have a tremendous effect on the availability of the free NHC. NHCs are highly basic compounds, and hence they can form very strong hydrogen bonds, which can result in a stabilization up to even $10-20$ kcal mol^{-1}.[1,5,82,121,123] While the stabilization by hydrogen bonding activates the aldehyde substrate, it may also occupy the NHC lone pair, which is the very site, to which the electrophilic substrate should bind in the reaction. Hydrogen bonding at this position has been, therefore, repeatedly invoked as a factor that diminishes the catalytic activity of NHCs.[127,129] For this reason, at

first glance the hydrogen bond between the solvent molecule and the NHC may seem rather contraproductive. Thus, next to the dissociative and associative mechanisms that were distinguished above, in which the carbene participates as a free or as a protonated species (i.e. azolium cation), hydrogen bonded carbenes should represent another degree of freedom for the carbene's lone pair, somewhere in between these two extremes.

Similarly to the associative mechanism detailed above, the hydrogen bond donor solvent molecule can be replaced by the substrate without forming an unstable, free NHC in the solution, through the transition state shown in Figure 3.65. The obtained free enthalpies of activation (for the reaction of 1,3-dimethylimidazol-2-ylidene with formaldehyde: $\Delta G^{\ddagger}_{\mathrm{solv}} = 7.4\,\mathrm{kcal\,mol^{-1}}$; with benzaldehyde: $\Delta G^{\ddagger}_{\mathrm{solv}} = 15.7\,\mathrm{kcal\,mol^{-1}}$; both in methanol) are quite low. Comparing this mechanism to the one that proceeds through the free carbene is not possible due to technical reasons: The COSMO-RS solvent model in all cases considers the best possible solute-solvent interactions, thus, it automatically forms a hydrogen bond between the NHC and the implicit solvent whenever the lone pair is available, hindering the calculation of a fully free carbene molecule (i.e. with an available lone pair, not blocked by protonation or hydrogen bonding). However, the values shown above for the mechanism in Figure 3.65 are very similar to the dissociation Gibbs free energy of a carbene-alcohol bond, i.e. that of producing a free NHC. A hypothetical free NHC, with no deactivating hydrogen bonds from the solvent, would need to react through yet another barrier to form the C-C bond with the substrate. Accordingly, it is reasonable to assume that the mechanism in Figure 3.65 is more feasible. Thus in protic (hydrogen bonding) solvents the dissociative mechanism can be rationalized as a substitution of the ammonium cation by the solvent at the hydrogen bond acceptor hypovalent carbon atom, followed by the reaction depicted in Figure 3.65. Such exchange of hydrogen bond donors at NHCs has been discussed before, and has been found to depend on steric effects and the hydrogen bond acceptor strength of the NHC in its rate and mechanism.[5,123] The reaction of the solvent-NHC hydrogen bonded complex with the substrate (Figure 3.65) can be considered as a special case of the associative mechanism depicted in Figure 3.59.

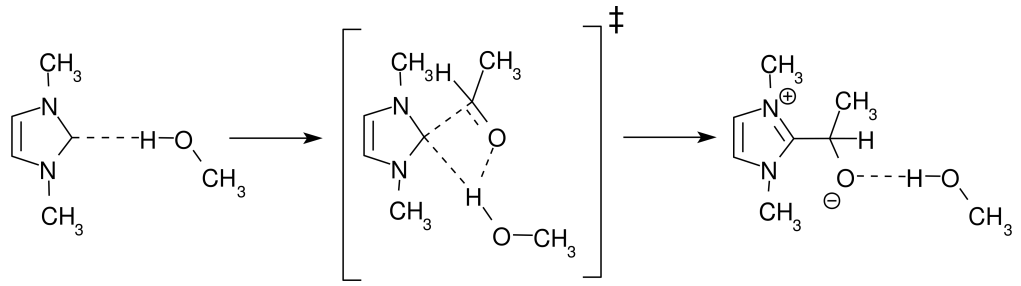

Figure 3.65.: Associative reaction of an NHC directly from its hydrogen bonded form without the formation of a free carbene species.

The presence of the anion in the solution next to the reacting species might also have significant effects on the differences in the barriers of the associative and dissociative reactions. The first question in this regard is if anions and cations remain associated in solution in the form of an ion pair, and can thereby affect the reaction, or if they instead dissociate into indiviual ions in the solution, and the reaction mechanism remains mostly unaffected by the anion. Ion pairing can be influenced by the solvent, and by the nature of the ions themselves. To uncover in what cases ion pairing might occur in these reaction mixtures, we performed umbrella sampling calculations in a classical molecular dynamics environment on a 1,3-dimethylimidazolium bromide ion pair, and a 1,3-dimethylimidazolium triflate ion pair in different solvents (see Section 3.7.2). While the chloride anion is considered highly coordinative, the triflate anion is considered non-coordinative in their e.g. imidazolium salts, for instance in ionic liquids.[327] In these calculations, the free energy was obtained as a function of the distance between the anion and cation, providing an estimate for the propensity of the given anion-cation pair to stay associated. The separation of the ions is in almost all cases endothermic, only in the most dissociating aqueous solution is the energy of dissociation close to zero. Based on these findings, imidazolium salts are apparently dissolved in all the investigated solvents as ion pairs. In the lack of such well-tested force field parameters for thiazolium and triazolium rings it is not possible to have such a quantitative insight for the corresponding salts. However, considering that those two cations are more acidic than imidazolium cations, it is reasonable to assume that they are stronger hydrogen bond donors, and therefore they would be even more strongly coordinated to the anions, and consequently the formation of ion pairs can be expected in these solutions as well.

Thus, the presence of the anions must be considered for the reactions, if the full picture is to be obtained regarding the two competing mechanisms. To this end, we chose a series of anions (halides, tetrafluoroborate and triflate) that are often applied in synthesis as counterions for the catalysts, and examined the Gibbs free energy barriers of the associative and dissociative paths in a series of solvents. Based on the obtained data, the difference between the barriers became lower, amounting to less than 11 kcal mol^{-1} in all cases (Tables 3.32 and 3.33). In fact, the preference varies between the two mechanisms, depending on the anion and on the solvent. In general, as observed above, the increasing polarity and hydrogen bonding ability of the solvent facilitates the dissociative mechanism, and hinders the associative one. The increasing size of the halide anions shifts the preference toward the dissociative mechanism, although for the reactions with the thiazolium cation the trend between bromide and iodide is reverse. The two other anions, tetrafluoroborate and triflate, apparently make the associative mechanism more dominant than bromide or iodide, exhibiting similar differences in the two barriers to those for chloride. Imidazolium-based salts appear to be the least favorable for the associative path to occur, while the very often applied triazolium catalyst shows the highest propensity to support this path.

Under closer scrutiny, the role of the anion in decreasing the difference between the barriers can be identified. The positive charge on the azolium cations is delocalized over the whole ring, while on the ammonium cation it is highly localized on the N-H unit. Therefore, although azolium cations have also been shown to be hydrogen bond

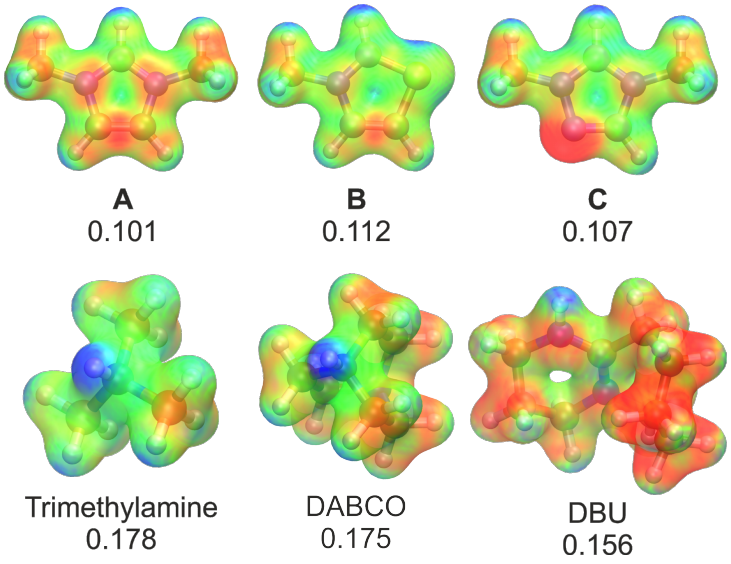

Figure 3.66.: Electrostatic potential maps of catalysts **A**, **B** and **C** (above), as well as the protonated trimethylamine, DABCO, and DBU (below). The more positive areas (blue) are less localized for the azolium cations (above) than for the protonated amine bases (below), which makes the latter group of compounds stronger hydrogen bond donors. The Hirshfeld charge (TPSSh-D3BJ/def2-TZVPP) at the mobile hydrogen atom is shown for each compound, supporting this hypothesis.

donors,[143,327,440] ammonium cations offer an even stronger donor site. These differences are clearly observable in the electrostatic potential maps of the azolium and ammonium ions, as well as the charges of the hydrogen bond donor sites (Figure 3.66). Thus, the strong hydrogen bond, formed between the ammonium ion and the anion, can compensate for the energy demand of moving the proton from the stronger base carbene to the weaker amine. This compensation effect can be estimated through the methatesis reaction [azolium$^+$ X$^-$] + HNMe$_3^+$ → azolium$^+$ + [HNMe$_3^+$X$^-$], showing the Gibbs free energy benefit of exchanging the azolium cation to an ammonium in interaction with anion **X** (Table 3.34). All anions interact apparently stronger with the ammonium cation than with any of the azolium species. Generally, the imidazolium cation **A** shows the lowest reaction Gibbs free energies, followed by the thiazolium cation **C**, while the least exergonic cation exchange was observed for the triazolium cation **B**. This trend is in full accordance with the discussion above, showing that the preference for the dissociative mechanism decreases in exactly this order. The Gibbs free energy is most negative in case of the halide anions, and moving toward the larger species with a delocalized charge the methatesis becomes less exergonic. Interestingly, the halides show an opposite trend, as the chloride — despite the significantly stronger interactions with the ammonium cation than with the azolium cation — decreases the least the propensity of the catalysts

Table 3.32.: DLPNO-CCSD(T)/CBS//TPSSh-D3BJ/def2-TZVPP difference between the Gibbs free energy barriers of the catalyst + formaldehyde + triethylamine reaction for the associative and dissociative mechanisms ($\Delta\Delta G^{\ddagger} = \Delta G^{\ddagger}_{assoc} - \Delta G^{\ddagger}_{dissoc}$, in kcal mol^{-1}) in non-polar media, in the presence of various anions. Negative values mean that the associative mechanism is faster in that particular case.

catalyst	anion	gas phase	hexane	toluene	Et_2O	THF
A	Cl^-	−5.2	−1.8	−0.9	−0.7	−0.3
A	Br^-	−1.2	0.9	2.0	2.0	2.4
A	I^-	0.5	2.0	3.0	2.9	3.3
A	$[BF_4]^-$	−3.7	−1.7	−0.5	−0.5	−0.2
A	$[CF_3SO_3]^-$	−4.7	−0.6	0.4	0.3	0.7
B	Cl^-	−6.9	−4.7	−3.6	−3.4	−3.2
B	Br^-	6.1	7.4	8.5	8.7	8.8
B	I^-	8.0	8.9	9.7	9.9	10.0
B	$[BF_4]^-$	−6.4	−4.3	−3.1	−3.0	−2.8
B	$[CF_3SO_3]^-$	−5.6	−3.8	−2.8	−2.7	−2.5
C	Cl^-	−3.1	−2.7	−1.8	−1.6	−1.4
C	Br^-	4.3	7.0	7.8	7.8	8.1
C	I^-	2.7	5.3	6.0	5.9	6.1
C	$[BF_4]^-$	−4.0	−2.6	−1.6	−1.6	−1.4
C	$[CF_3SO_3]^-$	−5.9	−2.0	−1.0	−1.0	−0.6

to undergo the associative mechanism (Tables 3.32 and 3.33). The explanation for this discrepancy might lie in the small size of the chloride anion, which allows some interaction through hydrogen bonding between the anion and the ammonium moiety also in transition state $\mathbf{TS}_{2\rightarrow IV}$ of the associative mechanism. Through this interplay, the system receives some stabilization also in this mechanism, albeit significantly less than in $\mathbf{TS}_{III\rightarrow IV}$ of the dissociative path, where the $HNMe_3^+Cl^-$ ion pair is separated from the reacting catalyst-substrate pair.

The effects above result in the conclusion that controlling hydrogen bonding and polarity effects of the solvent and the anion lead to a control over the reaction mechanism of N-heterocyclic carbene organocatalysis. The less polar solvents, and smaller halides or weakly hydrogen bonding anions lead to a preference in the associative mechanism, while the use of polar solvents and larger halides facilitates the dissociative mechanism. The numbers in Tables 3.32 and 3.33 show that switching between the mechanisms is possible. It is, however, very important to emphasize here the difficulties regarding the estimation of entropies in quantum chemical calculations, and it has been repeatedly discussed that entropy effects are significantly overestimated,[424,426,456] also for related reactions,[8] which results in an overestimation of the barriers for the associative reaction mechanism. Thus, while the trends for the shift in preference between the two mechanisms should be valid, it is possible that the actual numbers in Tables 3.32 and 3.33 should be somewhat more

Table 3.33.: DLPNO-CCSD(T)/CBS//TPSSh-D3BJ/def2-TZVPP difference between the Gibbs free energy barriers of the catalyst + formaldehyde + triethylamine reaction for the associative and dissociative mechanisms ($\Delta\Delta G^{\ddagger} = \Delta G^{\ddagger}_{assoc} - \Delta G^{\ddagger}_{dissoc}$, in kcal mol^{-1}) in polar solvents, in the presence of various anions. Negative values mean that the associative mechanism is faster in that particular case.

catalyst	anion	DMSO	Ethanol	Methanol	Water
A	Cl^-	0.5	1.7	1.8	0.3
A	Br^-	3.5	4.1	4.3	4.2
A	I^-	4.2	4.6	4.8	4.5
A	$[BF_4]^-$	0.9	2.1	2.3	1.9
A	$[CF_3SO_3]^-$	1.6	2.7	2.7	1.6
B	Cl^-	−2.2	−0.8	−0.5	−0.6
B	Br^-	9.5	10.0	10.0	9.2
B	I^-	10.5	10.8	10.7	9.7
B	$[BF_4]^-$	−1.8	−0.5	−0.3	−0.5
B	$[CF_3SO_3]^-$	−1.6	−0.2	0.0	0.3
C	Cl^-	−0.6	0.8	1.0	0.1
C	Br^-	8.8	9.1	9.1	8.0
C	I^-	6.7	7.2	7.1	5.8
C	$[BF_4]^-$	−0.6	0.8	0.9	−0.1
C	$[CF_3SO_3]^-$	0.3	1.3	1.3	0.3

Table 3.34.: DLPNO-CCSD(T)/CBS//TPSSh-D3BJ/def2-TZVPP Gibbs free energies (in kcal mol^{-1}) of the metathesis reaction [azolium$^+$ X$^-$] + $HNMe_3^+$ → azolium$^+$ + [$HNMe_3^+X^-$], showing the energy benefit of exchanging the azolium cation to an trimethylammonium cation in interaction with anion **X**.

	Cl	Br	I	$[BF_4]^-$	$[CF_3SO_3]^-$
A	−23.7	−21.7	−18.2	−13.1	−16.5
B	−16.5	−14.3	−12.2	−7.2	−10.5
C	−19.1	−17.0	−15.2	−11.0	−14.0

negative, and the associative mechanism slightly more preferred. The data presented here show that the associative mechanism, which avoids the formation of actual carbenes in the solution, has mild barriers, and should be considered in all cases when investigating the mechanism of NHC organocatalysis, especially in case of higher concentrations of the substrate, base and catalyst in the solution.

3.7.4. Summary and Conclusion

In the present computational study, two mechanisms were compared for the formation of the catalyst-substrate bond in NHC organocatalysis. These two mechanisms fundamentally differ in terms of the occurrence of free NHCs in the reaction mixture. In the widely accepted (dissociative) mechanism of this process, as described by Breslow,[52] the formation of free NHCs via the deprotonation of the azolium salt catalyst is required, and the resulting low concentration of carbenes in the solution offers the actual catalytic activity. In an alternative, associative mechanism,[6] the deprotonation of the very weakly acidic azolium salts is bypassed in a concerted process, in which the proton transfer and the catalyst-substrate bond formation occurs in a single elementary step. Depending on the mechanism, the selectivity of the reaction might be influenced, especially since in the transition state of the associative path the base is also present, and therefore its bulkiness and possible template effects can influence the outcome of the reaction as well. In a series of model reactions, imidazolium, triazolium, and thiazolium cations were considered as catalysts with varying substituents on the relevant nitrogen atoms, formaldehyde, acetaldehyde, benzaldehyde and acrolein as substrates, and trimethylamine, DBU, and DABCO as bases.

In the absence of solvents and anions the reaction follows the associative mechanism, avoiding, thereby, the formation of free carbenes in the solution. The reasons for this dominance were identified to be the high enthalpic benefit of the association of the components, and the interaction of the mobile proton on one hand with the azolium ring, avoiding the complete liberation of the reactive carbene lone pair, while on the other hand with the oxygen atom of the substrate, which activates this molecule for the nucleophilic attack of the catalyst. This complex network of stabilizing hydrogen bonding interactions can be, however, disrupted and partly substituted in the presence of polar and protic solvents, which offer alternative, modes of stabilization in case of the dissociative mechanism.

The azolium salts in a variety of organic solvents and water were found to stay associated within the same solvent shell in the form of ion pairs. The presence of anions vanishes most of the dominance of the associative mechanism, and the barriers become more similar. The underlying reason for this effect was identified to be the stronger interaction of the anion with the protonated base than with the azolium cation, which shifts the acid-base equilibrium toward the free carbene, and partially breaks up the azolium-base-substrate aggregates. In case of stronger hydrogen bond acceptor anions (e.g. halides), the dissociative process exhibits lower barriers, while in case of weak hydrogen bond acceptor anions (e.g. tetrafluoroborate and triflate), the associative path was found to be faster. An exception here was the chloride anion, which — due to its small size — can form stabilizing interactions with the hydrogen bond donor species also within the transition state of the associative path, retaining thereby the preference for this mechanism in many cases. Accordingly, the mechanism can be controlled through varying the anion and the solvent, and therefore introducing novel kinds of selectivities into these mechanism should also focus on carefully choosing these elements of the catalytic system.

The results above bring also new insight into the related biochemical reactions of vitamin B1, thiamine. Since in this reaction the thiazolium ring and the base that should deprotonate it are covalently bound, only the associative reaction mechanism is feasible. In the lack of significant entropic effects, the barriers of two model reactions of thiamine were found to be low, suggesting the viability of the associative mechanism in biological systems.

3.8. On the Carbene–Like Reactions of Imidazolium Acetate Ionic Liquids: Can Theory and Experiments Agree?

Sascha Gehrke[†,‡] , Werner Reckien[†] , Ivan Palazzo[§] , Tom Welton[§] , Oldamur Hollóczki[†,*]

European Journal of Organic Chemistry, 2019, Pages 504–511

DOI: 10.1002/ejoc.201801050

Received: July 05, 2018

Published: September 13, 2018

For this article a Supporting Information is available free of charge at:
`https://chemistry-europe.onlinelibrary.wiley.com/action/downloadSupplement?doi=10.1002%2Fejoc.201801050&file=ejoc201801050-sup-0001-SupMat.pdf`

Contributions to the manuscript:

- Setup and maintenance of all calculations
- Analysis of the trajectories
- Writing the technical part of the manuscript

[†]Mulliken Center for Theoretical Chemistry, University of Bonn, Beringstr. 4+6, D-53115 Bonn, Germany
[‡]Max Planck Institute for Chemical Energy Conversion, Stiftstr. 34–36, D-45470 Muelheim an der Ruhr, Germany
[§]Imperial College London, South Kensington Campus, London SW7 2AZ, UK
[*]E-mail: holloczki@gmail.com

The findings presented in the last chapters renders the detailed characteristics underlying the activity of organocatalysts as very complex. Therefore, it is no wonder that during the years several studies were published containing contradictive interpretations. In this chapter, some of these studies are revisited on a theoretical level and the results discussed in comparison with the findings obtained before.

Abstract

The N-heterocyclic carbene organocatalytic reactivity of the 1-ethyl-3-methylimidazolium acetate ionic liquid was investigated on the model reaction between this solvent and anisaldehyde. The formation of carbenes by a proton transfer from the cation to the anion was compared to a direct reaction mechanism, in which the proton transfer and the C–C bond formation between catalyst and substrate occurs in a single elementary step. Interestingly, the two reaction mechanisms show a much smaller difference in activation energies than those observed for analogous catalytic systems with neutral bases, showing that the mechanism might switch from one to the other at different temperatures or with different substrates. In this particular case, however, the direct reaction mechanism, avoiding free carbenes in the solution, is apparently more feasible. Based on the detailed analysis of this reaction path, the earlier contradictions between theory and experiments can be resolved, resulting in a consistent mechanistic picture for the related processes. Additionally, we show on the example of a platinum surface that introducing metal probes into the liquid may induce carbene–like reactions, as the formation of a strong coordinative bond between the carbene and a platinum atom at the surface is highly exothermic, shifting the acid–base equilibrium considerably.

3.8.1. Introduction

The rich chemistry of imidazole derivatives include an enormous variety of N-heterocyclic carbene (NHC)[35,40–42,230,232,233] related catalytic and organocatalytic applications. In the latter processes the carbene is often applied as a salt, which is supposed to be deprotonated by a proper base. These salts can be tailored in a way that they have a low melting point, forming ionic liquids (ILs),[133–136] which are used in a variety of organic synthesis. Clearly, there is a lot of potential to exploit these two properties of imidazolium derivatives simultaneously, where the material in question has a dual role in the reaction, serving both as a solvent and a catalyst.

This relation can be further improved if the counterion itself can serve as a base in the process, which can mobilize the proton at the imidazolium ring without the addition of an external base as an extra component in the reaction mixture. Indeed, for 1-alkyl-3-methylimidazolium acetate ILs carbene-like chemical properties were observed in the gas phase,[82] and in the liquid,[137] which attracted remarkable attention through the last decade. It has been shown that these ILs can react as a carbene with chalcogens,[137] metal ions[138] and oxides,[139,140] and carbon-dioxide[141,142] to form well-known carbene adducts of these substrates. Perhaps most interestingly, imidazolium acetate ILs have been shown to catalyze NHC-related organocatalytic reactions.[81] This concept was applied later in a bio fuel production process,[457,458] and has also been related to the degradation of cellulose dissolved in these ionic liquids.[306]

Although the aforementioned examples seem to indicate the availability of carbenes in imidazolium acetate ILs rather clearly, these species have not been observed by any direct spectroscopic technique in the bulk of these liquids,[459] a fact that — together with theoretical studies[143,144] — suggests that the concentration of spontaneously formed carbenes must be low at best. This contradiction induced an intensive scientific discussion, where the researchers — including us — aimed at either to observe the inherent presence of the carbene in the neat liquid,[144,460,461] or to find alternative reaction mechanisms that could explain these carbene-like reactions in the absence of the explicit formation of carbenes.[142,423,462]

Interestingly, the C-H bond of the mobile proton has been indicated by *ab initio* molecular dynamics simulations to stretch slightly longer in the presence of a neutral molecule e.g. CO_2.[144] These results raised the possibility that the proton transfer from the carbene to the anion in the liquid is induced by the substrate. In agreement with these observations, we discovered an alternative reaction mechanism for the reaction of CO_2 with 1-ethyl-3-methylimidazolium acetate $[C_2C_1Im][OAc]$ that avoids the explicit carbene formation in the liquid,[142] and in which the proton transfer from the cation to the anion and the C-C bond formation occur simultaneously instead. This reaction mechanism was confirmed later by *ab initio* molecular dynamics simulations[423] and further DFT calculations,[462] and it has been also shown to be a general mechanism for NHC organocatalysis.[6] It has been argued that the mechanism of these reactions is not related to carbenes at all, and the reactions in question can be better characterized as an electrophilic aromatic substitution mechanism of the azolium cation.[6] Although none of the organocatalytic reactions of ILs mentioned above has been investigated in detail, ac-

cording to these data it is reasonable to assume that those reactions can also follow such a direct, concerted path, which is more favorable than the dissociative path, involving the free NHC (Figure 3.67). In qualitative agreement with this reasoning, by a series of static calculations with continuum solvent models Yan *et al.* suggested that carbenes do not form from imidazolium acetates in solvents with a dielectric constant higher than $\epsilon = 5$.[423]

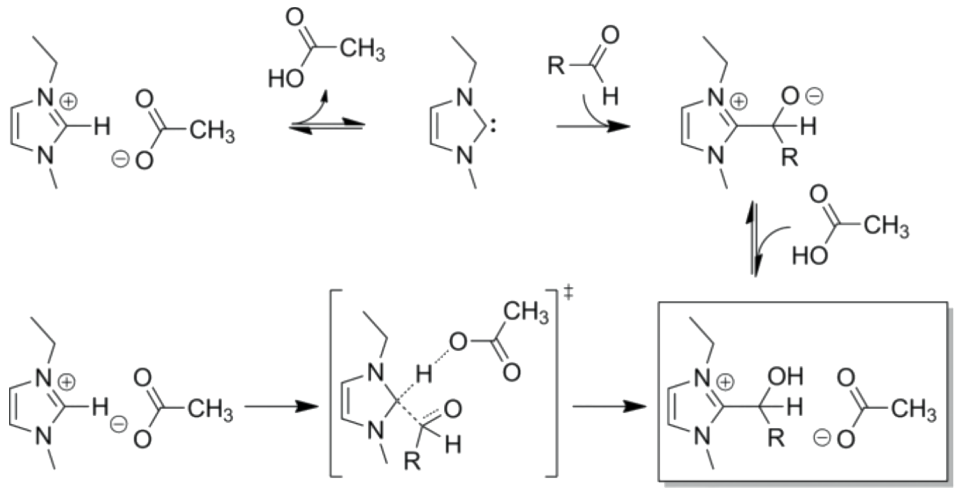

Figure 3.67.: The two possible reaction mechanisms for the catalyst-substrate bond formation in the organocatalytic benzoin condensation catalyzed by the 1-ethyl-3-methylimidazolium acetate solvent. The dissociative reaction mechanism (above) involves the formation of a free carbene, while in the direct — or associative — mechanism (below) the imidazolium cation reacts directly with the aldehyde substrate through an electrophilic aromatic substitution path.

However, in contrast to the theoretical results, the inherent presence of the NHC in $[C_2C_1Im][OAc]$ was recently reported based on electrochemical measurements.[460] In the cyclic voltammogram of the imidazolium-acetate IL such features were observed at elevated ($> 120°C$) temperatures, which were absent at room temperature, and also in other ILs with less basic anions. Since the other investigated anions could not produce a carbene from the cation, and since by raising the temperature somewhat less stable structures, such as the carbene and acetic acid in this case would be more populated, it is reasonable to interpret these results as the presence of the carbene. These arguments were verified through experiments, in which the NHC was generated artificially, aiding the assignment of the current peaks.

In a separate study, kinetic isotope effect measurements were performed on the reaction of the IL with anisaldehyde.[461] Since exchanging the hydrogen atom to a deuterium at position 2 of the imidazolium ring did not affect the reaction rate significantly, it was apparent that the proton transfer could not be the rate limiting step, suggesting the

spontaneous and facile formation of the NHCs in the IL.[461] Since the concerted mechanism, which had been indicated by various theoretical studies,[6,142,423] also involves the transfer of the proton in that single elementary reaction step, these experiments seem to contradict the theoretical calculations, while being in agreement with the electrochemical study.

Accordingly, there seems to be a conflict between the experimental and theoretical studies in the field, which alludes to the lack of understanding the present process in terms of reaction mechanisms. In this contribution we aim to resolve these contradictions, to understand the details of the related, and from the applications point of view highly potential reactions. To this end we present a series of static density functional theory (DFT) calculations, and *ab initio* molecular dynamics (AIMD) simulations to shed more light on the reaction mechanism of organocatalysis by imidazolium-acetate ionic liquids.

3.8.2. Models and Methods

Static DFT and *ab initio* Calculations

All quantum chemical calculations were performed by the ORCA 4.0 software package.[256,441] The geometries were optimized employing the TPSSh functional[278] enhanced by the D3 dispersion correction with Becke–Johnson damping[279,280] and applying the def2-TZVPP basis set.[282,283] For both the SCF cycle and the geometry optimization convergence criteria the tight settings of ORCA were used. The obtained stationary points were identified as minima by calculating the Hessian.

Based on the obtained structures, single point energies were calculated using the DLPNO-CCSD(T)[259–261] method, with tight settings for the localization as defined by Neese and Liakos. Afterwards, the single point energies with the def2-TZVPP and with the def2-QZVPP basis sets were extrapolated to the complete basis set limit.[262] The obtained electronic energies were corrected by the Gibbs free energy correction based on the Hessian of the DFT calculation.

Finally, the Gibbs free energies of solvation were calculated by the COSMO-RS method[287,442] employing the COSMOthermX14 program package.[443,444] To achieve this, the BP-TZVPD-FINE method of COSMOtherm was applied, which is based on single point energy calculations with the BP86 functional[445] and a def2-TZVPD basis set[282,283] by the Turbomole programm.[446]

Investigation of the Metal Interface

The adsorption of the ion pair and the carbene/acid system on the Pt(111) surface was studied by means of density functional theory (DFT) with the plane-wave code VASP.[463–466] The systems investigated are created by the clean, unreconstructed Pt(111) surface and the ion pair or carbene/acid system as adsorbate. A $\begin{pmatrix} 5 & 0 \\ 0 & 5 \end{pmatrix}$ supercell with three atomic layer was chosen ($a = b = 13.88$ Å, $\gamma = 120°$). The first two atomic layers were relaxed while the atoms of the lowermost layers were kept at their bulk-like positions.

All calculation were performed with the PBE functional in combination with an empirical dispersion correction (PBE-D3 with Becke–Johnson damping). The cutoff energy for the plane-wave valence basis was set to 400 eV. A $3 \times 3 \times 1$ k-point mesh was used for reciprocal-space integration.

Thermodynamic Integration

For the thermodynamic integration we followed an already proven protocol.[308,467,468] First, a simulation box containing 26 ion pairs of $[C_2C_1Im][OAc]$ was generated by PACKMOL with the experimental density of $1.027\,g\,mol^{-1}$ resulting in a cell vector of 19.29 Å. The following *ab initio* molecular dynamics simulations were performed by the QUICKSTEP code implemented in the CP2K program suite.[469] The electronic structure was modeled with the revPBE functional[275,470] enhanced by the D3 dispersion correction with Becke–Johnson damping[279,280] and the MOLOPT-DZVP basis set[471] for the valence electrons. The core electrons were handled with Goedecker–Teter–Hutter pseudopotentials.[472–474] The multigrid level was set to 5 with a cutoff criterion of 400 Ry and the convergence criterion for the SCF cycle was chosen to be 10^{-6}.

First, the cell was optimized with the default settings of the CG optimizer to avoid possible energy hotspots. Afterwards, the timestep was chosen to be 0.5 fs for the simulations. An equilibration run was performed for 7.5 ps in an NVT-ensemble, applying a massive Nosé–Hoover thermostat at a higher temperature ($T = 503$ K, $\tau = 100$ fs) to ensure the activation of all degrees of freedom. Afterwards, the massive option of the thermostat was deactivated and the target temperature was set to 303 K. An appropriate ion pair was chosen and the distance between the H2 and the corresponding carbon atom was set to 1.09 Å. The distance was enlarged with a constant speed of $0.0002\,Å\,fs^{-1}$ for 7 ps until a distance of 2.49 Å was reached.

Between a distance of 1.09 Å and 1.69 Å a snapshot of the system was taken every 0.05 Å. Afterwards this interval was enlarged to 0.1 Å. The obtained systems were equilibrated separately with the above mentioned settings and a additionally constrained distance between the relevant atoms for 20 ps at a temperature of 298 K. Finally, production runs of another 20 ps were performed printing out the Lagrange multiplier which gives the force necessary to constrain the distance in each step. For each distance the obtained forces were averaged and the corresponding distance–force plot was interpolated with the Akima spline method implemented in Xmgrace.[475] The Integral of the obtained function gives the Gibbs free energy potential.

With the aim to compare the carbene formation in the liquid phase with the gas phase static calculations, we prepared a single ion pair in a simulation box with the very same size and settings like above. Following the same protocol like for the ion pair in solution we were able to obtain an analogous potential for the gas phase.

3.8.3. Results and Discussion

First we investigated the reaction mechanism of the organocatalytic benzoin condensation of anisaldehyde catalyzed by the ionic liquid 1-ethyl-3-methylimidazolium acetate [C_2C_1Im][OAc], investigated earlier experimentally.[461] Although ionic liquids often contain moisture, the presence of water was neglected here. The effect of water on the basicity of the acetate anion in this particular ionic liquid has been investigated before theoretically[143] and experimentally as well,[141] and it has been shown that although at high concentrations of water reactions of the hydroxide anions can be observed instead of the acetate, but for reasonably dry solutions the carbene-like reactivity can be retained.[141,143] Accordingly, omitting the water content of the IL is a reasonable simplification.

As mentioned above, two possible reaction mechanisms are conceivable for this process (Figure 3.67), the dissociative pathway, which employs free carbenes in the solution, and the direct, concerted reaction path, which avoids the formation of free carbenes, and to which we will refer as associative mechanism. To assess and compare the feasibility of them, we performed static DFT and *ab initio* calculations to characterize energetically the intermediates and the transition states of these paths.

The dissociative mechanism (Figure 3.68) is initiated in the ion pair **I** by a proton transfer from the cation to the anion to yield **II**. This process is slightly exothermic for a single ion pair in the gas phase ($\Delta E = -0.3\,\mathrm{kcal\,mol^{-1}}$), in agreement with previous computational[82,144] and experimental[82] results. In **II** the carbene is not available for reacting with electrophilic substrates, since its lone pair is occupied in a hydrogen bond with the acetic acid molecule. In order to free this lone pair for the subsequent reaction steps of the dissociative path, **II** must dissociate to a free carbene and acetic acid **III**. This step is endothermic, it requires $\Delta E = 15.0\,\mathrm{kcal\,mol^{-1}}$, which is mainly due to the dissociation of this highly stable[82] hydrogen bond. This free nucleophilic carbene then reacts with the aldehyde through transition state $\mathbf{TS}_{\mathrm{III}\rightarrow\mathrm{IV}}$ to form the adduct **IV**, which can be protonated by the acetic acid, yielding the product **V**. The highest energy point of this path is $\mathbf{TS}_{\mathrm{III}\rightarrow\mathrm{IV}}$, which renders the barrier $\Delta E^{\dagger} = 19.2\,\mathrm{kcal\,mol^{-1}}$.

The associative mechanism (Figure 3.69) starts with the association of the anisaldehyde molecule to an ion pair, forming **2**. **2** rearranges into product **V** through an electrophilic aromatic substitution via $\mathbf{TS}_{2\rightarrow\mathrm{V}}$ in a single elementary step. This mechanism is practically identical to that observed before for the reaction of this ionic liquid with CO_2,[142,423,462] and the organocatalytic reactions catalyzed by azolium cations in the presence of amine bases.[6] The barrier of this path, defined by the relative energy of the aforementioned single transition state, is $13.1\,\mathrm{kcal\,mol^{-1}}$, notably lower than the $19.2\,\mathrm{kcal\,mol^{-1}}$ for the dissociative mechanism. Nonetheless, the difference between the two barriers is significantly smaller than for the amine bases in our earlier study,[6] where $20 - 30\,\mathrm{kcal\,mol^{-1}}$ activation energy differences were observed.

In the rate-limiting step of the dissociative mechanism the movement of the proton is not involved, hence the relative energies barely change when replacing the mobile position 2 hydrogen atom with a deuterium (Figure 3.68). In the associative mechanism the proton shift occurs simultaneously with the C–C bond formation in a single elementary step,

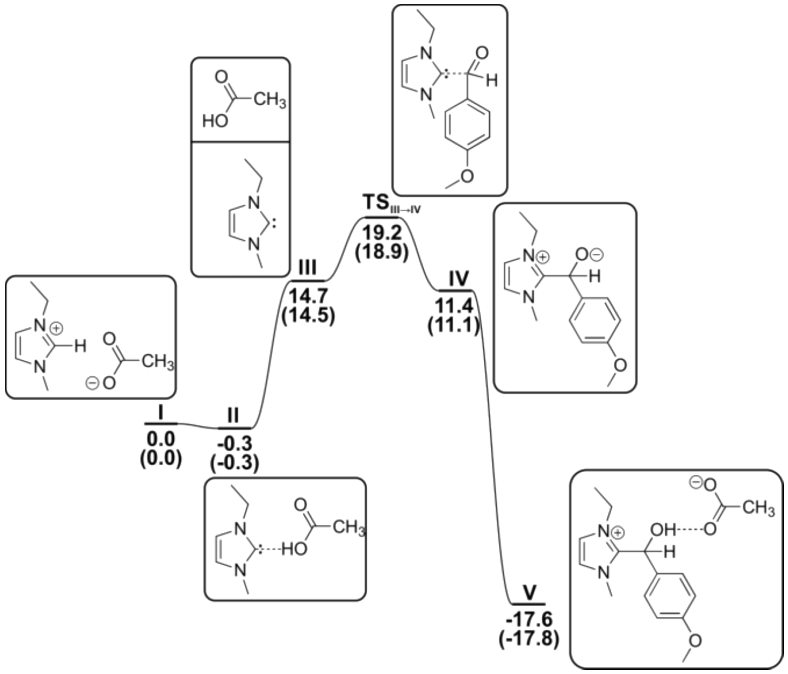

Figure 3.68.: Reaction energy profile (with zero point vibrational energies) of the dissociative mechanism for the reaction of 1-ethyl-3-methylimidazolium acetate with anisaldehyde. Data for the reaction, in which the cation is deuterated at position 2 are shown in parenthesis. The relative energies are given compared to the ion pair and a free, separated aldehyde. In the ΔE of **I**, **II**, and **III** the energy of the isolated aldehyde, while in the ΔE of $\mathbf{TS}_{\mathrm{III}\rightarrow\mathrm{IV}}$ and **IV** the energy of acetic acid is also included, these structures are omitted from the picture only for the sake of clarity.

and therefore one should expect to observe significant kinetic isotope effects, in clear contrast to the previous experimental findings.[461] However, recalculating the reaction energy profile with a deuteron at position 2 of the cation results in no significant changes in the relative energy of the corresponding transition state, and the energy barriers change no more than $0.3\,\mathrm{kcal\,mol^{-1}}$ (Figure 3.69). This surprising finding can be explained through the structural and normal mode analysis of $\mathbf{TS}_{2\rightarrow\mathrm{V}}$. The associative mechanism consists of a single, asynchronous concerted elementary step,[6] which means that the two processes are somewhat shifted apart along the reaction coordinate, with the proton transfer occurring earlier, and the C–C bond formation later in the reaction. On the resulting wide, plateau-like potential energy barrier the highest point, the transition state, is located closer to the second step. This is clearly visible in the structure of $\mathbf{TS}_{2\rightarrow\mathrm{V}}$, in which the O–H distance is very short (0.994 Å), while the C–H distance is long (1.967 Å); thus, the transfer of the proton is already completed. Kinetic isotope effects arise from the fact that the zero point vibration energies (ZPVE) are different in

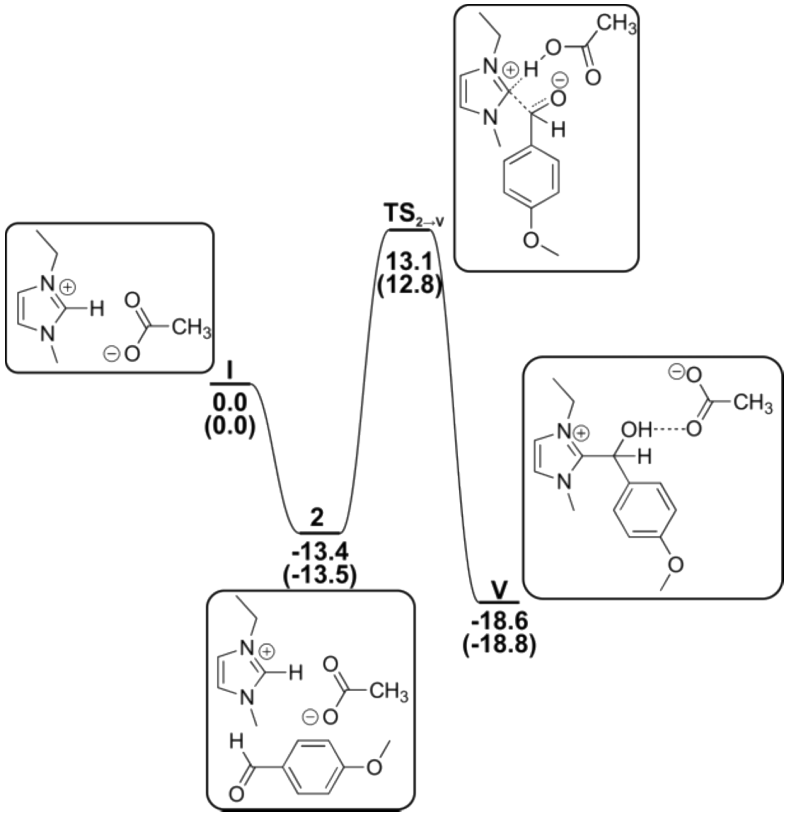

Figure 3.69.: Energy (with zero point vibrational energies) profile of the associative reaction of the $[C_2C_1Im][OAc]$ with anisaldehyde, with hydrogen and deuterium (in parenthesis) at the H2 position of the cation. The relative energies are given compared to the ion pair and a free, separated aldehyde.

the transition state and the minima of the potential energy surfaces. In the transition states, one of the normal modes becomes a translational mode of a (group of) atom(s), appearing in the calculations as an imaginary frequency. Hence, this normal mode has no contribution to the ZPVE of the transition state. Changing the mass of the atoms that are involved in this normal mode affects the vibrational energy, and therefore also the difference between the minimum and the transition state in ZPVE, producing a change in the effective barrier. In this case, however, the imaginary frequency does not involve a significant movement from the H2 (see Figure 3.70), hence changing its mass should not have any effect on the activation energy, and therefore, neither on the kinetics of the reaction. Accordingly, it is reasonable to conclude that the lack of kinetic isotope effect does not actually prove the spontaneous presence of carbenes in $[C_2C_1Im][OAc]$. Thus, we suggest that this direct reaction mechanism is no longer excluded in the liquid, and the formation of carbenes is not necessary for this carbene-like organocatalytic behavior.

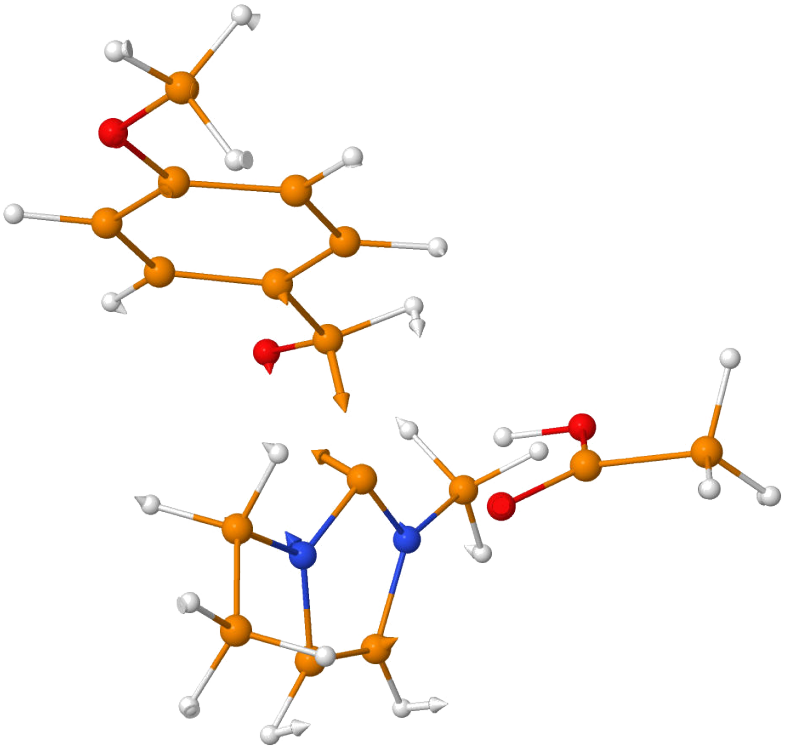

Figure 3.70.: Representation of the imaginary vibrational mode of the transition state in the associative mechanism for the reaction between $[C_2C_1Im][OAc]$ and anisaldehyde. It is visible how little the contribution is from the O(OAc)-H2 and C2-H2 vibrations.

The energetics above can be refined by considering solvent and thermal, including entropic effects. The proton transfer occurs between a cation and an anion, which converts the highly polar ion pair **I** (dipole moment $D = 9.57$) into two neutral molecules (dipole moments $D = 1.62$ and $D = 2.46$ for the acetic acid and the carbene, respectively). Even if such a transition is preferred in the gas phase, a polar solvent, just like the ionic liquid itself, would destabilize it greatly. Yan *et al.*[423] used a polarizable continuum model CPCM to account for the electronic effects of the solvent on the energy difference between **I** and **II**, and concluded that in polar environments (where $\epsilon > 5$) this proton transfer does not occur, and therefore **II** is absent in the solution. Here we chose to apply the COSMO-RS model (Conductor-like Screening Model for Real Solvents) for the reaction paths. In this model the electrostatic, hydrogen bonding and dispersion interaction energies are all included to estimate the solute-solvent interactions.

Since the molecularity of the two reactions is different, at the first glance it seems vital to include entropic effects also in the calculations. It is, however, necessary to point out that the routinely applied entropy calculations are based on the formalism used for the gas phase, and therefore they are of highly questionable relevance for processes in solu-

Table 3.35.: Differences between the activation Gibbs free energies of the associative and dissociative mechanisms ($\Delta G^{\dagger}_{\text{assoc}} - \Delta G^{\dagger}_{\text{dissoc}}$) at different temperatures with the COSMO-RS solvent model, with varying percentage of ΔS_{trans} and ΔS_{rot} considered. Negative values suggest the preference for the associative mechanism.

T/K	0 %	20 %	40 %	60 %	80 %	100 %
303	−5.9	−2.8	0.4	3.5	6.7	9.9
323	−6.8	−3.4	0.0	3.4	6.8	10.2
343	−7.8	−4.1	−0.5	3.2	6.8	10.5
363	−8.7	−4.8	−0.9	3.0	6.9	10.8
383	−9.6	−5.5	−1.3	2.8	7.0	11.1
403	−10.6	−6.2	−1.8	2.6	7.0	11.4

tion. In fact, it has been proven that the translational (ΔS_{trans}) and rotational (ΔS_{rot}) entropy loss is highly overestimated for association reactions in the liquid.[424–426,456] It has been even argued regarding a case study of protein binding affinities that the translational and rotational entropies make altogether negligible contribution to these association reactions in aqueous solutions.[456] In the present case the calculated entropies are of especially questionable relevance, since two of the three reacting molecules are, in fact, the solvent, and therefore the entropically unfavorable association to form e.g. **2** occurs already when dissolving anisaldehyde in the IL. Generally, a possible correction for the overestimation of solution phase entropies is the scaling of the rotational and translational entropy.[424–426,456]

Since the two barriers are relatively close in energy, varying scaling for these entropic contributions can change the preference for the two mechanisms. In Table 3.35 we collected the difference between the Gibbs free energies of the associative and dissociative mechanism with the COSMO-RS model ($\Delta G^{\dagger}_{\text{assoc}} - \Delta G^{\dagger}_{\text{dissoc}}$), and with a variety of scaling factors for ΔS_{trans} and ΔS_{rot} at different temperatures. The data shows the sensitivity of the conclusions to the way the entropies are considered. Scaling down ΔS_{trans} and ΔS_{rot} to 0 % favors the associative mechanism, and this preference increases by temperature. By leaving a large contribution of ΔS_{trans} and ΔS_{rot} in the Gibbs free energies, the dissociative mechanism appears to be more feasible, which is even more pronounced at higher temperatures.

In the light of the previous literature discussions regarding the necessity of scaling ΔS_{trans} and ΔS_{rot}, the data in Table 3.35 clearly suggests the need for a superior method to describe these effects. Accordingly, to account fully for the bulk structure and dynamics together with the necessary entropic effects, we performed *ab initio* molecular dynamics simulations with periodic boundary conditions on a model of the pure liquid. This technique, although computationally demanding, is an ideal tool for investigating simple reactions in the liquid phase, since it accounts for the movement and constant rearrangement of the molecules in the liquid, while describing the full electronic structure

explicitly. Instead of the highly complex reaction itself (with involved reaction coordinates), here we investigated with this technique the proton transfer from the cation to the anion, and the subsequent dissociation. Analysing this dissociation should reveal the true nature of dissociation/association processes in this solution in terms of free energies, which will aid us in assessing how large scaling would be reasonable for the translational and rotational entropies.

Since the proton transfer does not occur spontaneously in these systems in such *ab initio* molecular dynamics models,[143,144] we enforced it here with a thermodynamic integration approach, where the energetics of the process can be tracked along the reaction coordinate, viz. the increasing C2-H2 distance. The obtained graph shows a remarkably high energy demand ($> 26\,\mathrm{kcal\,mol^{-1}}$, Figure 3.71) to move the proton from the carbon atom of the cation toward the oxygen atom of the anion, and then elongate and break the hydrogen bond of the acetic acid-carbene complex. The high free energy demand of this process shows that the formation of a free carbene should occur only at elevated temperatures in solution, when this unstable isomer of an ion pair is also populated. This is in good qualitative agreement with the results of Chiarotto *et al.*,[460] observing the carbene formation in the voltammetry experiments only at 120 °C.

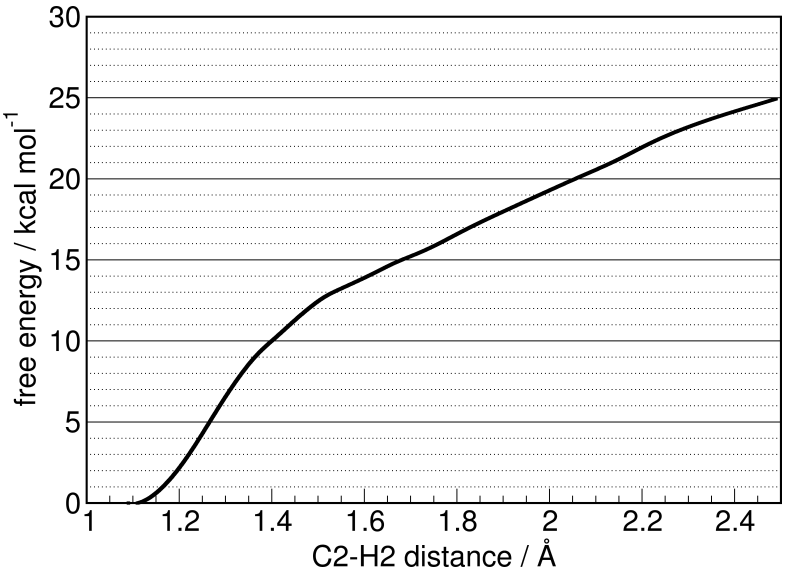

Figure 3.71.: Energy profile of the carbene formation process from thermodynamic integration. The thermodynamic integration was performed based on an AIMD simulation of 26 ion pairs of $[C_2C_1Im][OAc]$ applying the revPBE-D3 functional.

In contrast, static quantum chemical calculations with COSMO-RS solvent model and 100 % of the aforementioned $\Delta S_{\mathrm{trans}}$ and ΔS_{rot} contributions result in a Gibbs free energy difference between **I** and **III** of $\Delta G = 5.2\,\mathrm{kcal\,mol^{-1}}$. Thus, the static calculations that included the terms for the elusive translational and rotational entropy apparently

yield an even qualitatively different energetics for the carbene formation in the liquid compared to the more reliable technique of thermodynamic integration through *ab initio* molecular dynamics. The values are so different for the two methods that they lead to fully different conclusions for the presence of free carbenes in the solution. While the static calculations suggest a relatively easy access to the free carbene and the acetic acid, the molecular dynamics simulations – in agreement with earlier studies[423] – indicate that this process is considerably hindered by a substantial energy gap. Eliminating fully the translational and rotational entropy contributions produces, however, a Gibbs free energy difference between **I** and **II** that resembles most the data obtained from the superior simulations ($\Delta G = 20.3\,\mathrm{kcal\,mol^{-1}}$). These findings clearly suggest a low contribution of these entropic parts in the relative Gibbs free energies.

Based on these considerations, the Gibbs free energy barrier (with $\Delta S_{\mathrm{trans}}$ and ΔS_{rot} contributions scaled to 0 %) of the dissociative mechanism was found to be $\Delta G^{\dagger} = 20.8\,\mathrm{kcal\,mol^{-1}}$. In contrast, for the associative path a $\Delta G^{\dagger} = 14.9\,\mathrm{kcal\,mol^{-1}}$ was obtained, which shows that in the present case the associative mechanism is probably significantly faster, albeit both reaction mechanisms might occur. Even so, the data here suggest that with varying substrates the reaction might switch from one mechanism to the other. For this reason, from investigating the single examples for the trapping or catalytic activity of 1,3-di-alkylimidazolium acetate ILs computationally or experimentally general conclusions on these types of reactions cannot be drawn.

According to the considerations above it is especially intriguing to discuss again the voltammogram of the pure 1-ethyl-3-methylimidazolium acetate ionic liquid, which has been rationalized through the inherent presence of carbenes.[460] Since this measurement is related to the pure liquid itself, and to its reactivity, it is not specific to certain substrates or other reaction conditions. However, the setup of an electrochemical experiment always includes a probe, an electrode, which is sunk into the solution. Accordingly, the system one measures is not the bulk, but the interfacial region at the electrode. This is in most cases a very good measure to understand the composition or structure of the liquid, but in this case the introduction of a surface into the liquid might influence the process greatly.

The interfacial behavior of 1,3-dialkylimidazolium acetate ILs is largely unknown at electrode or other surfaces, although these regions may behave very differently compared to the actual bulk. Since at an interface solvation by the polar ionic liquid is incomplete, while the dynamics may also be different from the bulk, it is reasonable to assume that the carbene formation is affected by the electrode surface. Similarly, it has been shown that nitric acid, which is a strong acid in the bulk, behaves as a weak acid at the surface of water.[476] In fact, the very often applied glassy carbon electrodes are composed of a graphite ribbon network, which contains a myriad of confinements or pockets of curvatures at its surface.[477–479] Ionic liquid ions and ion pairs on porous carbon surfaces are known to enter confinements, having a significant contribution to the capacitance of supercapacitors.[480,481] In these regions of the surface the solvation is even more incomplete than at an ideally planar surface, affecting thereby the carbene formation even more severely.

An extreme case in terms of surface effects at electrodes can be envisioned with metal electrodes. Since carbenes are generally highly reactive species, they may effectively coordinate to a metal surface.[138–140,240] Considering the findings above, and that the presence of a substrate may trigger the NHC-like reactions from the imidazolium cation,[5,6,142,144,423,437,462] it is possible that carbene complexes at metal surfaces are formed without the presence of free carbenes in the solution. In such a case the electrode induces the carbene-like reactivity.

Thus, as an example, a Pt(111) surface was chosen here to investigate the effect of electrodes on the carbene formation of 1,3-dialkylimidazolium acetate ILs. A single **I** or **II** was adsorbed on the surface, and then the possible isomers were generated considering different orientation for the molecules with respect to each other and to the surface. The obtained most stable structures are shown in Figure 3.72.

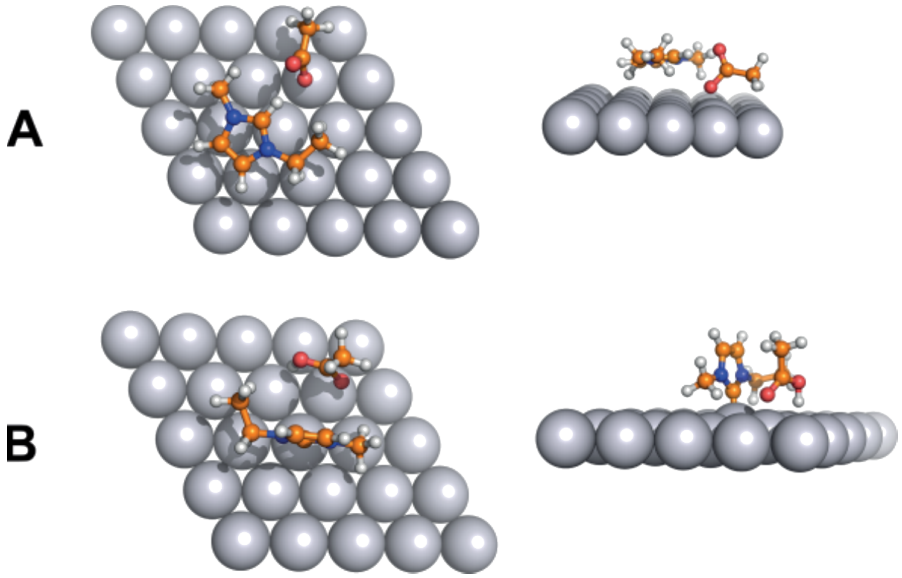

Figure 3.72.: The optimized structures at the Pt(111) surface. In structure **A** (top line, from two viewpoints) a single ion pair of [C_2C_1Im][OAc] is adsorbed on the platinum surface, while in structure **B** (bottom line, from two viewpoints) its hydrogen shift isomer is present at the interface as a relatively separated carbene and acetic acid pair.

The adsorption of an ion pair to the surface (structure **A**, Figure 3.72) is highly exothermic ($\Delta E_{\text{ads}} = -91.9\,\text{kcal}\,\text{mol}^{-1}$). However, the system is stabilized further by a surprisingly high $\Delta E = -9.1\,\text{kcal}\,\text{mol}^{-1}$ energy through a proton transfer, forming a carbene and an acetic acid at the surface (structure **B**, Figure 3.72). In contrast to **II**, in this very stable structure the two molecules are not bound through hydrogen bond to each other, and interacting with the surface independently; as the carbene forms a strong coordinative bond to one of the platinum atoms, while the acetate is pointing toward the surface with its carboxyl group. The strength of the carbene-platinum in-

terplay is clearly indicated by the out-of-plane position of the coordinated metal atom at the surface (Figure 3.72, bottom right). In agreement, the reorganisation energy of the surface (that is, the energy contribution of the structural changes in the orientation of the metal atoms) was found to be $\Delta E_{\text{reorg}} = 9.8\,\text{kcal}\,\text{mol}^{-1}$ for system **B**, as opposed to the $\Delta E_{\text{reorg}} = 1.9\,\text{kcal}\,\text{mol}^{-1}$ in case of the adsorbed ion pair **A**. The individual adsorption energy of the carbene and the acetic acid was also calculated separately, showing that the former molecule can be indeed very strongly bound to the surface by a $\Delta E_{\text{ads}} = -81.8\,\text{kcal}\,\text{mol}^{-1}$, while the latter species binds more weakly by a $\Delta E_{\text{ads}} = -22.7\,\text{kcal}\,\text{mol}^{-1}$.

It is interesting to compare the energetics of the dissociation of a single ion pair into an isolated acetic acid and a carbene molecule in the gas phase to that at the metal surface. While in the gas phase the dissociation is highly endothermic ($\Delta E = 22.8\,\text{kcal}\,\text{mol}^{-1}$, calculated by VASP with the PBE-D3BJ method), at the surface it is exothermic ($\Delta E = -9.1\,\text{kcal}\,\text{mol}^{-1}$ at the same level). Although the presence of the further ion pairs of the liquid phase will surely influence the energetics of this process, the trend is clearly shown here that the formation of a very strong C→Pt bond can induce the formation of carbenes from $[C_2C_1Im][OAc]$.

Considering these results it is reasonable to assume that in this particular kind of ionic liquid metal surfaces can be modified, and maybe even stabilized through carbene formation, which might have interesting applications in e.g. the synthesis of the corresponding metal nanoparticles. Regarding the electrochemical experiments that showed the presence of carbenes in $[C_2C_1Im][OAc]$,[460] however, these data above also have relevance. The results clearly show that in the presence of a surface, e.g. an electrode, the carbene formation might be induced artificially instead of observing the inherent carbene content of the liquid. In case of a metal electrode this effect is clearly very strong due to the aforementioned complex formation, but – as discussed above – the incomplete solvation should also have some (albeit significantly smaller) influence on the carbene formation. Having said that, and keeping the theoretical results and the discussion above in mind, the exciting electrochemical results by Chiarotto *et al.*[460] reveal that the interfacial region of these ionic liquids has a lot of important, yet hitherto unexplored features, which may be of special interest in future studies.

3.8.4. Conclusions

Motivated by the contradicting reports by theory and experiment in literature, we performed a theoretical study on the carbene-like activity of 1,3-dialkylimidazolium acetate ionic liquids. The quantum chemical calculations and the thermodynamic integration in an *ab initio* molecular dynamics environment show a high energy demand for the formation of free carbenes in solution from 1-ethyl-3-methylimidazolium acetate, in accordance with earlier theoretical results.[423] This indicates that the formation of free carbenes might only be possible at high temperatures, in good agreement with earlier voltammographic experiments.[460]

For the previously experimentally investigated model reaction of this ionic liquid with anisaldehyde two reaction mechanism were established. In the dissociative path the reaction is initiated by the formation of free carbenes through a proton transfer in solution, followed by the C–C bond forming reaction of this free carbene with the substrate, and the subsequent stabilizing protonation that stabilizes the product. In the associative mechanism, on the other hand, the proton transfer and the C–C bond formation occurs in the same elementary step, similarly to earlier suggestions regarding carbene organocatalysis[5,6,437] and the reactions of this ionic liquid with carbon dioxide.[142,423] We could show that kinetic isotope effects are not to be expected in either of the two possible mechanisms upon exchanging the mobile hydrogen to a deuterium, suggesting that the lack of these effects in earlier studies does not serve as proof in any direction.[461]

In the present case we found that the associative reaction mechanism is somewhat more favorable, but the energy difference is significantly lower than observed before for carbene organocatalysis with neutral bases.[6] For this reason it is possible that by applying different reaction conditions, substrates, or side chains at the imidazolium cation of the solvent/catalyst, the preference for the associative path vanishes, and the reaction occurs via the dissociative path. Accordingly, it is not possible to draw general conclusions regarding the mechanism of these carbene-like reactions, and the assessment of the mechanism has to be repeated for every single experimental setup.

In electrochemical studies one can study the neat liquid without the addition of any further components to the solution, which is a clear advantage of these experiments. However, the introduced electrodes create an extra surface, which may influence the carbene formation. As an extreme example, we considered a platinum surface, and we were able to show that the proton transfer is highly influenced by its presence, through offering a possible stabilization to the forming carbenes. At a glassy carbon surface such stabilization might not be possible, but the incompleteness of the solvation at the interface, and especially within interfacial cavities and other structural features should have a stark effect[476] on acid-base equilibria. In addition, based on the present findings regarding the reactions, it is interesting to consider such a redox process at the interface, in which – similarly to the associative reaction mechanism – the electron transfer from/to the electrode occurs simultaneously to the proton transfer to the anion.

Accordingly, the earlier reports in literature are, in fact, not contradicting, and it seems more likely that the theoretical and experimental studies are simply observing different aspects of the same system. While every single report is clearly valuable, and adds tremendously to the understanding of these systems in terms of their reactivity and structure, for the full characterization the joint interpretation of these results is necessary. In this respect, this complex system and problem is an excellent example how and why experiments and theory should collaborate intensively.

4. Conclusion and Outlook

Aims of the thesis were to investigate the interplay between NHCs and solvent molecules, especially with respect to their activity as potential organocatalysts. Due to the fact, that the active site of the carbene is also a very strong hydrogen bond acceptor,[82,120–128] it must be assumed that in the presence of hydrogen bond donor molecules the NHC is to a certain degree built into the solvent's hydrogen bond network. Subsequently, the catalytic active site is sterically blocked and the catalyst is inactive. In order that a reaction can occur the hydrogen bonding partner needs to be exchanged with the substrate molecule. Understanding this exchange process may be the key to an advanced control of the selectivity and activity of certain catalyst/solvent systems.

The investigation of dynamical properties — as the exchange of hydrogen bonding partners — necessitates simulations of sufficient length and size to assure a representative statistic of the process of interest. With the aim to enable such simulations, the first step discussed in Chapter 3.1 was to develop a model which represents the carbene ring unit. In order to make simulations of a broad number of different catalysts in various solvents available, the force field was designed in a way, that it can easily be combined with the already existing OPLS-AA,[255] force field for the substituents and solvent molecules, without the need of further reparametrization.

A particular problem that occurred during the development was that the carbene carbon atom's non-bonding potential is highly anisotropic,[123] due to the fact that both the electron lone pair of the carbene and the delocalized electron density of the aromatic ring can act as a hydrogen bond acceptor sites. In order to accommodate this special property, a certain amount of the partial charge was transferred from the carbene carbon atom to a massless ghost atom localized in the ring plane in front of the carbon atom. For the final fitting of the non-bonding parameters two hydrogen bonding reference potentials on the CCSD(T)/CBS level of theory were employed: One lying in the ring plane, the other one perpendicular to the plane. In this way it is determined, that the model in fact reproduces the structural motif of interest. The quality of this representation was proven by comparing the hydrogen bonding potential between a carbene and a methanol molecule calculated by the new force field and an OPLS-AA model of the methanol with the corresponding coupled cluster potential.

The ghost atom introduced to represent the anisotropy of the carbene was chosen to be nearly massless in order to preserve the molecule's moment of inertia. As a consequence of the definition of the acceleration $a = \frac{F}{m}$ the experienced acceleration a of the particle becomes exorbitantly high for a given force F due to it's very low mass. This could have resulted in unpredictable behavior of the new model in molecular dynamics simulations. In order to preclude this failure of the model a suited test project was necessary.

A project of this kind was found within the valorization of cellulose discussed in Chapter 3.2. It has been assumed, that the extraordinary good solvability of cellulose in imidazolium acetate ionic liquids[152,293] is due to the spontaneous formation of carbenes by a proton transfer from the imidazolium to the acetate. Unfortunately, the existence of the carbene species was discussed to be simultaneously responsible for the decomposition of the cellulose by catalyzing reactions of the sugar unit's aldehyde groups.[306]

Therefore, a broad study of simulations with smaller polysugars as well as with a cellulose bundle in the ionic liquid in presence and absence of carbenes was performed.

It was observed that the interaction between carbenes and carbohydrates is actually existing, but only in negligible quantity. Furthermore, the dissolution process of the cellulose bundle was not accelerated, but in contrast hindered by the presence of the carbenes. The obtained results were in line with other results achieved by static quantum chemistry calculation presented in the same work.

Apart from these findings — which were undoubtedly of great importance for the valorization community, although of lesser interest for the issue of this thesis — it could be shown that the new model also behaves well in larger simulation settings. Subsequently, the model was assumed to satisfy the first milestone of the thesis.

The aim of the second milestone was to establish a method for the quantification of the reorganization process of hydrogen bond networks. While the relatively simple methods based on a single autocorrelation function[213] are suffering from various biases, the reactive flux approach provides reliable, unbiased rate constants for the formation as well as for the cleavage of hydrogen bonds.[228,229,349] Moreover, it separates the hydrogen bond dynamics from the influence due to transport properties as diffusion.[228,229,349] Subsequently, an appropriate analysis tool was developed and implemented in the TRAVIS software package[18,316] as reported in Chapter 3.3.

As a first test the new tool was employed in a broad study including simulations of several ionic liquids and their mixtures. It could be shown, that the geometrical structure in this type of hydrogen bond was less linear than in water, indicating an angle of 60° to be well suited as a cutoff criterion. Further, it was found that an increase in temperature accelerated the dynamics. To complete the picture of the dynamical processes in ionic liquids the scope of the analysis was augmented by adapting the tool for the quantification of the dynamics of ionic networks. With the aid of this augmentation a correlation between the ionic network's dynamics and the viscosity of the liquids could be shown. Due to the fact, that the relatively high viscosity of ionic liquids is one factor which is strongly limiting their applicability, this finding may be of great help in the evaluation of the suitability of novel ionic liquid mixtures for certain applications.

During the study in Chapter 3.3 questions regarding the robustness of the method were raised. Especially, because the definition of a state as *"hydrogen bonded"* was done with the help of a geometrical criterion: the hydrogen–acceptor distance and the angle of the donor–hydrogen–acceptor assembly. It is generally possible to define the cutoffs for this criterion in different ways. Subsequently, it was unavoidable to gain knowledge about the influence of these parameters on the obtained results, in order to evaluate the stability of the method. Furthermore, the analysis is probably affected by different simulation settings — as the time between two snapshots or the total length of the trajectory.

With the aim to benchmark these impacts a systematic study was performed and presented in Chapter 3.4. The main finding of this work was, that the trajectory length should be at least by a factor of ten longer than the calculated hydrogen bond lifetime. The sensitivity for changes of the distance criterion was found to be relatively low and even lower for a deviation of the angle criterion.

During this benchmark the superiority of the reactive flux approach over the calculation of the lifetimes based on a single autocorrelation function could impressively be demonstrated: If the correlation between the fluidity of the system in question and the

corresponding hydrogen bond dynamics were considered, it was revealed that the lifetimes obtained by a single autocorrelation function showed a general linear relation independent on the type of system. This was due to a systematical, but purely mathematical and thereby artificial influence of transport properties as diffusion on the autocorrelation function. On the other hand, however, a linear relationship was still visible for each system when applying the reactive flow approach. However, the slope of this linear trend clearly differed dependent of the type of system. This means, that the reactive flux approach revealed the impact of the hydrogen bond dynamics on the fluidity of the liquid, which in fact is a real physical effect.

Finally, the implemented reactive flux method for the analysis of the dynamics of nonbonding interactions appeared to be well suited to satisfy the second milestone of the thesis.

The third milestone demanded an explicit study of the hydrogen bond dynamics of several carbene catalysts in different solvent systems as illustrated in Chapter 3.5. Approaching this task the achievements of the first two parts had to be combined. Subsequently, a large set of different NHCs was simulated applying the model obtained in the first milestone described in Chapter 3.1 in varying mixtures of THF and alcohols. Afterwards, the trajectories were analyzed concerning the statical and dynamical characteristics of the hydrogen bonds between carbenes and solvent molecules.

It was found, that the basicity of the carbene ring unit strongly correlated with the strength as well as the lifetimes of the corresponding hydrogen bonds. Thereby, the ring units mostly applied in organocatalysis — thiazole-2-ylidene and triazol-3-ylidene — were extraordinarily often found as free from hydrogen bonds and subsequently, were most available for catalytic reactions. In contrast, the most basic carbenes were often found in an unusual double hydrogen bond assembly, in which the lone pair of the carbene interacted simultaneously with the hydroxyl groups of two alcohol molecules. Meanwhile, the lifetimes gradually increased with the protonaffinities.

Due to the different ratios of free, single bonded, and double bonded carbenes, it could be concluded that the exchange mechanism may change depending on the basicity as well. For the weakly basic carbenes, the exchange followed a dissociative pathway with the occurrence of a free carbene form: The current hydrogen bonding partner was first released, forming a free carbene species. Afterwards, a new bonding partner was bound in a second, separated step. In contrast, for the strong basic carbenes the exchange followed an associative pathway: First, a second bonding partner was linked to the already hydrogen bonded carbene, forming the previous described three–body–assembly. In a second step, the bond to the initial bonding partner was broken. As a consequence, the exchange avoided the formation of a free carbene species in the case of the strongly basic NHCs. Due to a lower barrier for the associative pathway in comparison to the dissociative pathway, the exchange in the associative case was generally faster.

Furthermore, a strong impact of the substitution pattern on both, the carbene's ring and the alcohol, was revealed. If the steric demand of the side groups increased, free carbene species were found more often. At the same time, the number of three–body–assemblies dropped. Following from this, the preference for the exchange mechanism changed from the associative pathway for very small substituents towards the dissociative

pathway for bulkier side groups. As a result, the hydrogen bond lifetimes were elongated with increasing size of the substituents, due to the diminution of the faster associative pathway. If a certain steric demand was excelled this trend was inverted and the lifetimes were getting shorter with a further increase of the side group's size.

With regard to the objectives of this thesis, it should be noted that although both the ring type and the steric demand of the substituents of the carbene had an influence on the occurrence of a free carbene species, the reasons for this were essentially different. The choice of a ring type which preferred the free carbene form together with relatively low demanding side groups, can be expected to result in a catalyst which would be highly available for a potential reaction partner. In this case, the kinetics of the reaction would be mostly driven by the rate of the reaction itself or by the general transport rate of the substrate through the solvent, while on the other hand the influence of the hydrogen bond dynamics would be of lesser importance. However, if the freeness of the carbene was induced by steric hindrance of the active site, it has to be assumed, that not only the formation of hydrogen bonds would be hindered, but as well the reaction with a potential substrate. In other words, the carbene's active site would be permanently blocked, but not by a hydrogen bond but by the "catalyst" itself. Consequently, the carbene could barely assumed to be catalytic active at all.

Likewise, an impact of the ratio of alcohol to THF was found. Higher concentrations of alcohols in the solvent composition intensified the preference for the doubly bonded assembly, thus for the associative pathway. Subsequently, the hydrogen bond dynamics were getting faster.

In contrast to the relatively clear situation of model reactions, the circumstances in longer synthesis routes are more complex. In most cases, there is not only one conceivable reaction, but competitive reactions yielding undesirable side products. Since the hydrogen bond donor concentration of the solvent is an easy way to control not only the hydrogen bond situation of the catalyst, but as well the preference for a certain exchange mechanism, this might be a keystone in the control of selectivity if the competitive reaction partners show different capabilities to intervene into the hydrogen bond between catalyst and solvent in dependence of the exchange mechanism. Obviously, this is of a special interest if the reaction mechanism for the activation step is different. Therefore, the results targeted in the fourth milestone become crucial.

In order to achieve this last milestone, in Chapter 3.6 possible mechanisms for the activation step towards the Breslow intermediate were evaluated by static quantum chemical calculations for the reactions of the three carbene types mostly applied in catalysis — namely imidazole-2-ylidene,[98] triazole-3-ylidene,[56] and thiazole-2-ylidene[100] — with varying aldehydes. Thereby, it has been shown that the reaction is not only possible through the dissociative pathway originally proposed by Breslow,[52] but as well through a direct associative pathway. While in the dissociative case, a precursor cation is deprotonated by a base yielding a free carbene species, which reacts in a second step with the substrate in question, the deprotonation of the precursor occured simultaneously with the reaction of the forming carbene and the aldehyde in the associative case. According to the obtained results the reaction barrier of the novel mechanism is significantly lower compared to the one of Breslow's mechanism.

Albeit these findings are very interesting and may have the potential to completely change the view on NHC organocatalysis, the methods employed in Chapter 3.6 are relatively simple which may render their meaning to be questionable. The emerging question if the found mechanism is generally favored or if the preference for a certain pathway can be controlled by the experimental settings provoked deeper investigation of the matter in Chapter 3.7.

In this study the interaction of the hydrogen bond between the proton which is transferred to the base and the aldehyde's oxygen atom could be identified as the stabilizing part of the associative transition state. Subsequently, polar or protic solvent system which are characterized by a strong hydrogen bond network were found to destabilize this motif. As a consequence the associative pathway is energetically less favored which may change the general preference for the reaction mechanism. Moreover, it was shown that if the anion which has to be added to the batch together with the precursor cation is chosen to be able to form strong hydrogen bonds the associative barrier increases. This is not the case if an anion with weak hydrogen bond acceptor characteristics is chosen.

Of course, other variations of the system setup may play an essential role. One of these parameters to change is the applied base. While the bases applied in the studies of Chapters 3.6 and 3.7 were all amine bases, it is also possible to realize the same reaction with an anionic base. For instance, this is the case if the catalytic activity of imidazolium acetate ionic liquids is taken into account.

In the light of the complexity of the problem it is no wonder, that some recent reports concerning this substance are highly contradicting.[460,461] Therefore, in Chapter 3.8 a study is presented which aimed to explain previously published results of the kinetic isotope effect for the reaction of anisaldehyde in 1-ethyl-3-methylimidazolium acetate. Therein, it has been shown that if the acidic hydrogen atom is exchanged by a deuteron, the reaction kinetics do not change at all.[461] As a consequence, it was stated that the proton is not involved in the critical transition state, which points without a doubt towards the dissociative mechanism. However, we could demonstrate that in the associative mechanism the transition state is located relatively late, after the deprotonation formally already happened, even though the overall reaction is not resting in a stable deprotonated intermediate. As a result, the proton in question does not move in the transition state anymore and subsequently the kinetic isotope effect studies do not allow any conclusions on the mechanism to be drawn.

The re-interpretation of the experimental data in the last chapter reveals the difficulties to design a reliable experiment which is able to proof the mechanistics of the reaction. Nevertheless, here lies one of the most pressing tasks for future projects in my eyes. Although the obtained insights are without doubt helpful to understand the mechanistic details of NHC organocatalysis, it is desirable to validate the computations by proofing the principles in cooperation with an experimentalist. Unfortunately, the discussed experiments (trends in the H/D-exchange experiments in Chapter 3.5, general trends in terms of reactivity in Chapter 3.6, kinetic isotope effects in Chapter 3.8) can all be interpreted controversially. However, to allow a reliable validation a clear interpretation of the experimental findings is crucial.

A first step in finding such an experimental setup could be to approach the differentiation of the two proposed mechanisms. Generally, this can be realized by the application of a chiral base in an otherwise achiral environment. If the reaction occurs in a entioselective manner, this indicates a role of the base in the critical transition state and would therefore point towards the associative mechanism. Moreover, it has been shown for proline–organocatalysis, that the enantiomeric product ratio can precisely be predicted by simple DFT calculations of the corresponding transition states.[482] It will be interesting to see, if a comparable accuracy can be achieved for NHCs.

Apart from the experimental side, neither the theoretical processing of the matter is exhaustive. In Chapter 3.5 a method was presented to analyze the influence of different solvent systems on the exchange of hydrogen bonding partners, which can be exploited to estimate the availability of the catalyst to a substrate. Furthermore, in Chapters 3.3 and 3.4 the temperature dependence of the exchange rate was shown. However, the investigation of temperature driven effects on the reaction itself is still inadequate. As seen in Chapter 3.8 the accurate treatment of the entropy turned out to be a non-trivial task. One way to tackle this problem would be to calculate the free energy profile of the intrinsic reaction coordinate by molecular dynamics meta-simulations with an explicit solvent model, *e.g* by *ab initio* MD.

Further, in Chapter 3.8 a strong interplay of the carbene and a platinum surface was revealed. This interaction of carbenes and metals was also observed for nanoparticles.[241,242] Subsequently, it would be interesting to provide deeper insights into the impact of such surroundings on the details of the reaction. The strong interplay of carbene and metal might stabilize the dissociative transition state, or in contrary deactivate a formed carbene directly and thereby blocking the dissociative pathway completely. Potentially, this may be another way to control the selectivity of the reaction. Hypothetically, it would even be possible that a metal bound carbene is able to react through a reaction mechanism similar to the associative pathway described in Chapters 3.6 and 3.7 with the precursor's moving hydrogen atom exchanged by the metal entity. This would not only uncover a completely novel kind of carbene organocatalysis but also enables a route to valuable tandem reactions with both — the metal and the carbene — as catalysts.

Finally, it needs to be mentioned that there were reports[141,142] of reactions of NHCs with carbondioxide. In fact, the reaction of carbenes with CO_2 is very similar to the proposed associative mechanism of carbenes with aldehydes.[142,423] Nevertheless, the details and prospects of this special case of NHC reaction are still not fully investigated. Due to the emerging climate catastrophe due to the high CO_2 output of combustion power plants and engines, methods to capture and maybe even chemically activate carbondioxide are necessary. In this light, the potential of carbenes to be exploited in this sense should be examined in the near future.

As a final conclusion it can be stated, that the successful completion of the initially formulated milestone tasks of this thesis provide useful insights into the nature of carbene based catalyst-solvent-systems. These understandings will undoubtedly be helpful in the future development of appropriate solutions.

A. Appendix

A.1. Derivation of Equation 2.6

In statistical mechanics time correlation functions (TCFs) describe the correlation of a certain value $f(t)$ at time t with a value $g(t')$ at time t'. For the ensemble average of an equilibrium molecular dynamics simulation a TCF is invariant in time. In other words, the origin of the function can be arbitrarily shifted. Therefore,

$$\left\langle f(t)g(t')\right\rangle = \left\langle f(t+s)g(t'+s)\right\rangle \,, \tag{A.1}$$

where the chevrons denote the ensemble average. With a sophisticated choice of s as $s = -t'$ or $s = -t$ Equation A.1 can be written as

$$\left\langle f(t)g(t')\right\rangle = \left\langle f(t-t')g(0)\right\rangle = \left\langle f(0)g(t'-t)\right\rangle \,, \tag{A.2}$$

or simplified by defining $\tau = t' - t$ we can write

$$\left\langle f(t)g(t')\right\rangle = \langle f(-\tau)g(0)\rangle = \langle f(0)g(\tau)\rangle \,. \tag{A.3}$$

The derivative with respect to time of Equation A.3 reads

$$\frac{\mathrm{d}}{\mathrm{d}\tau}\langle f(-\tau)g(0)\rangle = \frac{\mathrm{d}}{\mathrm{d}\tau}\langle f(0)g(\tau)\rangle \,. \tag{A.4}$$

From the fact that both $f(0)$ as well as $g(0)$ are independent of t follows

$$-\left\langle \dot{f}(-\tau)g(0)\right\rangle = \left\langle f(0)\dot{g}(\tau)\right\rangle \,, \tag{A.5}$$

where the dot denotes the time derivative. According to Equations A.1 to A.3 we shift the origin of left side by τ we get

$$-\left\langle \dot{f}(0)g(\tau)\right\rangle = \left\langle f(0)\dot{g}(\tau)\right\rangle \,, \tag{A.6}$$

which is exactly Equation 2.6.

A.2. Derivation of Equation 2.8

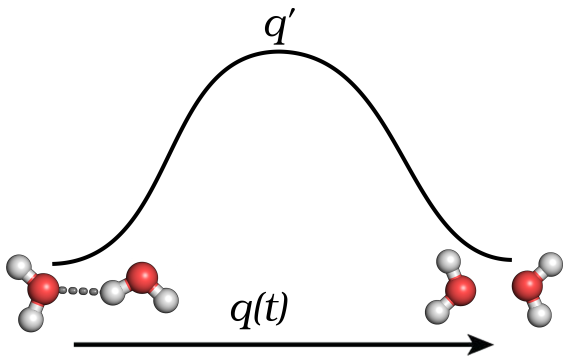

Figure A.1.: Schematic reaction coordinate of a hydrogen bond cleavage. The hydrogen bonded pair moves along the reaction coordinate $q(t)$ and has to overcome a barrier with a transition state at coordinate q'.

The cleavage of a hydrogen bond can be interpreted analogous to a chemical reaction. Thereby, the hydrogen bonded system is moving along a reaction coordinate $q(t)$ and if it overcomes a barrier with a transition state q' the hydrogen bond breaks. This process is shown schematically in Figure A.1.

In this interpretation the operator $h(t)$ is transformed into a functional $h[q(t)]$ of the reaction coordinate $q(t)$, which is equal unity if $q(t)$ is smaller than the transition state q' and zero otherwise. Therefore, the derivative of the operator with respect to time becomes

$$\frac{\mathrm{d}}{\mathrm{d}t}h[q(t)] = \dot{q}(t)\frac{\mathrm{d}}{\mathrm{d}q}h[q(t)] = -\dot{q}(t)\delta\left(q(t) - q'\right) , \tag{A.7}$$

with the Kronecker delta $\delta\left(q(t) - q'\right)$, and the dot denoting the time derivative. Analogously, one can write

$$\left\langle \dot{h}(0) \right\rangle = -\left\langle \dot{q}(0)\delta\left(q(0) - q'\right) \right\rangle \tag{A.8}$$

for the special case $t = 0$. Furthermore, the chevrons denote the ensemble average.

Obviously, the reaction coordinate $q(t)$ is a representation of a configuration, while $\dot{q}(t)$ is the associated velocity. Exploiting that configuration and velocity are uncorrelated, the term on the right side of Equation A.8 can be split into

$$\left\langle \dot{h}(0) \right\rangle = -\left\langle \dot{q}(0) \right\rangle \left\langle \delta\left(q - q'\right) \right\rangle . \tag{A.9}$$

In a system at equilibrium the distribution of velocities is even. As a consequence, the velocities ensemble average vanishes. Therefore,

$$\left\langle \dot{h}(0) \right\rangle = 0 , \tag{A.10}$$

which is Equation 2.8.

A.3. Technical Details of the Reactive Flux Analysis

The analysis of the reactive flux dynamics is done in three steps: step-by-step processing of the trajectory, correlating of the collected state functions and finally fitting of the data to the Luzar–Chandler model.

During the processing all pairs of anion and cation which are fulfilling the previously defined criteria for neighborhood on the one hand, and pairing or bonding on the other hand are identified. The neighboring criterion is defined by a cut-off distance between two certain atoms which is obtained from the first minimum in the corresponding RDFs. The criterion for hydrogen bonds consists of a distance between hydrogen atom and acceptor atom, obtained from the corresponding RDFs, and the angle between donor–hydrogen–acceptor, which is chosen based on the corresponding CDFs. For the ion pairs a cation and an anion is defined as a pair if they are nearest neighbors. If one or both of these states has changed compared to the previous step the current step number is saved for each involved pair.

After the processing is finished, the two functions — one for the pairing or bonding, one for the neighboring — are restored as arrays of zeroes and ones and Fourier transformed for every certain pair of cation and anion. In the Fourier space two new functions are obtained by multiplying the ion pair function with itself and with the neighboring function, respectively. The obtained result functions are transformed back into normal space. The Fourier transformation scheme is applied to speed up the calculation of the autocorrelation function of the pairing and the cross–correlation function of the pairing and the neighboring, following the Wiener–Khinchin theorem [483,484] and the cross–correlation theorem. After normalization the first result function is equal to the function $c(t)$ (see Section 2.1). From this function $c(t)$ the normalized second result function is subtracted to obtain the function $n(t)$. At least the derivative of $c(t)$ is calculated numerically.

Finally, a simplified steepest descent algorithm is applied to find two parameters k_d and k_f in a way that the root mean square displacement to Equation 2.13 is minimized. The lifetimes are obtained from the inverse k_d parameter.

A.4. Computational Details of Chapter 3.3

The systems were modeled by the OPLS force field[255], which was extended by the parameter set for the imidazolium ring unit developed by Canongia Lopez and Padua.[267] The parameters for the halides were taken from the same work.[267] The applied parameters for the triflate anions were taken from a previous publication of the same group.[266] This family of force fields has shown a good representations of the mass transport properties if the charges were scaled by a factor of 0.8. Thus, we scaled the charges of all cations and anions.

Another way to simulate ionic liquids with classical MD is the application of a polarizable force field like the drude model. The charges were split into two different point charges, one on the atomic core, the other one connected by a strong harmonic potential.[359] The distribution of the charges between the two point charges were chosen to represent the atomic polarizabilities.[360,485] Finally, the water molecules in the water containing mixtures were described by the SPC/E water model.[258]

To obtain unlike Lennard-Jones parameters, especially for the interactions between the different force fields, Lorentz–Berthelot mixing rules[486,487] ($\epsilon_{ij} = \sqrt{\epsilon_i \epsilon_j}$ and $\sigma_{ij} = \frac{1}{2}(\sigma_i + \sigma_j)$) were applied. Non-bonded interactions were computed only if the distance between the involved atoms was within a cutoff radius of 10 Å. Coulombic interactions beyond this distance were computed via the particle-particle particle-mesh solver[402] with an accuracy of 10^{-5}.

All the simulations were carried out by the LAMMPS software package[263] according to the following protocol:

1. The initial configuration of each cell with a composition like summarized in Table A.1 was generated applying PACKMOL[312], with a density chosen as equivalent to the respective experimental value. Possible hotspots in these configuration were removed by minimizing the energy of the geometry.

2. The system was simulated in an NVT-ensemble for 0.5 ns. The timestep for the integration of the Newton equations was chosen to be 1.0 fs. The temperature was controlled by a Nosé–Hoover chain thermostat ($\tau = 100$ fs).

3. The system was then simulated for 1.0 ns in an NpT-ensemble, to relax the cells to the optimal density of the applied force fields. Constant pressure and temperature were provided by applying a Nosé–Hoover-chain thermostat ($\tau = 100$ fs) and a Nosé–Hoover barostat ($p = 1$ bar, $\tau = 1000$ fs), respectively.[403–405] Over the last 0.5 ns the box volume was averaged.

4. The system was mildly forced to the obtained average volume over 0.1 ns. Finally, the ensemble was switched back to NVT, assuring a constant temperature again by Nosé–Hoover-chain thermostat ($\tau = 100$ fs). The final density during the simulations are summarized in Table A.2.

5. After an equilibration period for 5.0 ns, the production runs were performed for 10.0 ns, saving the coordinates of the systems in every 1 ps. For the last 200 ps the

snapshots were saved in every 1 fs, to get a sufficient resolution in the analysis of the non-covalent dynamics.

Table A.1.: Compositions of the investigated systems.

pure $[C_4C_1Im][Br]$			
Model	$[C_4C_1Im]$	[Br]	
ff	500	500	
pol-ff	500	500	
Temperature dependent $[C_4C_1Im][OTf]$			
T in K	$[C_4C_1Im]$	[OTf]	
293	300	300	
323	300	300	
353	300	300	
373	300	300	
393	300	300	
$[C_4C_1Im][OTf]$/water mixtures			
x of H_2O	$[C_4C_1Im]$	[OTf]	H_2O
0.39	197	197	303
0.58	288	288	212
0.66	330	330	170
0.82	410	410	90
$[C_4C_1Im][OTf]$/[Cl] mixtures			
x of [Cl]	$[C_4C_1Im]$	[OTf]	[Cl]
0.000	300	300	–
0.192	500	404	96
0.303	501	349	152
0.402	500	299	201

Table A.2.: Densities of the simulated systems in g cm^{-3}.

$[C_4C_1Im][Br]$	ff	1.140943
	pol-ff	0.980296
$[C_4C_1Im][OTf]$	293 K	1.289345
	323 K	1.254602
	353 K	1.229592
	373 K	1.208724
	393 K	1.194788
$[C_4C_1Im][Br]/H_2O$	0.39	1.260310
	0.58	1.270363
	0.66	1.278284
	0.82	1.282257
$[C_4C_1Im][Br]/[Cl]$	0.000	1.278982
	0.192	1.216546
	0.303	1.211863
	0.402	1.193510

A.5. Computational Details of Chapter 3.6

All quantum chemical calculations were performed by the ORCA program.[256] Full geometry optimizations were performed at the TPSSh-D3BJ/def2-TZVP level of theory,[278–280,283] followed by a frequency calculation to verify the nature of the obtained critical point. The electronic energy of the system was calculated at the DLPNO-CCSD(T)/CBS level, using a localization approach[259,260] and a CBS extrapolation scheme reported earlier.[262] To the CCSD(T) energies the thermal corrections obtained at the DFT method were applied, providing the Gibbs free energy values presented here. Finally, the vibrational frequencies were recalculated applying the conductor-like polarizable continuum model (CPCM)[488,489] for THF, toluene, and DMSO without further re-optimization.

Bibliography

[1] S. Gehrke and O. Hollóczki, *Phys. Chem. Chem. Phys.*, 2016, **18**, 22070–22080.

[2] S. Gehrke, K. Schmitz and O. Hollóczki, *J. Phys. Chem. B*, 2017, **121**, 4521–4529.

[3] S. Gehrke, M. von Domaros, R. Clark, O. Hollóczki, M. Brehm, T. Welton, A. Luzar and B. Kirchner, *Faraday discuss.*, 2018, **206**, 219–245.

[4] S. Gehrke and B. Kirchner, *J. Chem. Eng. Data*, 2020, **65**, 1146–1158.

[5] S. Gehrke and O. Hollóczki, *Chem.Eur. J.*, 2018, **24**, 11594–11604.

[6] S. Gehrke and O. Hollóczki, *Angew. Chem. Int. Ed.*, 2017, **56**, 16395–16398.

[7] S. Gehrke and O. Hollóczki, *Chem. Eur. J.*, 2020, **26**, 10140–10151.

[8] S. Gehrke, W. Reckien, I. Palazzo, T. Welton and O. Hollóczki, *Eur. J. Org. Chem.*, 2019, **2019**, 504–511.

[9] S. Gehrke, H. T. Alznauer, H. A. Karimi-Varzaneh and J. A. Becker, *J. Chem. Phys.*, 2017, **147**, 214703.

[10] C. J. Smith, S. Gehrke, O. Hollóczki, D. V. Wagle, M. P. Heitz and G. A. Baker, *J. Chem. Phys.*, 2018, **148**, 193845.

[11] J. Ingenmey, S. Gehrke and B. Kirchner, *ChemSusChem*, 2018, **11**, 1900–1910.

[12] D. Riemer, W. Schilling, A. Goetz, Y. Zhang, S. Gehrke, I. Tkach, O. Hollóczki and S. Das, *ACS Cat.*, 2018, **8**, 11679–11687.

[13] S. Gehrke, R. Macchieraldo and B. Kirchner, *Phys. Chem. Chem. Phys.*, 2019, **21**, 4988–4997.

[14] R. Macchieraldo, S. Gehrke, N. K. Batchu, B. Kirchner and K. Binnemans, *J. Phys. Chem. B*, 2019, **123**, 4400–4407.

[15] T. Stettner, S. Gehrke, P. Ray, B. Kirchner and A. Balducci, *ChemSusChem*, 2019, **12**, 3827–3836.

[16] O. Hollóczki and S. Gehrke, *Sci. Rep.*, 2019, **9**, 1–7.

[17] O. Hollóczki and S. Gehrke, *ChemPhysChem*, 2020, **21**, 9–12.

[18] M. Brehm, M. Thomas, S. Gehrke and B. Kirchner, *J. Chem. Phys.*, 2020, **152**, 164105.

[19] C. J. Smith, D. V. Wagle, N. Bhawawet, S. Gehrke, O. Hollóczki, S. V. Pingali, H. O'Neill and G. A. Baker, *The Journal of Physical Chemistry B*, 2020, **124**, 7647–7658.

[20] R. Elfgen, S. Gehrke and O. Hollóczki, *ChemSusChem*, 2020, **13**, 5449.

[21] D. Bourissou, O. Guerret, F. P. Gabbai and G. Bertrand, *Chem. Rev.*, 2000, **100**, 39–92.

[22] L. Nyulászi, T. Veszprémi and A. Forró, *Phys. Chem. Chem. Phys.*, 2000, **2**, 3127–3129.

[23] W. A. Herrmann, *Angew. Chem. Int. Ed.*, 2002, **41**, 1290–1309.

[24] V. César, S. Bellemin-Laponnaz and L. H. Gade, *Chem. Soc. Rev.*, 2004, **33**, 619–636.

[25] V. Nair, S. Bindu and V. Sreekumar, *Angew. Chem. Int. Ed.*, 2004, **43**, 5130–5135.

[26] R. H. Crabtree, *J. Organomet. Chem.*, 2005, **690**, 5451–5457.

[27] J. C. Garrison and W. J. Youngs, *Chem. Rev.*, 2005, **105**, 3978–4008.

[28] S. P. Nolan, *N-Heterocyclic carbenes in synthesis*, John Wiley & Sons, 2006.

[29] C. Samojłowicz, M. Bieniek and K. Grela, *Chem. Rev.*, 2009, **109**, 3708–3742.

[30] R. H. Crabtree, *Coord. Chem. Rev.*, 2013, **257**, 755–766.

[31] D. J. Nelson and S. P. Nolan, *Chem. Soc. Rev.*, 2013, **42**, 6723–6753.

[32] S. Bellemin-Laponnaz and S. Dagorne, *Chem. Rev.*, 2014, **114**, 8747–8774.

[33] C. Fliedel and P. Braunstein, *J. Organomet. Chem.*, 2014, **751**, 286–300.

[34] F. Izquierdo, S. Manzini and S. P. Nolan, *Chem. Commun.*, 2014, **50**, 14926–14937.

[35] G. Frenking, M. Solà and S. F. Vyboishchikov, *J. Organomet. Chem.*, 2005, **690**, 6178–6204.

[36] P. L. Arnold and S. Pearson, *Coordin. Chem. Rev.*, 2007, **251**, 596–609.

[37] O. Schuster, L. Yang, H. G. Raubenheimer and M. Albrecht, *Chem. Rev.*, 2009, **109**, 3445–3478.

[38] S. Díez-González, *N-Heterocyclic carbenes: from laboratory curiosities to efficient synthetic tools*, Royal Society of Chemistry, 2011.

[39] H. Stetter, R. Y. Raemsch and H. Kuhlmann, *Synthesis*, 1976, **1976**, 733–735.

[40] N. Marion, S. Díez-González and S. P. Nolan, *Angew. Chem. Int. Ed.*, 2007, **46**, 2988–3000.

[41] D. Enders, O. Niemeier and A. Henseler, *Chem. Rev.*, 2007, **107**, 5606–5655.

[42] D. Enders and T. Balensiefer, *Acc. Chem. Res.*, 2004, **37**, 534–541.

[43] C. S. Cazin, *N-Heterocyclic carbenes in transition metal catalysis and organocatalysis*, Springer Science & Business Media, 2010, vol. 32.

[44] C. Eijkman, *Archiv für pathologische Anatomie und Physiologie und für klinische Medicin*, 1897, **148**, 523–532.

[45] U. Suzuki and T. Shimamura, *Tokyo Kagaku Kaishi*, 1911, **32**, 4–7.

[46] K. Lohmann and P. Schuster, *Biochem. Ztschr.*, 1937, **294**, 188–214.

[47] D. Green, W. Westerfeld, B. Vennesland, W. Knox *et al.*, *J. Biol. Chem.*, 1942, **145**, 69–84.

[48] T. Ukai, R. Tanaka and T. Dokawa, *J. Pharm. Soc. Jpn*, 1943, **63**, 296–300.

[49] S. Mizuhara and P. Handler, *J. Am. Chem. Soc.*, 1954, **76**, 571–573.

[50] S. Mizuhara and R. Tamura, *Proc. Jap. Acad.*, 1951, **27**, 709–714.

[51] R. Breslow, *J. Am. Chem. Soc.*, 1957, **79**, 1762–1763.

[52] R. Breslow, *J. Am. Chem. Soc.*, 1958, **80**, 3719–3726.

[53] R. Breslow, *Annals of the New York Academy of Sciences*, 1962, **98**, 445–452.

[54] A. Lapworth, *J. Chem. Soc. Trans.*, 1904, **85**, 1206–1214.

[55] J. C. Sheehan and D. Hunneman, *J. Am. Chem. Soc.*, 1966, **88**, 3666–3667.

[56] D. Enders, K. Breuer, G. Raabe, J. Runsink, J. H. Teles, J.-P. Melder, K. Ebel and S. Brode, *Angew. Chem. Int. Ed.*, 1995, **34**, 1021–1023.

[57] R. L. Knight and F. J. Leeper, *J. Chem. Soc., Perkin Trans. 1*, 1998, 1891–1894.

[58] J. Teles, J.-P. Melder, K. Ebel, R. Schneider, E. Gehrer, W. Harder, S. Brode, D. Enders, K. Breuer and G. Raabe, *Helv. Chim. Acta*, 1996, **79**, 61–83.

[59] M. S. Kerr, J. Read de Alaniz and T. Rovis, *J. Am. Chem. Soc.*, 2002, **124**, 10298–10299.

[60] A. J. Arduengo, *Acc. Chem. Res.*, 1999, **32**, 913–921.

[61] K. Zeitler, *Angew. Chem. Int. Ed.*, 2005, **44**, 7506–7510.

[62] D. M. Flanigan, F. Romanov-Michailidis, N. A. White and T. Rovis, *Chem. Rev.*, 2015, **115**, 9307–9387.

[63] J. Moore and T. Rovis, *Aldrichimica Acta*, 2009, **42**, 55–66.

[64] T. Dudding and K. N. Houk, *Proc. Natl. Acad. Sci.*, 2004, **101**, 5770–5775.

[65] O. Hollóczki, Z. Kelemen and L. Nyulászi, *J. Org. Chem.*, 2012, **77**, 6014–6022.

[66] A. Berkessel, S. Elfert, K. Etzenbach-Effers and J. H. Teles, *Angew. Chem. Int. Ed.*, 2010, **49**, 7120–7124.

[67] A. Berkessel, V. R. Yatham, S. Elfert and J.-M. Neudörfl, *Angew. Chem. Int. Ed.*, 2013, **52**, 11158–11162.

[68] Y.-J. Kim and A. Streitwieser, *J. Am. Chem. Soc.*, 2002, **124**, 5757–5761.

[69] A. M. Magill, K. J. Cavell and B. F. Yates, *J. Am. Chem. Soc.*, 2004, **126**, 8717–8724.

[70] R. S. Massey, C. J. Collett, A. G. Lindsay, A. D. Smith and A. C. O'Donoghue, *J. Am. Chem. Soc.*, 2012, **134**, 20421–20432.

[71] A. Berkessel, S. Elfert, V. R. Yatham, J.-M. Neudörfl, N. E. Schlörer and J. H. Teles, *Angew. Chem. Int. Ed.*, 2012, **51**, 12370–12374.

[72] M. Paul, P. Sudkaow, A. Wessels, N. E. Schlörer, J.-M. Neudörfl and A. Berkessel, *Angew. Chem. Int. Ed.*, 2018, **57**, 8310–8315.

[73] B. Maji and H. Mayr, *Angew. Chem. Int. Ed.*, 2012, **51**, 10408–10412.

[74] D. A. DiRocco, K. M. Oberg and T. Rovis, *J. Am. Chem. Soc.*, 2012, **134**, 6143–6145.

[75] Y. Reddi and R. B. Sunoj, *Org. Lett.*, 2012, **14**, 2810–2813.

[76] Z. Li, D. Wei, Y. Wang, Y. Zhu and M. Tang, *J. Org. Chem.*, 2014, **79**, 3069–3078.

[77] R. C. Johnston, D. T. Cohen, C. C. Eichman, K. A. Scheidt and P. H.-Y. Cheong, *Chem. Sci.*, 2014, **5**, 1974–1982.

[78] S. M. Langdon, C. Y. Legault and M. Gravel, *J. Org. Chem.*, 2015, **80**, 3597–3610.

[79] D. Meyer, P. Neumann, R. Ficner and K. Tittmann, *Nat. Chem. Biol.*, 2013, **9**, 488.

[80] H. Zeng, K. Wang, Y. Tian, Y. Niu, L. Greene, Z. Hu and J. K. Lee, *Int. J. Mass Spec.*, 2014, **369**, 92–97.

[81] Z. Kelemen, O. Hollóczki, J. Nagy and L. Nyulászi, *Org. Biomol. Chem.*, 2011, **9**, 5362–5364.

[82] O. Hollóczki, D. Gerhard, K. Massone, L. Szarvas, B. Németh, T. Veszprémi and L. Nyulászi, *New J. Chem.*, 2010, **34**, 3004–3009.

[83] M. W. Washabaugh and W. P. Jencks, *Biochemistry*, 1988, **27**, 5044–5053.

[84] M. W. Washabaugh and W. P. Jencks, *J. Am. Chem. Soc.*, 1989, **111**, 674–683.

[85] M. W. Washabaugh and W. P. Jencks, *J. Am. Chem. Soc.*, 1989, **111**, 683–692.

[86] R. W. Alder, P. R. Allen and S. J. Williams, *J. Chem. Soc., Chem. Commun.*, 1995, 1267–1268.

[87] T. L. Amyes, S. T. Diver, J. P. Richard, F. M. Rivas and K. Toth, *J. Am. Chem. Soc.*, 2004, **126**, 4366–4374.

[88] Y. Chu, H. Deng and J.-P. Cheng, *J. Org. Chem.*, 2007, **72**, 7790–7793.

[89] E. M. Higgins, J. A. Sherwood, A. G. Lindsay, J. Armstrong, R. S. Massey, R. W. Alder and A. C. O'Donoghue, *Chem. Commun.*, 2011, **47**, 1559–1561.

[90] H. Hall Jr, *J. Am. Chem. Soc.*, 1957, **79**, 5444–5447.

[91] X. Zhao, D. A. DiRocco and T. Rovis, *J. Am. Chem. Soc.*, 2011, **133**, 12466–12469.

[92] R. De Vreese and M. D'hooghe, *Beilstein J. Org. Chem.*, 2012, **8**, 398.

[93] H.-W. Wanzlick and E. Schikora, *Angew. Chem.*, 1960, **72**, 494–494.

[94] H.-W. Wanzlick and E. Schikora, *Chem. Ber.*, 1961, **94**, 2389–2393.

[95] H. Wanzlick, *Angew. Chem. Int. Ed.*, 1962, **1**, 75–80.

[96] A. Igau, H. Grutzmacher, A. Baceiredo and G. Bertrand, *J. Am. Chem. Soc.*, 1988, **110**, 6463–6466.

[97] A. Igau, A. Baceiredo, G. Trinquier and G. Bertrand, *Angew. Chem. Int. Ed.*, 1989, **28**, 621–622.

[98] A. J. Arduengo III, R. L. Harlow and M. Kline, *J. Am. Chem. Soc.*, 1991, **113**, 361–363.

[99] A. J. Arduengo III, H. R. Dias, R. L. Harlow and M. Kline, *J. Am. Chem. Soc.*, 1992, **114**, 5530–5534.

[100] A. J. Arduengo, J. R. Goerlich and W. J. Marshall, *Liebigs Annalen*, 1997, **1997**, 365–374.

[101] A. J. Arduengo, F. Davidson, H. R. Dias, J. R. Goerlich, D. Khasnis, W. J. Marshall and T. Prakasha, *J. Am. Chem. Soc.*, 1997, **119**, 12742–12749.

[102] Y.-T. Chen, G. L. Barletta, K. Haghjoo, J. T. Cheng and F. Jordan, *J. Org. Chem.*, 1994, **59**, 7714–7722.

[103] J. Crosby and G. E. Lienhard, *J. Am. Chem. Soc.*, 1970, **92**, 5707–5716.

[104] D. S. Kemp, *J. Am. Chem. Soc.*, 1970, **92**, 2553–2554.

[105] J. Crosby, R. Stone and G. E. Lienhard, *J. Am. Chem. Soc.*, 1970, **92**, 2891–2900.

[106] D. M. Lemal, R. A. Lovald and K. I. Kawano, *J. Am. Chem. Soc.*, 1964, **86**, 2518–2519.

[107] J. Castells, F. López-Calahorra, F. Geijo, R. Pérez-Dolz and M. Bassedas, *J. Heterocycl. Chem.*, 1986, **23**, 715–720.

[108] J. Castells, L. Domingo, F. López-Calahorra and J. Martí, *Tetrahedron Lett.*, 1993, **34**, 517–520.

[109] J. Castells, F. Lopez-Calahorra and L. Domingo, *J. Org. Chem.*, 1988, **53**, 4433–4436.

[110] Y. A. Muller, Y. Lindqvist, W. Furey, G. E. Schulz, F. Jordan and G. Schneider, *Structure*, 1993, **1**, 95–103.

[111] R. Breslow and R. Kim, *Tetrahedron Lett.*, 1994, **35**, 699–702.

[112] F. López-Calahorra and R. Rubires, *Tetrahedron*, 1995, **51**, 9713–9728.

[113] R. Breslow and C. Schmuck, *Tetrahedron Lett.*, 1996, **37**, 8241–8242.

[114] F. López-Calahorra, E. Castro, A. Ochoa and J. Martí, *Tetrahedron Lett.*, 1996, **37**, 5019–5022.

[115] J. Martí, F. López-Calahorra and J. M. Bofill, *J. Mol. Struct.: THEOCHEM*, 1995, **339**, 179–194.

[116] I. Nakanishi, S. Itoh, T. Suenobu and S. Fukuzumi, *Angew. Chem. Int. Ed.*, 1998, **37**, 992–994.

[117] J. Guin, S. De Sarkar, S. Grimme and A. Studer, *Angew. Chem. Int. Ed.*, 2008, **47**, 8727–8730.

[118] Y. Du, Y. Wang, X. Li, Y. Shao, G. Li, R. D. Webster and Y. R. Chi, *Org. Lett.*, 2014, **16**, 5678–5681.

[119] N. A. White and T. Rovis, *J. Am. Chem. Soc.*, 2014, **136**, 14674–14677.

[120] N. R. Dhumal, H. J. Kim and J. Kiefer, *J. Phys. Chem. A*, 2009, **113**, 10397–10404.

[121] O. Hollóczki, P. Terleczky, D. Szieberth, G. Mourgas, D. Gudat and L. Nyulászi, *J. Am. Chem. Soc.*, 2010, **133**, 780–789.

[122] M. Thomas, M. Brehm, O. Hollóczki and B. Kirchner, *Chem. Eur. J.*, 2014, **20**, 1622–1629.

[123] O. Hollóczki, *Phys. Chem. Chem. Phys.*, 2016, **18**, 126–140.

[124] A. J. I. Arduengo, S. F. Gamper, M. Tamm, J. C. Calabrese, F. Davidson and H. A. Craig, *J. Am. Chem. Soc.*, 1995, **117**, 572–573.

[125] J. A. Cowan, J. A. Clyburne, M. G. Davidson, R. L. W. Harris, J. A. Howard, P. Küpper, M. A. Leech and S. P. Richards, *Angew. Chem. Int. Edit.*, 2002, **114**, 1490–1492.

[126] L. A. Leites, G. I. Magdanurov, S. S. Bukalov and R. West, *Mendeleev Commun.*, 2008, **18**, 14–15.

[127] M. Feroci, I. Chiarotto, F. D'Anna, G. Forte, R. Noto and A. Inesi, *Electrochim. Acta*, 2015, **153**, 122–129.

[128] O. Hollóczki and L. Nyulászi, *Org. Biomol. Chem.*, 2011, **9**, 2634–2640.

[129] M. H. Dunn, M. L. Cole and J. B. Harper, *RSC Advances*, 2012, **2**, 10160–10162.

[130] T. Matsumoto, M. Ohishi and S. Inoue, *J. Org. Chem.*, 1985, **50**, 603–606.

[131] C. Burstein, S. Tschan, X. Xiulan and F. Glorius, *Synthesis*, 2006, 2418–2439.

[132] Z. Kelemen, O. Hollóczki, J. Oláh and L. Nyulászi, *RSC Adv.*, 2013, **3**, 7970–7978.

[133] T. Welton, *Chem. Rev.*, 1999, **99**, 2071–2083.

[134] R. D. Rogers and K. R. Seddon, *Science*, 2003, **302**, 792–793.

[135] J. F. Brennecke, R. D. Rogers and K. R. Seddon, *Ionic Liquids IV. Not Just Solvents Anymore.*, American Chemical Society, Washington, 2007.

[136] T. Welton, *Green Chem.*, 2011, **13**, 225–225.

[137] H. Rodríguez, G. Gurau, J. D. Holbrey and R. D. Rogers, *Chem. Commun.*, 2011, **47**, 3222–3224.

[138] O. Hollóczki, *Inorg. Chem.*, 2013, **53**, 835–846.

[139] S. Schernich, M. Laurin, Y. Lykhach, H.-P. Steinrück, N. Tsud, T. Skála, K. C. Prince, N. Taccardi, V. Matolín, P. Wasserscheid *et al.*, *J. Phys. Chem. let.*, 2012, **4**, 30–35.

[140] S. Wellens, N. R. Brooks, B. Thijs, L. Van Meervelt and K. Binnemans, *Dalton Trans.*, 2014, **43**, 3443–3452.

[141] G. Gurau, H. Rodríguez, S. P. Kelley, P. Janiczek, R. S. Kalb and R. D. Rogers, *Angew. Chem. Int. Ed.*, 2011, **50**, 12024–12026.

[142] Z. Kelemen, B. Péter-Szabó, E. Székely, O. Hollóczki, D. S. Firaha, B. Kirchner, J. Nagy and L. Nyulászi, *Chem. Eur. J.*, 2014, **20**, 13002–13008.

[143] M. Brehm, H. Weber, A. S. Pensado, A. Stark and B. Kirchner, *Phys. Chem. Chem. Phys.*, 2012, **14**, 5030–5044.

[144] O. Hollóczki, D. S. Firaha, J. Friedrich, M. Brehm, R. Cybik, M. Wild, A. Stark and B. Kirchner, *J. Phys. Chem. B*, 2013, **117**, 5898–5907.

[145] S. Scheiner, *Hydrogen bonding: a theoretical perspective*, Oxford University Press on Demand, 1997.

[146] G. R. Desiraju and T. Steiner, *The Weak Hydrogen Bond: in Structural Chemistry and Biology*, International Union of Crystal, 2001, vol. 9.

[147] T. Steiner, *Angew. Chem. Int. Ed.*, 2002, **41**, 48–76.

[148] M. Meot-Ner, *Chem. Rev.*, 2005, **105**, 213–284.

[149] J. Thar and B. Kirchner, *J. Phys. Chem. A*, 2006, **110**, 4229–4237.

[150] I. Rozas, *Phys. Chem. Chem. Phys.*, 2007, **9**, 2782–2790.

[151] G. Gilli and P. Gilli, *The nature of the hydrogen bond: outline of a comprehensive hydrogen bond theory*, Oxford University Press, 2009, vol. 23.

[152] B. Kirchner, *Ionic Liquids*, Springer Berlin Heidelberg, 2010, vol. 290, pp. 213–262.

[153] V. Kempter and B. Kirchner, *J. Mol. Struct.*, 2010, **972**, 22–34.

[154] S. B. C. Lehmann, M. Roatsch, M. Schoppke and B. Kirchner, *Phys. Chem. Chem. Phys.*, 2010, **12**, 7473–7486.

[155] K. Wendler, J. Thar, S. Zahn and B. Kirchner, *J. Phys. Chem. A*, 2010, **114**, 9529–9536.

[156] S. J. Grabowski, *Chem. Rev.*, 2011, **111**, 2597–2625.

[157] P. A. Hunt, C. R. Ashworth and R. P. Matthews, *Chem. Soc. Rev.*, 2015, **44**, 1257–1288.

[158] M. Kohagen, M. Brehm, Y. Lingscheid, R. Giernoth, J. Sangoro, F. Kremer, S. Naumov, C. Iacob, J. Kärger, R. Valiullin and B. Kirchner, *J. Phys. Chem. B*, 2011, **115**, 15280–15288.

[159] K. Shinokita, A. V. Cunha, T. L. Jansen and M. S. Pshenichnikov, *J. Chem. Phys.*, 2015, **142**, 212450.

[160] J. Y. Shin, Y.-L. Wang, S. A. Yamada, S. T. Hung and M. D. Fayer, *J. Phys. Chem. B*, 2019, **123**, 2094–2105.

[161] G. R. Desiraju, *Angew. Chem. Int. Ed.*, 2011, **50**, 52–59.

[162] S. J. Grabowski, *Hydrogen bonding: new insights*, Springer, 2006, vol. 3.

[163] A. J. Stone, *J. Chem. Theory Comput.*, 2005, **1**, 1128–1132.

[164] L. V. Slipchenko and M. S. Gordon, *J. Comput. Chem.*, 2007, **28**, 276–291.

[165] A. Stone and M. Alderton, *Mol. Phys.*, 2002, **100**, 221–233.

[166] A. Stone, *The theory of intermolecular forces*, OUP Oxford, 2nd edn, 2013.

[167] F. Weinhold and C. R. Landis, *Valency and bonding: a natural bond orbital donor-acceptor perspective*, Cambridge University Press, 2005.

[168] I. Bakó, Á. Bencsura, K. Hermannson, S. Bálint, T. Grósz, V. Chihaia and J. Oláh, *Phys. Chem. Chem. Phys.*, 2013, **15**, 15163–15171.

[169] E. D. Glendening, C. R. Landis and F. Weinhold, *J. Comput. Chem.*, 2013, **34**, 1429–1437.

[170] R. M. Badger and S. H. Bauer, *J. Chem. Phys.*, 1937, **5**, 839–851.

[171] M. Tichy, *Adv. Org. Chem.*, 1965, **5**, 115–298.

[172] C. Sandorfy, *Hydrogen Bonds*, Springer, 1984, pp. 41–84.

[173] N. Asprion, H. Hasse and G. Maurer, *Fluid Phase Equilib.*, 2001, **186**, 1–25.

[174] M. Meot-Ner, *Chem. Rev.*, 2012, **112**, PR22–PR103.

[175] A. Cohen and C. Reid, *J. Chem. Phys.*, 1956, **25**, 790–791.

[176] M. Saunders and J. B. Hyne, *J. Chem. Phys.*, 1958, **29**, 1319–1323.

[177] S. Forsen, *Acta Chem. Scand.*, 1959, **13**, 1472–1473.

[178] E. D. Becker, *J. Chem. Phys.*, 1959, **31**, 269–270.

[179] M. Maiwald, H. Li, T. Schnabel, K. Braun and H. Hasse, *J. Supercrit. Fluids*, 2007, **43**, 267–275.

[180] S. Reiser, N. McCann, M. Horsch and H. Hasse, *J. Supercrit. Fluids*, 2012, **68**, 94–103.

[181] E. Arunan, G. R. Desiraju, R. A. Klein, J. Sadlej, S. Scheiner, I. Alkorta, D. C. Clary, R. H. Crabtree, J. J. Dannenberg, P. Hobza *et al.*, *Pure and applied chemistry*, 2011, **83**, 1637–1641.

[182] E. Arunan, G. R. Desiraju, R. A. Klein, J. Sadlej, S. Scheiner, I. Alkorta, D. C. Clary, R. H. Crabtree, J. J. Dannenberg, P. Hobza *et al.*, *Pure and Applied Chemistry*, 2011, **83**, 1619–1636.

[183] G. A. Jeffrey and G. A. Jeffrey, *An introduction to hydrogen bonding*, Oxford university press New York, 1997, vol. 32.

[184] O. Conde and J. Teixeira, *Mol. Phys.*, 1984, **53**, 951–959.

[185] S. Chen and J. Teixeira, *Adv. Chem. Phys*, 1986, **64**, 1–46.

[186] E. Castner Jr, Y. Chang, Y. Chu and G. Walrafen, *J. Chem. Phys.*, 1995, **102**, 653–659.

[187] R. Rey, K. B. Møller and J. T. Hynes, *J. Phys. Chem. A*, 2002, **106**, 11993–11996.

[188] J. B. Asbury, T. Steinel, C. Stromberg, K. Gaffney, I. Piletic and M. Fayer, *J. Chem. Phys.*, 2003, **119**, 12981–12997.

[189] C. Lawrence and J. Skinner, *Chem. Phys. Lett.*, 2003, **369**, 472–477.

[190] S. A. Yamada, W. H. Thompson and M. D. Fayer, *J. Chem. Phys.*, 2017, **146**, 234501.

[191] M. Balasubramanian, A. Reynolds, T. J. Blair and M. Khalil, *Chem. Phys.*, 2019, **519**, 38–44.

[192] H.-K. Nienhuys, S. Woutersen, R. A. van Santen and H. J. Bakker, *J. Chem. Phys.*, 1999, **111**, 1494–1500.

[193] S. Woutersen, Y. Mu, G. Stock and P. Hamm, *Chem. Phys.*, 2001, **266**, 137–147.

[194] J. Eaves, J. Loparo, C. J. Fecko, S. Roberts, A. Tokmakoff and P. Geissler, *Proc. Natl. Acad. Sci.*, 2005, **102**, 13019–13022.

[195] J. J. Loparo, S. T. Roberts and A. Tokmakoff, *J. Chem. Phys.*, 2006, **125**, 194521.

[196] S. Park and M. D. Fayer, *Proc. Natl. Acad. Sci. U. S. A.*, 2007, **104**, 16731–16738.

[197] T. Schnabel, A. Srivastava, J. Vrabec and H. Hasse, *J. Phys. Chem. B*, 2007, **111**, 9871–9878.

[198] B. Qiao, C. Krekeler, R. Berger, L. Delle Site and C. Holm, *J. Phys. Chem. B*, 2008, **112**, 1743–1751.

[199] J. Thar, M. Brehm, A. P. Seitsonen and B. Kirchner, *J. Phys. Chem. B*, 2009, **113**, 15129–15132.

[200] W. Zhao, F. Leroy, B. Heggen, S. Zahn, B. Kirchner, S. Balasubramanian and F. Müller-Plathe, *J. Am. Chem. Soc.*, 2009, **131**, 15825–15833.

[201] B. S. Mallik and J. I. Siepmann, *J. Phys. Chem. B*, 2010, **114**, 12577–12584.

[202] M. Kohagen, M. Brehm, J. Thar, W. Zhao, F. Müller-Plathe and B. Kirchner, *J. Phys. Chem. B*, 2011, **115**, 693–702.

[203] I. Skarmoutsos, T. Welton and P. A. Hunt, *Phys. Chem. Chem. Phys.*, 2014, **16**, 3675–3685.

[204] J. Jeon, C.-S. Hsieh, Y. Nagata, M. Bonn and M. Cho, *J. Chem. Phys.*, 2017, **147**, 044707.

[205] A. Strate, J. Neumann, V. Overbeck, A.-M. Bonsa, D. Michalik, D. Paschek and R. Ludwig, *J. Chem. Phys.*, 2018, **148**, 193843.

[206] S. Das, B. Mukherjee and R. Biswas, *J. Chem. Phys.*, 2018, **148**, 193839.

[207] A. Rahman and F. H. Stillinger, *J. Chem. Phys.*, 1971, **55**, 3336–3359.

[208] M. Mezei and D. L. Beveridge, *J. Chem. Phys.*, 1981, **74**, 622–632.

[209] L. Onsager, *Phys. Rev.*, 1931, **37**, 405.

[210] L. Onsager, *Phys. Rev.*, 1931, **38**, 2265.

[211] D. Chandler, *J. Chem. Phys.*, 1978, **68**, 2959–2970.

[212] B. J. Berne, *Multiple Time Scales*, Elsevier, 1985, pp. 419–436.

[213] D. C. Rapaport, *Mol. Phys.*, 1983, **50**, 1151–1162.

[214] L. W. Flanagin, P. B. Balbuena, K. P. Johnston and P. J. Rossky, *J. Phys. Chem.*, 1995, **99**, 5196–5205.

[215] T. I. Mizan, P. E. Savage and R. M. Ziff, *J. Comput. Chem.*, 1996, **17**, 1757–1770.

[216] T. I. Mizan, P. E. Savage and R. M. Ziff, *J. Phys. Chem.*, 1996, **100**, 403–408.

[217] J. Marti, J. Padro and E. Guardia, *J. Chem. Phys.*, 1996, **105**, 639–649.

[218] L. Saiz, J. Padro and E. Guardia, *Mol. Phys.*, 1999, **97**, 897–905.

[219] J. Marti, *Phys. Rev. E*, 2000, **61**, 449.

[220] D. A. Zichi and P. J. Rossky, *J. Chem. Phys.*, 1986, **84**, 2814–2822.

[221] A. C. Belch and S. A. Rice, *J. Chem. Phys.*, 1987, **86**, 5676–5682.

[222] F. Sciortino and S. Fornili, *J. Chem. Phys.*, 1989, **90**, 2786–2792.

[223] F. Sciortino, P. H. Poole, H. E. Stanley and S. Havlin, *Phys. Rev. Lett.*, 1990, **64**, 1686.

[224] I. Ohmine and H. Tanaka, *Chem. Rev.*, 1993, **93**, 2545–2566.

[225] A. Luzar and D. Chandler, *Hydrogen Bond Networks*, Springer, 1994, pp. 239–246.

[226] F. W. Starr, J. K. Nielsen and H. E. Stanley, *Phys. Rev. Lett.*, 1999, **82**, 2294.

[227] M. Matsumoto and K. Gubbins, *J. Chem. Phys.*, 1990, **93**, 1981–1994.

[228] A. Luzar and D. Chandler, *Nature*, 1996, **379**, 55–57.

[229] A. Luzar, *J. Chem. Phys.*, 2000, **113**, 10663–10675.

[230] F. E. Hahn and M. C. Jahnke, *Angew. Chem. Int. Edit.*, 2008, **47**, 3122–3172.

[231] T. Dröge and F. Glorius, *Angew. Chem. Int. Edit.*, 2010, **49**, 6940–6952.

[232] D. Martin, M. Melaimi, M. Soleilhavoup and G. Bertrand, *Organometallics*, 2011, **30**, 5304–5313.

[233] M. N. Hopkinson, C. Richter, M. Schedler and F. Glorius, *Nature*, 2014, **510**, 485.

[234] L. Stryer, *Biochemistry*, Freeman, 4th edn, 1995.

[235] T. Kano, K. Sasaki and K. Maruoka, *Org. Lett.*, 2005, **7**, 1347–1349.

[236] Y. Suzuki, K. Yamauchi, K. Muramatsu and M. Sato, *Chem. Commun.*, 2004, 2770–2771.

[237] J. L. Moore and T. Rovis, *Asymmetric Organocatalysis*, Springer, 2010, pp. 118–144.

[238] F. Bonnette, T. Kato, M. Destarac, G. Mignani, F. P. Cossío and A. Baceiredo, *Angew. Chem. Int. Edit.*, 2007, **46**, 8632–8635.

[239] T. Weidner, J. E. Baio, A. Mundstock, C. Große, S. Karthäuser, C. Bruhn and U. Siemeling, *Aust. J. Chem.*, 2011, **64**, 1177–1179.

[240] C. M. Crudden, J. H. Horton, I. I. Ebralidze, O. V. Zenkina, A. B. McLean, B. Drevniok, Z. She, H.-B. Kraatz, N. J. Mosey, T. Seki *et al.*, *Nat. Chem.*, 2014, **6**, 409–414.

[241] J. Vignolle and T. D. Tilley, *Chem. Commun.*, 2009, 7230–7232.

[242] E. A. Baquero, S. Tricard, J. C. Flores, E. de Jesús and B. Chaudret, *Angew. Chem. Int. Edit.*, 2014, **53**, 13220–13224.

[243] M. Heger, J. Altnöder, A. Poblotzki and M. A. Suhm, *Phys. Chem. Chem. Phys.*, 2015, **17**, 13045–13052.

[244] H. C. Gottschalk, J. Altnöder, M. Heger and M. A. Suhm, *Angew. Chem. Int. Edit.*, 2016, **55**, 1921–1924.

[245] W. L. Jorgensen, J. Chandrasekhar, J. D. Madura, R. W. Impey and M. L. Klein, *J. Chem. Phys.*, 1983, **79**, 926–935.

[246] S. Izadi, R. Anandakrishnan and A. V. Onufriev, *J. Phys. Chem. let.*, 2014, **5**, 3863–3871.

[247] M. W. Mahoney and W. L. Jorgensen, *J. Chem. Phys.*, 2000, **112**, 8910–8922.

[248] F. H. Stillinger and A. Rahman, *J. Chem. Phys.*, 1974, **60**, 1545–1557.

[249] E. Aldeco-Perez, A. J. Rosenthal, B. Donnadieu, P. Parameswaran, G. Frenking and G. Bertrand, *Science*, 2009, **326**, 556–559.

[250] A. J. Arduengo III, J. R. Goerlich and W. J. Marshall, *J. Am. Chem. Soc.*, 1995, **117**, 11027–11028.

[251] O. Hollóczki and L. Nyulászi, *J. Org. Chem*, 2008, **73**, 4794–4799.

[252] K. F. Donnelly, A. Petronilho and M. Albrecht, *Chem. Commun.*, 2013, **49**, 1145–1159.

[253] S. Solé, H. Gornitzka, W. W. Schoeller, D. Bourissou and G. Bertrand, *Science*, 2001, **292**, 1901–1903.

[254] V. Lavallo, Y. Canac, B. Donnadieu, W. W. Schoeller and G. Bertrand, *Science*, 2006, **312**, 722–724.

[255] W. L. Jorgensen, D. S. Maxwell and J. Tirado-Rives, *J. Am. Chem. Soc.*, 1996, **118**, 11225–11236.

[256] F. Neese, *WIREs Comput. Mol. Sci.*, 2012, **2**, 73–78.

[257] C. M. Breneman and K. B. Wiberg, *J. Comput. Chem.*, 1990, **11**, 361–373.

[258] H. Berendsen, J. Grigera and T. Straatsma, *J. Phys. Chem.*, 1987, **91**, 6269–6271.

[259] C. Riplinger, B. Sandhoefer, A. Hansen and F. Neese, *J. Chem. Phys.*, 2013, **139**, 134101.

[260] D. G. Liakos, M. Sparta, M. K. Kesharwani, J. M. Martin and F. Neese, *J. Chem. Theory Comput.*, 2015, **11**, 1525–1539.

[261] D. G. Liakos and F. Neese, *J. Chem. Theory Comput.*, 2015, **11**, 4054–4063.

[262] D. G. Liakos and F. Neese, *J. Phys. Chem. A*, 2012, **116**, 4801–4816.

[263] S. Plimpton, *J. Comp. Phys.*, 1995, **117**, 1–19.

[264] W. D. Cornell, P. Cieplak, C. I. Bayly, I. R. Gould, K. M. Merz, D. M. Ferguson, D. C. Spellmeyer, T. Fox, J. W. Caldwell and P. A. Kollman, *J. Am. Chem. Soc.*, 1995, **117**, 5179–5197.

[265] S. V. Sambasivarao and O. Acevedo, *J. Chem. Theory Comput.*, 2009, **5**, 1038–1050.

[266] J. N. Canongia Lopes, J. Deschamps and A. A. Pádua, *J. Phys. Chem. B*, 2004, **108**, 2038–2047.

[267] J. N. Canongia Lopes and A. A. Pádua, *J. Phys. Chem. B*, 2006, **110**, 19586–19592.

[268] N. A. McDonald and W. L. Jorgensen, *J. Phys. Chem. B*, 1998, **102**, 8049–8059.

[269] C. D. Boden and G. Pattenden, *J. Comput. Aid. Mol. Des.*, 1999, **13**, 153–166.

[270] W. L. Jorgensen and N. A. McDonald, *J. Mol. Struc. Theochem*, 1998, **424**, 145–155.

[271] A. D. Becke, *Phys. Rev. A*, 1988, **38**, 3098.

[272] C. Lee, W. Yang and R. G. Parr, *Phys. Rev. B*, 1988, **37**, 785.

[273] B. Miehlich, A. Savin, H. Stoll and H. Preuss, *Chem. Phys. Lett.*, 1989, **157**, 200–206.

[274] A. D. Becke, *J. Chem. Phys.*, 1993, **98**, 5648–5652.

[275] J. P. Perdew, K. Burke and M. Ernzerhof, *Phys. Rev. Lett.*, 1996, **77**, 3865.

[276] J. P. Perdew, M. Ernzerhof and K. Burke, *J. Chem. Phys.*, 1996, **105**, 9982–9985.

[277] C. Adamo and V. Barone, *J. Chem. Phys.*, 1999, **110**, 6158–6170.

[278] J. Tao, J. P. Perdew, V. N. Staroverov and G. E. Scuseria, *Phys. Rev. Lett.*, 2003, **91**, 146401.

[279] S. Grimme, J. Antony, S. Ehrlich and H. Krieg, *J. Chem. Phys.*, 2010, **132**, 154104.

[280] S. Grimme, S. Ehrlich and L. Goerigk, *J. Comput. Chem.*, 2011, **32**, 1456–1465.

[281] S. Grimme, *J. Chem. Phys.*, 2003, **118**, 9095–9102.

[282] A. Schäfer, H. Horn and R. Ahlrichs, *J. Chem. Phys.*, 1992, **97**, 2571–2577.

[283] F. Weigend and R. Ahlrichs, *Phys. Chem. Chem. Phys.*, 2005, **7**, 3297–3305.

[284] R. S. Mulliken, *J. Chem. Phys.*, 1955, **23**, 1833–1840.

[285] P.-O. Lowdin, *Adv. Quantum Chem.*, 1970, **5**, 185.

[286] A. E. Reed, R. B. Weinstock and F. Weinhold, *J. Chem. Phys.*, 1985, **83**, 735–746.

[287] A. Klamt, *J. Phys. Chem.*, 1995, **99**, 2224–2235.

[288] D. Yin and A. D. MacKerell, *J. Comput. Chem.*, 1998, **19**, 334–348.

[289] D. Hagberg, G. Karlström, B. O. Roos and L. Gagliardi, *J. Am. Chem. Soc.*, 2005, **127**, 14250–14256.

[290] W. L. Jorgensen, *J. Am. Chem. Soc.*, 1981, **103**, 335–340.

[291] H. J. Berendsen, J. P. Postma, W. F. van Gunsteren and J. Hermans, *Intermolecular forces*, Springer, 1981, pp. 331–342.

[292] M. Downing, L. M. Eaton, R. L. Graham, M. H. Langholtz, R. D. Perlack, A. F. T. Jr, B. Stokes and C. C. Brandt, *Biomass as Feedstock for a Bioenergy and Bioproducts Industry: The Technical Feasibility of a Billion-Ton Annual Supply*, U.S. Department of Energy and U.S. Department of Agriculture, DE-AC05-00OR22725 edn, 2011.

[293] M. Isik, H. Sardon and D. Mecerreyes, *Int. J. Mol. Sci.*, 2014, **15**, 11922–11940.

[294] S. Zhu, Y. Wu, Q. Chen, Z. Yu, C. Wang, S. Jin, Y. Ding and G. Wu, *Green Chem.*, 2006, **8**, 325–327.

[295] H. Wang, G. Gurau and R. D. Rogers, *Structures and Interactions of Ionic Liquids*, Springer, 2014, pp. 79–105.

[296] N. Sun, M. Rahman, Y. Qin, M. L. Maxim, H. Rodríguez and R. D. Rogers, *Green Chem.*, 2009, **11**, 646–655.

[297] R. P. Swatloski, S. K. Spear, J. D. Holbrey and R. D. Rogers, *J. Am. Chem. Soc.*, 2002, **124**, 4974–4975.

[298] H. Wang, G. Gurau and R. D. Rogers, *Chem. Soc. Rev.*, 2012, **41**, 1519–1537.

[299] R. C. Remsing, G. Hernandez, R. P. Swatloski, W. W. Massefski, R. D. Rogers and G. Moyna, *J. Phys. Chem. B*, 2008, **112**, 11071–11078.

[300] B. D. Rabideau and A. E. Ismail, *Phys. Chem. Chem. Phys*, 2015, **17**, 5767.

[301] Y. Fukaya, K. Hayashi, M. Wadab and H. Ohno, *Green Chem.*, 2008, **10**, 44–46.

[302] H. Liu, K. L. Sale, B. M. Holmes, B. A. Simmons and S. Singh, *J. Phys. Chem. B*, 2010, **114**, 4293–4301.

[303] A. Pinkert, K. N. Marsh, S. Pang and M. P. Staiger, *Chem. Rev.*, 2009, **109 (12)**, 6712–6728.

[304] B. Lu, A. Xu and J. Wang, *Green Chem.*, 2014, **16**, 1326–1335.

[305] B. D. Rabideau, A. Agarwal and A. E. Ismail, *J. Phys. Chem. B*, 2014, **118 (6)**, 1621–1629.

[306] M. T. Clough, K. Geyer, P. A. Hunt, S. Son, U. Vagt and T. Welton, *Green Chem.*, 2015, **17**, 231–243.

[307] J. P. Armstrong, C. Hurst, R. G. Jones, P. Licence, K. R. J. Lovelock, C. J. Satterley and I. J. Villar-Garcia, *Phys. Chem. Chem. Phys.*, 2007, **9**, 982–990.

[308] F. Malberg, M. Brehm, O. Hollóczki, A. S. Pensado and B. Kirchner, *Phys. Chem. Chem. Phys.*, 2013, **15**, 18424–18436.

[309] T. L. Greaves and C. J. Drummond, *Chem. Rev.*, 2008, **108**, 206–237.

[310] T. L. Greaves and C. J. Drummond, *Chem. Rev.*, 2015, **115**, 11379–11448.

[311] M. Y. Lui, L. Crowhurst, J. P. Hallett, P. A. Hunt, H. Niedermeyer and T. Welton, *Chem. Sci.*, 2011, **2**, 1491–1496.

[312] L. Martínez, R. Andrade, E. G. Birgin and J. M. Martínez, *J. Comput. Chem.*, 2009, **30**, 2157–2164.

[313] S. Kossmann, J. Thar, B. Kirchner, P. A. Hunt and T. Welton, *J. Chem. Phys.*, 2006, **124**, 174506.

[314] O. Hollóczki, F. Malberg, T. Welton and B. Kirchner, *Phys. Chem. Chem. Phys.*, 2014, **16**, 16880–16890.

[315] B. Kirchner, F. Malberg, D. S. Firaha and O. Hollóczki, *J. Phys. Condens. Matter*, 2015, **27**, 463002.

[316] M. Brehm and B. Kirchner, *J. Chem. Inf. Model.*, 2011, **51**, 2007–2023.

[317] T. G. A. Youngs, J. D. Holbrey, C. L. Mullan, S. E. Norman, M. C. Lagunas, C. D'Agostino, M. D. Mantle, L. F. Gladden, D. T. Bowron and C. Hardacre, *Chem. Sci.*, 2011, **2**, 1594.

[318] B. D. Rabideau, A. Agarwal and A. E. Ismail, *J. Phys. Chem. B*, 2013, **117**, 3469–3479.

[319] E. I. Izgorodina, *Phys. Chem. Chem. Phys.*, 2011, **13**, 4189–4207.

[320] H. K. Kashyap, C. S. Santos, H. V. R. Annapureddy, N. S. Murthy, C. J. Margulis and E. W. Castner, Jr, *Faraday Discuss.*, 2012, **154**, 133–143.

[321] B. Kirchner, O. Hollóczki, J. N. Canongia Lopes and A. A. H. Pádua, *WIREs Comp. Mol. Sci.*, 2014, 202–214.

[322] E. I. Izgorodina, Z. L. Seeger, D. L. Scarborough and S. Y. Tan, *Chem. Rev.*, 2017, **117**, 6696–6754.

[323] Z. Hu and C. J. Margulis, *Proc. Natl. Acad. Sci. U.S.A.*, 2006, **103**, 831–836.

[324] S. M. Urahata and M. C. C. Ribeiro, *J. Chem. Phys.*, 2004, **120**, 1855–1863.

[325] Y. T. Wang and G. A. Voth, *J. Am. Chem. Soc.*, 2005, **127**, 12192–12193.

[326] J. N. Canongia Lopes and A. A. H. Pádua, *J. Phys. Chem. B*, 2006, **110**, 3330–3335.

[327] H. Weber, O. Hollóczki, A. S. Pensado and B. Kirchner, *J. Chem. Phys.*, 2013, **139**, 084502.

[328] K. Shimizu, C. E. Bernardes and J. N. Canongia Lopes, *J. Phys. Chem. B*, 2014, **118**, 567–576.

[329] M. Brehm, H. Weber, M. Thomas, O. Hollóczki and B. Kirchner, *ChemPhysChem*, 2015, **16**, 3271–3277.

[330] O. Hollóczki, M. Macchiagodena, H. Weber, M. Thomas, M. Brehm, A. Stark, O. Russina, A. Triolo and B. Kirchner, *ChemPhysChem*, 2015, **16**, 3325–3333.

[331] T. Steiner and G. R. Desiraju, *Chem. Commun.*, 1998, **8**, 891–892.

[332] P. A. Hunt, B. Kirchner and T. Welton, *Chem. Eur. J.*, 2006, **12**, 6762–6775.

[333] S. Zahn, F. Uhlig, J. Thar, C. Spickermann and B. Kirchner, *Angew. Chem. Int. Ed.*, 2008, **47**, 3639–3641.

[334] I. Skarmoutsos, D. Dellis, R. P. Matthews, T. Welton and P. A. Hunt, *J. Phys. Chem. B*, 2012, **116**, 4921–4933.

[335] K. Fumino, A. Wulf and R. Ludwig, *Angew. Chem. Int. Ed.*, 2008, **47**, 3830–3834.

[336] R. Cooper, A. M. Zolot, J. A. Boatz, D. P. Sporleder and J. A. Stearns, *J. Phys. Chem. A*, 2013, **117**, 12419–12428.

[337] K. Fumino, A.-M. Bonsa, B. Golub, D. Paschek and R. Ludwig, *ChemPhysChem*, 2015, **16**, 299–304.

[338] H. Tokuda, S. Tsuzuki, M. A. B. H. Susan, K. Hayamizu and M. Watanabe, *J. Phys. Chem. B*, 2006, **110(39)**, 19593–19600.

[339] F. Müller-Plathe and W. F. van Gunsteren, *J. Chem. Phys.*, 1995, **103**, 4745–4756.

[340] B. L. Bhargava and S. Balasubramanian, *J. Chem. Phys.*, 2005, **123**, 144505.

[341] T. G. A. Youngs and C. Hardacre, *ChemPhysChem*, 2008, **9**, 1548–1558.

[342] A. S. Pensado, M. Brehm, J. Thar, A. P. Seitsonen and B. Kirchner, *ChemPhysChem*, 2012, **13**, 1845–1853.

[343] H. V. Spohr and G. N. Patey, *J. Chem. Phys.*, 2008, **129**, 064517.

[344] H. V. Spohr and G. N. Patey, *J. Chem. Phys.*, 2009, **130**, 104506.

[345] H. V. Spohr and G. N. Patey, *J. Chem. Phys.*, 2010, **132**, 154504.

[346] Y. Zhang and E. J. Maginn, *J. Chem. Phys.*, 2015, **6**, 700–705.

[347] S. N. Butler and F. Müller-Plathe, *ChemPhysChem*, 2012, **13**, 1791–1801.

[348] F. H. Stillinger, *Theory And Molecular Models For Water*, Wiley, Bell Laboratories, Murray Hill, New Jersey, Advances in Chemical Physics, Volume XXXI edn, 1975.

[349] A. Luzar and D. Chandler, *Phys. Rev. Lett.*, 1996, **76**, 928–931.

[350] A. Luzar, *Faraday Discuss.*, 1996, **103**, 29–40.

[351] S. Bandyopadhyay, S. Chakraborty and B. Bagchi, *J. Am. Chem. Soc.*, 2005, **127**, 16660–16667.

[352] J. Chanda and S. Bandyopadhyay, *J. Phys. Chem. B*, 2006, **110**, 23443–23449.

[353] L. Hua, X. Huang, R. Zhou and B. J. Berne, *J. Phys. Chem. B*, 2006, **110**, 3704–3711.

[354] R. Rousseau, E. Schreiner, A. Kohlmeyer and D. Marx, *Biophys. J.*, 2004, **86**, 1393–1407.

[355] E. Schreiner, C. Nicolini, B. Ludolph, R. Ravindra, N. Otte, A. Kohlmeyer, R. Rousseau, R. Winter and D. Marx, *Phys. Rev. Lett.*, 2004, **92**, 148101.

[356] H. Xu and B. Berne, *J. Phys. Chem. B*, 2001, **105**, 11929–11932.

[357] E. Marin-Rimoldi, J. K. Shah and E. J. Maginn, *Fluid Ph. Equilibria*, 2016, **407**, 117–125.

[358] P. Hänggi, P. Talkner and M. Borkovec, *Rev. Mod. Phys.*, 1990, **62**, 251.

[359] A. Dequidt, J. Devémy and A. A. H. Pádua, *J. Chem. Inf. Model.*, 2016, **56**, 260–268.

[360] C. E. S. Bernardes, K. Shimizu, J. N. C. Lopes, P. Marquetand, E. Heid, O. Steinhauser and C. Schroder, *Phys. Chem. Chem. Phys.*, 2016, **18**, 1665–1670.

[361] G. García-Miaja, J. Troncoso and L. Romaní, *J. Chem. Thermodyn.*, 2009, **41**, 161–166.

[362] D. T. Bowron, C. D'Agostino, L. F. Gladden, C. Hardacre, J. D. Holbrey, M. C. Lagunas, J. McGregor, M. D. Mantle, C. L. Mullan and T. G. A. Youngs, *J. Phys. Chem. B*, 2010, **114**, 7760–7768.

[363] O. Borodin, *J. Phys. Chem. B*, 2009, **113**, 11463–11478.

[364] A. Elaiwi, P. B. Hitchcock, K. R. Seddon, N. Srinivasen, Y. Tan, T. Welton and J. A. Zora, *J. Chem. Soc., Dalton Trans.*, 1995, , 3467–3472.

[365] C. P. Fredlake, J. M. Crosthwaite, D. G. Hert, S. N. V. K. Aki and J. F. Brennecke, *J. Chem. Eng. Data*, 2004, **49**, 954–964.

[366] C. Hardacre, J. D. Holbrey, C. L. Mullan, T. G. A. Youngs and D. T. Bowron, *J. Chem. Phys.*, 2010, **133**, 074510.

[367] D. S. Firaha, M. Thomas, O. Hollóczki, M. Korth and B. Kirchner, *J. Chem. Phys.*, 2016, **145**, 204502.

[368] M.-L. Ge, R.-S. Zhao, Y.-F. Yi, Q. Zhang and L. S. Wang, *J. Chem. Eng. Data*, 2008, **53(10)**, 2408–2411.

[369] M. T. Clough, C. R. Crick, J. Gräsvik, P. A. Hunt, H. Niedermeyer, T. Welton and O. P. Whitaker, *Chem. Sci.*, 2015, **6**, 1101–1114.

[370] B. Mbondo Tsamba, S. Sarraute, M. Traïkia and P. Husson, *J. Chem. Eng. Data*, 2014, **59**, 1747–1754.

[371] J.-M. Andanson, X. Meng, M. Traïkia and P. Husson, *J. Chem. Thermodyn.*, 2016, **94**, 169–176.

[372] G. McHale, C. Hardacre, R. Ge, N. Doy, R. W. Allen, J. M. MacInnes, M. R. Bown and M. I. Newton, *Anal. Chem.*, 2008, **80**, 5806–5811.

[373] M. Shamsipur, A. A. M. Beigi, M. Teymouri, S. M. Pourmortazavi and M. Irandoust, *J. Mol. Liq.*, 2010, **157**, 43–50.

[374] M. L. Batista, L. I. Tomé, C. M. Neves, J. R. Gomes and J. A. Coutinho, *J. Mol. Liq.*, 2014, **192**, 26–31.

[375] R. L. Gardas and J. A. P. Coutinho, *AIChE J.*, 2009, **55**, 1274–1290.

[376] B. Kirchner, C. Spickermann, W. Reckien and C. A. Schalley, *J. Am. Chem. Soc.*, 2009, **132**, 484–494.

[377] F. H. Stillinger, *Science*, 1980, **209**, 451–457.

[378] A. Luzar, S. Svetina and B. Žekš, *Chem. Phys. Lett.*, 1983, **96**, 485–490.

[379] A. Luzar, *J. Chem. Phys.*, 1989, **91**, 3603–3613.

[380] N. Asprion, H. Hasse and G. Maurer, *J. Chem. Eng. Data*, 1998, **43**, 74–80.

[381] T. Schnabel, J. Vrabec and H. Hasse, *Chem. Ing. Tech.*, 2007, **79**, 1421–1422.

[382] T. Schnabel, J. Vrabec and H. Hasse, *Fluid Phase Equilib.*, 2008, **263**, 144–159.

[383] K. Langenbach, C. Engin, S. Reiser, M. Horsch and H. Hasse, *AIChE J.*, 2015, **61**, 2926–2932.

[384] G. R. Desiraju, *Acc. Chem. Res.*, 2002, **35**, 565–573.

[385] S. Cha and D. Kim, *J. Chem. Phys.*, 2018, **148**, 193827.

[386] Z. Ren, A. S. Ivanova, D. Couchot-Vore and S. Garrett-Roe, *J. Phys. Chem. Lett.*, 2014, **5**, 1541–1546.

[387] G. Desiraju and T. Steiner, *Chem. Commun.*, 1998, **8**, 891–892.

[388] G. Rutkai, A. Köster, G. Guevara-Carrion, T. Janzen, M. Schappals, C. W. Glass, M. Bernreuther, A. Wafai, S. Stephan and M. Kohns, *Comput. Phys. Commun.*, 2017, **221**, 343–351.

[389] H. Hasse and J. Lenhard, *Mathematics as a Tool*, Springer, 2017, pp. 93–115.

[390] G. Guevara-Carrion, H. Hasse and J. Vrabec, *Multiscale Molecular Methods in Applied Chemistry*, Springer, 2011, pp. 201–249.

[391] G. Guevara-Carrion, J. Vrabec and H. Hasse, *Int. J. Thermophys.*, 2012, **33**, 449–468.

[392] G. Guevara-Carrion, J. Vrabec and H. Hasse, *Fluid Phase Equilib.*, 2012, **316**, 46–54.

[393] E. von Harbou, R. Behrens, J. Berje, A. Brächer and H. Hasse, *Chem. Ing. Tech.*, 2017, **89**, 369–378.

[394] T. Kikutsuji, K. Kim and N. Matubayasi, *J. Chem. Phys.*, 2019, **150**, 204502.

[395] M. P. Lautenschlaeger and H. Hasse, *Fluid Phase Equilib.*, 2019, **482**, 38–47.

[396] J. Cioslowski, *Science*, 1991, **252**, 1566–1568.

[397] U. Koch and P. L. Popelier, *J. Phys. Chem.*, 1995, **99**, 9747–9754.

[398] M. Reiher and B. Kirchner, *J. Phys. Chem. A*, 2003, **107**, 4141–4146.

[399] F. Stillinger, *Philos. Trans. Royal Soc. B*, 1977, **278**, 97–112.

[400] J. Neumann, B. Golub, L.-M. Odebrecht, R. Ludwig and D. Paschek, *J. Chem. Phys.*, 2018, **148**, 193828.

[401] Y. Zhang and E. J. Maginn, *J. Phys. Chem. B*, 2012, **116**, 10036–10048.

[402] R. W. Hockney and J. W. Eastwood, *Computer simulation using particles*, CRC Press, 1988.

[403] S. Nosé, *J. Chem. Phys.*, 1984, **81**, 511–519.

[404] S. Nosé, *Mol. Phys.*, 1984, **52**, 255–268.

[405] G. J. Martyna, M. L. Klein and M. Tuckerman, *J. Chem. Phys.*, 1992, **97**, 2635–2643.

[406] R. L. Gardas, M. G. Freire, P. J. Carvalho, I. M. Marrucho, I. M. Fonseca, A. G. Ferreira and J. A. Coutinho, *J. Chem. Eng. Data*, 2007, **52**, 80–88.

[407] M. Tariq, P. J. Carvalho, J. A. Coutinho, I. M. Marrucho, J. N. C. Lopes and L. P. Rebelo, *Fluid Phase Equilib.*, 2011, **301**, 22–32.

[408] N. Mac Dowell, F. Llovell, N. Sun, J. Hallett, A. George, P. Hunt, T. Welton, B. Simmons and L. Vega, *J. Phys. Chem. B*, 2014, **118**, 6206–6221.

[409] Y. Hiraga, A. Kato, Y. Sato and R. L. Smith Jr, *J. Chem. Eng. Data*, 2015, **60**, 876–885.

[410] K. R. Harris, L. A. Woolf and M. Kanakubo, *J. Chem. Eng. Data*, 2005, **50**, 1777–1782.

[411] H. F. Almeida, J. N. Canongia Lopes, L. P. Rebelo, J. a. A. Coutinho, M. G. Freire and I. M. Marrucho, *J. Chem. Eng. Data*, 2016, **61**, 2828–2843.

[412] Y. Hiraga, K. Koyama, Y. Sato and R. L. Smith Jr, *J. Chem. Thermodyn.*, 2017, **108**, 7–17.

[413] I. Alkorta and J. Elguero, *J. Phys. Chem.*, 1996, **100**, 19367–19370.

[414] J. P. Pezacki, *Can. J. Chem.*, 1999, **77**, 1230–1240.

[415] M. Eigen, *Angew. Chem. Int. Ed.*, 1964, **3**, 1–19.

[416] M. E. Tuckerman, D. Marx, M. L. Klein and M. Parrinello, *Science*, 1997, **275**, 817–820.

[417] D. M. Wilkins, D. E. Manolopoulos, S. Pipolo, D. Laage and J. T. Hynes, *J. Phys. Chem. Lett.*, 2017, **8**, 2602–2607.

[418] M. Thomas, M. Brehm and B. Kirchner, *Phys. Chem. Chem. Phys.*, 2015, **17**, 3207–3213.

[419] B.-S. Li, Y. Wang, R. S. Proctor, Y. Zhang, R. D. Webster, S. Yang, B. Song and Y. R. Chi, *Nat. Commun.*, 2016, **7**, 12933.

[420] Z. Fu, J. Xu, T. Zhu, W. W. Y. Leong and Y. R. Chi, *Nat. Chem.*, 2013, **5**, 835–839.

[421] D. W. MacMillan, *Nature*, 2008, **455**, 304.

[422] J. Mahatthananchai and J. W. Bode, *Acc. Chem. Res.*, 2014, **47**, 696–707.

[423] F. Yan, N. R. Dhumal and H. J. Kim, *Phys. Chem. Chem. Phys.*, 2017, **19**, 1361–1368.

[424] S. Tobisch and T. Ziegler, *J. Am. Chem. Soc.*, 2004, **126**, 9059–9071.

[425] H. Zhu and T. Ziegler, *J. Organomet. Chem.*, 2006, **691**, 4486–4497.

[426] D. H. Wertz, *J. Am. Chem. Soc.*, 1980, **102**, 5316–5322.

[427] D. H. Nouri and D. J. Tantillo, *J. Org. Chem.*, 2006, **71**, 3686–3695.

[428] J. Knorr, P. Sokkar, S. Schott, P. Costa, W. Thiel, W. Sander, E. Sanchez-Garcia and P. Nuernberger, *Nat. Commun.*, 2016, **7**, 12968.

[429] B. Galabov, D. Nalbantova, P. v. R. Schleyer and H. F. Schaefer III, *Acc. Chem. Res.*, 2016, **49**, 1191–1199.

[430] B. Horecker and P. Smyrniotis, *J. Am. Chem. Soc.*, 1953, **75**, 1009–1010.

[431] E. Racker, G. de la Haba and I. Leder, *J. Am. Chem. Soc.*, 1953, **75**, 1010–1011.

[432] O. Hollóczki, *Chemistry–A European Journal*, 2020, **26**, 4885–4894.

[433] F. Lopez-Calahorra, J. Castells, L. Domingo, J. Marti and J. M. Bofill, *Heterocycles*, 1994, **37**, 1579–1597.

[434] N. Konstandaras, M. H. Dunn, E. T. Luis, M. L. Cole and J. B. Harper, *Org. Biomol. Chem.*, 2020, **18**, 1910–1917.

[435] H. Hall Jr, *J. Am. Chem. Soc.*, 1957, **79**, 5441–5444.

[436] S. Tshepelevitsh, A. Kütt, M. Lõkov, I. Kaljurand, J. Saame, A. Heering, P. G. Plieger, R. Vianello and I. Leito, *Eur. J. Org. Chem.*, 2019, **2019**, 6735–6748.

[437] D. Rico del Cerro, R. Mera-Adasme, A. W. King, J. E. Perea-Buceta, S. Heikkinen, T. Hase, D. Sundholm and K. Wähälä, *Angew. Chem. Int. Ed.*, 2018, **57**, 11613–11617.

[438] N. V. Tzouras, F. Nahra, L. Falivene, L. Cavallo, M. Saab, K. Van Hecke, A. Collado, C. J. Collett, A. D. Smith, C. S. Cazin *et al.*, *Chem. Eur. J.*, 2020, **26**, 4515–4519.

[439] N. V. Tzouras, M. Saab, W. Janssens, T. Cauwenbergh, K. Van Hecke, F. Nahra and S. P. Nolan, *Chem. Eur. J.*, 2020, **26**, 5541–5551.

[440] J. Blasius, R. Elfgen, O. Hollóczki and B. Kirchner, *Phys. Chem. Chem. Phys.*, 2020, **22**, 10726–10737.

[441] F. Neese, *WIREs Comput. Mol. Sci.*, 2018, **8**, e1327.

[442] A. Klamt, V. Jonas, T. Bürger and J. C. Lohrenz, *J. Phys. Chem. A*, 1998, **102**, 5074–5085.

[443] F. Eckert and A. Klamt, *AIChE Journal*, 2002, **48**, 369–385.

[444] A. Klamt, *Wiley Interdisciplinary Reviews: Computational Molecular Science*, 2018, **8**, e1338.

[445] O. Treutler and R. Ahlrichs, *J. Chem. Phys.*, 1995, **102**, 346–354.

[446] R. Ahlrichs, M. Bär, M. Häser, H. Horn and C. Kölmel, *Chem. Phys. Lett.*, 1989, **162**, 165–169.

[447] E. R. Johnson, S. Keinan, P. Mori-Sánchez, J. Contreras-García, A. J. Cohen and W. Yang, *J. Am. Chem. Soc.*, 2010, **132**, 6498–6506.

[448] J. Contreras-García, W. Yang and E. R. Johnson, *J. Phys. Chem. A*, 2011, **115**, 12983–12990.

[449] E. Pastorczak and C. Corminboeuf, *J. Chem. Phys.*, 2017, **146**, 120901.

[450] T. Lu and F. Chen, *J. Comput. Chem.*, 2012, **33**, 580–592.

[451] M. S. Taylor and E. N. Jacobsen, *Angew. Chem. Int. Ed.*, 2006, **45**, 1520–1543.

[452] P. R. Schreiner, *Chem. Soc. Rev.*, 2003, **32**, 289–296.

[453] R. R. Knowles and E. N. Jacobsen, *Proc. Natl. Acad. Sci.*, 2010, **107**, 20678–20685.

[454] A. G. Doyle and E. N. Jacobsen, *Chem. Rev.*, 2007, **107**, 5713–5743.

[455] W. Cleland and M. M. Kreevoy, *Science*, 1994, **264**, 1887–1890.

[456] Y. B. Yu, P. L. Privalov and R. S. Hodges, *Biophys. J.*, 2001, **81**, 1632–1642.

[457] D. D. Liu and E. Y.-X. Chen, *Green Chem.*, 2014, **16**, 964–981.

[458] D. D. Liu, Y. Zhang and E. Y.-X. Chen, *Green Chem.*, 2012, **14**, 2738–2746.

[459] M. Thomas, M. Brehm, O. Hollóczki, Z. Kelemen, L. Nyulászi, T. Pasinszki and B. Kirchner, *J. Chem. Phys.*, 2014, **141**, 024510.

[460] I. Chiarotto, M. Feroci and A. Inesi, *New J. Chem.*, 2017, **41**, 7840–7843.

[461] N. Daud, E. Bakis, J. Hallett, C. Weber and T. Welton, *Chem. Commun.*, 2017, **53**, 11154–11156.

[462] M. Dong, J. Gao, C. Liu and D. Zhang, *J. Phys. Chem. B*, 2017, **121**, 10276–10284.

[463] G. Kresse and J. Hafner, *Phys. Rev. B*, 1993, **47**, 558.

[464] G. Kresse and J. Hafner, *Phys. Rev. B*, 1994, **49**, 14251.

[465] G. Kresse and J. Furthmüller, *Comp. Mat. Sci.*, 1996, **6**, 15–50.

[466] G. Kresse and J. Furthmüller, *Phys. Rev. B*, 1996, **54**, 11169.

[467] M. Sprik and G. Ciccotti, *J. Chem. Phys.*, 1998, **109**, 7737–7744.

[468] M. Brüssel, P. J. Di Dio, K. Muñiz and B. Kirchner, *Int. J. Mol. Sci.*, 2011, **12**, 1389–1409.

[469] J. VandeVondele, M. Krack, F. Mohamed, M. Parrinello, T. Chassaing and J. Hutter, *Comp. Phys. Commun.*, 2005, **167**, 103–128.

[470] Y. Zhang and W. Yang, *Phys. Rev. Lett.*, 1998, **80**, 890.

[471] J. VandeVondele and J. Hutter, *J. Chem. Phys.*, 2007, **127**, 114105.

[472] S. Goedecker, M. Teter and J. Hutter, *Phys. Rev. B*, 1996, **54**, 1703.

[473] C. Hartwigsen, S. Gœdecker and J. Hutter, *Phys. Rev. B*, 1998, **58**, 3641.

[474] M. Krack, *Theor. Chem. Acc.*, 2005, **114**, 145–152.

[475] H. Akima, *JACM*, 1970, **17**, 589–602.

[476] E. S. Shamay, V. Buch, M. Parrinello and G. L. Richmond, *J. Am. Chem. Soc.*, 2007, **129**, 12910–12911.

[477] G. Jenkins and K. Kawamura, *Nature*, 1971, **231**, 175.

[478] B. O'Malley, I. Snook and D. McCulloch, *Phys. Rev. B*, 1998, **57**, 14148.

[479] P. Harris, *Philos. Mag.*, 2004, **84**, 3159–3167.

[480] C. Merlet, B. Rotenberg, P. A. Madden, P.-L. Taberna, P. Simon, Y. Gogotsi and M. Salanne, *Nat. Mater.*, 2012, **11**, 306.

[481] C. Merlet, C. Péan, B. Rotenberg, P. A. Madden, B. Daffos, P.-L. Taberna, P. Simon and M. Salanne, *Nat. Commun.*, 2013, **4**, 2701.

[482] S. Bahmanyar, K. Houk, H. J. Martin and B. List, *J. Am. Chem. Soc.*, 2003, **125**, 2475–2479.

[483] N. Wiener *et al.*, *Acta math.*, 1930, **55**, 117–258.

[484] A. Khintchine, *Math. Ann.*, 1934, **109**, 604–615.

[485] G. Lamoureux and B. Roux, *J. Phys. Chem. B*, 2006, **110**, 3308–3322.

[486] H. A. Lorentz, *Ann. Phys.*, 1881, **248**, 127–136.

[487] D. Berthelot, *Compt. Rendus*, 1898, **126**, 1703–1855.

[488] V. Barone and M. Cossi, *J. Phys. Chem. A*, 1998, **102**, 1995–2001.

[489] T. N. Truong and E. V. Stefanovich, *Chem. Phys. Lett.*, 1995, **240**, 253–260.

Acknowledgments

Even though I wrote this thesis down, it would never have been made without the numberless helping hands of many people. Therefore, it is important to me to write some short words of gratitude at this point.

First of all, I thank my supervisor Prof. Dr. Barbara Kirchner for the freedom to grow on my own on the one hand, but being always available if necessary on the other.

Second, I thank Prof. Dr. Thomas Bredow for being the second referee of the thesis and Prof. Dr. Helmut Baltruschat and Prof. Dr. Jan Börner for completing the committee.

Special thanks go to Dr. Oldamur Hollóczki, who taught me a lot about how to write scientific articles. During finalizing the thesis, I realized once again what a tremendous progress I made over the last years.

Of course, I thank the current and former members of the Kirchner group and furthermore the entire Mulliken Center for providing a calm and peaceful environment with a countless number of people which were always ready to share their expertise.

Moreover, I thank the *International Max Planck Research School on Reactive Structure Analysis for Chemical Reactions (IMPRS RECHARGE)* not only for funding the first three years of my thesis, but as well for giving me the opportunity to broaden my scientific horizon and meet a lot of interesting and pleasant people.

Last but not least, I want to thank Anne for tolerating my existence at the *"science-is-not-always-fun"*-days during the last five years.